Dissertation
submitted to the
Combined Faculties for the Natural Sciences and for Mathematics
of the Ruperto-Carola University of Heidelberg, Germany
for the degree of
Doctor of Natural Sciences

presented by
Diplom-Physiker Martin Kiffner
born in Munich, Germany
Oral examination: 16.05.2007

Coherence effects in vacuum-induced processes

Referees: **Prof. Dr. C. H. Keitel**

Prof. Dr. P. Schmelcher

Zusammenfassung

Quanteninterferenzen und Kohärenzeffekte in der Wechselwirkung von Atomen mit dem quantisierten elektromagnetischen Feld werden theoretisch untersucht. Ein allgemeine Mastergleichung zur Beschreibung der Wechselwirkung von Atomen mit dem Strahlungsfeld wird vorgestellt. Das Zusammenspiel von Komplementarität und Interferenz in Bezug auf Energie und Zeit wird anhand des Fluoreszenzlichts eines einzelnen, lasergetriebenen Atoms diskutiert. Hierbei führt die Kohärenz der spontanen Prozesse zur Quanteninterferenz im Resonanzfluoreszenzspektrum. Die vakuum-induzierte Dipol-Dipol Wechselwirkung wird in Systemen bestehend aus zwei Mehrniveau-Atomen analysiert. Es wird gezeigt, dass die Wechselwirkung zwischen orthogonalen Dipolmomenten verschiedener Atome nicht nur die Systemdynamik entscheidend beeinflußt, sondern auch bewirkt, dass benachbarte, nahezu entartete Zeeman-Unterzustände des atomaren Niveauschemas im Allgemeinen nicht vernachlässigt werden können. Potentielle Anwendungen von Dipol-Dipol wechselwirkenden Mehrniveau-Atomen für die Realisierung von dekohärenzfreien Unterräumen und die Erzeugung von Verschränkung zwischen atomaren Zuständen werden aufgezeigt. Die Erzeugung eines verschränkten Zustandes des Strahlungsfeldes mit einer makroskopischen Zahl von Photonen wird anhand eines Ein-Atom Lasers diskutiert.

Abstract

Quantum interference and coherence effects in the interaction of atoms with the quantized electromagnetic field are investigated theoretically. A general master equation for the description of atom-field interactions is introduced. The interplay of the concepts of complementarity and interference in the time-energy domain are studied on the basis of the fluorescence light emitted by a single laser-driven atom, where the coherence of spontaneous processes gives rise to quantum interference in the spectrum of resonance fluorescence. The vacuum-induced dipole-dipole interaction in pairs of multi-level atoms is analyzed. It is shown that the interaction between orthogonal transition dipole moments of different atoms does not only influence the system dynamics crucially, but implies that the few-level approximation in general cannot be applied to near-degenerate Zeeman sublevels of the atomic level scheme. Potential applications of dipole-dipole interacting multi-level atoms for the implementation of decoherence-free subspaces and the generation of entanglement between atomic states are examined. The generation of an entangled state of the radiation field with a macroscopic number of photons is discussed on the basis of a single-atom laser.

Within the framework of this thesis, the following articles were published in refereed journals:

- M. Kiffner, J. Evers, and C. H. Keitel, *Quantum interference enforced by time-energy complementarity*, Phys. Rev. Lett. **96**, 100403 (2006).
- M. Kiffner, J. Evers, and C. H. Keitel, *Interference in the resonance fluorescence of two incoherently coupled transitions*, Phys. Rev. A **73**, 063814 (2006).
- J. Evers, M. Kiffner, M. Macovei, and C. H. Keitel, *Geometry-dependent dynamics of two Λ-type atoms via vacuum-induced coherences*, Phys. Rev. A **73**, 023804 (2006).

Articles accepted for publication in refereed journals:

- M. Kiffner, J. Evers, and C. H. Keitel, *Coherent control in a decoherence-free subspace of a collective multi-level system*, to appear in Phys. Rev. A.

Articles submitted for publication in refereed journals:

- M. Kiffner, J. Evers, and C. H. Keitel, *Breakdown of the few-level approximation in collective systems*, submitted to Phys. Rev. A.
- M. Kiffner, M. S. Zubairy, J. Evers, and C. H. Keitel, *Two-mode single-atom laser as a source of entangled light*, submitted to Phys. Rev. A.

Contents

Introduction

The development of quantum mechanics at the beginning of the 20th century was initiated by a series of failures of classical physics. A number of experiments revealed that Maxwell's theory of classical electrodynamics can neither account for the corpuscular properties of the radiation field nor the stability of atoms. On the other hand, classical mechanics was unable to explain the wavelike behavior of matter, and a variety of other examples could be added. The establishment of a comprehensive quantum theory took several decades and was complicated by the counterintuitive and peculiar nature of the quantum phenomena.

The interpretation of the emerging theory of quantum mechanics was facilitated by a thorough investigation of interference experiments. For example, a series of famous thought experiments based on Young's two-slit experiment were designed to shed new light on the apparent contradictions in connection with the wave-particle duality of matter and light [1, 2]. The problem of seemingly inconsistent predictions of quantum mechanics was then resolved within the famous Einstein-Bohr dialogue [2], where Heisenberg's uncertainty relation was employed to show that the wave- and the particle features of the interfering quantities can never be observed simultaneously. This striking result is the most famous example for the principle of complementarity. According to Niels Bohr [2], complementarity in general encompasses a class of phenomena where a set of observables cannot be measured precisely under the same experimental conditions. Since complementarity is one of the most salient features of quantum mechanics, it has been investigated in various experimental and theoretical studies and continues to challenge our understanding of the quantum world.

Interference phenomena did not only play a crucial role during the early days of the quantum theory, but remained in the focus of interest until now. While the discussion and interpretation of quantum interference effects is sometimes an involved task, it was often rewarded by an improved understanding of physical processes. In some cases, new interference experiments continued to initiate further development of the theory. An example is the famous Hanbury-Brown and Twiss experiment, which provided evidence for second-order correlations in a thermal field [3]. This experiment gave rise to a systematic investigation of the quantum nature of the radiation field, and caused the development of the quantum theory of optical coherence [4]. Eventually, the invention of the laser and its technical improvement made the various aspects of this theory accessible to the experiment, and the field of quantum optics was launched.

During the last decades, the field of atom-laser interactions evolved at a stunning pace and opened up a rich variety of new and intriguing physical phenomena. A lot of excitement was created by interference effects like electromagnetically induced transparency, the stopping of light and lasing without inversion, for example. These phenomena can be attributed to laser-induced coherences between atomic states. Further, it has been shown that quantum optical systems can provide tests for fundamental concepts of quantum mechanics like the principle of complementarity or Bell's inequalities. Remarkable success has also been achieved in the field of high-precision measurements. A prominent example is the development of atomic clocks which serve as a time standard and are at the heart of the global positioning system (GPS). Moreover, the invention of sophisticated laser cooling and trapping methods allowed to study ultra-cold quantum gases and culminated in the realization of Bose-Einstein condensates and the trapping of single atoms and ions.

The general trend of the tremendous progress in quantum optics can be described by the increasing ability to control single quantum systems. This achievement does not only provide new insight into fundamental processes, but constitutes a necessary requirement for the fields of quantum computation and quantum information theory [5]. This flourishing field of quantum physics aims at a speedup of classical computations and at secure communication via quantum cryptography. An important resource for many schemes in quantum computation and quantum information is entanglement, which was first discussed in a thought experiment by Einstein, Podolsky and Rosen [6]. Einstein described the strange correlations that occur in the context with non-separable states as a "spooky action at a distance," and the counterintuitive implications of entanglement are still puzzling and fascinating nowadays. In particular, there is still an ongoing debate about general criteria which allow to quantify the degree of entanglement in a quantum system unambiguously.

While the physical implementation of small quantum processors and basic quantum algorithms has been achieved recently [7], the scaling of these schemes to larger systems is a challenging and as yet unresolved task. A major difficulty arises from the interaction of a quantum system with its environment, which leads to decoherence [8, 9]. In atomic systems, a crucial source of decoherence is represented by spontaneous emission which results from the interaction of the atom with the infinitely many field modes of the quantized electromagnetic field. Several schemes for the control and modification of spontaneous emission have been investigated, and many of them are based on quantum interference effects in single atoms or in collective systems. In the ideal case, these control mechanisms would allow for a complete suppression of spontaneous emission such that the decohering processes are avoided. Fortunately, this very ambitious goal is not a necessary requirement for the implementation of quantum computing schemes. For most applications, it suffices to suppress spontaneous emission in a subspace of the total state space of the system, and these subspaces are termed decoherence-free subspaces (DFS).

In this thesis, several interference and coherence effects in the interaction of atoms with the vacuum are put forward. On the one hand, fundamental aspects like the intimate connection between the concepts of interference and complementarity are addressed. On the other hand, the role of vacuum-induced processes for the generation of entanglement and the possibility to realize decoherence-free subspaces are discussed. More specifically, the general model for atom-field interactions which is the basis for all calculations in subsequent chapters is presented in **part I**. In **part II**, we demonstrate that the interplay of the concepts of complementarity and interference can be transferred from the familiar position-momentum domain to the time-energy domain. In particular, we show that the fluorescence light emitted by a single laser-driven atom displays a clear signature of quantum interference. While the mere presence of the interference effect is a surprising and counterintuitive result, it is additionally enabled by spontaneous processes which usually destroy the coherence in the system. In **part III**, the vacuum-induced dipole-dipole interaction between multi-level atoms is discussed. This coupling is mediated via the exchange of photons between dipole transitions of different atoms and is of second order in the atom-field interaction [10, 11]. Any analysis which goes beyond the simple model of a pair of two-level atoms involves the interaction between orthogonal dipoles of different atoms. While these coupling terms have frequently been neglected in previous works, we show that these terms do not only influence the system dynamics crucially (chapter 3), but imply that the few-level approximation cannot be applied to near-degenerate Zeeman sublevels of the atomic level scheme (chapter 4). As a potential application, we show that a pair of dipole-dipole interacting multi-level atoms exhibits a decoherence-free subspace and can be prepared in a long-lived entangled state (chapter 5). In this setup, entanglement of the atomic states is created by the coherent part of the dipole-dipole interaction. From a conceptual point of view, it is interesting to ask whether the role of the atoms and the radiation field can be reversed, i.e., can an atomic system act as a source of entangled light? This question is investigated in **part IV**, where we show that a single-atom laser can give rise to an entangled state of the field inside a doubly resonant cavity. After this brief overview, we now provide a more detailed description of the individual chapters.

In **chapter 1**, a mathematical model for the interaction of a collection of atoms with the quantized electromagnetic field is presented. Each atom is modeled by two near-degenerate multiplets that may consist of an arbitrary but finite number of states. These multiplets correspond to the angular momentum eigenstates of the atoms. We employ the master equation approach and provide a detailed derivation of the equation of motion for the reduced density operator of the atoms. All essential approximations that enter the calculation are discussed in detail. The master equation derived in this chapter is quite general and encompasses various physical phenomena. For single-atom systems, it accounts for spontaneous emission on individual dipole transitions as well as for vacuum-induced quantum interference effects associated with the cross-decay of two dipole transitions (see chapter 2). In systems comprised of more than one atom, additional coupling terms occur. Some of

these terms are collective decay rates which account for a modification of spontaneous emission of one atom due to the presence of the other atoms. In addition, the vacuum-induced coupling between the atoms gives rise to a coherent interaction which results in energy shifts of the collective states. These collective parameters are in the focus of part III of this thesis. In particular, the master equation derived in chapter 1 accounts for the coupling between orthogonal transition dipole moments of different atoms that have frequently been neglected in the previous literature (see chapter 3). Finally, the master equation can be extended such that the reduced density operator does not only describe the atomic degrees of freedom, but also the quantum state of a finite number of field modes, for example. This situation is investigated in chapter 6. Note that the master equation derived in chapter 1 is not only the starting point for all calculations in subsequent chapters, but in our general form an advancement of previous work.

The interplay of the concepts of complementarity and interference in the time-energy domain are studied in **chapter 2**. Here we present a system where different temporal paths lead to interference in the energy domain. The analysis is carried out on the basis of the resonance fluorescence of a single four-level atom in an external magnetic field. Two dipole transitions that are only coupled by spontaneous emission are driven by a monochromatic laser field. We find that the spectrum of resonance fluorescence exhibits a clear signature of quantum interference between photons emitted on two different dipole transitions of the atomic level scheme. Since the two transitions in question start and end up in different atomic states, the mere presence of this interference effect is a surprising result which needs to be explained. In addition, the degree of interference in the fluorescence spectrum can be controlled by means of the external magnetic field to a large extend. For a suitably chosen magnetic field strength, the relative weight of the Rayleigh line can be completely suppressed, even for low intensities of the coherent driving field. The second observable is total fluorescence intensity emitted by the atom, and we find that is not affected by interference. In order to explain our results, we employ the principle of complementarity, applied to time and energy. For the system considered here, it claims that it is impossible to observe the temporal and the energy aspect of the radiative cascade of the atom at the same time. If the fluorescence spectrum is observed, the photon emission times are indeterminate. The interference in the fluorescence spectrum can thus be explained in terms of interferences between transition amplitudes that correspond to different time orders of photon emissions. Since the considered atomic level scheme can be found, e.g., in $^{198}Hg^{+}$ ions, our model system turns out to be an ideal candidate for the experimental verification of vacuum-induced interference effects. These effects have been studied extensively by theoretical means in V-type three-level atoms, but could not be confirmed experimentally in atomic systems due to the stringent conditions of near-degenerate levels and non-orthogonal dipole moments [11].

The third part of this thesis consists of three chapters and deals with the vacuum-induced dipole-dipole coupling in pairs of multi-level atoms. In **chapter 3**, two nearby three-level atoms in Λ-configuration are considered. If the distance of the

two atoms is small on a scale given by the relevant transition wavelength, the dipole-dipole interaction between transitions of different atoms gives rise to a collective quantum dynamics of the system. We show that in general, the dipole-dipole interaction does not only couple transitions with parallel dipole moments. On the contrary, even transitions with perpendicular dipole moments may interact via the exchange of photons. We give an interpretation of this effect and show that it may crucially influence the system dynamics. As an example observable, we study the resonance fluorescence intensity emitted by the atoms that are driven by two laser fields with different frequencies. For a fixed setup of driving fields and detectors, the spatial orientation of the two-atom pair decides if the system reaches a true constant steady state or if it exhibits periodic oscillations in the long-time limit. These oscillations are directly observable in the fluorescence intensity emitted by the atoms. The geometry-dependent dynamics of the system can be traced back to the interaction between orthogonal dipoles of different atoms. Potential applications of this effect include three-dimensional precision measurements of relative positions and distances of the two atoms.

An important consequence of the results in chapter 3 is investigated in **chapter 4**, where the validity of the few-level approximation in dipole-dipole interacting collective systems is discussed. As an example system, we consider a pair of dipole-dipole interacting four-level atoms, each modelled by two complete sets of angular momentum multiplets. The ground state of each atom is a S_0 singlet state, and the excited state multiplet is a P_1 triplet which consists of three Zeeman sublevels. Here we show that the otherwise ubiquitous few-level approximation in general leads to incorrect results if it is applied to the magnetic sublevels of this system. For this, we prove that the dipole-dipole induced energy shifts between collective two-atom states depend on the length of the vector connecting the atoms, but not on its orientation, if complete and degenerate multiplets are considered. On the contrary, the artificial omission of Zeeman sublevels breaks the rotational symmetry and leads to incorrect eigenenergies of the system. We find that the breakdown of the few-level approximation can be traced back to the dipole-dipole coupling of transitions with orthogonal dipole moments that were studied in chapter 3. A careful analysis of the nature of the dipole-dipole coupling enables us to identify special geometries in which one or two of the excited states of each atom can be neglected, such that the few-level approximation is recovered. Our results are relevant for future experimental and theoretical studies of dipole-dipole interacting few-level systems.

In **chapter 5**, a decoherence-free subspace (DFS) in a system of two dipole-dipole interacting multi-level atoms is investigated. For this, we consider the two-atom system introduced in chapter 4, where each four-level atom is modeled by two complete sets of angular momentum multiplets. We first establish conditions which warrant the existence of a DFS in the two-atom system of interest. It is shown that the collective state space of this system contains a four-dimensional DFS if the distance between the atoms approaches zero. In the following, possible applications of this DFS for the storage and processing of quantum information are discussed. For this, the coherent and incoherent system dynamics is analyzed in detail. We

determine the eigenstates and energies of the collective system and provide explicit expressions for the dipole-dipole induced energy shifts of these states. It is found that our results are in agreement with the general findings established in chapter 4. The evaluation of the decay rates of the antisymmetric collective states shows that spontaneous emission of states inside the DFS is strongly suppressed, provided that the separation of the atoms is sufficiently small. For potential applications of this DFS in quantum information processing, it must be possible to prepare the system inside the DFS. We show that the antisymmetric states can be populated selectively by means of an external laser field. Further, the possibility to induce a controlled quantum dynamics between a pair of antisymmetric states is investigated. While a static magnetic field can only induce a limited dynamics, any single-qubit operation can be performed within the DFS if a radiofrequency field is applied. Finally, we employ the concurrence as a measure of entanglement and show that the symmetric and antisymmetric collective states are entangled. This entanglement is created by the coherent part of the dipole-dipole interaction and originates from the interaction of the atoms with the vacuum.

The quantum state of the radiation field created by an atomic system is analyzed in **Chapter 6**. While we have seen in chapter 5 that the atom-field interaction can give rise to entangled atomic states, we now demonstrate that a single atom can act as a source for an entangled state of the radiation field. For this, we consider a laser where the gain medium consists of a single atom trapped inside a cavity. The atom interacts with two (nondegenerate) cavity modes on separate transitions. In addition, two other transitions of the atomic four-level system are driven by laser fields. The complete system consists of the atomic degrees of freedom and the cavity modes, and its dynamics is described by a master equation. We then derive an equation of motion for the quantum state of the two cavity modes alone and include cavity losses into our model. An inequality based on the correlation of the field operators serves as a sufficient criterion for the entanglement of the cavity field. We find that the single-atom laser is a source of entangled light over a wide range of control parameters and initial states of the cavity field. In contrast to other schemes like parametric down-conversion, an entangled state with a macroscopic number of photons can be created. Our system may find applications in the fields of quantum computation and quantum information which require entanglement as a key resource.

Part I

Mathematical model

Chapter 1

Master equation for a collection of interacting multi-level atoms

1.1 Introduction

All physical phenomena that are discussed in subsequent chapters of this thesis require a model for the interaction of atoms with the quantized electromagnetic field. Thus in this chapter, we describe the underlying mathematical method that allows to determine the physical observables we are interested in. Here we employ the master equation approach which is a standard technique in the description of atom-field interactions. The master equation describes the time evolution of the reduced density operator of the atomic system, and the infinite number of field modes of the quantized electromagnetic field act as a reservoir which changes only slightly due to the presence of the atoms. For a variety of physically relevant initial states of the radiation field, it is justified to introduce a number of approximations which simplify the equation of motion for the atomic system considerably.

The master equation technique has been applied to various atomic systems. For example, the master equation for a single two-level atom is a standard component of most textbooks on quantum optics, and the more general case of a single multi-level atom has been considered, e.g., in [11]. The master equation for M identical two-level atoms coupled to the vacuum was introduced by Lehmberg [12, 13], and its derivation can also be found in a textbook by Agarwal [10]. A generalization of this system to the case of M non-identical two-level atoms that are placed in a thermal field or in a squeezed vacuum was considered in [11] and [14], respectively. A large number of physical phenomena in systems of M two-level atoms were investigated theoretically and experimentally (see Sec. 3.1).

On the contrary, systems that are comprised of two or more atoms with more than two internal states are much less common in the literature. A master equation for M identical multi-level atoms can be found in [15, 16], for example. Here the states within the excited and ground state multiplet were assumed to be degenerate.

A system of two three-level atoms with non-degenerate multiplets was considered in [17], where the emphasis was on a new type of vacuum-induced coupling terms between transitions with orthogonal dipole moments. These coupling terms were frequently neglected in previous studies, and will be discussed in detail in chapters 3 and 4.

In this chapter, we consider a collection of M identical multi-level atoms, and each atom is modeled by two near-degenerate multiplets with an arbitrary number of states. Note that we explicitly allow the states within each multiplet to be non-degenerate. The multiplets correspond to the angular momentum eigenstates of the atoms, and the level splitting within each manifold can be identified with the Zeeman splitting of the magnetic sublevels. Since the master equation for this quite general multi-atom multi-level system is not part of the standard literature yet, we provide a detailed derivation of its explicit form in Secs. 1.2 and 1.3. In particular, we illustrate all approximations that enter the calculation to clarify its scope of validity.

Since the master equation only describes the dynamics of the reduced atomic density operator, the quantum state of the radiation field is inaccessible. Fortunately, physical observables which involve correlation functions of the electromagnetic field can be expressed in terms of correlation functions of atomic operators. This procedure is illustrated in chapters 2 and 3, where we discuss the resonance fluorescence of a single atom and a pair of atoms, respectively. Since the atomic correlation functions can be evaluated via the master equation, it is generally not required to determine the quantum state of the radiation field.

On the contrary, in some physical problems one is especially interested in the quantum state of the radiation field created by the atomic system. This situation is considered in chapter 6, where the quantum state inside a two-mode cavity is determined. In this case, the two cavity modes of interest are separated from the reservoir, and the density operator of the system describes the quantum state of the atoms and the two cavity modes.

The derivation process of the master equation for M identical multi-level atoms is split in two parts. In Sec. 1.2, we give a detailed description of the system and set up its Hamiltonian. Starting from Zwanzig's exact master equation for the reduced density operator of the atoms, we recall the major steps which lead to the general master equation in Born approximation. The derivation of the explicit form of the master equation for M identical multi-level atoms is provided in Sec. 1.3. Some calculations are deferred to Appendix 1.A.

1.2 Description of the system and general approach

We consider a collection of M identical atoms that are located at different positions $\boldsymbol{r}_\mu$ ($\mu \in \{1, \ldots, M\}$) in space. An example for a geometrical setup of five atoms is shown in Fig. 1.1(a). Each atom is modeled by a finite number of L atomic states,

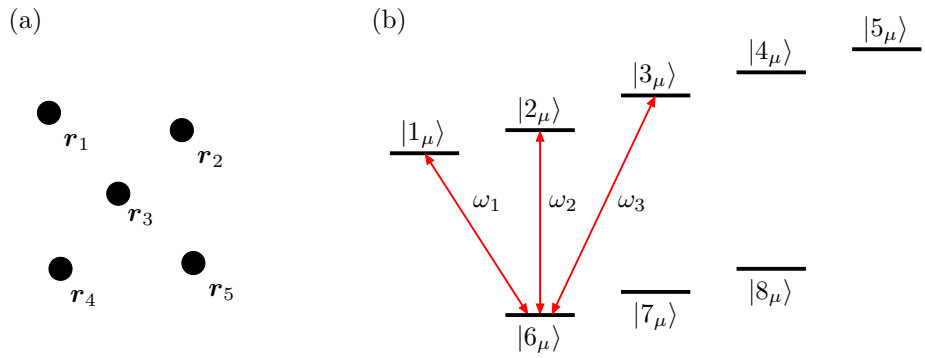

Figure 1.1: (a) Geometrical setup of $M = 5$ atoms. We neglect the center of mass motion of the atoms and assume their positions to be fixed. (b) Level scheme with $L = 8$ states. The ground and excited state multiplets consist of three and five states, respectively. In order to keep the drawing concise, only those dipole transitions which involve the ground state $|6_\mu\rangle$ are indicated by red arrows, and the transition frequencies are labeled by ω_i. Note that the splitting of the excited and ground state multiplets is not to scale. In particular, all frequency differences $(\omega_i - \omega_j)$ are assumed to be much smaller than the frequencies ω_i themselves.

and the k-th state of atom μ is labeled by $|k_\mu\rangle$ ($k \in \{1, \ldots, L\}$). Since we consider a collection of identical atoms, we assume that the states $|k_\mu\rangle$ and $|k_\nu\rangle$ for $\mu \neq \nu$ represent the same physical state. The subscript μ indicates that $|k_\mu\rangle$ belongs to the state space of atom μ, and the energy of state $|k_\mu\rangle$ is denoted by E_k.

We assign to each dipole transition of the atomic level scheme a number i and a transition frequency ω_i. This assignment can be chosen at will, but must be kept fixed throughout the derivation. The total number of dipole transitions is denoted by D. To the i-th dipole transition of atom μ corresponds a pair of raising and lowering operators that are labeled by $S_{i+}^{(\mu)}$ and $S_{i-}^{(\mu)}$, respectively. These transition operators are defined as

$$S_{i+}^{(\mu)} = |l_\mu\rangle\langle k_\mu| \quad \text{and} \quad S_{i-}^{(\mu)} = |k_\mu\rangle\langle l_\mu|\,, \tag{1.1}$$

where $|k_\mu\rangle$ is the ground state and $|l_\mu\rangle$ is the excited state of the i-th dipole transition.

Although the number of the relevant atomic states L is arbitrary, we assume that the atomic levels can be divided into a group of ground states and a group of excited states. In particular, we suppose that the ground and excited state multiplets are near-degenerate. This means that the frequency splitting between any two states that belong to the same multiplet is much smaller than all transition frequencies ω_i. It follows that all possible differences $(\omega_i - \omega_j)$ are much smaller than the mean transition frequency ω_0,

$$(\omega_i - \omega_j) \ll \omega_0\,, \quad \text{where} \quad \omega_0 = \frac{1}{D}\sum_{i=1}^{D}\omega_i \quad \text{and} \quad i, j \in \{1, \ldots, D\}\,. \tag{1.2}$$

An example for an atomic level scheme with $L = 8$ states is shown in Fig. 1.1(b). Here the ground and excited state multiplets consist of three and five states, respectively.

Note that our approach can easily be generalized to systems with more than two near-degenerate multiplets. If the difference between the mean transition frequencies of the various multiplet transitions is much larger than the inverse lifetimes of the atomic states, each pair of an excited and ground state multiplet can be treated independently. It follows that the contributions from all pairs of ground and excited state multiplets can be added to obtain the total master equation.

After the introduction of these definitions, we can establish the Hamiltonian of the complete system which is comprised of the atoms and the quantized electromagnetic field. We begin with the Hamiltonian $H_{\rm A}$ which governs the free time evolution of the atoms,

$$H_{\rm A} = \sum_{\mu=1}^{M} \sum_{k=1}^{L} E_k A_{kk}^{(\mu)} \,, \tag{1.3}$$

where $A_{kk}^{(\mu)} = |k_\mu\rangle\langle k_\mu|$. The free Hamiltonian of the radiation field is given by

$$H_{\rm F} = \sum_{\boldsymbol{k}s} \hbar\omega_k a_{\boldsymbol{k}s}^\dagger a_{\boldsymbol{k}s} \,, \tag{1.4}$$

and $a_{\boldsymbol{k}s}$ ($a_{\boldsymbol{k}s}^\dagger$) are the annihilation (creation) operators that correspond to a field mode with wave vector $\boldsymbol{k}$, unit polarization vector $\boldsymbol{\epsilon}_{\boldsymbol{k}s}$ ($s \in \{1, 2\}$) and frequency ω_k. In electric-dipole approximation, the interaction between the atoms and the radiation field is described by [18, 19]

$$V = -\sum_{\mu=1}^{M} \hat{\boldsymbol{d}}^{(\mu)} \cdot \hat{\boldsymbol{E}}(\boldsymbol{r}_\mu) \,, \tag{1.5}$$

where $\hat{\boldsymbol{d}}^{(\mu)}$ is the electric-dipole moment operator of atom μ,

$$\hat{\boldsymbol{d}}^{(\mu)} = \sum_{i=1}^{D} \left[\boldsymbol{d}_i S_{i+}^{(\mu)} + \text{H.c.} \right] . \tag{1.6}$$

The complex vector $\boldsymbol{d}_i$ denotes the dipole moment of the i-th dipole transition, and the electric field operator $\hat{\boldsymbol{E}}$ is defined as

$$\hat{\boldsymbol{E}}(\boldsymbol{r}) = i\hbar \sum_{\boldsymbol{k}s} \boldsymbol{u}_{\boldsymbol{k}s}(\boldsymbol{r}_\mu) a_{\boldsymbol{k}s} + \text{H.c.} \,. \tag{1.7}$$

In this equation, the mode function $\boldsymbol{u}_{\boldsymbol{k}s}(\boldsymbol{r})$ reads

$$\boldsymbol{u}_{\boldsymbol{k}s}(\boldsymbol{r}) = \frac{1}{\hbar} \sqrt{\frac{\hbar\omega_k}{2\varepsilon_0 v}} \boldsymbol{\epsilon}_{\boldsymbol{k}s} e^{i\boldsymbol{k}\cdot\boldsymbol{r}} \,, \tag{1.8}$$

where v is the quantization volume and $\boldsymbol{\epsilon}_{\boldsymbol{k}s}$ is the unit polarization vector that corresponds to the wave vector $\boldsymbol{k}$ ($s \in \{1, 2\}$).

The time evolution of the quantum state ϱ of the atoms and the radiation field is determined by Schrödinger's equation,

$$\partial_t \varrho = -\frac{i}{\hbar}[H, \varrho]\,, \tag{1.9}$$

where the complete Hamiltonian is $H = H_\mathrm{A} + H_\mathrm{F} + V$. The Schrödinger equation (1.9) can be transformed into an exact equation of motion for the reduced density operator $\varrho_\mathrm{A} = \mathrm{Tr}_\mathrm{F}[\varrho]$ of the atoms [4, 10, 20]. This equation is known as Zwanzig's master equation,

$$i\hbar\partial_t \mathcal{P}\varrho(t) = \mathcal{P}\mathcal{L}\mathcal{P}\varrho + \mathcal{P}\mathcal{L}\mathcal{Q}\left[\mathcal{U}_{QQ}(t)\mathcal{Q}\varrho(0) - \frac{i}{\hbar}\int_0^t d\tau\, \mathcal{U}_{QQ}(\tau)\mathcal{Q}\mathcal{L}\mathcal{P}\varrho(t-\tau)\right]\,. \tag{1.10}$$

Here the time-independent projection operator $\mathcal{P}$ is defined as

$$\mathcal{P}\varrho(t) = \varrho_\mathrm{F}(0) \otimes \mathrm{Tr}_\mathrm{F}[\varrho(t)] = \varrho_\mathrm{F}(0) \otimes \varrho_\mathrm{A}(t)\,, \tag{1.11}$$

and $\varrho_\mathrm{F}(0) = \mathrm{Tr}_\mathrm{A}[\varrho(0)]$ denotes the reduced density operator of the radiation field at $t = 0$. The projection operator $\mathcal{P}$ satisfies $\mathcal{P}^2 = \mathcal{P}$, and $\mathcal{P}\varrho$ is essentially given by the reduced density operator ϱ_A of the atoms that we are interested in. The projection operator $\mathcal{Q} = \mathbb{1} - \mathcal{P}$ is complementary to $\mathcal{P}$ and obeys $\mathcal{Q}^2 = \mathcal{Q}$. The Liouville operator of the system is defined as

$$\mathcal{L}(\,\cdot\,) = [H_\mathrm{A} + H_\mathrm{F} + V, \,\cdot\,]\,, \tag{1.12}$$

and the centered dot denotes the position of the argument of $\mathcal{L}$. With the definitions

$$\mathcal{L}_\mathrm{A}(\,\cdot\,) = [H_\mathrm{A}, \,\cdot\,]\,, \qquad \mathcal{L}_\mathrm{R}(\,\cdot\,) = [H_\mathrm{R}, \,\cdot\,]\,, \qquad \mathcal{L}_\mathrm{int}(\,\cdot\,) = [V, \,\cdot\,]\,, \tag{1.13}$$

$\mathcal{L}$ can be written as $\mathcal{L}_\mathrm{A} + \mathcal{L}_\mathrm{R} + \mathcal{L}_\mathrm{int}$. Since the total Hamiltonian in Eq. (1.9) and hence the Liouville operator in Eq. (1.12) are time-independent, the time evolution operator reads

$$\mathcal{U}_{QQ}(t) = \exp\left[-i\mathcal{Q}\mathcal{L}\mathcal{Q}t/\hbar\right]\,. \tag{1.14}$$

Basic assumptions. In order to simplify the exact master equation (1.10), we assume that the total density operator factorizes into a product state at $t = 0$, $\varrho(0) = \varrho_\mathrm{F}(0) \otimes \varrho_\mathrm{A}(0)$. It follows that the term $\mathcal{Q}\varrho(0)$ in Eq. (1.10) vanishes. Here we suppose that the radiation field is initially in the vacuum state $\varrho_\mathrm{F}(0) = |0_\mathrm{F}\rangle\langle 0_\mathrm{F}|$. This state is a stationary state with respect to H_F,

$$[H_\mathrm{F}, \varrho_\mathrm{F}(0)] = 0\,, \tag{1.15}$$

and the expectation value of the interaction Hamiltonian V with respect to $\varrho_\mathrm{F}(0)$ vanishes,

$$\mathrm{Tr}_\mathrm{F}\left[\varrho_\mathrm{F}(0)V\right] = 0\,. \tag{1.16}$$

With Eqs. (1.15) and (1.16), one can show that the superoperators in Eq. (1.13) satisfy

$$\mathcal{P}\mathcal{L}_{\rm A} = \mathcal{L}_{\rm A}\mathcal{P}\,, \quad \mathcal{P}\mathcal{L}_{\rm R} = \mathcal{L}_{\rm R}\mathcal{P} = 0 \quad \text{and} \quad \mathcal{P}\mathcal{L}_{\rm int}\mathcal{P} = 0\,. \tag{1.17}$$

It follows that the master equation (1.10) can be written as [4, 10]

$$\partial_t \mathcal{P}\varrho(t) = -\frac{i}{\hbar}\mathcal{L}_{\rm A}\mathcal{P}\varrho - \frac{1}{\hbar^2}\mathcal{P}\mathcal{L}_{\rm int}\int_0^t d\tau\, \mathcal{U}_{QQ}(\tau)\mathcal{L}_{\rm int}\mathcal{P}\varrho(t-\tau)\,. \tag{1.18}$$

Born approximation. We now introduce the first approximation which is known as the Born approximation. The second term in Eq. (1.10) is at least of second order in the interaction Hamiltonian V. Higher orders arise since the time evolution operator $\mathcal{U}_{QQ}$ also contains $\mathcal{L}_{\rm int}$. If the coupling between the atoms and the radiation field is sufficiently weak, it is justified to restrict the analysis to the leading order in $\mathcal{V}$ such that the interaction term $\mathcal{L}_{\rm int}$ in $\mathcal{U}_{QQ}$ can be neglected,

$$\mathcal{U}_{QQ}(t) \approx \exp\left[-i\mathcal{Q}\left(\mathcal{L}_{\rm A} + \mathcal{L}_{\rm F}\right)\mathcal{Q}t/\hbar\right]\,. \tag{1.19}$$

This approximation means that an emitted photon does not react back on the atom. The general master equation in Born approximation then reads

$$\partial_t \mathcal{P}\varrho(t) = -\frac{i}{\hbar}\mathcal{L}_{\rm A}\mathcal{P}\varrho - \frac{1}{\hbar^2}\mathcal{P}\mathcal{L}_{\rm int}\int_0^t d\tau\, U(\tau)\left[\mathcal{L}_{\rm int}\mathcal{P}\varrho(t-\tau)\right]U^\dagger(\tau)\,, \tag{1.20}$$

where

$$U(t) = \exp[-i(H_{\rm A} + H_{\rm F})t/\hbar]\,. \tag{1.21}$$

With the definition of the projection operator $\mathcal{P}$ in Eq. (1.11) and the short-hand notation $\varrho_{\rm F}(0) = \varrho_{\rm F}$, we obtain from Eq. (1.20) the equation of motion for the reduced atomic density operator $\varrho_{\rm A}$,

$$\boxed{\partial_t \varrho_{\rm A} = -\frac{i}{\hbar}[H_{\rm A}, \varrho_{\rm A}] - \frac{1}{\hbar^2}\int_0^t d\tau \mathrm{Tr}_{\rm F}\Big(\big[V, U(\tau)\big[V, \varrho_{\rm F}\otimes\varrho_{\rm A}(t-\tau)\big]U^\dagger(\tau)\big]\Big)\,.} \tag{1.22}$$

This equation has been derived under quite general conditions and does not only apply to a collective system of multi-level atoms. On the contrary, the interaction Hamiltonian V is only constrained by Eq. (1.16), but its explicit form has not been employed so far. In addition, the assumption that V is time-independent is not essential and can be relaxed [4, 10], which leads to a slight modification of Eq. (1.22).

1.3 Derivation of the master equation

We now derive from Eq. (1.22) the explicit form of the master equation for a collection of M multi-level atoms. We begin with the evaluation of the double commutator

in Eq. (1.22). To this end, we introduce the operator

$$\tilde{V}(t) = U^\dagger(t)\, V\, U(t) = -i\hbar \sum_{\boldsymbol{k}s} \Big[D_{\boldsymbol{k}s}(t)\tilde{a}_{\boldsymbol{k}s}(t) - D^\dagger_{\boldsymbol{k}s}(t)\tilde{a}^\dagger_{\boldsymbol{k}s}(t) \Big] \,, \tag{1.23}$$

which is the interaction Hamiltonian transformed into the interaction picture with respect to $H_\mathrm{A} + H_\mathrm{F}$. In this equation, the operators $D_{\boldsymbol{k}s}(t)$, $\tilde{a}_{\boldsymbol{k}s}(t)$ and $\tilde{a}^\dagger_{\boldsymbol{k}s}(t)$ are given by

$$\begin{aligned} D_{\boldsymbol{k}s}(t) &= \sum_{\mu=1}^{M} \boldsymbol{u}_{\boldsymbol{k}s}(\boldsymbol{r}_\mu) \cdot \left\{ \sum_{i=1}^{D} \Big[\boldsymbol{d}_i S^{(\mu)}_{i+} e^{i\omega_i t} + \mathrm{H.c.} \Big] \right\} , \\ \tilde{a}_{\boldsymbol{k}s}(t) &= a_{\boldsymbol{k}s}\, e^{-i\omega_k t} \,, \qquad \text{and} \qquad \tilde{a}^\dagger_{\boldsymbol{k}s}(t) = a^\dagger_{\boldsymbol{k}s}\, e^{i\omega_k t} \,. \end{aligned} \tag{1.24}$$

With the definition in Eq. (1.23) and the relation $U(\tau) = U^\dagger(-\tau)$, the commutator in Eq. (1.22) can be written as

$$\begin{aligned} [\tilde{V}(0), [\tilde{V}(-\tau), \varrho_\mathrm{F} \otimes \tilde{\varrho}_\mathrm{A}(t-\tau)]] =& \tilde{V}(0)\tilde{V}(-\tau)\varrho_\mathrm{F} \otimes \tilde{\varrho}_\mathrm{A}(t-\tau) \\ & - \tilde{V}(-\tau)\varrho_\mathrm{F} \otimes \tilde{\varrho}_\mathrm{A}(t-\tau)\tilde{V}(0) + \mathrm{H.c.} \,, \end{aligned} \tag{1.25}$$

where $\tilde{\varrho}_\mathrm{A}(t-\tau) = \exp\left[-iH_\mathrm{A}\tau/\hbar\right] \varrho_\mathrm{A}(t-\tau) \exp\left[iH_\mathrm{A}\tau/\hbar\right]$. Note that only the first two terms on the right hand side of Eq. (1.25) have to be determined, the remaining parts can be obtained by Hermitian conjugation. In the master equation (1.22), the first term in Eq. (1.25) gives rise to the following expression,

$$(\triangle) = -\frac{1}{\hbar^2} \int_0^t d\tau \mathrm{Tr}_\mathrm{F} \Big(\tilde{V}(0)\tilde{V}(-\tau)\varrho_\mathrm{F} \otimes \tilde{\varrho}_\mathrm{A}(t-\tau) \Big) \,. \tag{1.26}$$

Next we evaluate the trace over the vacuum modes in Eq. (1.26). Since the initial state of the radiation field ϱ_F is the vacuum, the various field correlation functions are found to be

$$\begin{aligned} &\mathrm{Tr}[\tilde{a}_{\boldsymbol{k}s}(t)\tilde{a}_{\boldsymbol{k}'s'}(t')\,\varrho_\mathrm{F}] = \mathrm{Tr}[\tilde{a}^\dagger_{\boldsymbol{k}s}(t)\tilde{a}^\dagger_{\boldsymbol{k}'s'}(t')\,\varrho_\mathrm{F}] = \mathrm{Tr}[\tilde{a}^\dagger_{\boldsymbol{k}s}(t)\tilde{a}_{\boldsymbol{k}'s'}(t')\,\varrho_\mathrm{F}] = 0 \,, \\ &\mathrm{Tr}[\tilde{a}_{\boldsymbol{k}s}(t)\tilde{a}^\dagger_{\boldsymbol{k}'s'}(t')\,\varrho_\mathrm{F}] = \delta_{\boldsymbol{k}\boldsymbol{k}'}\delta_{ss'} e^{-i\omega_k(t-t')} \,. \end{aligned} \tag{1.27}$$

With these relations, Eq. (1.26) can be written as

$$(\triangle) = -\int_0^t d\tau \sum_{\boldsymbol{k}s} D_{\boldsymbol{k}s}(0) D^\dagger_{\boldsymbol{k}s}(-\tau) \tilde{\varrho}_\mathrm{A}(t-\tau) e^{-i\omega_k\tau} \,. \tag{1.28}$$

Rotating-wave approximation. We proceed with our second approximation which is known as the rotating-wave approximation (RWA). According to the definition (1.24) of $D_{\boldsymbol{k}s}(t)$, the expression $(\triangle)$ contains all possible products of the atomic

raising and lowering operators $S_{i+}^{(\mu)}$ and $S_{i-}^{(\mu)}$. If we transformed ($\triangle$) into the interaction picture with respect to $H_{\rm A}$, all terms proportional to $S_{i+}^{(\mu)}S_{j+}^{(\nu)}$ and $S_{i-}^{(\mu)}S_{j-}^{(\nu)}$ would oscillate at a frequency $\pm(\omega_i+\omega_j)$. On the contrary, the terms proportional to $S_{i+}^{(\mu)}S_{j-}^{(\nu)}$ and $S_{i-}^{(\mu)}S_{j+}^{(\nu)}$ would oscillate at a frequency $\pm(\omega_i-\omega_j)$. Since we assumed that the differences $(\omega_i-\omega_j)$ between the resonance frequencies are much smaller than the frequencies ω_i themselves, it is justified to keep only the resonant terms in ($\triangle$) which are proportional to $S_{i+}^{(\mu)}S_{j-}^{(\nu)}$ and $S_{i-}^{(\mu)}S_{j+}^{(\nu)}$,

$$(\triangle) = -\sum_{\mu,\nu=1}^{M}\sum_{i,j=1}^{D}\left[S_{i+}^{(\mu)}S_{j-}^{(\nu)}X_{ij}^{\mu\nu}(t)+S_{i-}^{(\mu)}S_{j+}^{(\nu)}Y_{ij}^{\mu\nu}(t)\right], \tag{1.29}$$

where the operators $X_{ij}^{\mu\nu}(t)$ and $Y_{ij}^{\mu\nu}(t)$ are defined as

$$\begin{aligned} X_{ij}^{\mu\nu}(t) &= \int_0^t d\tau \sum_{\boldsymbol{k}s}\left[\boldsymbol{u}_{\boldsymbol{k}s}(\boldsymbol{r}_\mu)\cdot\boldsymbol{d}_i\right]\left[\boldsymbol{u}_{\boldsymbol{k}s}^*(\boldsymbol{r}_\nu)\cdot\boldsymbol{d}_j^*\right]e^{i(\omega_j-\omega_k)\tau}\tilde{\varrho}_{\rm A}(t-\tau)\,,\\ Y_{ij}^{\mu\nu}(t) &= \int_0^t d\tau \sum_{\boldsymbol{k}s}\left[\boldsymbol{u}_{\boldsymbol{k}s}(\boldsymbol{r}_\mu)\cdot\boldsymbol{d}_i^*\right]\left[\boldsymbol{u}_{\boldsymbol{k}s}^*(\boldsymbol{r}_\nu)\cdot\boldsymbol{d}_j\right]e^{-i(\omega_j+\omega_k)\tau}\tilde{\varrho}_{\rm A}(t-\tau)\,. \end{aligned} \tag{1.30}$$

We emphasize that the RWA performed in Eq. (1.28) is not equivalent to a RWA on the level of the interaction Hamiltonian V [10]. In particular, we would miss important terms that contribute to the energy shifts of collective states in multi-atom systems if we had performed the RWA already in Eq. (1.5).

If we proceed with the remaining terms in Eq. (1.22) in a similar fashion, the master equation can be written as

$$\begin{aligned} \partial_t\varrho_{\rm A}(t) = &-\frac{i}{\hbar}\left[H_{\rm A},\varrho_{\rm A}(t)\right]\\ &+\sum_{\mu,\nu=1}^{M}\sum_{i,j=1}^{D}\left\{\left[S_{j-}^{(\nu)}X_{ij}^{\mu\nu},S_{i+}^{(\mu)}\right]+\left[S_{j-}^{(\nu)},\left(X_{ji}^{\nu\mu}\right)^\dagger S_{i+}^{(\mu)}\right]\right.\\ &\qquad\left.+\left[S_{j+}^{(\nu)}Y_{ij}^{\mu\nu},S_{i-}^{(\mu)}\right]+\left[S_{j+}^{(\nu)},\left(Y_{ji}^{\nu\mu}\right)^\dagger S_{i-}^{(\mu)}\right]\right\}. \end{aligned} \tag{1.31}$$

We continue with the evaluation of the operators $X_{ij}^{\mu\nu}$ and $Y_{ij}^{\mu\nu}$ in Eq. (1.30). First, we introduce a cutoff in the summation on the wave vectors $\boldsymbol{k}$ since the interaction Hamiltonian V in Eq. (1.5) does not correctly describe the interaction of the atom with high-frequency field modes which lead to relativistic effects [19]. Here we only consider wave vectors which obey $|\boldsymbol{k}|\leq k_{\rm C}$, where $ck_{\rm C}=\omega_{\rm C}$ is the cutoff frequency. This frequency is much larger than all relevant transition frequencies ω_i of the atoms, but smaller than $m_ec^2/\hbar$, where m_e is the electron mass. It follows that quasi-resonant absorption and emission processes are still correctly described,

but virtual emissions and reabsorbtions of "relativistic" high-frequency photons are not taken into account [19]. Next we replace the summation over the discrete wave vectors $\boldsymbol{k}$ in Eq. (1.30) by an integral over the continuum modes,

$$\sum_{\boldsymbol{k}s} \quad \rightarrow \quad \frac{v}{(2\pi c)^3} \int_0^{\omega_{\mathrm{C}}} d\omega_k \omega_k^2 \int d\Omega_k \sum_s . \tag{1.32}$$

Here we expressed the integral over the three-dimensional k-space in terms of spherical coordinates and changed the integration over k into an integral over frequencies $\omega_k = ck$. The operators $X_{ij}^{\mu\nu}$ and $Y_{ij}^{\mu\nu}$ in Eq. (1.30) then become

$$X_{ij}^{\mu\nu}(t) = \int_0^t d\tau \mathcal{X}_{ij}^{\mu\nu}(\tau) \tilde{\varrho}_{\mathrm{A}}(t-\tau) \quad \text{and} \quad Y_{ij}^{\mu\nu}(t) = \int_0^t d\tau \mathcal{Y}_{ij}^{\mu\nu}(\tau) \tilde{\varrho}_{\mathrm{A}}(t-\tau) , \tag{1.33}$$

where

$$\begin{aligned}
\mathcal{X}_{ij}^{\mu\nu}(\tau) =& \frac{1}{2\varepsilon_0 \hbar (2\pi c)^3} \int_0^{\omega_{\mathrm{C}}} d\omega_k \omega_k^3 \int d\Omega_k \sum_s e^{i\boldsymbol{k}\cdot\boldsymbol{R}_{\mu\nu}} \left[\boldsymbol{\epsilon}_{\boldsymbol{k}s} \cdot \boldsymbol{d}_i\right] \left[\boldsymbol{\epsilon}_{\boldsymbol{k}s}^* \cdot \boldsymbol{d}_j^*\right] e^{i(\omega_j - \omega_k)\tau} , \\
\mathcal{Y}_{ij}^{\mu\nu}(\tau) =& \frac{1}{2\varepsilon_0 \hbar (2\pi c)^3} \int_0^{\omega_{\mathrm{C}}} d\omega_k \omega_k^3 \int d\Omega_k \sum_s e^{i\boldsymbol{k}\cdot\boldsymbol{R}_{\mu\nu}} \left[\boldsymbol{\epsilon}_{\boldsymbol{k}s} \cdot \boldsymbol{d}_i^*\right] \left[\boldsymbol{\epsilon}_{\boldsymbol{k}s}^* \cdot \boldsymbol{d}_j\right] e^{-i(\omega_j + \omega_k)\tau} .
\end{aligned} \tag{1.34}$$

In this equation, the vector $\boldsymbol{R}_{\mu\nu} = \boldsymbol{r}_\mu - \boldsymbol{r}_\nu$ denotes the relative coordinates of atom μ with respect to atom ν. Note that the integrals in Eq. (1.34) would be divergent if we had not introduced the cutoff frequency ω_{C}.

Markov approximation. As a consequence of the exponential factor $\exp[-i\omega_k\tau]$ in Eq. (1.34), the functions $\mathcal{X}_{ij}^{\mu\nu}(\tau)$ and $\mathcal{Y}_{ij}^{\mu\nu}(\tau)$ tend very rapidly to zero when τ increases. We assume here that these two functions are approximately zero if $\tau \gg \tau_c$, where τ_c is the width of $\mathcal{X}_{ij}^{\mu\nu}(\tau)$ and $\mathcal{Y}_{ij}^{\mu\nu}(\tau)$ in τ. The parameter τ_c can be identified as the correlation time of the vacuum fluctuations of the free electromagnetic field [18, 19]. This correlation time is shorter than the period $2\pi/\omega_i$ of all relevant transitions. In particular, τ_c is much smaller than the lifetimes $T_{\mathrm{A}} = 1/\gamma$ of the atomic levels which determine the time scale of the evolution of $\varrho_{\mathrm{A}}(t)$. The existence of the two very different time scales $\tau_c \ll T_{\mathrm{A}}$ allows us to simplify the integrals in Eq. (1.33) considerably. First, we can assume that the interaction with the radiation field does not change the atomic state $\varrho_{\mathrm{A}}(t)$ appreciable during the correlation time τ_c. Therefore, we can replace $\tilde{\varrho}_{\mathrm{A}}(t-\tau)$ by $\varrho_{\mathrm{A}}(t)$ in Eq. (1.33),

$$\tilde{\varrho}_{\mathrm{A}}(t-\tau) = \exp\left[-iH_{\mathrm{A}}\tau/\hbar\right] \varrho_{\mathrm{A}}(t-\tau) \exp\left[iH_{\mathrm{A}}\tau/\hbar\right] \approx \varrho_{\mathrm{A}}(t) , \tag{1.35}$$

which means that the time evolution of $\varrho_{\mathrm{A}}(t)$ is governed by the unperturbed Hamiltonian H_{A} for short times. In addition, it is justified to extend the upper bound in

the integration over τ in Eq. (1.33) to infinity,

$$X_{ij}^{\mu\nu}(t) = \int_0^\infty d\tau \mathcal{X}_{ij}^{\mu\nu}(\tau)\varrho_{\rm A}(t) \quad \text{and} \quad Y_{ij}^{\mu\nu}(t) = \int_0^\infty d\tau \mathcal{Y}_{ij}^{\mu\nu}(\tau)\varrho_{\rm A}(t)\,. \tag{1.36}$$

The two approximations which led from Eq. (1.33) to Eq. (1.36) are known as the Markov approximation [4, 10, 18]. We now employ the relation $\int_0^\infty e^{ix\tau}d\tau = \pi\delta(x) + i\,\mathcal{P}_{\rm c}1/x$ (here $\mathcal{P}_{\rm c}$ denotes the Cauchy principal part) and evaluate the integrals over τ in Eq. (1.36). This yields

$$X_{ij}^{\mu\nu}(t) = \left(\Gamma_{ij}^{\mu\nu} + iM_{ij}^{\mu\nu}\right)\varrho_{\rm A}(t) \quad \text{and} \quad Y_{ij}^{\mu\nu}(t) = -i\left(P_{ij}^{\mu\nu}\right)^*\varrho_{\rm A}(t)\,, \tag{1.37}$$

where

$$\Gamma_{ij}^{\mu\nu} = \frac{\pi}{2\varepsilon_0\hbar(2\pi c)^3}\int_0^{\omega_{\rm C}} d\omega_k\omega_k^3\left[\boldsymbol{d}_i^{\rm T}\overleftrightarrow{F}(\omega_k/c, \boldsymbol{R}_{\mu\nu})\,\boldsymbol{d}_j^*\right]\delta(\omega_k-\omega_0)\,, \tag{1.38}$$

$$P_{ij}^{\mu\nu} = \frac{1}{2\varepsilon_0\hbar(2\pi c)^3}\mathcal{P}_{\rm c}\int_0^{\omega_{\rm C}} d\omega_k\omega_k^3\left[\boldsymbol{d}_i^{\rm T}\overleftrightarrow{F}(\omega_k/c, \boldsymbol{R}_{\mu\nu})\,\boldsymbol{d}_j^*\right]\frac{1}{\omega_0+\omega_k}\,, \tag{1.39}$$

$$M_{ij}^{\mu\nu} = \frac{1}{2\varepsilon_0\hbar(2\pi c)^3}\mathcal{P}_{\rm c}\int_0^{\omega_{\rm C}} d\omega_k\omega_k^3\left[\boldsymbol{d}_i^{\rm T}\overleftrightarrow{F}(\omega_k/c, \boldsymbol{R}_{\mu\nu})\,\boldsymbol{d}_j^*\right]\frac{1}{\omega_0-\omega_k}\,. \tag{1.40}$$

In these definitions, we approximated the frequencies ω_i and ω_j by the mean frequency $\omega_0 = 1/D\sum_{i=1}^D\omega_i$. This is justified since we assumed that the differences $(\omega_i-\omega_j)$ are much smaller than the mean transition frequency ω_0. The components of the tensor $\overleftrightarrow{F}$ which enters Eqs. (1.38)-(1.40) are given by ($p,q\in\{1,2,3\}$)

$$\overleftrightarrow{F}_{pq}(k,\boldsymbol{R}) = \int d\Omega_k\sum_s e^{i\boldsymbol{k}\cdot\boldsymbol{R}}\left[\boldsymbol{\epsilon}_{\boldsymbol{k}s}\right]_p\left[\boldsymbol{\epsilon}_{\boldsymbol{k}s}^*\right]_q\,, \tag{1.41}$$

and the explicit form of these tensor components is presented in Appendix 1.A. Since the range of integration extends over the complete solid angle, the tensor in Eq. (1.41) depends only on the absolute value of $\boldsymbol{k}$. In addition, the components of this tensor are real, which has already been employed in the derivation of Eq. (1.37). We find that the parameters in Eqs. (1.38)-(1.40) obey the following symmetry relations,

$$\Gamma_{ij}^{\mu\nu} = \left(\Gamma_{ji}^{\nu\mu}\right)^*, \quad P_{ij}^{\mu\nu} = \left(P_{ji}^{\nu\mu}\right)^*, \quad M_{ij}^{\mu\nu} = \left(M_{ji}^{\nu\mu}\right)^*. \tag{1.42}$$

These relations together with Eq. (1.37) allow us to cast the master equation (1.31) into the following form,

$$\begin{aligned}\partial_t \varrho_{\mathrm{A}}(t) = &-\frac{i}{\hbar}\left[H_{\mathrm{A}}, \varrho_{\mathrm{A}}(t)\right] + i \sum_{\substack{\mu,\nu=1 \\ \mu\neq\nu}}^{M} \sum_{i=1}^{D} \sum_{j=1}^{D} \Omega_{ij}^{\mu\nu} \left[S_{i+}^{(\mu)} S_{j-}^{(\nu)}, \varrho_{\mathrm{A}}(t)\right] \\ &- \sum_{\mu,\nu=1}^{M} \sum_{i=1}^{D} \sum_{j=1}^{D} \Gamma_{ij}^{\mu\nu} \left(S_{i+}^{(\mu)} S_{j-}^{(\nu)} \varrho_{\mathrm{A}}(t) + \varrho_{\mathrm{A}}(t) S_{i+}^{(\mu)} S_{j-}^{(\nu)} - 2 S_{j-}^{(\nu)} \varrho_{\mathrm{A}}(t) S_{i+}^{(\mu)}\right) \\ &- i \sum_{\mu=1}^{M} \sum_{i=1}^{D} \sum_{j=1}^{D} \left\{ M_{ij}^{\mu\mu} \left[S_{i+}^{(\mu)} S_{j-}^{(\mu)}, \varrho_{\mathrm{A}}(t)\right] - \left(P_{ij}^{\mu\mu}\right)^{*} \left[S_{i-}^{(\mu)} S_{j+}^{(\mu)}, \varrho_{\mathrm{A}}(t)\right] \right\} . \end{aligned} \tag{1.43}$$

The parameters $\Omega_{ij}^{\mu\nu} = P_{ij}^{\mu\nu} - M_{ij}^{\mu\nu}$ which occur in the second term of the first line in Eq. (1.43) will be discussed below. Here we first concentrate on the two terms in the last line of Eq. (1.43) which depend on $M_{ij}^{\mu\mu} = M_{ij}$ and $P_{ij}^{\mu\mu} = P_{ij}$. Note that we omitted the index μ since the parameters in Eqs. (1.39) and (1.40) depend only on the indices i and j if $\mu = \nu$. In order to give an interpretation for the parameters M_{ij} and P_{ij} for $i = j$, let $S_{i+}^{(\mu)} = |k_\mu\rangle\langle l_\mu|$ be the transition operator from state $|l_\mu\rangle$ of atom μ to state $|k_\mu\rangle$ of the same atom. Since $S_{i+}^{(\mu)} S_{i-}^{(\mu)} = |k_\mu\rangle\langle k_\mu| = A_{kk}^{(\mu)}$ and $S_{i-}^{(\mu)} S_{i+}^{(\mu)} = A_{ll}^{(\mu)}$, the parameters M_{ii} and P_{ii} represent a frequency shift of the atomic levels which is related to the Lamb shift.

However, we emphasize that the correct values for the Lamb shift of the atomic levels cannot be obtained within the framework of the present theory. A rigorous treatment of this effect requires a fully relativistic theory and renormalization procedures. Here we assume that the correct values for the atomic level shifts have been incorporated into the energies of the atomic states.

We proceed with a short discussion of the parameters M_{ij} and P_{ij} for $i \neq j$. In this case, the terms proportional to M_{ij} and P_{ij} represent a coherent coupling between two atomic levels of the same atom. However, these terms only contribute if two conditions are simultaneously fulfilled. First, the dipole moments $\boldsymbol{d}_i$ and $\boldsymbol{d}_j$ must be non-orthogonal since M_{ij}, $P_{ij} \sim \boldsymbol{d}_i \cdot \boldsymbol{d}_j^{*}$. Second, at least one of the operators $S_{i+}^{(\mu)} S_{j-}^{(\mu)}$ or $S_{i-}^{(\mu)} S_{j+}^{(\mu)}$ must be different from zero (for $i \neq j$). However, these two conditions can usually not be fulfilled at the same time in atomic systems [11]. In particular, they are never fulfilled simultaneously for the atomic systems considered in this thesis, and hence we omit these terms.

In conclusion, we can remove all terms in the last line of Eq. (1.43) if the Lamb shifts are incorporated into the energies of the atomic levels. We thus arrive at the

master equation in its final form,

$$\partial_t \varrho_{\rm A}(t) = -\frac{i}{\hbar}\left[H_{\rm A}, \varrho_{\rm A}(t)\right] + i\sum_{\substack{\mu,\nu=1\\ \mu\neq\nu}}^{M}\sum_{i=1}^{D}\sum_{j=1}^{D}\Omega_{ij}^{\mu\nu}\left[S_{i+}^{(\mu)}S_{j-}^{(\nu)}, \varrho_{\rm A}(t)\right] \tag{1.44}$$

$$-\sum_{\mu=1}^{M}\sum_{i=1}^{D}\sum_{j=1}^{D}\gamma_{ij}\left(S_{i+}^{(\mu)}S_{j-}^{(\mu)}\varrho_{\rm A}(t) + \varrho_{\rm A}(t)S_{i+}^{(\mu)}S_{j-}^{(\mu)} - 2S_{j-}^{(\mu)}\varrho_{\rm A}(t)S_{i+}^{(\mu)}\right)$$

$$-\sum_{\substack{\mu,\nu=1\\ \mu\neq\nu}}^{M}\sum_{i=1}^{D}\sum_{j=1}^{D}\Gamma_{ij}^{\mu\nu}\left(S_{i+}^{(\mu)}S_{j-}^{(\nu)}\varrho_{\rm A}(t) + \varrho_{\rm A}(t)S_{i+}^{(\mu)}S_{j-}^{(\nu)} - 2S_{j-}^{(\nu)}\varrho_{\rm A}(t)S_{i+}^{(\mu)}\right).$$

In the second line of Eq. (1.44), we introduced the parameters

$$\gamma_{ij} = \Gamma_{ij}^{\mu\mu} = \sqrt{\gamma_i\gamma_j}\frac{\boldsymbol{d}_i\cdot\boldsymbol{d}_j^*}{|\boldsymbol{d}_i|\,|\boldsymbol{d}_j|}, \tag{1.45}$$

where

$$\gamma_i = \frac{\omega_0^3\,|\boldsymbol{d}_i|^2}{6\pi\varepsilon_0\hbar c^3}. \tag{1.46}$$

The derivation of the expressions for γ_{ij} and γ_i can be found in Appendix 1.A. For $i=j$, $\gamma_{ii}=\gamma_i$ is the half-decay rate of the i-th atomic dipole transition. The parameters γ_{ij} for $i\neq j$ describe the cross-damping between a pair of transitions i and j of the same atom. According to Eq. (1.45), the cross decay rates γ_{ij} depend on the mutual orientation of the associated dipole moments $\boldsymbol{d}_i$ and $\boldsymbol{d}_j$. These parameters describe the decay-induced coherence between atomic dipole transitions and will be discussed in detail in chapter 2. In particular, we show that these spontaneously created coherences give rise to quantum interference effects. Note that the cross decay rates γ_{ij} contribute to the master equation provided that the dipole moments $\boldsymbol{d}_i$ and $\boldsymbol{d}_j$ are non-orthogonal. Due to the term $S_{j-}^{(\mu)}\varrho_{\rm A}(t)S_{i+}^{(\mu)}$ in the second line of Eq. (1.44), it is not required that one of the operators $S_{i+}^{(\mu)}S_{j-}^{(\mu)}$ or $S_{i-}^{(\mu)}S_{j+}^{(\mu)}$ is different from zero at the same time. This is in contrast to the parameters M_{ij} and P_{ij} $(i\neq j)$ which were discussed below Eq. (1.43).

The parameters in the third line of the master equation (1.44) are given by

$$\Gamma_{ij}^{\mu\nu} = \frac{1}{\hbar}\left[\boldsymbol{d}_i^{\rm T}\,\overleftrightarrow{\chi}_{\rm im}(\boldsymbol{R}_{\mu\nu})\,\boldsymbol{d}_j^*\right], \tag{1.47}$$

and a derivation of this result is presented in Appendix 1.A. In this equation, $\overleftrightarrow{\chi}_{\rm im}$ denotes the imaginary part of the tensor $\overleftrightarrow{\chi}$ whose components for $p,q\in\{1,2,3\}$ are given by

$$\overleftrightarrow{\chi}_{pq}(\boldsymbol{R}) = \frac{1}{4\pi\varepsilon_0}\left[k_0^2\delta_{pq} + \frac{\partial^2}{\partial R_p\partial R_q}\right]\frac{1}{R}e^{ik_0R}$$

$$= \frac{k_0^3}{4\pi\varepsilon_0}\left[\delta_{pq}\left(\frac{1}{\eta}+\frac{i}{\eta^2}-\frac{1}{\eta^3}\right) - \frac{[\boldsymbol{R}]_p[\boldsymbol{R}]_q}{R^2}\left(\frac{1}{\eta}+\frac{3i}{\eta^2}-\frac{3}{\eta^3}\right)\right]e^{i\eta}, \tag{1.48}$$

and $\eta = k_0 R$. In the first line of Eq. (1.48), the derivatives are taken with respect to the Cartesian components $R_p = [\boldsymbol{R}]_p$ of the vector $\boldsymbol{R}$. Note that in the last line of Eq. (1.44), terms with $\mu = \nu$ are excluded in the summation over the atomic indices μ and ν. The parameters $\Gamma_{ij}^{\mu\nu}$ are thus only present in collective systems and can be interpreted as collective decay rates. They arise from the interaction between two dipole transitions which belong to different atoms and describe the modification of spontaneous emission of one atom due to the presence of the other atoms. A more detailed discussion of these terms is provided in chapters 3-5 of part III.

Next we discuss the parameters

$$\begin{aligned} \Omega_{ij}^{\mu\nu} &= P_{ij}^{\mu\nu} - M_{ij}^{\mu\nu} \\ &= \frac{1}{\hbar}\left[\boldsymbol{d}_i^{\mathrm{T}} \overleftrightarrow{\chi}_{\mathrm{re}}(\boldsymbol{R}_{\mu\nu})\, \boldsymbol{d}_j^*\right] \end{aligned} \tag{1.49}$$

which occur in the second term of the first line in Eq. (1.44). Here $\overleftrightarrow{\chi}_{\mathrm{re}}$ denotes the real part of the tensor $\overleftrightarrow{\chi}$ in Eq. (1.48), and the derivation of Eq. (1.49) can be found in Appendix 1.A. As for the parameters $\Gamma_{ij}^{\mu\nu}$, the terms proportional to $\Omega_{ij}^{\mu\nu}$ only contribute to the master equation (1.44) in collective systems and arise from the interaction between a pair of dipoles which belong to different atoms. In contrast to the collective decay rates $\Gamma_{ij}^{\mu\nu}$, the parameters $\Omega_{ij}^{\mu\nu}$ give rise to a *coherent* coupling between two dipole transitions of different atoms. This is a remarkable result, since this coherent interaction arises solely from the vacuum-mediated coupling between different atoms. The influence of the coherent part of the dipole-dipole interaction on the quantum dynamics of collective systems is investigated in depth in chapters 3-5 of part III.

The parameters $\Gamma_{ij}^{\mu\nu}$ and $\Omega_{ij}^{\mu\nu}$ obey an important symmetry property which allows to reduce the number of independent parameters in the master equation (1.44). According to their definitions in Eqs. (1.47) and (1.49), $\Gamma_{ij}^{\mu\nu}$ and $\Omega_{ij}^{\mu\nu}$ depend on the atomic indices μ, ν via the atomic separation vector $\boldsymbol{R}_{\mu\nu} = \boldsymbol{r}_\mu - \boldsymbol{r}_\nu$. Since the tensor $\overleftrightarrow{\chi}(\boldsymbol{R})$ in Eq. (1.48) does not depend on the sign of the vector $\boldsymbol{R}$,

$$\overleftrightarrow{\chi}(-\boldsymbol{R}) = \overleftrightarrow{\chi}(\boldsymbol{R})\,, \quad \text{we have} \quad \Gamma_{ij}^{\mu\nu} = \Gamma_{ij}^{\nu\mu} \quad \text{and} \quad \Omega_{ij}^{\mu\nu} = \Omega_{ij}^{\nu\mu}\,. \tag{1.50}$$

Together with Eq. (1.42) we can establish the following relations,

$$\begin{aligned} \Gamma_{ij}^{\mu\nu} = \Gamma_{ij}^{\nu\mu} &= \left(\Gamma_{ji}^{\mu\nu}\right)^* = \left(\Gamma_{ji}^{\nu\mu}\right)^*\,, \\ \Omega_{ij}^{\mu\nu} = \Omega_{ij}^{\nu\mu} &= \left(\Omega_{ji}^{\mu\nu}\right)^* = \left(\Omega_{ji}^{\nu\mu}\right)^*\,. \end{aligned} \tag{1.51}$$

In particular, this shows that the parameters $\Gamma_{ii}^{\mu\nu}$ and $\Omega_{ii}^{\mu\nu}$ are real. In part III of this thesis, we focus on systems that consist of two atoms. Since their relative position is described by a single separation vector $\boldsymbol{R}$, we can omit the superscripts μ and ν and denote the parameters $\Gamma_{ij}^{\mu\nu}$ and $\Omega_{ij}^{\mu\nu}$ by $\Gamma_{ij}(\boldsymbol{R})$ and $\Omega_{ij}(\boldsymbol{R})$, respectively.

So far, we only considered the interaction of M atoms via the vacuum field. In the presence of external laser fields, an additional term

$$-\frac{i}{\hbar}\left[H_{\rm L}(t),\varrho(t)\right] \tag{1.52}$$

has to be added to the right hand side of Eq. (1.44). Here the time-dependent Hamiltonian $H_{\rm L}(t)$ describes the interaction between the atoms and the laser fields (see chapters 2-6). In the following, we assume that the Rabi frequencies and detunings that are associated with the laser fields are much smaller than the mean transition frequency ω_0. In this case, it is justified to assume that the other terms in Eq. (1.44) which arise due to the atom-vacuum coupling are not affected by the presence of the laser fields [18].

1.A Calculation of the parameters $\Gamma_{ij}^{\mu\nu}$ and $\Omega_{ij}^{\mu\nu}$

Here we outline the calculation of the generalized decay rates and collective energy shifts which enter the master equation (1.44) derived in Chapter 1. We begin with the general expression for the decay rates in Eq. (1.38) and obtain

$$\begin{aligned}\Gamma_{ij}^{\mu\nu} =& \frac{\pi}{2\varepsilon_0\hbar(2\pi c)^3}\int_0^{\omega_\mathrm{C}} d\omega_k \omega_k^3 \left[\boldsymbol{d}_i^{\mathrm{T}} \overleftrightarrow{F}(\omega_k/c, \boldsymbol{R}_{\mu\nu})\, \boldsymbol{d}_j^*\right] \delta(\omega_k-\omega_0)\\ =& \frac{k_0^3}{16\varepsilon_0\hbar\pi^2}\left[(\boldsymbol{d}_i)^{\mathrm{T}} \overleftrightarrow{F}(k_0, \boldsymbol{R}_{\mu\nu})\, \boldsymbol{d}_j^*\right]. \end{aligned} \tag{1.53}$$

Note that $k_0 = \omega_0/c$ is the mean wavenumber of all dipole transitions, see Eq. (1.2). In order to derive explicit expressions for the parameters $\Gamma_{ij}^{\mu\nu}$, we determine the tensor $\overleftrightarrow{F}(k, \boldsymbol{R})$ which has been defined in Eq. (1.41). Since the polarization vectors of the radiation field satisfy the relation [19]

$$\sum_s [\boldsymbol{\epsilon}_{\boldsymbol{k}s}]_p\, [\boldsymbol{\epsilon}_{\boldsymbol{k}s}^*]_q = \delta_{pq} - \frac{k_p k_q}{k^2}, \tag{1.54}$$

we arrive at

$$\overleftrightarrow{F}_{pq}(k, \boldsymbol{R}) = \int_0^{2\pi} d\phi_k \int_0^{\pi} d\theta_k \sin\theta_k e^{i\boldsymbol{k}\cdot\boldsymbol{R}} \left(\delta_{pq} - \frac{k_p k_q}{k^2}\right), \tag{1.55}$$

where $\boldsymbol{k} = k(\sin\theta_k\cos\phi_k, \sin\theta_k\sin\phi_k, \cos\theta_k)$. For $\boldsymbol{R} = 0$, the evaluation of the integral yields

$$\overleftrightarrow{F}_{pq}(k, \boldsymbol{R}=\boldsymbol{0}) = \frac{8}{3}\pi\delta_{pq}. \tag{1.56}$$

Since we have $\boldsymbol{R}_{\mu\nu} = 0$ for $\mu = \nu$, we obtain from Eq. (1.53)

$$\Gamma_{ij}^{\mu\mu} = \frac{\omega_0^3}{6\varepsilon_0\hbar\pi c^3}\, \boldsymbol{d}_i \cdot \boldsymbol{d}_j^*. \tag{1.57}$$

Together with the definition of the half-decay rates γ_i in Eq. (1.46), we can establish the result presented in Eq. (1.45).

The general expression of the tensor $\overleftrightarrow{F}$ for $\boldsymbol{R} \neq 0$ is found to be

$$\begin{aligned}\overleftrightarrow{F}_{pq}(k, \boldsymbol{R}) =& 4\pi\left\{\delta_{pq}\left[\left(\frac{1}{\zeta} - \frac{1}{\zeta^3}\right)\sin\zeta + \frac{1}{\zeta^2}\cos\zeta\right]\right.\\ &\left. - \frac{[\boldsymbol{R}]_p\,[\boldsymbol{R}]_q}{R^2}\left[\left(\frac{1}{\zeta} - \frac{3}{\zeta^3}\right)\sin\zeta + \frac{3}{\zeta^2}\cos\zeta\right]\right\},\\ =& 4\pi\mathrm{Im}\left\{\left[\delta_{pq}\left(\frac{1}{\zeta} + \frac{i}{\zeta^2} - \frac{1}{\zeta^3}\right) - \frac{[\boldsymbol{R}]_p[\boldsymbol{R}]_q}{R^2}\left(\frac{1}{\zeta} + \frac{3i}{\zeta^2} - \frac{3}{\zeta^3}\right)\right] e^{i\zeta}\right\}, \end{aligned} \tag{1.58}$$

where $\zeta = kR$. Note that the general expression (1.58) reduces to the special result in Eq. (1.57) in the limit $R \to 0$. If Eq. (1.58) is plugged in Eq. (1.53), we obtain ($\eta = k_0 R$)

$$\Gamma_{ij}^{\mu\nu} = \frac{3}{2}\frac{\sqrt{\gamma_i\gamma_j}}{|\boldsymbol{d}_i|\,|\boldsymbol{d}_j|}\left\{\boldsymbol{d}_i\cdot\boldsymbol{d}_j^*\left[\left(\frac{1}{\eta}-\frac{1}{\eta^3}\right)\sin\eta+\frac{1}{\eta^2}\cos\eta\right]\right. \tag{1.59}$$
$$\left. -\frac{[\boldsymbol{d}_i\cdot\boldsymbol{R}_{\mu\nu}]\,[\boldsymbol{d}_j^*\cdot\boldsymbol{R}_{\mu\nu}]}{R_{\mu\nu}^2}\left[\left(\frac{1}{\eta}-\frac{3}{\eta^3}\right)\sin\eta+\frac{3}{\eta^2}\cos\eta\right]\right\}.$$

This rather complicated expression can be cast into a compact form via the tensor $\overleftrightarrow{\chi}_{\rm im}$, which denotes the imaginary part of the tensor $\overleftrightarrow{\chi}$ that has been introduced in Eq. (1.48). With Eq. (1.53) and the relation

$$\overleftrightarrow{\chi}_{\rm im}(\boldsymbol{R}) = \frac{k_0^3}{16\pi^2\varepsilon_0}\overleftrightarrow{F}(k_0,\boldsymbol{R})\,, \tag{1.60}$$

we arrive at Eq. (1.47).

We now turn to the evaluation of the parameters $\Omega_{ij}^{\mu\nu} = P_{ij}^{\mu\nu} - M_{ij}^{\mu\nu}$,

$$\Omega_{ij}^{\mu\nu} = \frac{1}{\varepsilon_0\hbar(2\pi c)^3}\mathcal{P}_{\rm c}\int_0^\infty d\omega_k\left[\boldsymbol{d}_i^{\rm T}\overleftrightarrow{F}\left(\omega_k/c,\boldsymbol{R}_{\mu\nu}\right)\boldsymbol{d}_j^*\right]\frac{\omega_k^4}{\omega_k^2-\omega_0^2}\,. \tag{1.61}$$

With the identity

$$\frac{\omega_k^2}{\omega_k^2-\omega_0^2} = 1 + \frac{\omega_0^2}{\omega_k^2-\omega_0^2}\,, \tag{1.62}$$

we split the integral in two parts,

$$\Omega_{ij}^{\mu\nu} = \frac{1}{\varepsilon_0\hbar(2\pi c)^3}\left\{\int_0^{\omega_{\rm C}} d\omega_k\omega_k^2\left[\boldsymbol{d}_i^{\rm T}\overleftrightarrow{F}\left(\omega_k/c,\boldsymbol{R}_{\mu\nu}\right)\boldsymbol{d}_j^*\right]\right.$$
$$\left. +\,\omega_0^2\,\mathcal{P}_{\rm c}\int_0^{\omega_{\rm C}} d\omega_k\left[\boldsymbol{d}_i^{\rm T}\overleftrightarrow{F}\left(\omega_k/c,\boldsymbol{R}_{\mu\nu}\right)\boldsymbol{d}_j^*\right]\frac{\omega_k^2}{\omega_k^2-\omega_0^2}\right\}. \tag{1.63}$$

We begin with the evaluation of the first integral in Eq. (1.63). Note that we dropped the symbol $\mathcal{P}_{\rm c}$ in front of this integral since there are no poles in this expression. If we change the integration from ω_k to k and employ Eq. (1.55), we find

$$(\square) = \frac{1}{\varepsilon_0\hbar(2\pi)^3}\int_0^{k_{\rm C}} dk k^2\left[\boldsymbol{d}_i^{\rm T}\overleftrightarrow{F}\left(k,\boldsymbol{R}_{\mu\nu}\right)\boldsymbol{d}_j^*\right]$$
$$= \frac{1}{\varepsilon_0\hbar}\sum_{p,q=1}^{3}\left[\boldsymbol{d}_i\right]_p\left[\boldsymbol{d}_j^*\right]_q\frac{1}{(2\pi)^3}\int d^3k e^{i\boldsymbol{k}\cdot\boldsymbol{R}_{\mu\nu}}\left(\delta_{pq}-\frac{k_p k_q}{k^2}\right)\Theta(k_{\rm c}-k)\,. \tag{1.64}$$

In the last line of Eq. (1.64), we introduced the unit step function $\Theta(k_\mathrm{c}-k)$ which is equal to one for $k \leq k_\mathrm{c}$ and zero if $k > k_\mathrm{c}$. The presence of this function allows to extend the range of integration over the complete k space. Here we replace the unit step function $\Theta(k_\mathrm{c}-k)$ by the smooth step function $k_\mathrm{c}^2/(k^2+k_\mathrm{c}^2)$ which is approximately equal to unity for $k \ll k_\mathrm{c}$ and approximately zero for $k \gg k_\mathrm{c}$. With this replacement, the integral in the second line of Eq. (1.64) can be expressed in terms of the regularized transverse δ function (see, e.g., Complement $\mathrm{A_I}$ in [19]),

$$\begin{aligned}\delta_{pq}^{\perp}(\boldsymbol{R}) &= \frac{1}{(2\pi)^3}\int d^3k e^{i\boldsymbol{k}\cdot\boldsymbol{R}}\left(\delta_{pq}-\frac{k_p k_q}{k^2}\right)\frac{k_\mathrm{c}^2}{k^2+k_\mathrm{c}^2}\\ &= g_{pq}(\boldsymbol{R})+\frac{1}{4\pi R^3}\left(\frac{3\,[\boldsymbol{R}]_p\,[\boldsymbol{R}]_q}{R^2}-\delta_{pq}\right)f(\boldsymbol{R})\,, \end{aligned} \tag{1.65}$$

where

$$\begin{aligned} g_{pq}(\boldsymbol{R}) &= \frac{k_\mathrm{c}^2}{8\pi R}\left(\frac{[\boldsymbol{R}]_p\,[\boldsymbol{R}]_q}{R^2}+\delta_{pq}\right)e^{-k_\mathrm{c}R}\,,\\ f(\boldsymbol{R}) &= 1-\left(1+k_\mathrm{c}R+\frac{1}{2}k_\mathrm{c}^2R^2\right)e^{-k_\mathrm{c}R}\,. \end{aligned} \tag{1.66}$$

Since the cutoff frequency ω_c is on the order of $m_e c^2/\hbar$, the inverse wave number $1/k_\mathrm{c}$ is of the order of the spatial extend of a single atom. From the definitions in Eq. (1.66), it follows that we can set $g_{pq}(\boldsymbol{R}) \approx 0$ and $f(\boldsymbol{R}) \approx 1$ for $R \gg 1/k_\mathrm{c}$. Since we assume that the interatomic distance between any two atoms is much larger than $1/k_\mathrm{c}$, we obtain

$$(\square) = \frac{1}{\hbar}\left[\boldsymbol{d}_i^{\mathrm{T}}\overleftrightarrow{V}(\boldsymbol{R}_{\mu\nu})\boldsymbol{d}_j^{*}\right]\,, \tag{1.67}$$

where

$$\overleftrightarrow{V}_{pq}(\boldsymbol{R}) = \frac{1}{4\pi\varepsilon_0}\frac{1}{R^3}\left(3\frac{[\boldsymbol{R}]_p\,[\boldsymbol{R}]_q}{R^2}-\delta_{pq}\right)\,. \tag{1.68}$$

It follows that the contribution $(\square)$ in Eq. (1.64) represents the interaction potential of two static dipoles.

We now turn to the second term in Eq. (1.63),

$$(\lozenge) = \frac{1}{4\pi\varepsilon_0\hbar}\frac{\omega_0^2}{2\pi^2c^3}\mathcal{P}_\mathrm{c}\int_0^{\omega_\mathrm{c}} d\omega_k\left[\boldsymbol{d}_i^{\mathrm{T}}\overleftrightarrow{F}\left(\omega_k/c,\boldsymbol{R}_{\mu\nu}\right)\boldsymbol{d}_j^{*}\right]\frac{\omega_k^2}{\omega_k^2-\omega_0^2}\,. \tag{1.69}$$

Note that the integrand exhibits a pole at $\omega_k=\omega_0$. Since the cutoff frequency ω_c is much larger than the mean transition frequency ω_0, we can extend the upper limit of integration to infinity. The relevant principal value integrals can be evaluated via

the residue theorem and are given by ($\tau > 0$)

$$\mathcal{P}_{\rm c}\int_0^\infty d\omega_k \frac{\omega_k}{\omega_k^2-\omega_0^2}\sin(\omega_k\tau) = \frac{1}{2}\pi\cos(\omega_0\tau)\,,$$

$$\mathcal{P}_{\rm c}\int_0^\infty d\omega_k \frac{1}{\omega_k\left(\omega_k^2-\omega_0^2\right)}\sin(\omega_k\tau) = -\frac{\pi}{2\omega_0^2}\left[1-\cos(\omega_0\tau)\right]\,,$$

$$\mathcal{P}_{\rm c}\int_0^\infty d\omega_k \frac{1}{\omega_k^2-\omega_0^2}\cos(\omega_k\tau) = -\frac{\pi}{2\omega_0}\sin(\omega_0\tau)\,. \tag{1.70}$$

If these relations are substituted in Eq. (1.69), we arrive at

$$(\lozenge) = \frac{1}{\hbar}\left\{\boldsymbol{d}_i^{\rm T}\left[\overleftrightarrow{\chi}_{\rm re}(\boldsymbol{R}_{\mu\nu}) - \overleftrightarrow{V}(\boldsymbol{R}_{\mu\nu})\right]\boldsymbol{d}_j^*\right\}\,, \tag{1.71}$$

where $\overleftrightarrow{\chi}_{\rm re}$ is the real part of the tensor $\overleftrightarrow{\chi}$ in Eq. (1.48). Finally, the combination of Eqs. (1.67) and (1.71) yields

$$\Omega_{ij}^{\mu\nu} = \frac{1}{\hbar}\left[\boldsymbol{d}_i^{\rm T}\,\overleftrightarrow{\chi}_{\rm re}(\boldsymbol{R}_{\mu\nu})\,\boldsymbol{d}_j^*\right]\,. \tag{1.72}$$

This is the result presented in Eq. (1.49), and can be written as ($\eta = k_0 R$)

$$\begin{aligned}\Omega_{ij}^{\mu\nu} =& \frac{3}{2}\frac{\sqrt{\gamma_i\gamma_j}}{|\boldsymbol{d}_i|\,|\boldsymbol{d}_j|}\left\{\boldsymbol{d}_i\cdot\boldsymbol{d}_j^*\left[\left(\frac{1}{\eta}-\frac{1}{\eta^3}\right)\cos\eta - \frac{1}{\eta^2}\sin\eta\right]\right. \\ &\left. -\frac{\left[\boldsymbol{d}_i\cdot\boldsymbol{R}_{\mu\nu}\right]\left[\boldsymbol{d}_j^*\cdot\boldsymbol{R}_{\mu\nu}\right]}{R_{\mu\nu}^2}\left[\left(\frac{1}{\eta}-\frac{3}{\eta^3}\right)\cos\eta - \frac{3}{\eta^2}\sin\eta\right]\right\}\,.\end{aligned} \tag{1.73}$$

Part II

Quantum interference enforced by time-energy complementarity

Chapter 2

Interference in the resonance fluorescence of two incoherently coupled transitions

2.1 Introduction

Since the emergence of quantum mechanics, quantum interference has been regarded as one of the most exciting and intriguing aspects of quantum theory [11]. In general, quantum interference occurs whenever an initial state of a quantum system is connected to a final state by several indistinguishable transition amplitudes. These transition amplitudes are frequently identified with the various pathways or "histories" connected with the time evolution of the quantum system. Although interference effects are present in almost all areas of quantum mechanics, some of them particularly attracted the attention of many scientists.

As a first example, we would like to mention vacuum-induced interference effects, where the interfering pathways are realized by atom-vacuum interactions. A standard representative for a physical system that displays vacuum-induced coherence and interference effects is the so-called V-system. This atomic level scheme is comprised of two near-degenerate excited levels and one ground state (see Fig. 2.1). Many authors demonstrated that a rich variety of interference effects should be observable in this system, and most of them are potentially interesting for applications. These effects include the modification and quenching of spontaneous emission [10, 21–23], and several schemes to control spontaneous emission by means of external fields have been suggested [24–27]. Furthermore, it has been shown that quantum interference leads to strong modifications of the spectrum of resonance fluorescence, and for suitable parameters the complete suppression of resonance fluorescence is achievable [28–31]. The emitted fluorescence light also displays highly nonclassical features like extremely strong intensity-intensity correlations and squeezing [32, 33].

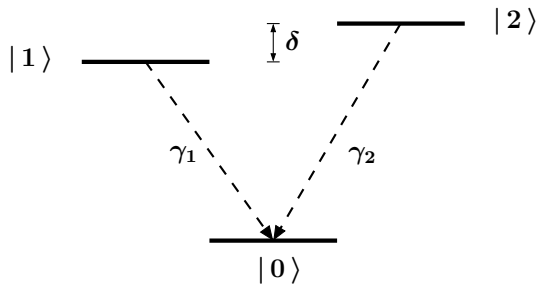

Figure 2.1: The level scheme in V-configuration is comprised of two excited states and one ground state. Each excited state can decay spontaneously to the ground state $|0\rangle$, and the decay rates are labeled by γ_1 and γ_2. The parameter δ denotes the frequency splitting of the excited states. For non-orthogonal dipole moments $\boldsymbol{d}_1 = \langle 1|\hat{\boldsymbol{d}}|0\rangle$ and $\boldsymbol{d}_2 = \langle 2|\hat{\boldsymbol{d}}|0\rangle$, this system displays a rich variety of vacuum-induced interference effects.

We emphasize that all these schemes rest on two stringed conditions. First, the excited states must be near-degenerate, i.e., the frequency splitting δ of the upper levels must not exceed the natural linewidth of the transitions which is determined by the spontaneous decay rates γ_1, γ_2. Second, the dipole moments $\boldsymbol{d}_1$ and $\boldsymbol{d}_2$ associated with the $|1\rangle \leftrightarrow |0\rangle$ and $|2\rangle \leftrightarrow |0\rangle$ transitions must be at least non-orthogonal. If these two requirements are fulfilled, the interference terms

$$\gamma_{ij} = \sqrt{\gamma_i \gamma_j}\, \frac{\boldsymbol{d}_i \cdot \boldsymbol{d}_j^*}{|\boldsymbol{d}_i|\ |\boldsymbol{d}_j|} \tag{2.1}$$

for $i \neq j$ will contribute to the master equation (1.44) and change the system dynamics. All the interference effects cited above can be traced back to the cross-decay rates proportional to $\sqrt{\gamma_i \gamma_j}$.

However, the requirements of near-degenerate levels and non-orthogonal dipole transitions are very hard to meet in an experiment, and appropriate atomic systems are not known up to now. In order to circumvent this problem, an experiment with a molecular system has been performed [34], but the experimental results could not be reproduced yet [35]. A recent experiment demonstrates the existence of spontaneously generated coherences between spin states in quantum dots [36].

One of the most famous interference effects is certainly Young's double-slit experiment [1, 4, 11]. A beautiful realization of this experiment was performed by Eichmann *et. al.* [37] and subsequently discussed by several authors [38–40]. In this experiment, the slits are represented by two $^{198}Hg^{+}$ ions in a trap that are irradiated by a coherent laser field, and the interference pattern formed by the scattered light was observed. Starting from the early days of quantum mechanics, the two-slit experiment has been employed to explore fundamental concepts of quantum mechanics such as the principle of complementarity. According to Niels Bohr [2], complementarity arises from the inseparability of detector and object. This leads to

mutually exclusive observables that cannot be measured precisely under the same experimental conditions. Here we adopt this point of view and say that two observables are complementary if the experimental conditions that allow for an exact measurement of one of them eliminate the possibility to determine the other observable precisely. In the case of wave-particle duality in a two-slit experiment, one can decide to observe either the interference pattern exposing wave-like features, or particle properties by measuring the path taken. The interference pattern is observed under conditions where it is principally impossible to know through which of the two slits each object has moved. On augmenting the experiment by any means which in principle allow to measure the path taken, the interference pattern vanishes. Celebrated thought experiments like Feynman's light microscope [41] and Einstein's recoiling slits [2] employ the position-momentum uncertainty relation to demonstrate that it is impossible to observe the wave and the particle nature of the interfering quantities (for example, electrons or photons) at the same time. In recent years, a proposal by Scully *et. al.* [42] rose the question whether the principle of complementarity is always enforced by the uncertainty relation. This touches the delicate question if the principle of complementarity is more fundamental than the uncertainty relation. In [42], a two-slit experiment with Rydberg atoms was proposed, and the authors claimed that the loss of interference due to which-way information cannot be explained in terms of the position-momentum uncertainty relation. This interpretation was challenged by Storey *et. al.* [43] who argued that the momentum transfer in the proposed experiment [42] is in agreement with the position-momentum uncertainty relation if which-way information is obtained. A lively debate on the interrelation between the principle of complementarity and the position-momentum uncertainty relation followed [44–49]. According to a recent which-way experiment with an atom interferometer [50], the principle of complementarity and the position-momentum relation are indeed not equivalent. Here the authors claim that the loss of interference due to which-way information can only be explained in terms of correlations between the which-way detector and the atomic motion, but not in terms of the momentum transfer associated with the path detection.

Up to now, the discussion of complementarity was focused on spatially separated pathways resulting in an interference pattern in position space. Here, we demonstrate that quantum optical experiments can reveal complementarity of time and energy. In this class of setups, different temporal paths lead to interference in the energy domain. An attempt to extend interference and complementarity to the time-energy domain raises several questions. First, it is not obvious what the equivalence is of (spatial) pathway interference in the time-energy domain. How can paths differing "in time" be realized, and what makes these paths indistinguishable in principle, as required for interference? Finally, what is the role of the time-energy uncertainty relation, which is special in that time is a parameter rather than an operator in quantum mechanics?

In the following, we discuss these questions on the basis of the resonance fluorescence of a single laser-driven atom with a $J = 1/2$ to $J = 1/2$ transition as found, e.g., in

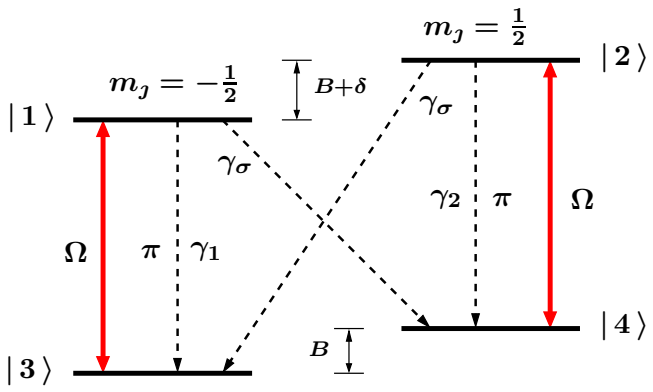

Figure 2.2: Schematic representation of the four-level atom of interest. The two upper and lower levels are Zeeman sublevels with $m_J = \pm\frac{1}{2}$. Each upper state can decay by dipole allowed transitions to both ground states. The coupling between the laser field and the π transitions is characterized by the Rabi frequency Ω. γ_1, γ_2 and γ_σ are spontaneous decay rates. The Zeeman splitting of the magnetic sublevels is not to scale.

$^{198}Hg^+$ ions [51–53]. A schematic representation of this four-level system is shown in Fig. 2.2. The transitions $|2\rangle \leftrightarrow |3\rangle$ and $|1\rangle \leftrightarrow |4\rangle$ couple to σ^+ and σ^- polarized light, respectively, and will be referred to as the σ transitions. By contrast, the π transitions $|1\rangle \leftrightarrow |3\rangle$ and $|2\rangle \leftrightarrow |4\rangle$ couple to light linearly polarized along $\boldsymbol{e}_z$, and the frequency difference δ between the two π transitions can be adjusted by means of an external magnetic field. The schematic setup of the discussed experiment is shown in Fig. 2.3. An atom is located at the point of origin and irradiated by a monochromatic laser beam that couples only to the π transitions, and the detector records either the spectrum of resonance fluorescence or the total intensity. With a suitable polarization filter in front of the detector, only the light emitted on the π transitions or the the light emitted on the σ transitions is measured.

Our main findings can be summarized as follows. We show that complementarity enforces a signature of interference in the spectrum of resonance fluorescence emitted on the π transitions, whereas the total fluorescence intensity exhibits no interference. The results can be described quantitatively via the time-energy uncertainty relation, but no conclusion about the hierarchy between the uncertainty relation and complementarity can be drawn from our results. Further, we demonstrate that the interference in the fluorescence spectrum results from vacuum-induced coherences. This result can be traced back to the fact that the dipole moments associated with the two π transitions are antiparallel. Since the level scheme with antiparallel dipole moments in Fig. 2.2 can be found in real atoms, we provide a realistic experimental setup to verify the presence of vacuum-induced interference effects.

However, it cannot be expected that this four-level system displays the same interference effects that were predicted for the V-system with parallel dipole moments

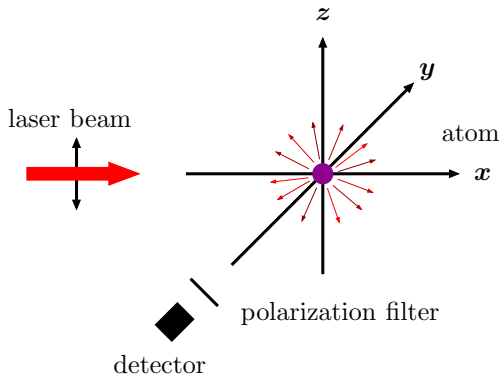

Figure 2.3: Considered experimental setup showing the atom interacting with the laser field. Either the total intensity or the spectrum of resonance fluorescence is observed. With a suitable polarization filter in front of the detector, only the light emitted on the π transitions or the the light emitted on the σ transitions of the atomic level scheme is measured (see Fig. 2.2).

since there is a striking difference between them. In the case of the V-system, both transitions from the upper levels end up in the same ground state, while the two π transitions of our four-level system start and end up in different states that are orthogonal to each other. In view of this, it is surprising that the system in Fig. 2.2 displays interference effects at all. The detailed explanation of this result is provided with the discussion of all our results (see Sec. 2.5).

This chapter is organized as follows. In Sec. 2.2, we discuss the master equation for the laser-driven four-level atom in Fig. 2.2 and describe the polarization-dependent detection scheme which allows to discriminate between the fluorescence light that stems from the π- and the σ transitions. The fluorescence light emitted on the π transitions is discussed in Sec. 2.4, where we show that the total intensity emitted on the π transitions is not affected by interference. On the other hand, a formal argument immediately clarifies that the spectrum of resonance fluorescence emitted on the π transitions does show a signature of quantum interference. The coherent and incoherent spectrum of resonance fluorescence is examined in Secs. 2.3.1 and 2.3.2, respectively, and Sec. 2.3.3 demonstrates how the interference terms alter the fluorescence spectrum for different regimes of the driving field strength. We then turn to the fluorescence spectrum emitted on the σ transitions that only consists of an incoherent part (see Sec. 2.4).
A detailed discussion of all our results is provided in Sec. 2.5. In particular, the interference effect in the spectrum of resonance fluorescence is explained in terms of interferences between transition amplitudes that correspond to different time orders of photon emissions. Our interpretation is supported by a formal argument and a thorough study of the continuous transition from perfect frequency resolution to perfect temporal resolution of the detector. Finally, a summary of our results is given in Sec. 2.6.

2.2 Equation of motion and detection scheme

We now return to the level scheme in Fig. 2.2. Note that we allow the Zeeman splitting of the excited and the ground state magnetic sublevels to be different, since the Landé g factors will not necessarily be the same for these two multiplets. For example, in the case of the $6s\,^2S_{1/2} - 6p\,^2P_{1/2}$ transition in $^{198}Hg^+$ the g factor for the excited states is given by 2/3, and for the ground states it takes on its maximum value of 2. The matrix elements of the electric-dipole moment operator $\hat{\boldsymbol{d}}$ can be found from the the Wigner-Eckart theorem [54] and are given by

$$\begin{aligned} \boldsymbol{d}_1 = \langle 1|\hat{\boldsymbol{d}}|3\rangle = -\frac{1}{\sqrt{3}}\,\mathcal{D}\,\boldsymbol{e}_z\,, \qquad \boldsymbol{d}_2 = \langle 2|\hat{\boldsymbol{d}}|4\rangle = -\boldsymbol{d}_1 \\ \boldsymbol{d}_3 = \langle 2|\hat{\boldsymbol{d}}|3\rangle = \sqrt{\frac{2}{3}}\,\mathcal{D}\,\boldsymbol{\epsilon}^{(-)}\,, \qquad \boldsymbol{d}_4 = \langle 1|\hat{\boldsymbol{d}}|4\rangle = \boldsymbol{d}_3^*\,. \end{aligned} \tag{2.2}$$

In this equation, the circular polarization vector is defined as $\boldsymbol{\epsilon}^{(-)} = (\boldsymbol{e}_x - i\,\boldsymbol{e}_y)/\sqrt{2}$ and $\mathcal{D}$ denotes the reduced dipole matrix element. We assign to each of the four dipole-allowed transitions a resonance frequency ω_i ($i \in \{1,2,3,4\}$). If the splitting between the magnetic sublevels vanishes (i.e. $B = \delta = 0$), these four frequencies are equal.

We are interested in the time evolution of our four level system driven by a monochromatic field of frequency ω_L that is linearly polarized along the z axis,

$$\boldsymbol{E}(t) = E_0\,e^{-i\omega_L t}\,\boldsymbol{e}_z + \text{c.c.}\,, \tag{2.3}$$

and c.c. stands for the complex conjugate. With this choice of polarization, the electric field couples only to the two antiparallel dipole moments $\boldsymbol{d}_1$ and $\boldsymbol{d}_2$. In the rotating wave approximation, the interaction Hamiltonian takes the form

$$V = \big(\,A_{13} - A_{24}\,\big)\,\hbar\Omega\,e^{-i\omega_L t} + \text{h.c.}\,, \tag{2.4}$$

where the atomic transition operators are defined as $A_{ij} = |i\rangle\langle j|$, and the Rabi frequency is given by $\Omega = E_0\,\mathcal{D}/(\sqrt{3}\,\hbar)$. The atomic Hamiltonian can be written as

$$H_0 = \hbar\omega_1\,A_{11} + \hbar(\omega_2 + B)\,A_{22} + \hbar B\,A_{44}\,, \tag{2.5}$$

where ω_1 stands for the resonance frequency of the $1 \leftrightarrow 3$ transition and $\omega_2 = \omega_1 + \delta$ is the resonance frequency on the $2 \leftrightarrow 4$ transition. In a rotating frame defined by the unitary transformation

$$W = \exp\big[\big(\,A_{11} + A_{22}\,\big)\,i\omega_L t\big]\,, \tag{2.6}$$

the master equation for the density operator $\tilde{\varrho} = W\varrho W^\dagger$ reads

$$\dot{\tilde{\varrho}} = -\frac{i}{\hbar}\,[H, \tilde{\varrho}] + \mathcal{L}_\gamma\tilde{\varrho}\,. \tag{2.7}$$

In this equation, the Hamiltonian is given by

$$\begin{aligned} H = &- \hbar\big[\,\Delta\, A_{11} + (\Delta - \delta)\, A_{22} - B\,(A_{22} + A_{44})\,\big] \\ &+ \big[\,(\,A_{13} - A_{24}\,)\,\hbar\Omega \,+\, \text{h.c.}\,\big]\,, \end{aligned} \tag{2.8}$$

$\Delta = \omega_L - \omega_1$ is the detuning of the driving field from resonance with the $1 \leftrightarrow 3$ transition, and $\Delta - \delta$ is the detuning on the $2 \leftrightarrow 4$ transition. According to Eq. (1.44) of Chapter 1 and with the dipole moments in Eq. (2.2), the damping term $\mathcal{L}_\gamma \tilde{\varrho}$ takes the form

$$\begin{aligned} \mathcal{L}_\gamma \tilde{\varrho} \;\; = \;\; & -\frac{1}{2} \sum_{i,\,j=1}^{2} \gamma_{ij} \,\Big(S_i^+ S_j^- \,\tilde{\varrho} + \tilde{\varrho} S_i^+ S_j^- - 2 S_j^- \,\tilde{\varrho} S_i^+ \Big) \\ & - \frac{\gamma_\sigma}{2} \sum_{i=3}^{4} \Big(S_i^+ S_j^- \,\tilde{\varrho} + \tilde{\varrho} S_i^+ S_j^- - 2 S_j^- \,\tilde{\varrho} S_i^+ \Big)\,. \end{aligned} \tag{2.9}$$

Since we are dealing with a single-atom system, we introduced a simplified notation for the atomic transition operators $S_i^\pm$. These operators are defined as

$$S_1^+ = A_{13}\,, \;\; S_2^+ = A_{24}\,, \;\; S_3^+ = A_{23}\,, \;\; S_4^+ = A_{14}\,, \tag{2.10}$$

and $S_i^- = (S_i^+)^\dagger$. The decay constant on each of the σ transitions is denoted by γ_σ, the parameters γ_{ij} are determined by

$$\gamma_{ij} = \frac{\boldsymbol{d}_i \cdot \boldsymbol{d}_j^*}{|\boldsymbol{d}_i|\,|\boldsymbol{d}_j|} \sqrt{\gamma_i \gamma_j} \qquad i,\, j \in \{1, 2\}\,, \tag{2.11}$$

and γ_1 and γ_2 are the decay constants of the π transitions (see Fig. 2.2). Note that in contrast to Chapter 1, the parameters γ_σ, γ_1 and γ_2 are full decay rates rather than half-decay rates. This explains the factor $1/2$ in Eq. (2.9). For $i = j$, the parameters γ_{ij} in Eq. (2.9) are equal to the decay rates of the π transitions, $\gamma_{11} = \gamma_1$ and $\gamma_{22} = \gamma_2$. Although γ_1 and γ_2 are equal in our setup, we will continue to label them differently to facilitate the physical interpretation later on. Since $\boldsymbol{d}_1$ and $\boldsymbol{d}_2$ are antiparallel, the cross-damping terms are given by $\gamma_{12} = \gamma_{21} = -\sqrt{\gamma_1 \gamma_2}$. These terms allow for the possibility of coherence transfer from the excited to the ground state doublet.

The decay rates γ_1, γ_2, γ_σ can be related to the total decay rate $\gamma = \gamma_1 + \gamma_\sigma = \gamma_2 + \gamma_\sigma$ of each of the two excited states through the branching probabilities b_π and b_σ,

$$\gamma_1 = \gamma_2 = b_\pi \gamma \quad \text{and} \quad \gamma_\sigma = b_\sigma \gamma\,. \tag{2.12}$$

According to the Clebsch-Gordan coefficients, we have $b_\pi = 1/3$ and $b_\sigma = 2/3$. Although we will keep the symbols b_π and b_σ in formulas, we will always assume these values whenever a concrete evaluation is performed, e.g. in figures.

Next we employ the normalization condition $\mathrm{Tr}(\tilde{\varrho}) = 1$ to eliminate the matrix element $\tilde{\varrho}_{44}$ from the master equation (2.7) that can be cast into the form

$$\partial_t \boldsymbol{R}(t) = \mathcal{M}\, \boldsymbol{R}(t) \,+\, \boldsymbol{I}\,. \tag{2.13}$$

Here $\mathcal{M}$ represents a generalized 15×15 Bloch matrix, the vector $\boldsymbol{I}$ is an inhomogeneity with components

$$\boldsymbol{I} = \big(0,0,0,0,0,0,0,i\,\Omega,0,0,0,0,0,-i\,\Omega^*,0\big)^{\mathrm{T}} \tag{2.14}$$

and the vector $\boldsymbol{R}$ contains the matrix elements $\tilde{\varrho}_{ij} = \langle i|\tilde{\varrho}|j\rangle$ of the density operator,

$$\boldsymbol{R} = \big(\tilde{\varrho}_{11},\tilde{\varrho}_{12},\tilde{\varrho}_{13},\tilde{\varrho}_{14},\tilde{\varrho}_{21},\tilde{\varrho}_{22},\tilde{\varrho}_{23},\tilde{\varrho}_{24},\tilde{\varrho}_{31},\tilde{\varrho}_{32},\tilde{\varrho}_{33},\tilde{\varrho}_{34},\tilde{\varrho}_{41},\tilde{\varrho}_{42},\tilde{\varrho}_{43}\big)^{\mathrm{T}} . \tag{2.15}$$

The stationary solution of Eq. (2.13) is formally given by $\boldsymbol{R}_{\mathrm{st}} = -\mathcal{M}^{-1}\boldsymbol{I}$, and an evaluation of the latter equation yields

$$\begin{aligned}
\tilde{\varrho}_{11} &= \frac{1}{2}\,\frac{|\Omega|^2}{\gamma^2/4+\delta^2/4+(\Delta-\delta/2)^2+2|\Omega|^2}\,, \\
\tilde{\varrho}_{33} &= \frac{1}{2}\,\frac{\gamma^2/4+\Delta^2+|\Omega|^2}{\gamma^2/4+\delta^2/4+(\Delta-\delta/2)^2+2|\Omega|^2}\,, \\
\tilde{\varrho}_{44} &= \frac{1}{2}\,\frac{\gamma^2/4+(\Delta-\delta)^2+|\Omega|^2}{\gamma^2/4+\delta^2/4+(\Delta-\delta/2)^2+2|\Omega|^2}\,, \\
\tilde{\varrho}_{13} &= \frac{1}{2}\,\frac{(\Delta-i\gamma/2)\,\Omega}{\gamma^2/4+\delta^2/4+(\Delta-\delta/2)^2+2|\Omega|^2}\,, \\
\tilde{\varrho}_{24} &= \frac{1}{2}\,\frac{(\delta-\Delta+i\gamma/2)\,\Omega}{\gamma^2/4+\delta^2/4+(\Delta-\delta/2)^2+2|\Omega|^2}\,.
\end{aligned} \tag{2.16}$$

The remaining non-zero components of $\boldsymbol{R}_{\mathrm{st}}$ are determined by

$$\tilde{\varrho}_{11} = \tilde{\varrho}_{22}\,, \qquad \tilde{\varrho}_{31} = \tilde{\varrho}_{13}^* \qquad \text{and} \qquad \tilde{\varrho}_{42} = \tilde{\varrho}_{24}^*\,. \tag{2.17}$$

In the case of the degenerate system, the population of the two ground levels will be equal and we have $\tilde{\varrho}_{13} = -\tilde{\varrho}_{24}$. Note that the minus sign arises since the dipole moments $\boldsymbol{d}_1$ and $\boldsymbol{d}_2$ are antiparallel, and the coherences $\tilde{\varrho}_{14}$ and $\tilde{\varrho}_{23}$ are equal to zero because the driving field does not couple to the σ transitions.

In this chapter we focus on the total intensity and the spectral distribution of the fluorescence light emitted by the atom in steady state. The total intensity

$$I_{\mathrm{st}} = \big\langle\, \hat{\boldsymbol{E}}^{(-)}(\boldsymbol{r},t)\cdot\hat{\boldsymbol{E}}^{(+)}(\boldsymbol{r},t)\,\big\rangle_{\mathrm{st}} \tag{2.18}$$

is given by the normally ordered first-order correlation function of the electric field, and the spectrum of resonance fluorescence is determined by the Fourier transform of the two-time correlation function of the electric field [18],

$$S(\omega) = \frac{1}{2\pi}\int\limits_{-\infty}^{\infty} e^{-i\omega\tau}\,\big\langle\, \hat{\boldsymbol{E}}^{(-)}(\boldsymbol{r},t+\tau)\cdot\hat{\boldsymbol{E}}^{(+)}(\boldsymbol{r},t)\,\big\rangle_{\mathrm{st}}\,d\tau\,. \tag{2.19}$$

In these equations, $\hat{\boldsymbol{E}}^{(-)}$ $\left(\hat{\boldsymbol{E}}^{(+)}\right)$ denotes the negative (positive) frequency part of the electric field operator. At a point $\boldsymbol{r} = r\hat{\boldsymbol{r}}$ in the far-field zone, the negative frequency part of the electric field operator is found to be [10]

$$\hat{\boldsymbol{E}}^{(-)}(\boldsymbol{r},t) = \hat{\boldsymbol{E}}^{(-)}_{\rm free}(\boldsymbol{r},t) - \frac{\eta}{r}\sum_{i=1}^{4}\omega_i^2\,\hat{\boldsymbol{r}}\times(\,\hat{\boldsymbol{r}}\times\boldsymbol{d}_i\,)\;\tilde{S}_i^{+}(\hat{t})\,e^{i\omega_L\hat{t}}\,, \tag{2.20}$$

where $\hat{t} = t - \frac{r}{c}$ is the retarded time, $\eta = 1/(4\pi\varepsilon_0 c^2)$ and $\tilde{S}_i^{\pm}(t) = \exp(\mp i\omega_L t)\,S_i^{\pm}(t)$. The first term stands for the negative frequency part of the free field. It does not contribute to the normally ordered correlation functions in Eqs. (2.18) and (2.19) as long as the point of observation lies outside the driving field [55]. The second term describes the retarded dipole field generated by the atom situated at the point of origin.

Throughout this chapter we assume that the point of observation lies in the y direction, where the z and x axes are defined by the polarization and the direction of propagation of the laser beam, respectively. An evaluation of the cross products in Eq. (2.20) shows then that the light emitted on the π transitions is linearly polarized along $\boldsymbol{e}_z$, whereas the light emitted on the σ transitions is linearly polarized along $\boldsymbol{e}_x$. The advantage of this detection scheme is that one can easily discriminate between the light emitted on the π and σ transitions by means of a polarization filter. For this reason we will discuss the fluorescence light of the π- and σ transitions separately.

2.3 Spectrum of resonance fluorescence – π transitions

We begin with a brief discussion of the steady-state intensity recorded by a broadband detector that observes the light emitted on the π transitions. According to Eqs. (2.18) and (2.20), we have

$$I^{\pi}_{\rm st} = \phi_\pi \sum_{i,\,j=1}^{2}\gamma_{ij}\,\langle\,\tilde{S}_i^{+}\tilde{S}_j^{-}\,\rangle_{\rm st}\,, \tag{2.21}$$

where it was assumed that $\omega_1 \approx \omega_2$ to obtain a common prefactor ϕ_π that we set equal to one in the following. The terms γ_{ij} are defined in Eq. (2.11), and $\gamma_{12} = \gamma_{21} = -\sqrt{\gamma_1\gamma_2}$ describe the cross-damping between the π transitions that arises as a consequence of quantum interference. However, these interference terms do not contribute to the total intensity, regardless of what the steady state solution might be, because the ground states are orthogonal,

$$\langle\,\tilde{S}_1^{+}\tilde{S}_2^{-}\,\rangle_{\rm st} = \big\langle\,|1\rangle\langle 3|\;|4\rangle\langle 2|\,\big\rangle_{\rm st} = 0\,. \tag{2.22}$$

Consequently, the intensity emitted on the π transitions is not altered by interference terms and simply proportional to the population of the excited states,

$$I^{\pi}_{\rm st} = b_\pi\gamma(\tilde{\varrho}_{11} + \tilde{\varrho}_{22})\,. \tag{2.23}$$

We now turn to the the spectrum of resonance fluorescence emitted on the π transitions. With the help of Eqs. (2.19) and (2.20) we arrive at

$$S^{\pi}(\tilde{\omega}) = \frac{1}{\pi} \sum_{i,j=1}^{2} \gamma_{ij} \, \mathrm{Re} \int_{0}^{\infty} e^{-i\tilde{\omega}\tau} \langle \, \tilde{S}_i^{+}(\hat{t}+\tau) \tilde{S}_j^{-}(\hat{t}) \, \rangle_{\mathrm{st}} \, d\tau \; , \tag{2.24}$$

where $\tilde{\omega} = \omega - \omega_L$ is the difference between the observed frequency and the laser frequency. In contrast to Eq. (2.22), the terms proportional to γ_{12} are now determined by the *two-time averages* $\langle \, \tilde{S}_1^{+}(\hat{t}+\tau)\tilde{S}_2^{-}(\hat{t}) \, \rangle_{\mathrm{st}}$ rather than by the one-time averages. Indeed, we find that the correlation function

$$G_{12}(\tau) = -\sqrt{\gamma_1 \gamma_2} \, \langle \, \tilde{S}_1^{+}(\hat{t}+\tau)\tilde{S}_2^{-}(\hat{t}) \, \rangle_{\mathrm{st}} \tag{2.25}$$

is different from zero for $\tau > 0$; a plot of G_{12} is shown in Fig. 2.4. But this implies that there is quantum interference in the spectrum of the light emitted on the π transitions, although there is no interference in the total intensity. To illustrate this result we decompose the transition operators in Eq. (2.25) in mean values and fluctuations according to

$$\tilde{S}_i^{\pm} = \langle \, \tilde{S}_i^{\pm} \, \rangle_{\mathrm{st}} \mathbb{1} \; + \; \delta \tilde{S}_i^{\pm} \; . \tag{2.26}$$

The correlation function $G_{12}(\tau)$ becomes then

$$G_{12}(\tau) = -\sqrt{\gamma_1 \gamma_2} \, \left[\, \langle \, \delta\tilde{S}_1^{+}(\hat{t}+\tau)\delta\tilde{S}_2^{-}(\hat{t}) \, \rangle_{\mathrm{st}} + \langle \, \tilde{S}_1^{+} \, \rangle_{\mathrm{st}} \langle \, \tilde{S}_2^{-} \, \rangle_{\mathrm{st}} \, \right] . \tag{2.27}$$

The two-time average of the fluctuations can be calculated from the generalized Bloch equations and the quantum regression theorem (see the Appendix). It decays exponentially with a time constant on the order of γ^{-1} and does not contribute to G_{12} in the long-time limit $\tau \to \infty$. The mean values $\langle \, \tilde{S}_1^{+} \, \rangle_{\mathrm{st}} = \tilde{\varrho}_{31}$ and $\langle \, \tilde{S}_2^{+} \, \rangle_{\mathrm{st}} = \tilde{\varrho}_{42}$ are given by matrix elements of the steady-state density-operator in Eq. (2.16) and are both different from zero. This is obvious from a physical point of view since the laser field creates a coherence on both transitions $1 \leftrightarrow 3$ and $2 \leftrightarrow 4$. Consequently, the long-time limit of G_{12} reads $G_{12}(\infty) = -\sqrt{\gamma_1\gamma_2} \langle \, \tilde{S}_1^{+} \, \rangle_{\mathrm{st}} \langle \, \tilde{S}_2^{-} \, \rangle_{\mathrm{st}}$. It follows that the interference terms will affect the coherent and incoherent spectrum of resonance fluorescence.

Before we give expressions for the spectral distribution of the emitted light, we calculate the respective contributions of coherent and incoherent scattering to the intensity I_{st}^{π}. To this end we apply the decomposition of the transition operators Eq. (2.26) to Eq. (2.21). This allows us to write I_{st}^{π} as the sum of four terms,

$$I_{\mathrm{st}}^{\pi} = I_{\mathrm{coh}}^{0} + I_{\mathrm{coh}}^{\mathrm{int}} + I_{\mathrm{inc}}^{0} + I_{\mathrm{inc}}^{\mathrm{int}} \; . \tag{2.28}$$

The first two terms account for the contribution of coherent scattering (subscript "coh") and are given by

$$I_{\mathrm{coh}}^{0} \;\; = \;\; \gamma_1 \, |\langle \, \tilde{S}_1^{+} \, \rangle_{\mathrm{st}}|^2 + \gamma_2 \, |\langle \, \tilde{S}_2^{+} \, \rangle_{\mathrm{st}}|^2 \, , \tag{2.29}$$

$$I_{\mathrm{coh}}^{\mathrm{int}} \;\; = \;\; -2\sqrt{\gamma_1\gamma_2} \, \mathrm{Re} \langle \, \tilde{S}_1^{+} \, \rangle_{\mathrm{st}} \langle \, \tilde{S}_2^{-} \, \rangle_{\mathrm{st}} \, . \tag{2.30}$$

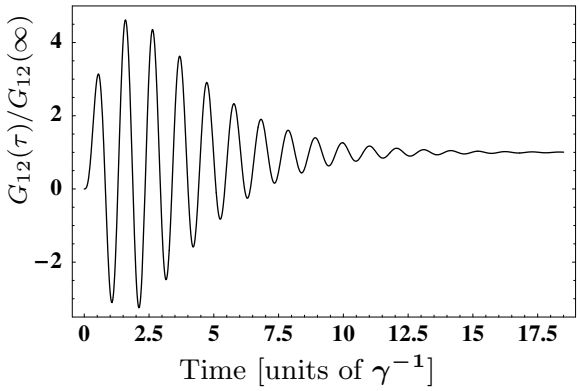

Figure 2.4: Plot of the correlation function G_{12} in relation to its long-time limit $G_{12}(\infty) = -\sqrt{\gamma_1\gamma_2}\langle\, \tilde{S}_1^+ \,\rangle_{\rm st}\langle\, \tilde{S}_2^- \,\rangle_{\rm st}$ for the degenerate system. The parameters are $\Omega = 3\times 10^7\, s^{-1}$, $\Delta = 5\times 10^6\, s^{-1}$ and $\gamma = 10^7\, s^{-1}$. G_{12} has to vanish at $\tau = 0$ since the ground states are orthogonal.

In this equation, $I^0_{\rm coh}$ stands for the contribution of terms proportional to γ_{11} and γ_{22}, and $I^{\rm int}_{\rm coh}$ is the weight of the interference terms that can be positive or negative. By contrast, the sum of $I^0_{\rm coh}$ and $I^{\rm int}_{\rm coh}$ is the weight of the Rayleigh line that is always positive. The last two terms in Eq. (2.28) denote the contribution of incoherent scattering (subscript "inc"),

$$I^0_{\rm inc} = \gamma_1\,\langle\, \delta\tilde{S}_1^+\delta\tilde{S}_1^- \,\rangle_{\rm st} + \gamma_2\,\langle\, \delta\tilde{S}_2^+\delta\tilde{S}_2^- \,\rangle_{\rm st}\,, \tag{2.31}$$

$$I^{\rm int}_{\rm inc} = -2\sqrt{\gamma_1\gamma_2}\,{\rm Re}\,\langle\, \delta\tilde{S}_1^+\delta\tilde{S}_2^- \,\rangle_{\rm st}\,. \tag{2.32}$$

Since the ground states are orthogonal, Eq. (2.26) allows to establish the relation

$$\langle\, \delta\tilde{S}_1^+\delta\tilde{S}_2^- \,\rangle_{\rm st} = -\langle\, \tilde{S}_1^+ \,\rangle_{\rm st}\langle\, \tilde{S}_2^- \,\rangle_{\rm st}\,. \tag{2.33}$$

If this expression is applied to Eq. (2.32), it follows from Eq. (2.30) that the interference terms $I^{\rm int}_{\rm coh}$ and $I^{\rm int}_{\rm inc}$ are of opposite sign, i.e.,

$$I^{\rm int}_{\rm coh} = -I^{\rm int}_{\rm inc}\,. \tag{2.34}$$

This relation clarifies that the interference terms alter the weights of the coherent and the incoherent part of the spectrum, whereas the total intensity remains unchanged. Note that this is in contrast to the V-system with nonorthogonal transition dipole moments mentioned in the introduction, where both the fluorescence spectrum and the total intensity show a signature of interference [11, 21, 30, 31].

We now turn to the spectral distribution of the fluorescence light and employ Eq. (2.26) to write the spectrum of resonance fluorescence in Eq. (2.24) as the sum

of the coherent and the incoherent spectrum, $S^{\pi}(\tilde{\omega}) = S^{\pi}_{\rm coh}(\tilde{\omega}) + S^{\pi}_{\rm inc}(\tilde{\omega})$, where

$$S^{\pi}_{\rm coh}(\tilde{\omega}) = \left(I^{0}_{\rm coh} + I^{\rm int}_{\rm coh}\right)\delta(\tilde{\omega})\,, \tag{2.35}$$

$$S^{\pi}_{\rm inc}(\tilde{\omega}) = \frac{1}{\pi}\sum_{i,\,j=1}^{2}\gamma_{ij}\,{\rm Re}\int_{0}^{\infty} e^{-i\tilde{\omega}\tau}\langle\,\delta\tilde{S}^{+}_{i}(\hat{t}+\tau)\delta\tilde{S}^{-}_{j}(\hat{t})\,\rangle_{\rm st}\,d\tau\,. \tag{2.36}$$

These two contributions will be discussed in the following sections.

2.3.1 Coherent spectrum of resonance fluorescence

The coherent part of the fluorescence spectrum consists of the Rayleigh peak centered at $\omega = \omega_L$. In order to get a better understanding of how the weight of this line is affected by interference, we write it as

$$I^{0}_{\rm coh} + I^{\rm int}_{\rm coh} = |\sqrt{\gamma_1}\langle\,\tilde{S}^{+}_{1}\,\rangle_{\rm st} - \sqrt{\gamma_2}\langle\,\tilde{S}^{+}_{2}\,\rangle_{\rm st}|^2\,. \tag{2.37}$$

In this equation, $\langle\,\tilde{S}^{+}_{1}\,\rangle_{\rm st}$ is proportional to the scattering amplitude on the $1 \leftrightarrow 3$ transition and $-\langle\,\tilde{S}^{+}_{2}\,\rangle_{\rm st}$ corresponds to the scattering amplitude on the $2 \leftrightarrow 4$ transition. Note that the minus sign arises since the dipoles $\boldsymbol{d}_1$ and $\boldsymbol{d}_2$ are antiparallel. Depending on the relative phase and the absolute values of the coherences $\langle\,\tilde{S}^{+}_{1}\,\rangle_{\rm st}$ and $\langle\,\tilde{S}^{+}_{2}\,\rangle_{\rm st}$, there will be constructive or destructive interference in the coherent part of the spectrum. We will now demonstrate that the degree of interference in the coherent spectrum can be controlled by means of the difference δ between the resonance frequencies of the π transitions. Therefore, we write Eq. (2.37) as

$$I^{0}_{\rm coh} + I^{\rm int}_{\rm coh} = I^{0}_{\rm coh}\left[\,1 + C\,\right]\,, \tag{2.38}$$

where $C = I^{\rm int}_{\rm coh}/I^{0}_{\rm coh}$ is the relative weight of the interference terms. An explicit expression for C can be found with the help of the definitions in Eq. (2.30) and the steady-state solution for $\tilde{\varrho}$ in Eq. (2.16),

$$C = \frac{\gamma^2/4 + \Delta(\Delta-\delta)}{\gamma^2/4 + \delta^2/4 + (\Delta-\delta/2)^2}\,. \tag{2.39}$$

The absolute value of this quantity can be regarded as the degree of interference in the coherent spectrum. Figure 2.5 shows a plot of C as a function of δ for two different (negative) detunings Δ. It is evident that C is equal to one in the case of the degenerate system. Therefore, we have perfect constructive interference for $\delta = 0$. In this case, the detunings on both π transitions are equal and hence we have $\langle\,\tilde{S}^{+}_{1}\,\rangle_{\rm st} = -\langle\,\tilde{S}^{+}_{2}\,\rangle_{\rm st}$, the two transitions are now perfectly equivalent. In addition, the weight of the Rayleigh line is then, apart from the branching probability b_π, identical to the corresponding expression for a two-level atom [56].

As $|\delta|$ increases, $C(\delta)$ decreases monotonically and becomes zero at $\delta_0 = \Delta\big[1 + \gamma^2/(4\Delta^2)\big]$. Note that δ_0 can be either positive or negative, depending on the

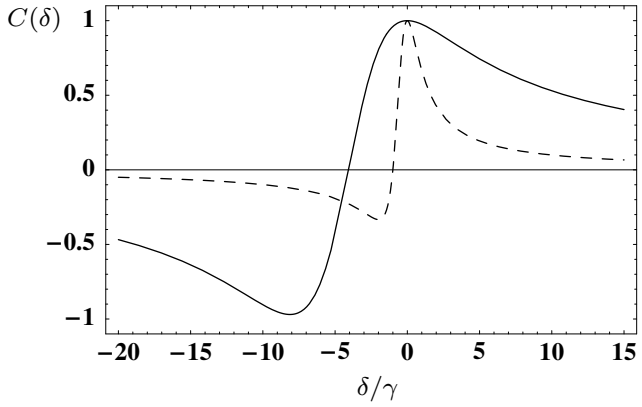

Figure 2.5: Plot of the relative weight of the interference terms $C(\delta)$ for different values of the detuning Δ of the laser field from the $1 \leftrightarrow 3$ transition. The parameters are given by $\gamma = 10^7 s^{-1}$, $\Delta = -4 \times 10^7 s^{-1}$ (solid line) and $\Delta = -5 \times 10^6 s^{-1}$ (dashed line).

sign of Δ. In the case of $\Delta^2 \gg \gamma^2$, we have $\delta_0 \approx \Delta$. This implies that the interference term vanishes if the laser field is resonant with the $2 \leftrightarrow 4$ transition. The minimum of the curve is reached at $\delta_{\min} = 2\Delta(1 + \gamma^2/(4\Delta^2))$ and given by $C(\delta_{\min}) = -1/(1 + \gamma^2/(2\Delta^2))$. Consequently, $C(\delta_{\min})$ tends to -1 provided that $\Delta^2 \gg \gamma^2$. The weight of the Rayleigh peak becomes then zero as a consequence of destructive interference, and the emitted radiation is solely incoherent. Note that this situation occurs if the detunings on the $1 \leftrightarrow 3$ and $2 \leftrightarrow 4$ transitions are approximately equal and of opposite sign. In this case, the coherences $\langle \tilde{S}_1^+ \rangle_{\rm st}$ and $\langle \tilde{S}_2^+ \rangle_{\rm st}$ cancel each other in Eq. (2.37). Finally, C tends to zero as $|\delta|$ becomes much larger than $|\Delta|$ and γ. This is due to the fact that the interference term in Eq. (2.30) consists of the product of $\langle \tilde{S}_1^+ \rangle_{\rm st}$ and $\langle \tilde{S}_2^+ \rangle_{\rm st}$. If the detuning on one of the two π transitions becomes very large, $I_{\rm coh}^{\rm int}$ tends to zero, whereas $I_{\rm coh}^0$ remains different from zero.

2.3.2 Incoherent spectrum of resonance fluorescence

It is possible to evaluate the expression for $S_{\rm inc}^{\pi}$ in Eq. (2.36) analytically, an outline of the calculation can be found in the Appendix. However, the general result is too bulky to present it here. We just mention that the spectrum does only depend on the difference δ between the Zeeman splittings of the ground and excited states, but not on the parameter B (see Fig. 2.2). In the case of the degenerate system, we find

$$S_{\rm inc}^{\pi}(\tilde{\omega}) = b_\pi \frac{\gamma}{\pi} \frac{\gamma^2 + 2|\Omega|^2 + \tilde{\omega}^2}{\gamma^2/4 + \Delta^2 + 2|\Omega|^2} \frac{2\gamma|\Omega|^4}{|P(-i\tilde{\omega})|^2} , \tag{2.40}$$

where $P(z)$ is a cubic polynomial as a function of z that is defined as

$$P(z) = \frac{1}{4}(z+\gamma)\left[(2z+\gamma)^2 + 4\Delta^2\right] + 2(2z+\gamma)|\Omega|^2 \,. \tag{2.41}$$

Apart from the branching probability b_π, this result is *exactly* the same as the incoherent spectrum of resonance fluorescence of a two-level atom [56].

As soon as δ becomes different from zero, the incoherent spectrum differs considerably from the two-level spectrum. This is demonstrated in Fig. 2.6(a) which displays $S^\pi_{\rm inc}$ for $\delta = 0$ (dashed line) and $\delta = -4 \times 10^6 s^{-1}$ (solid line). For $\delta \neq 0$, an additional central peak occurs whose width is much smaller than the decay rate γ.

Section 2.3.1 provides a detailed discussion of the weight of the interference term $I^{\rm int}_{\rm coh}$ in the coherent spectrum. These results can also be applied to the weight of the interference term $I^{\rm int}_{\rm inc}$ in the inelastic spectrum by means of Eq. (2.34). For example, it follows that the weight of the interference term $I^{\rm int}_{\rm inc}$ in the inelastic spectrum vanishes for $\delta = \delta_0$. This situation is shown in Fig. 2.6(b), where the width and the weight of the additional peak is larger than in (a). For $\delta = \delta_{\rm min}$ and the parameters of Fig. 2.6, we know from Sec. 2.3.1 that the weight of the Rayleigh line is approximately zero. The corresponding incoherent spectrum is shown in

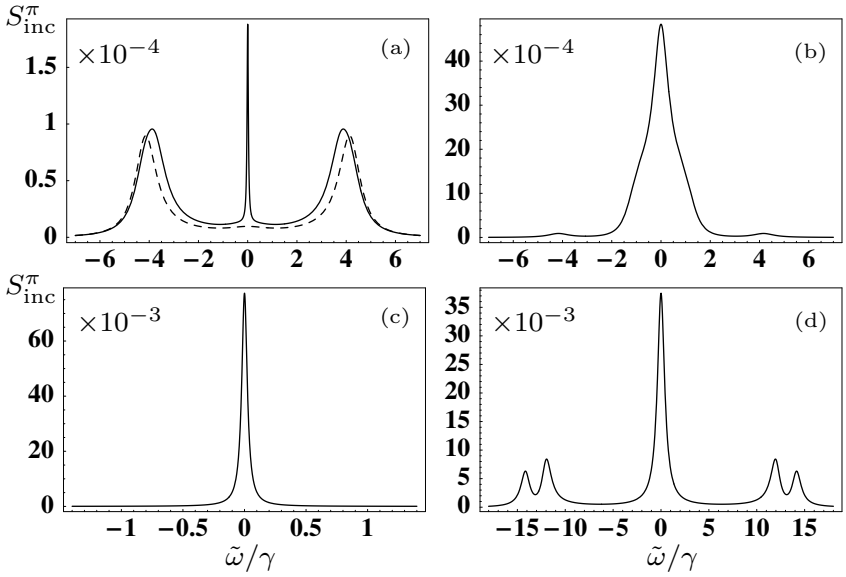

Figure 2.6: Incoherent spectrum of resonance fluorescence according to Eq. (2.36). Plot (a) shows $S^\pi_{\rm inc}$ for the degenerate system (dashed line) and for $\delta = -4 \times 10^6 s^{-1}$ (solid line), the other parameters are $\gamma = 10^7 s^{-1}$, $\Delta = -4 \times 10^7 s^{-1}$ and $\Omega = 6 \times 10^6 s^{-1}$. In (b) and (c) the values of δ are given by $\delta = \delta_0$ and $\delta = \delta_{\rm min}$, respectively, the other parameters are the same than in (a). Plot (d) shows the incoherent spectrum for the set of parameters $\Delta = -5 \times 10^6 s^{-1}$, $\Omega = 6 \times 10^7 s^{-1}$, $\gamma = 10^7 s^{-1}$ and $\delta = -8 \times 10^7 s^{-1}$.

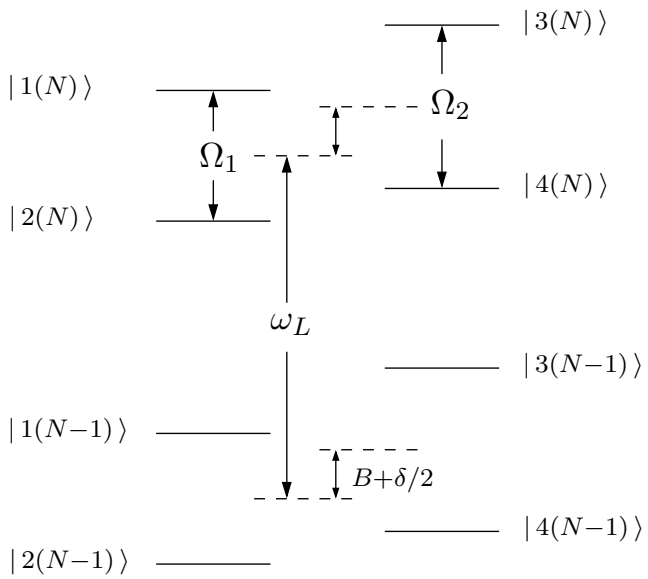

Figure 2.7: Dressed state analog of the bare state system in Fig. 2.2. The frequency of the laser field is labeled by ω_L. For $\delta \neq 0$, the detuning of the laser field will be different on each of the π transitions. There are thus two effective Rabi frequencies Ω_1 and Ω_2 involved. The splitting of the dressed states for fixed N is not to scale.

Fig. 2.6(c). Instead of the elastic delta-peak in the coherent spectrum we thus have a very narrow peak that occurs in the incoherent spectrum.

Finally, Fig. 2.6(d) shows $S^{\pi}_{\rm inc}$ for a strong laser field. In this case, the weight of the interference terms is negligible as can be verified with the help of Eq. (2.30). However, the incoherent spectrum still deviates from the Mollow spectrum if $\delta \neq 0$. This can be easily understood with the aid of the dressed states [18, 57] of the system. If N denotes the number of laser photons of frequency ω_L, the dressed states can be expressed in terms of the bare states as follows,

$$\begin{aligned} |1(N)\rangle &= e^{i\phi}\sin\Theta_1\,|1,\,N\rangle + \cos\Theta_1\,|3,\,N+1\rangle\,, \\ |2(N)\rangle &= e^{i\phi}\cos\Theta_1\,|1,\,N\rangle - \sin\Theta_1\,|3,\,N+1\rangle\,, \end{aligned} \tag{2.42}$$

where $\tan 2\Theta_1 = 2\,|\Omega|/\Delta$ and

$$\begin{aligned} |3(N)\rangle &= e^{i\phi}\sin\Theta_2\,|2,\,N\rangle - \cos\Theta_2\,|4,\,N+1\rangle\,, \\ |4(N)\rangle &= e^{i\phi}\cos\Theta_2\,|2,\,N\rangle + \sin\Theta_2\,|4,\,N+1\rangle\,, \end{aligned} \tag{2.43}$$

with $\tan 2\Theta_2 = 2\,|\Omega|/(\Delta-\delta)$ ($0 < \Theta_1,\,\Theta_2 < \pi/2$, $e^{i\phi} = \Omega/|\Omega|$). Figure 2.7 shows the relative position of the dressed states for two manifolds with N and $(N-1)$ laser photons, respectively. Note that $|1(N)\rangle$ and $|2(N)\rangle$ are separated by a frequency interval of $\Omega_1 = \sqrt{4|\Omega|^2+\Delta^2}$, whereas the spacing between $|3(N)\rangle$ and $|4(N)\rangle$ is given by $\Omega_2 = \sqrt{4|\Omega|^2+(\Delta-\delta)^2}$. The sidebands in the spectrum of the

π transitions result from the transitions $|1(N)\rangle \rightarrow |2(N-1)\rangle$, $|2(N)\rangle \rightarrow |1(N-1)\rangle$, $|3(N)\rangle \rightarrow |4(N-1)\rangle$ and $|4(N)\rangle \rightarrow |3(N-1)\rangle$. Consequently, they will be located at the frequencies $\omega_L \pm \Omega_1$ and $\omega_L \pm \Omega_2$. For $\delta \neq 0$, we thus expect four sideband peaks symmetrically placed around the laser frequency ω_L, precisely as in Fig. 2.6(d).

2.3.3 Influence of the interference terms on the fluorescence spectrum

In this Section we investigate how the interference terms alter the fluorescence spectrum emitted on the π transitions. Here we only consider the degenerate system that is distinguished by maximal constructive (destructive) interference in the coherent (incoherent) part of the fluorescence spectrum, see Sec. 2.3. If the interference terms in Eq. (2.24) are omitted, the fluorescence spectrum reads

$$S_0^{\pi}(\tilde{\omega}) = \frac{1}{\pi} \sum_{i=1}^{2} \gamma_{ii} \, \mathrm{Re} \int_0^{\infty} e^{-i\tilde{\omega}\tau} \langle \, \tilde{S}_i^{+}(\hat{t}+\tau) \tilde{S}_i^{-}(\hat{t}) \, \rangle_{\mathrm{st}} \, d\tau \; . \tag{2.44}$$

The fluorescence spectra with and without the interference terms according to Eqs. (2.24) and (2.44) are shown in Fig. 2.8 for different parameters of the laser field. If the saturation parameter defined in Eq. (2.49) is much larger than unity, the weight of the interference terms goes to zero. However, Fig. 2.8(a) demonstrates that the interference terms still alter the shape of the fluorescence spectrum in the region of the sideband peaks. The spectrum S^{π} with interference terms is identical to the fluorescence spectrum of a two-level atom (see Sec 2.3), and thus the ratio between the central and the sideband peaks reads $1:3:1$. For the spectrum without the interference terms and a branching probability of $b_{\pi} = 1/3$, this ratio reads $7:15:7$.

Figure 2.8(b) shows S^{π} and S_0^{π} for low saturation. In this case, the spectrum without interference terms is distinguished by a narrow peak centered at the laser frequency that occurs in addition to the elastic Rayleigh peak. A numerical analysis shows that S_0^{π} can be written as

$$S_0^{\pi}(\tilde{\omega}) \approx I_{\mathrm{coh}}^{0} \, \delta(\tilde{\omega}) \; + \; S_{\mathrm{inc}}^{\pi}(\tilde{\omega}) \; + \; S_{\mathrm{peak}}^{\pi}(\tilde{\omega}) \, . \tag{2.45}$$

In this equation, the first term represents the Rayleigh peak whose weight misses the interference term $I_{\mathrm{coh}}^{\mathrm{int}}$ that is present in Eq. (2.35). The second term stands for the incoherent spectrum according to Eq. (2.40). The last term describes a Lorentzian of weight $I_{\mathrm{coh}}^{\mathrm{int}}$ and width Γ_{π} that is centered at the laser frequency,

$$S_{\mathrm{peak}}^{\pi}(\tilde{\omega}) = \frac{I_{\mathrm{coh}}^{\mathrm{int}}}{\pi} \, \frac{\Gamma_{\pi}}{\tilde{\omega}^2 + \Gamma_{\pi}^2} \; . \tag{2.46}$$

The weight of the extra peak S_{peak}^{π} is determined by the constraint that the total intensity is independent of the interference terms (see Sec. 2.3). Therefore, S_{peak}^{π} has to compensate for the reduced weight of the Rayleigh line of S_0^{π} as compared

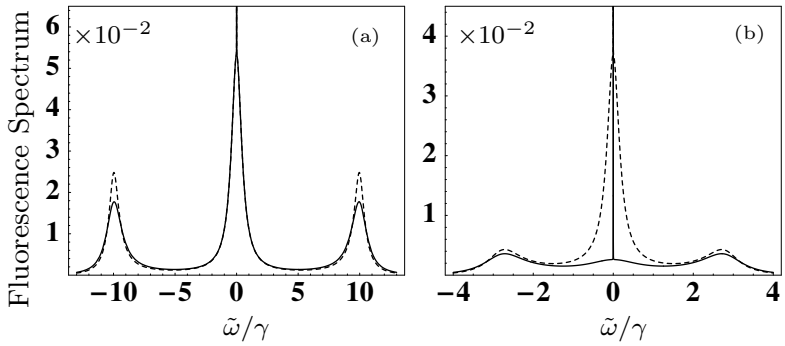

Figure 2.8: Fluorescence spectrum for the degenerate system according to Eq. (2.24). The solid line (dashed line) shows the spectrum with (without) the interference terms proportional to γ_{12}, γ_{21}. The Rayleigh peak (the vertical line at $\omega = \omega_L$) is present both with and without interference terms. Note that its weight is larger if the interference terms are taken into account. However, the sums of the integrated coherent and incoherent spectra with and without the interference terms are identical, making the total intensity independent of the interference terms. In (a), the parameters are $\Omega = 5 \times 10^7\, s^{-1}$, $\Delta = 0$ and $\gamma = 10^7\, s^{-1}$. For (b), we have $\Omega = 10^7\, s^{-1}$, $\Delta = 2 \times 10^7\, s^{-1}$ and $\gamma = 10^7\, s^{-1}$.

to the spectrum with interference terms. In general, the width Γ_π of the extra peak $S^\pi_{\rm peak}$ is smaller than the decay rate γ. If the saturation parameter s is much smaller than unity, we find ($b_\pi = 1/3$)

$$I^{\rm int}_{\rm coh} \approx \frac{\gamma}{12}(1-2s)s \quad \text{and} \quad \Gamma_\pi \approx 2\frac{\gamma}{9}(3-5s)s\,. \tag{2.47}$$

Figure 2.8(b) allows to summarize the effect of the interference terms on the fluorescence spectrum in the case of low saturation as follows. The spectrum without interference terms displays a narrow peak $S^\pi_{\rm peak}$ of finite width at the laser frequency that is absent if the interference terms are taken into account. Therefore, quantum interference cancels the incoherent response of the atom at the laser frequency ω_L.

In conclusion, the experimental observation of the fluorescence spectrum confirming the solid lines in Fig. 2.8 would give evidence for vacuum-mediated interference effects as described by terms proportional to γ_{12}. So far, interference effects of this kind have not been observed in atomic systems.

2.4 Spectrum of resonance fluorescence – σ transitions

This Section is concerned with a brief discussion of the fluorescence spectrum emitted on the σ transitions. Since the laser field does not couple to these transitions, the

spectrum contains only an incoherent part. We arrive at

$$S^{\sigma}(\tilde{\omega}) = \phi_{\sigma}\frac{b_{\sigma}\gamma}{\pi}\sum_{i=3}^{4}\mathrm{Re}\int_{0}^{\infty}e^{-i\tilde{\omega}\tau}\langle\,\delta\tilde{S}_{i}^{+}(\hat{t}+\tau)\delta\tilde{S}_{i}^{-}(\hat{t})\,\rangle_{\mathrm{st}}\,d\tau\;, \tag{2.48}$$

where ϕ_{σ} is a geometrical factor that we set equal to one in the following. It has been pointed out in Sec. 2.2 that the light emitted on the σ transitions is linearly polarized along $\boldsymbol{e}_x$ if the point of observation lies in the y direction. Therefore, the cross terms $\langle\,\delta\tilde{S}_{3}^{+}(\hat{t}+\tau)\delta\tilde{S}_{4}^{-}(\hat{t})\,\rangle_{\mathrm{st}}$ and $\langle\,\delta\tilde{S}_{4}^{+}(\hat{t}+\tau)\delta\tilde{S}_{3}^{-}(\hat{t})\,\rangle_{\mathrm{st}}$ will, in principle, contribute to the spectrum in Eq. (2.48). However, we find that the latter two-time averages are equal to zero. For different driving schemes where the laser field couples to the σ transitions, the cross-correlation terms have to be taken into account as is the case in the work of Polder et. al. [51]. The exact analytical expression for S^{σ} is too bulky to display it here. Instead we will discuss S^{σ} in the case of the degenerate system ($B=\delta=0$) and for different regimes of the driving field strength that will be characterized by means of the saturation parameter

$$s = \frac{2|\Omega|^2}{\Delta^2+\gamma^2/4}\;. \tag{2.49}$$

In the range from a weak to a moderately strong laser field ($s<1$), a numerical analysis reveals that S^{σ} can be written as

$$S^{\sigma}(\tilde{\omega}) \;\approx\; b_{\sigma}/b_{\pi}\,S^{\pi}_{\mathrm{inc}}(\tilde{\omega}) + S^{\sigma}_{\mathrm{peak}}(\tilde{\omega})\;. \tag{2.50}$$

In this equation, the first term stands for the incoherent spectrum of a two-level atom according to Eq. (2.40). The prefactor b_{σ}/b_{π} accounts for the different branching probability of the σ transitions as compared to the π transitions. The second term represents a narrow peak that is centered at the laser frequency $\omega=\omega_L$. It can be modeled as a Lorentzian of weight $\mathcal{W}_{\sigma}$ and width Γ_{σ},

$$S^{\sigma}_{\mathrm{peak}}(\tilde{\omega}) = \frac{\mathcal{W}_{\sigma}}{\pi}\,\frac{\Gamma_{\sigma}}{\tilde{\omega}^2+\Gamma_{\sigma}^2}\;. \tag{2.51}$$

The weight of $S^{\sigma}_{\mathrm{peak}}$ is determined by the total intensity emitted on the σ transitions,

$$I^{\sigma}_{\mathrm{st}} = b_{\sigma}\gamma(\tilde{\varrho}_{11}+\tilde{\varrho}_{22})\,, \tag{2.52}$$

and the weight of $b_{\sigma}/b_{\pi}\,S^{\pi}_{\mathrm{inc}}$. We arrive at

$$\mathcal{W}_{\sigma} = 4\,b_{\sigma}\gamma|\tilde{\varrho}_{13}|^2\,, \tag{2.53}$$

where $\tilde{\varrho}_{13}$ is given in Eq. (2.16). The width Γ_{σ} of the additional peak is smaller than the decay rate γ. If s is much smaller than unity, the width and the weight of $S^{\sigma}_{\mathrm{peak}}$ are given by

$$\begin{aligned}\mathcal{W}_{\sigma} &\approx b_{\sigma}\frac{\gamma}{2}(1-2s)s\,,\\ \Gamma_{\sigma} &\approx b_{\sigma}\frac{\gamma}{4}\big[2-(2+b_{\sigma})s\big]s\;.\end{aligned} \tag{2.54}$$

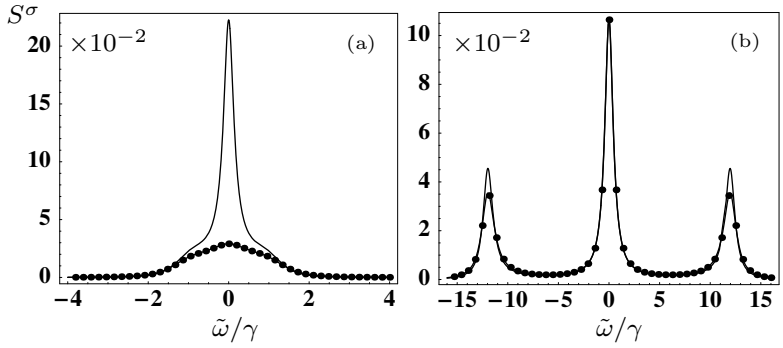

Figure 2.9: Spectrum of resonance fluorescence emitted on the σ transitions (solid line) in comparison with the fluorescence spectrum of a two-level atom (dotted line). The parameters in (a) are $\Omega = 5 \times 10^6\, s^{-1}$, $\Delta = 6 \times 10^6\, s^{-1}$ and $\gamma = 10^7\, s^{-1}$. In (b), the parameters are $\Omega = 6 \times 10^7\, s^{-1}$, $\Delta = 0$ and $\gamma = 10^7\, s^{-1}$. Note that S^σ deviates slightly from the Mollow triplet in the region of the sideband peaks in (b).

At the same time, the contribution of $S^\pi_{\rm inc}\, b_\sigma/b_\pi$ to S^σ is small such that the spectrum is dominated by the central narrow peak $S^\sigma_{\rm peak}$. If the field strength is increased, the weight of the extra peak $S^\sigma_{\rm peak}$ gets smaller. Figure 2.9(a) shows S^σ (solid line) and $S^\pi_{\rm inc}\, b_\sigma/b_\pi$ (dotted line) for a moderately strong laser field, the saturation parameter is on the order of unity. Nevertheless, the spectrum S^σ is still dominated by the sharp peak $S^\sigma_{\rm peak}$ that exceeds the central peak of the two-level spectrum by one order of magnitude.

For a strong driving field ($s \gg 1$), the weight of $S^\sigma_{\rm peak}$ goes to zero and the central peak of S^σ coincides with the corresponding peak of the Mollow spectrum. However, the sideband peaks of S^σ differ from those of a two-level atom as can be seen from Fig. 2.9(b). In the secular limit, it is advantageous to employ the dressed state picture in order to obtain analytic expressions for the sideband peaks, being well separated from the central peak whose analytic form can be taken over from the well-known results for a two-level atom [18, 56]. The fluorescence spectrum for a resonant driving field can be achieved by a tedious but straightforward calculation that follows the procedure of Chapter VI.E in [18],

$$\begin{aligned} S^\sigma(\tilde{\omega}) \;\approx\; & \gamma \frac{b_\sigma}{8\pi}\, \frac{\Gamma_{\rm sb}}{\Gamma_{\rm sb}^2 + (\Omega_1 - \tilde{\omega})^2} \\ & + \gamma \frac{b_\sigma}{4\pi}\, \frac{\gamma/2}{\gamma^2/4 + \tilde{\omega}^2} + \gamma \frac{b_\sigma}{8\pi}\, \frac{\Gamma_{\rm sb}}{\Gamma_{\rm sb}^2 + (\Omega_1 + \tilde{\omega})^2}\,, \end{aligned} \tag{2.55}$$

where $\Omega_1 = \sqrt{4|\Omega|^2 + \Delta^2}$. A comparison of the latter equation with the corresponding expression for the Mollow spectrum reveals that the weights of the sideband peaks differ only by the branching probability b_σ. For the width of the sideband

peaks in Eq. (2.55) we find

$$\Gamma_{\rm sb} = \frac{1}{4}\sqrt{\gamma_1\gamma_2} + \frac{\gamma}{2} = \frac{1}{4}(3 - b_\sigma)\gamma\,. \tag{2.56}$$

Note that the second equality is obtained by virtue of Eq. (2.12) . The ratio between the heights of the central peak at $\tilde{\omega} = 0$ and the sideband peaks at $\tilde{\omega} = \pm\Omega_1$ is found to be $3 - b_\sigma$. For $b_\sigma = 2/3$, the peak ratio is thus $3 : 7 : 3$. By contrast, the peak ratio of the Mollow spectrum reads $1 : 3 : 1$. A precise measurement of the peak ratio would thus provide a means of determining the branching probability b_σ of the degenerate system experimentally.

Note that the width of the sideband peaks in Eq. (2.56) depends on the cross-damping terms $\sqrt{\gamma_1\gamma_2}$ that appear in the master equation through the spontaneous emission term $\mathcal{L}_\gamma\tilde{\varrho}$ in Eq. (2.9). If these interference terms were not present, the peak ratio would not depend on the branching probabilities and would be given by $1 : 2 : 1$. The spectrum emitted on the σ transitions shows thus an indirect signature of interference.

2.5 Discussion

In Section 2.3 we have shown that the interference terms proportional to γ_{12} contribute only to the spectrum of resonance fluorescence, but not to the total intensity in Eq. (2.21). In the following, we demonstrate that this result is a consequence of the principle of complementarity, applied to time and energy.

If the total intensity is measured, complementarity does not impose any restrictions on the time resolution of the measurement since the photon energies are not observed. It is thus possible to observe the temporal aspect of the radiative cascade, i.e. one could determine the photon emission times. The time evolution of the driven atom is then most suitably described in the bare state basis. For example, assume that the atom is initially in ground state $|3\rangle$. The laser field will induce Rabi oscillations between the excited state $|1\rangle$ and $|3\rangle$. Immediately after the spontaneous emission of a photon, the atom is found in ground state $|3\rangle$ (π transition) or $|4\rangle$ (σ transition). Subsequently, this sequence of Rabi oscillations and a spontaneous emission event is repeated. In this description, each emission process on one of the π transitions is independent of the other π transition. In particular, the transition amplitudes associated with the emission of a *single* π photon on one transition do neither share a common initial state nor a common final state with the transition amplitudes associated with the other π transition. Since quantum interference does only occur if various indistinguishable transition amplitudes connect a common initial state to a common final state, we must conjecture that the total intensity is not affected by interference.

The lack of interference in the total intensity can also be explained by drawing an analogy to the two-slit experiment. It is well known that the interference pattern vanishes as soon as it is principally possible to know through which of the two slits

each object (electrons or photons) has moved. Similarly, the internal states of our atom can be regarded as a which-way marker. Since the experimental conditions allow, at least in principle, to determine the atomic ground state immediately after the detection of a π-photon, one could decide on which of the two π-transitions the photon was emitted. Consequently, the observer could reveal the quantum path taken by the system and hence there is no signature of interference. Note that this argument requires that the retardation between the times of emission and detection is much smaller than the time between successive emissions. This condition can typically be achieved in atomic systems.

A totally different situation arises if the detector measures the spectrum of resonance fluorescence and hence the energy of the emitted photons. Since time and energy are complementary observables, the temporal aspect of the radiative cascade is not accessible simultaneously. In order to illustrate this point, we consider a quantitative description of time-energy complementarity that can be achieved via the time-energy uncertainty. If the photon energies are determined with a precision of $\Delta\omega$, the time-energy uncertainty relation enforces that the time of observation has to be at least on the order of $1/\Delta\omega$. Since the observer can only notice the detection of a photon after the observation time has elapsed, the photon emission times are indeterminate within a time interval of $\Delta t = 1/\Delta\omega$. For the moment we envisage an ideal measurement of the fluorescence spectrum. In this case, the atom will emit (infinitely) many photons during the (infinite) time of observation. In addition, the photon emission times are indeterminate, and thus the time order in which these photons have been emitted is unknown. It follows that the transition amplitudes corresponding to the various time orderings of the photons will interfere.

The energy aspect of the cascade of spontaneously emitted photons is most suitably described in the dressed state picture rather than in the bare state picture. We illustrate the interference mechanism on the basis of Fig. 2.10 that shows a cascade of only two photons in the dressed state picture, one emitted on a π transition and the other on a σ transition. Assume that the atom is initially in the dressed state $|4(N)\rangle$. In one of the two cascades, the atom decays first to the state $|4(N-1)\rangle$ by the emission of a π photon on the bare state transition $|2\rangle \rightarrow |4\rangle$. The subsequent emission of a σ photon takes the atom to the state $|1(N-2)\rangle$ within the manifold with $N-2$ laser photons. In the second cascade, the time order of the two photons is reversed. The atom decays now first to the state $|1(N-1)\rangle$ by the emission of a σ photon, and then to the final state $|1(N-2)\rangle$ under the emission of a π photon. In contrast to the first cascade, this π photon is now emitted on the bare state transition $|1\rangle \rightarrow |3\rangle$. Since the two cascades in Fig. 2.10 have the same initial and final states, and since it is in principle impossible to determine the quantum path taken by the system, the two transition amplitudes corresponding to different time orders of photon emissions interfere. In one of the transition amplitudes the π photon stems from the $|2\rangle \rightarrow |4\rangle$ transition, and in the other from the $|1\rangle \rightarrow |3\rangle$ transition. Exactly this mechanism gives rise to the interference effects in the fluorescence spectrum that are mediated by the cross-damping terms in Eq. (2.24). Note that the difference δ between the resonance frequencies of the π transitions enters the definition of

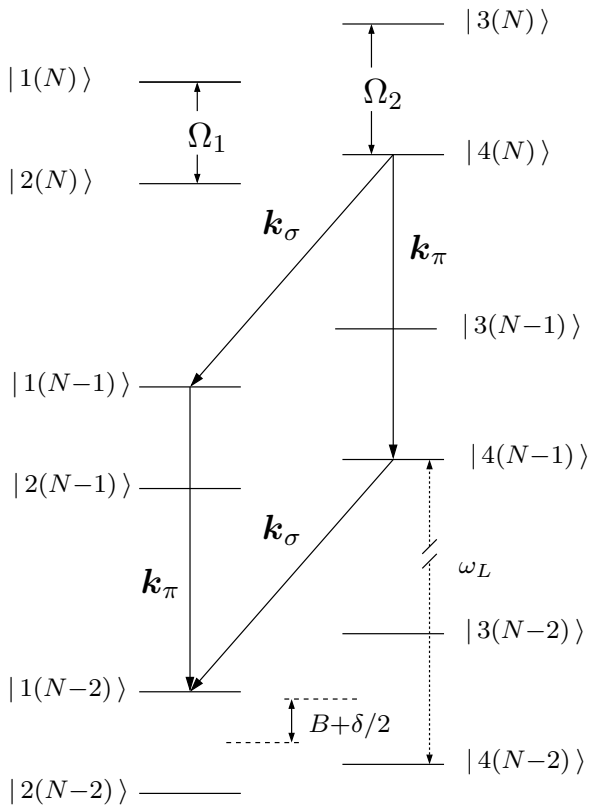

Figure 2.10: Radiative cascade in the dressed states of the system [see Eqs. (2.42) and (2.43)]. The splitting of the dressed states for a fixed number of laser photons N is not to scale. Each of the two indicated cascades involves the emission of a π photon and a σ photon with wave vector $\boldsymbol{k}_\pi$ and $\boldsymbol{k}_\sigma$, respectively. Depending on the time order of their emission, the π photon is either emitted on transition $|4(N)\rangle \rightarrow |4(N-1)\rangle$ or $|1(N-1)\rangle \rightarrow |1(N-2)\rangle$, corresponding to the bare state transitions $|2\rangle \rightarrow |4\rangle$ and $|1\rangle \rightarrow |3\rangle$, respectively. Since the final and initial states of the two cascades are identical, the corresponding transition amplitudes may interfere.

the dressed states Eqs. (2.42) and (2.43) asymmetrically, giving rise to different probabilities for the two cascades. This explains why the degree of interference is maximal only for $\delta = 0$ and decreases with increasing $|\delta|$ (see Sec. 2.3).

The provided explanation can also be employed to illustrate why there is no interference in the fictitious situation of perpendicular dipole moments $\boldsymbol{d}_1$ and $\boldsymbol{d}_2$. In this case, a photon can either stem from $\boldsymbol{d}_1$ or $\boldsymbol{d}_2$, but not from both transitions. It is then impossible to realize both cascades in Fig. 2.10, and hence there is no interference. Moreover, it becomes now clear why the spectrum emitted on the σ transitions depends on the interference terms γ_{12} and γ_{21}. For antiparallel dipole moments $\boldsymbol{d}_1$ and $\boldsymbol{d}_2$ there are two transition amplitudes that involve the emission of a σ photon , and for perpendicular dipole moments there would be only one. We emphasize that

the discussion has been restricted to a cascade of only two photons for the sake of simplicity. In principle, all possible cascades with an arbitrary number of photons have to be considered, but the general idea remains the same.

It is also possible to provide an explanation for the interference in the coherent spectrum, but the elastic scattering events cannot be visualized in the dressed state basis. However, in the case of low saturation ($s \ll 1$) the process of elastic scattering can be illustrated in the bare state basis such that the atom hops from one ground state to another by the absorption of a laser photon and the emission of a scattered photon. The excited states act as intermediate states and can be adiabatically eliminated. Since it is impossible to tell on which of the two π transitions the photon was scattered, it is plausible that one has to sum the scattering amplitudes first and then take the absolute value squared in order to obtain the weight of the Rayleigh line in Eq. (2.38).

Next we demonstrate how the interfering transition amplitudes that correspond to different time orders of photon emissions enter the expression for the spectrum of resonance fluorescence in Eq. (2.24). Let a_π ($a_\pi^\dagger$) be the annihilation (creation) operator of a photon in a mode of the radiation field that is actually observed by the detector, being sensitive only to photons emitted on the π transitions. The rate at which the photon number in this particular mode changes is given by

$$R_\pi(t) = \partial_t \, \langle \, a_\pi^\dagger(t) a_\pi(t) \, \rangle \; . \tag{2.57}$$

If one follows the lines of Chapter 7 in [10], one can show that the steady-state value of R_π is proportional to the spectrum of resonance fluorescence,

$$\lim_{t\to\infty} R_\pi(t) \sim S^\pi(c\,|\boldsymbol{k}_\pi| - \omega_L) \; . \tag{2.58}$$

In this equation, $\boldsymbol{k}_\pi$ denotes the wave vector that corresponds to the observed mode a_π, and c is the speed of light. In order to evaluate the left hand side of Eq. (2.58), we will label the basis states $|i(N);\,\{n\}\rangle$ of the total system (atom + laser field + vacuum modes) by three quantum numbers, namely the dressed states i, the number of laser photons N and the state of the vacuum modes $\{n\}$. The mean value on the right hand side of Eq. (2.57) becomes then

$$\langle \, a_\pi^\dagger(t) a_\pi(t) \, \rangle = \sum_{i=1}^{4} \sum_{N,\,\{n\}} |C^i_{N,\{n\}}(t)|^2 \, N_\pi(\{n\}) \; , \tag{2.59}$$

where $|C^i_{N,\{n\}}(t)|^2$ is the probability to find the system at time t in state $|i(N);\,\{n\}\rangle$ and $N_\pi(\{n\})$ is the expectation value of $a_\pi^\dagger a_\pi$ in this state. We assume that the system is in some initial state $|\psi_0\rangle$ at time $t = 0$ with all vacuum modes being empty. If the time evolution operator is labeled by $U(t,0)$, the transition amplitude from the initial state $|\psi_0\rangle$ to the final state $|i(N);\,\{n\}\rangle$ can be written as

$$C^i_{N,\{n\}}(t) = \langle i(N);\,\{n\}|U(t,0)|\psi_0\rangle \; . \tag{2.60}$$

Let us assume that the final state contains q scattered photons that are characterized by their wave and polarization vectors, $\{n\} = \{\boldsymbol{k}_\pi \boldsymbol{\epsilon}_\pi, \boldsymbol{k}_2 \boldsymbol{\epsilon}_2, \ldots, \boldsymbol{k}_q \boldsymbol{\epsilon}_q\}$. We do not attempt to evaluate Eq. (2.60) explicitly, but in principle one would introduce $q-1$ intermediate states and arrange the q scattered photons into a certain order. But since there is no distinguished time order of the scattered photons, there are, in principle, $q!$ transition amplitudes involved in the evaluation of Eq. (2.60) that will all interfere.

In conclusion, we demonstrated that the interference in the spectrum from the π transitions can be explained in terms of interference between transition amplitudes that correspond to different time orders of photon emissions. If the spectrum of resonance fluorescence is observed, the principle of complementarity enforces that these transition amplitudes are indistinguishable. If the total intensity is recorded by a broadband detector, the temporal aspect of the radiative cascade can in principle be observed. Consequently, the possibility of interference between different time orders of photon emissions is ruled out. The preceding discussion of our results also implies that the experimental setup—potentially after the photon emissions—decides if interference takes place, a feature that is also known from quantum eraser schemes [49, 58].

We now refine our analysis and consider a detector with a finite frequency resolution $\Delta\omega$ that allows us to study the continuous transition from perfect frequency resolution to perfect time resolution. For simplicity, we consider only the degenerate system ($B = \delta = 0$). If a filter of bandwidth λ and setting frequency ω is placed in front of a broadband detector, the spectrum can be determined with an accuracy of λ, and the temporal resolution is on the order of λ^{-1}. The spectrum of resonance fluorescence emitted on the π transitions reads then [59]

$$S^\pi(\tilde{\omega}, \lambda) = \frac{1}{\pi} \sum_{i,\,j=1}^{2} \gamma_{ij}\, \mathrm{Re} \int_0^\infty e^{-i\tilde{\omega}\tau} e^{-\lambda\tau} \langle\, \tilde{S}_i^+(\hat{t}+\tau) \tilde{S}_j^-(\hat{t})\, \rangle_{\mathrm{st}}\, d\tau\,. \tag{2.61}$$

In the absence of interference terms the spectrum will be denoted by $S_0^\pi(\tilde{\omega}, \lambda)$ and is obtained from Eq. (2.61) by omitting the terms proportional to γ_{12} and γ_{21}. For the rest of this Section we assume that the saturation parameter s is much smaller than unity. To a first approximation, the incoherent contribution to the spectrum with interference terms can then be neglected. In the presence of the filter, the coherent δ-peak becomes a Lorentzian of width λ and weight $I_{\mathrm{coh}}^0 + I_{\mathrm{coh}}^{\mathrm{int}}$, and thus we obtain

$$S^\pi(\tilde{\omega}, \lambda) \approx \frac{I_{\mathrm{coh}}^0 + I_{\mathrm{coh}}^{\mathrm{int}}}{\pi} \frac{\lambda}{\tilde{\omega}^2 + \lambda^2}\,. \tag{2.62}$$

Similarly, we neglect the contribution of S_{inc}^π to the spectrum without interference terms in Eq. (2.45), the δ-peak becomes a Lorentzian of width λ and weight I_{coh}^0, and S_{peak}^π is replaced by a Lorentzian of width $\Gamma_\pi + \lambda$ and weight $I_{\mathrm{coh}}^{\mathrm{int}}$,

$$S_0^\pi(\tilde{\omega}, \lambda) \approx \frac{I_{\mathrm{coh}}^0}{\pi} \frac{\lambda}{\tilde{\omega}^2 + \lambda^2} + \frac{I_{\mathrm{coh}}^{\mathrm{int}}}{\pi} \frac{\Gamma_\pi + \lambda}{\tilde{\omega}^2 + (\Gamma_\pi + \lambda)^2}\,. \tag{2.63}$$

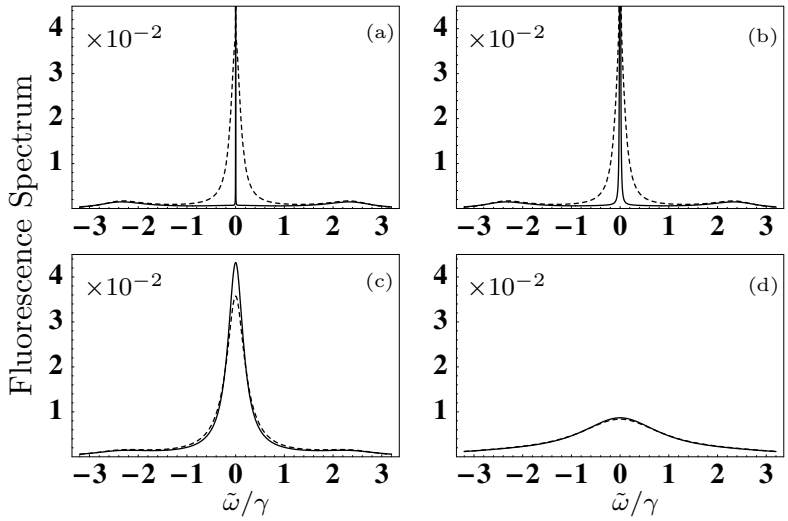

Figure 2.11: The solid lines show the fluorescence spectra recorded with a finite frequency resolution λ. The dashed curves are the spectra without the interference terms proportional to γ_{12}, γ_{21} in Eq. (2.61). The parameters are $\Omega = 7{\times}10^6 s^{-1}$, $\Delta = 2{\times}10^7 s^{-1}$, $\gamma = 10^7 s^{-1}$ and $B = \delta = 0$. This corresponds to a saturation parameter of $s = 0.235$ and a mean number of photons per unit time of approximately $9.4{\times}10^5 s^{-1}$. The filter bandwidths are given by (a) $\lambda = 10^2 s^{-1}$, (b) $\lambda = 10^4 s^{-1}$, (c) $\lambda = 1.9 \times 10^6 s^{-1}$ and (d) $\lambda = 10^7 s^{-1}$.

Figure 2.11 shows the fluorescence spectrum according to Eq. (2.61) (solid lines) for different values of the filter bandwidth λ and for low saturation. The dashed lines are the spectra without the interference terms. In Fig. 2.11(a), the bandwidth λ is much smaller than Γ_π. Therefore, the widths of the lines $S^\pi(\tilde{\omega}, \lambda)$ and $S_0^\pi(\tilde{\omega}, \lambda)$ are clearly distinct. If λ is increased, the differences between the spectra with and without the interference terms diminish until both curves are virtually identical for $\lambda = \gamma$ [Fig. 2.11(d)].

These results can be understood as follows. With an increasing filter bandwidth λ, the smallest time interval Δt that can be resolved by the detector without violating the time-energy uncertainty gets shorter. Therefore, the observer can in principle obtain more information about the quantum path taken by the atom. Consequently, we expect that the signature of interference in the fluorescence spectrum diminishes for increasing λ. This is in agreement with Fig. 2.11 and completely analogous to a two-slit experiment, where the visibility of the interference pattern is reduced at the cost of which-path information and vice versa [60].

Furthermore, we demonstrate that the time-energy uncertainty relation allows to estimate the smallest filter bandwidth λ for which the spectra with and without interference terms should be indistinguishable. Since the total number of photons emitted per unit time is equal to $\gamma(\tilde{\varrho}_{11} + \tilde{\varrho}_{22})$, the mean time between successive

photon emissions is determined by $\bar{\Theta} = 1/[\gamma(\tilde{\varrho}_{11} + \tilde{\varrho}_{22})]$. If the bandwidth λ is chosen such that the temporal resolution could be much better than the mean time between successive photon emissions, i.e. $\lambda^{-1} \ll \bar{\Theta} = 1/[\gamma(\tilde{\varrho}_{11} + \tilde{\varrho}_{22})]$, we have

$$\lambda \gg \gamma(\tilde{\varrho}_{11} + \tilde{\varrho}_{22}) \approx (1 - s)s\gamma/2 \; . \tag{2.64}$$

Under these conditions, the radiative cascade of photons could be observed in a time resolved way and it is extremely unlikely that more than one spontaneous emission takes place during the time of observation. Since this rules out the interference mechanism as described in Sec. 2.5, the signature of interference in the fluorescence spectrum should disappear. But if inequality (2.64) holds, it follows that $\lambda \gg \Gamma_\pi$, and in this case $S^\pi(\tilde{\omega}, \lambda)$ and $S_0^\pi(\tilde{\omega}, \lambda)$ are indeed indistinguishable as can be seen from Eqs. (2.62) and (2.63). This is confirmed by Fig. 2.11(d) that shows $S_0^\pi(\tilde{\omega}, \lambda)$ and $S^\pi(\tilde{\omega}, \lambda)$ for a bandwidth λ that is about ten times larger than the mean number of photons emitted per unit time. The two spectra are now virtually indistinguishable.

It remains to explain the sharp peaks in the incoherent spectrum. To this end we return to Fig. 2.6 that shows the incoherent spectrum $S_{\rm inc}^\pi$ for several values of the parameter δ. A narrow central peak occurs only in case of the non-degenerate system ($\delta \neq 0$), and thus only if the weight of the Rayleigh line deviates from its maximal value attained at $\delta = 0$. Therefore, the narrow central peak in the incoherent spectrum may be regarded as a (partially) broadened coherent peak. This broadening can be understood as follows. Except for $\delta = 0$, the two π transitions are not equivalent since the absolute value and the phase of the coherences $\langle\, \tilde{S}_1^+ \,\rangle_{\rm st}$ and $\langle\, \tilde{S}_2^+ \,\rangle_{\rm st}$ will be different. The time that the atom spends on the $1 \leftrightarrow 3$ transition can thus be regarded as a dark period with respect to the $2 \leftrightarrow 4$ transition and vice versa. This suggests that the sharp peaks in the incoherent spectrum can be explained in terms of electron shelving [61–63]. This explanation is also applicable to the sharp peak in the spectrum from the σ transitions. Figure 2.12 illustrates the scattering events that give rise to this peak. If the atom is initially in state $|3\rangle$, a scattering event can bring it to state $|4\rangle$ (solid arrows). The scattered photon has then been emitted on one of the σ transitions. Before the next photon can be

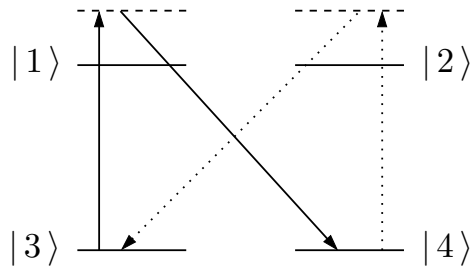

Figure 2.12: Schematic representation of elastic scattering events into the $3 \to 1 \to 4$ (solid arrows) and $4 \to 2 \to 3$ channels (dotted arrows). These processes account for the sharp peak in the fluorescence spectrum S^σ emitted on the σ transitions.

scattered on that same transition, a similar scattering process has to take place into the $4 \rightarrow 2 \rightarrow 3$ channel (dotted arrows). Consequently, every emission on one of the σ transitions is followed by a dark period on that same transition.

It should be mentioned that related interference effects between transition amplitudes corresponding to different time orders of photon emissions do also play a role in other systems. A discussion of these effects in the fluorescence spectrum of a two-level atom can be found in [64] and in Sec. 2.2.3 of [65], for example. In addition, it was shown that interference in the time-energy domain can occur in the intensity correlations between different spectral components of the fluorescence light emitted by a two-level atom [66–68]. However, the distinguished feature of the system presented here is that this mechanism gives rise to interference effects between the two π transitions that do not share a common state.

We would also like to point out that the work presented here is related to recent double-slit experiments in the time-energy domain [69, 70]. In these experiments, ultra-short laser pulses of atto- or femtosecond duration open different time windows for the photoionization of an atom. If the energy spectrum of the photoelectrons is measured, these time-slits are indistinguishable and an interference pattern is observed.

2.6 Summary

We have shown that the system in Figs. 2.2 and 2.3 exhibits a signature of quantum interference in the spectrum of resonance fluorescence under conditions of no interference in the total intensity, being enforced by the principle of complementarity. For the system considered here, it claims that it is impossible to observe the temporal and the energy aspect of the radiative cascade of the atom at the same time. If the fluorescence spectrum is observed, the photon emission times are indeterminate. The interference in the fluorescence spectrum can thus be explained in terms of interferences between transition amplitudes that correspond to different time orders of photon emissions.

It has been shown that the degree of interference in the fluorescence spectrum emitted on the π transitions can be controlled by means of an external magnetic field. In particular, the degree of interference in the coherent part of the spectrum can be adjusted from perfect constructive to perfect destructive interference. Under conditions of perfect destructive interference, the weight of the Rayleigh line is completely suppressed. If the difference δ between the resonance frequencies of the π transitions is different from zero, the incoherent spectrum emitted on the π transitions contains a very narrow peak whose width is smaller than the decay rate γ. This peak has been identified as a partially broadened coherent peak and can be explained in terms of electron shelving.

The spectrum emitted on the σ transitions contains only an incoherent part. In the case of a weak driving field and for the degenerate system, the fluorescence spec-

trum displays a narrow peak that can be regarded as broadened coherent peak. For a strong driving field, the widths of the sideband peaks differ from the Mollow spectrum. We have shown that the ratio between the peak heights of the central and the sideband peaks display an indirect signature of interference. In addition, a measurement of the relative peak heights allows to determine the branching probability b_σ of the spontaneous decay of each excited state into the σ channel.

2.A Calculation of the two-time averages

In this section we outline how the functions

$$S_{ij}(\tilde{\omega}) = \mathrm{Re} \int_0^\infty e^{-i\tilde{\omega}\tau} \langle\, \delta\tilde{S}_i^+(\hat{t}+\tau)\delta\tilde{S}_j^-(\hat{t})\,\rangle_{\mathrm{st}}\, d\tau \;. \tag{2.65}$$

can be evaluated by means of the quantum regression theorem [71, 72]. To this end we introduce the operators $\mathcal{A}_{ij}$ that are connected to the atomic transition operators A_{ij} (taken in the Schrödinger picture) by

$$\mathcal{A}_{ij} = W^\dagger A_{ij} W \;, \tag{2.66}$$

where the unitary transformation W is defined in Eq. (2.6). In particular, the operators $\tilde{S}_i^\pm$ introduced in Sec. (2.2) can be identified with the operators $\mathcal{A}_{ij}$ according to

$$\tilde{S}_1^+ = \mathcal{A}_{13}\,, \quad \tilde{S}_2^+ = \mathcal{A}_{24}\,, \quad \tilde{S}_3^+ = \mathcal{A}_{23}\,, \quad \tilde{S}_4^+ = \mathcal{A}_{14}\;. \tag{2.67}$$

The corresponding Heisenberg operators are then defined as

$$\mathcal{A}_{ij}(t) = U^\dagger(t,0)\,\mathcal{A}_{ij}\,U(t,0)\;, \tag{2.68}$$

and the time evolution operator has been labeled by U. A straightforward calculation shows that the mean values of the these Heisenberg operators are directly related to the matrix elements of the reduced density operator $\tilde{\varrho}$ in the rotating frame,

$$\langle\, \mathcal{A}_{ij}(t)\,\rangle = \mathrm{Tr}_{\mathrm{A}}\big[A_{ij}\tilde{\varrho}(t)\big] = \tilde{\varrho}_{ji}(t)\;. \tag{2.69}$$

In this equation, $\mathrm{Tr}_{\mathrm{A}}[\,\cdot\,]$ denotes the trace over atomic degrees of freedom. Next we arrange the operators $\mathcal{A}_{ij}$ in a column vector

$$\boldsymbol{L} = (\mathcal{A}_{11}, \mathcal{A}_{21}, \mathcal{A}_{31}, \mathcal{A}_{41}, \mathcal{A}_{12}, \mathcal{A}_{22}, \mathcal{A}_{32}, \mathcal{A}_{42}, \mathcal{A}_{13}, \mathcal{A}_{23}, \mathcal{A}_{33}, \mathcal{A}_{43}, \mathcal{A}_{14}, \mathcal{A}_{24}, \mathcal{A}_{34})^{\mathrm{T}}$$

such that $\langle\, \boldsymbol{L}(t)\,\rangle$ coincides with the Bloch vector $\boldsymbol{R}(t)$ of Eq. (2.15), i.e. $\langle\, \boldsymbol{L}(t)\,\rangle = \boldsymbol{R}(t)$. It follows that the mean values $\langle\, \boldsymbol{L}(t)\,\rangle$ obey the generalized Bloch Equation (2.13). If we decompose each component of $\boldsymbol{L}$ in mean values an fluctuations according to $\mathcal{A}_{ij} = \delta\mathcal{A}_{ij} + \langle\, \mathcal{A}_{ij}\,\rangle_{\mathrm{st}}\mathbb{1}$, we can cast $\langle\, \boldsymbol{L}\,\rangle$ into the form

$$\langle\, \boldsymbol{L}(t)\,\rangle = \langle\, \delta\boldsymbol{L}(t)\,\rangle + \langle\, \boldsymbol{L}\,\rangle_{\mathrm{st}}\;, \tag{2.70}$$

where $\langle\, \boldsymbol{L}\,\rangle_{\mathrm{st}} = \boldsymbol{R}_{\mathrm{st}} = -\mathcal{M}^{-1}\boldsymbol{I}$. If Eq. (2.70) is plugged into Eq. (2.13) we obtain a homogeneous equation of motion for the fluctuations,

$$\partial_t \langle\, \delta\boldsymbol{L}(t)\,\rangle = \mathcal{M}\,\langle\, \delta\boldsymbol{L}(t)\,\rangle\;. \tag{2.71}$$

The two-time correlation functions $\langle\, \delta L_i(\hat{t}+\tau)\delta L_j(\hat{t})\,\rangle$ for $i \in \{1,\ldots,15\}$ and fixed j can be written in vector notation as $\boldsymbol{g}^j(\hat{t},\tau) = \langle\, \delta\boldsymbol{L}(\hat{t}+\tau)\delta L_j(\hat{t})\,\rangle$. According to

the quantum regression theorem, $\boldsymbol{g}^j$ obeys the same equation of motion than the one-time averages $\langle\, \delta \boldsymbol{L}(t)\,\rangle$,

$$\partial_\tau \boldsymbol{g}^j = \mathcal{M}\, \boldsymbol{g}^j \qquad \text{for} \quad \tau \geq 0\ . \tag{2.72}$$

If $\boldsymbol{G}^j(\hat{t}, z)$ denotes the Laplace transform of $\boldsymbol{g}^j(\hat{t}, \tau)$ with respect to τ, it follows

$$\boldsymbol{G}^j(\hat{t}, z) = [z\,\mathbb{1} - \mathcal{M}]^{-1}\, \boldsymbol{g}^j(\hat{t}, 0)\ . \tag{2.73}$$

We need the Laplace transform at $z = i\tilde{\omega}$ in steady state to determine the functions $S_{ij}(\tilde{\omega})$ of Eq. (2.65). With the definitions

$$\boldsymbol{R}^j = \lim_{\hat{t}\to\infty} \boldsymbol{g}^j(\hat{t}, 0) \quad \text{and} \quad \boldsymbol{K}^j(\tilde{\omega}) = \lim_{\hat{t}\to\infty} \boldsymbol{G}^j(\hat{t}, z = i\tilde{\omega}) \tag{2.74}$$

we arrive at

$$\boldsymbol{K}^j(\tilde{\omega}) = \left[i\tilde{\omega}\,\mathbb{1} - \mathcal{M}\right]^{-1} \boldsymbol{R}^j\ . \tag{2.75}$$

The relevant correlation functions that are needed for the evaluation of Eq. (2.36) and (2.48) are then given by

$$\begin{aligned} S_{11}(\tilde{\omega}) &= \mathrm{Re}\left[\boldsymbol{K}^3(\tilde{\omega})\right]_9 \qquad S_{21}(\tilde{\omega}) = \mathrm{Re}\left[\boldsymbol{K}^3(\tilde{\omega})\right]_{14} \\ S_{22}(\tilde{\omega}) &= \mathrm{Re}\left[\boldsymbol{K}^8(\tilde{\omega})\right]_{14} \qquad S_{12}(\tilde{\omega}) = \mathrm{Re}\left[\boldsymbol{K}^8(\tilde{\omega})\right]_9 \\ S_{33}(\tilde{\omega}) &= \mathrm{Re}\left[\boldsymbol{K}^7(\tilde{\omega})\right]_{10} \qquad S_{44}(\tilde{\omega}) = \mathrm{Re}\left[\boldsymbol{K}^4(\tilde{\omega})\right]_{13}\ . \end{aligned} \tag{2.76}$$

Finally, we remark that Eq. (2.61) can be evaluated if one replaces $i\tilde{\omega}$ in Eq. (2.75) by $i\tilde{\omega} + \lambda$.

Part III

Dipole-dipole interaction beyond the two-level approximation

Chapter 3

Geometry-dependent dynamics via vacuum-induced coherences

3.1 Introduction

In collections of nearby atoms, the various particles can interact via the common vacuum radiation field in a process where a (virtual) photon emitted by one of the atoms is re-absorbed by another atom. This process is illustrated in Fig. 3.1 for a pair of two-level atoms with excited state $|e\rangle$ and ground state $|g\rangle$. If the distance between two particles does not significantly exceed the involved transition wavelength, this exchange of photons gives rise to a collective quantum dynamics of the system, which can significantly deviate from a corresponding single-particle dynamics. Collective effects have been studied in various physical systems. Apart from larger ensembles of nearby quantum objects which require a statistical treatment [10–12, 73–83], also few-particle quantum systems have attained considerable interest [14, 17, 84–97]. These systems reveal interesting cooperative effects, but are still small enough such that the constituents can be treated individually. Sub- and superradiance was studied, e.g., in [10, 12, 73, 78], while two-atom resonance fluorescence was discussed in [84]. Other studies include frequency shifts [87], collective quantum jumps [89, 90], two-photon resonances [88], or entanglement [91–93]. Some of these effects have been verified experimentally [94–97]. Further references on collective two-atom systems can be found, e.g., in [14, 75]. Most of these works have focussed on two-level systems, often restricted to somewhat special geometries. For example, the alignment of the transition dipole moments, the interatomic distance vectors, the laser field wave vectors and the observation direction are often assumed fixed and parallel or perpendicular to each other.

The exchange of photons between a pair of atoms as depicted in Fig. 3.1 requires that the polarization of the emitted photon matches the absorbing transition [10, 11]. Thus usually this dipole-dipole interaction is thought to couple only non-orthogonal transition dipole moments. This restriction is in complete analogy to the stringent

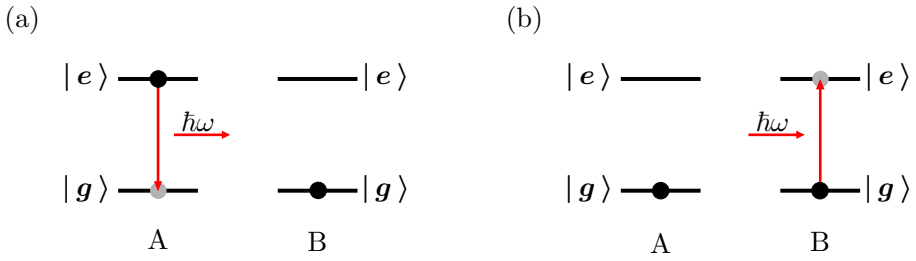

Figure 3.1: Illustration of the dipole-dipole interaction for a pair of two-level atoms. (a) Atom A deexcites and emits a photon with energy $\hbar\omega$. Atom B is in its ground state. (b) Atom B is excited to the state $|e\rangle$ by the absorption of the photon previously emitted by atom A. The total process in which the excitation of one atom is transferred to the other atom is of second order in the atom-field interaction.

conditions for the appearance of spontaneous-emission interference in single-particle systems, which was studied in chapters 1 and 2.

Recently, a collection of two nearby three-level systems in V-configuration was studied in a more general geometric setup [17], with the emphasis on vacuum-mediated couplings. Interestingly, the authors found a new type of vacuum-induced coherences, which arises from dipole-dipole coupling of transitions with *orthogonal* dipole moments. In [17], however, only little physical interpretation of the effect is given, and no external driving field but the vacuum was considered.

Thus in this chapter, we study two nearby laser-driven three-level systems in Λ-configuration as shown in Fig. 3.2. We demonstrate that the vacuum-induced dipole-dipole coupling of orthogonal transition dipole moments can crucially influence the dynamics of the laser-driven system. For otherwise fixed parameters and experimental setup, the relative position of the two atoms alone can decide whether the system has a stationary steady state or not. The non-stationary steady states occur even though each of the involved atomic transitions is driven by a single laser field only. As an example observable, we discuss the total fluorescence intensity emitted by the composite system, which is either stationary or "blinks" at a characteristic frequency in the long-time limit. In the final part, we give a physical interpretation for the new coherences, and show that the coupling of orthogonal dipole moments can be explained in terms of the dipole radiation pattern.

Our results are of relevance for experimental realizations of collective few-level systems. If the system geometry is not fixed to one of few special cases, then additional interactions between the considered transitions lead to a non-trivial modification of the dynamics. Furthermore, unwanted couplings to additional transitions can occur via the vacuum, even if no laser field is applied to the unwanted transitions. Then, for example, a few-level approximation of the system may break down (see chapter 4). Finally, the geometry-dependent effects provide an extended set of observables in the study of samples of nearby atoms. Potential applications include

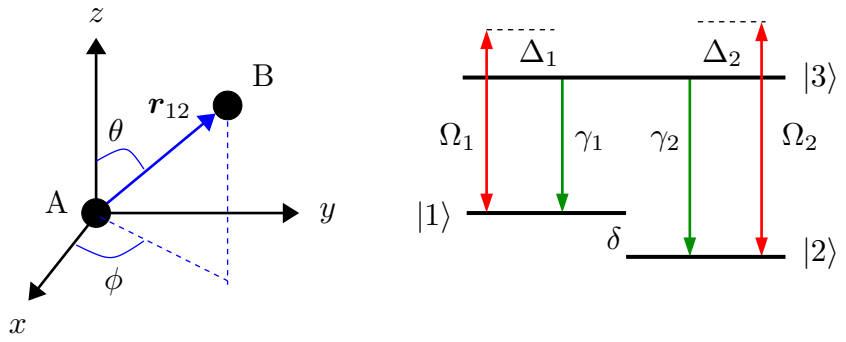

Figure 3.2: The system setup. Atom A is located in the coordinate origin, atom B at $\boldsymbol{r}_{12}$, as shown in the left part of the figure. In our coordinate system, the atomic separation vector is parameterized by the length r_{12} and the angles θ, ϕ. Internally, both atoms (A,B) are three-level systems in Λ configuration as shown in the right subfigure. Ω_1 (Ω_2) is the Rabi frequency of the driving laser field coupling to transition $1 \leftrightarrow 3$ ($2 \leftrightarrow 3$) with detuning Δ_1 (Δ_2). The two lower states have frequency difference δ. The spontaneous decay rates are γ_1, γ_2.

three-dimensional precision measurements of relative positions and distances of the involved particles.

This chapter is organized as follows. In Sec. 3.2, we introduce the system of interest and analytically derive the expressions for the emitted fluorescence intensity. In the following Sec. 3.3, we numerically solve the master equation and present our results. In Sec. 3.4, we provide a physical interpretation of the new coherences and explain why orthogonal transition dipoles can be coupled. Finally, our results are discussed and summarized in Sec. 3.5.

3.2 Analytical considerations

We consider two three-level systems in Λ-configuration as shown in Fig. 3.2. We place the origin of the coordinate system at the location of the first atom, $\boldsymbol{r}_1 = (0,0,0)^{\mathrm{T}}$, and the second atom is located at $\boldsymbol{r}_2 = \boldsymbol{r}_{12} = r_{12}\,(\sin\theta\cos\phi, \sin\theta\sin\phi, \cos\theta)^{\mathrm{T}}$. Thus the atomic separation vector is $\boldsymbol{r}_{12}$. The two lower states of the atomic level scheme in Fig. 3.2(a) have an energy separation δ. The two transition dipole moments of each individual atom are orthogonal to each other as, e.g., for the case of Zeeman sublevels. For simplicity, we assume real dipole moments. The dipole moment $\boldsymbol{d}_1$ of the $1 \leftrightarrow 3$ transition is taken to be identical for both atoms, and aligned in the x direction. The second dipole moment $\boldsymbol{d}_2$ corresponding to the $2 \leftrightarrow 3$ transition is oriented along the y direction for both atoms. The free time evolution of the two

atoms is described by the Hamiltonian

$$H_{\rm A} = \hbar \sum_{\mu=1}^{2} \sum_{j=1}^{3} \omega_j \, A_{jj}^{(\mu)} \,, \tag{3.1}$$

where $A_{jj}^{(\mu)} = |j_\mu\rangle\langle j_\mu|$, and $\hbar\omega_j$ is the energy of state $|j\rangle$ of each of the atoms. The atoms interact with two classical laser fields that are characterized by their frequencies ν_j, polarization unit vectors $\boldsymbol{\epsilon}_j$ and amplitudes $\mathcal{E}_j$. Both fields propagate in z direction. In rotating-wave approximation (RWA), the interaction of the two atoms with the driving laser fields is governed by

$$H_{\rm L} = -\hbar \sum_{\mu=1}^{2} \left[\Omega_1(\boldsymbol{r}_\mu) e^{-i\nu_1 t} S_{1+}^{(\mu)} + \Omega_2(\boldsymbol{r}_\mu) e^{-i\nu_2 t} S_{2+}^{(\mu)} + \text{H.c.} \right] , \tag{3.2}$$

where the atomic transition operators are defined as

$$S_{1+}^{(\mu)} = |3_\mu\rangle\langle 1_\mu| \,, \qquad S_{1-}^{(\mu)} = |1_\mu\rangle\langle 3_\mu| \,, \tag{3.3}$$

$$S_{2+}^{(\mu)} = |3_\mu\rangle\langle 2_\mu| \,, \qquad S_{2-}^{(\mu)} = |2_\mu\rangle\langle 3_\mu| \,. \tag{3.4}$$

The Rabi frequencies in Eq. (3.2) are given by

$$\Omega_j(\boldsymbol{r}) = \Omega_j \exp[i\boldsymbol{k}_j \cdot \boldsymbol{r}] \,, \quad \text{where} \quad \Omega_j = (\boldsymbol{d}_j \cdot \boldsymbol{\epsilon}_j)\mathcal{E}_j/\hbar \tag{3.5}$$

and $\boldsymbol{k}_j = \nu_j \boldsymbol{e}_z/c$ are the wave vectors of the laser fields.

In a suitable interaction picture, the master equation for the atomic density operator ϱ can be written as (see chapter 1)

$$\begin{aligned}
\partial_t \varrho = & -i \sum_{\mu=1}^{2} \sum_{j=1}^{2} \left[\Delta_j A_{jj}^{(\alpha)}, \varrho \right] + i \sum_{\mu=1}^{2} \sum_{j=1}^{2} \left[\left(S_{j+}^{(\mu)} \Omega_j(\boldsymbol{r}_\mu) + \text{H.c.} \right), \varrho \right] \\
& - \sum_{\mu=1}^{2} \sum_{j=1}^{2} \gamma_j \left(S_{j+}^{(\mu)} S_{j-}^{(\mu)} \varrho + \varrho S_{j+}^{(\mu)} S_{j-}^{(\mu)} - 2 S_{j-}^{(\mu)} \varrho S_{j+}^{(\mu)} \right) \\
& - \sum_{j=1}^{2} \left\{ \Gamma_j^{dd} \left(S_{j+}^{(2)} S_{j-}^{(1)} \varrho + \varrho S_{j+}^{(2)} S_{j-}^{(1)} - 2 S_{j-}^{(1)} \varrho S_{j+}^{(2)} \right) + \text{H.c.} \right\} \\
& - \sum_{\substack{\mu,\nu=1 \\ \mu\neq\nu}}^{2} \left\{ \Gamma_{vc}^{dd} \left(S_{2+}^{(\mu)} S_{1-}^{(\nu)} \varrho + \varrho S_{2+}^{(\mu)} S_{1-}^{(\nu)} - 2 S_{1-}^{(\nu)} \varrho S_{2+}^{(\mu)} \right) e^{i\Delta t} + \text{H.c.} \right\} \\
& + \sum_{j=1}^{2} \left\{ i\Omega_j^{dd} \left[S_{j+}^{(2)} S_{j-}^{(1)}, \varrho \right] + \text{H.c.} \right\} + \sum_{\substack{\mu,\nu=1 \\ \mu\neq\nu}}^{2} \left\{ i\Omega_{vc}^{dd} \left[S_{2+}^{(\mu)} S_{1-}^{(\nu)}, \varrho \right] e^{i\Delta t} + \text{H.c.} \right\} .
\end{aligned} \tag{3.6}$$

In this equation, we have $\Delta = \delta + \Delta_2 - \Delta_1 = \nu_2 - \nu_1$, where $\delta = \omega_{12}$, $\Delta_i = \nu_i - \omega_{3i}$, and $\omega_{ij} = \omega_i - \omega_j$. Note that the fourth and fifth lines of Eq. (3.6) contain a

time-dependent exponential factor that oscillates with Δ. Thus the residual time dependence can be traced back to the frequency difference of the two driving laser fields, even though each atomic transition is driven by a single laser field only. The first term on the right hand side of Eq. (3.6) contains the detunings Δ_i of the driving laser fields and is due to the chosen interaction picture. The second contribution with $\Omega_j(\boldsymbol{r}_\mu)$ contains the interaction with the driving laser fields. The term with γ_j describes the usual individual spontaneous decay on each of the transitions, where the spontaneous emission rate on transition $3 \leftrightarrow j$ is given by $2\gamma_j$. The term proportional to Γ_j^{dd} contains the dipole-dipole cross-decay between a dipole of one of the atoms and the corresponding parallel dipole of the other atom. The contribution with Ω_j^{dd} is the corresponding dipole-dipole energy shift. Finally, Γ_{vc}^{dd} and Ω_{vc}^{dd} are the cross-coupling and the energy shift related to dipole-dipole interaction between a dipole of one of the atoms and the *perpendicular* dipole of the other atom. These are due to the peculiar vacuum-coupling of transitions with perpendicular dipole moments, which do not occur in single-atom systems. The physical interpretation of these terms will be given in section 3.5. The explicit expressions for the dipole-dipole coupling constants are given by (see chapter 1)

$$\Gamma_j^{dd} = \Gamma_{jj} = \frac{1}{\hbar}\left[\boldsymbol{d}_j^{\mathrm{T}} \overleftrightarrow{\chi}_{\mathrm{im}}(\boldsymbol{r}_{12})\, \boldsymbol{d}_j\right], \tag{3.7}$$

$$\Omega_j^{dd} = \Omega_{jj} = \frac{1}{\hbar}\left[\boldsymbol{d}_j^{\mathrm{T}} \overleftrightarrow{\chi}_{\mathrm{re}}(\boldsymbol{r}_{12})\, \boldsymbol{d}_j\right], \tag{3.8}$$

$$\Gamma_{vc}^{dd} = \Gamma_{21} = \frac{1}{\hbar}\left[\boldsymbol{d}_2^{\mathrm{T}} \overleftrightarrow{\chi}_{\mathrm{im}}(\boldsymbol{r}_{12})\, \boldsymbol{d}_1\right], \tag{3.9}$$

$$\Omega_{vc}^{dd} = \Omega_{21} = \frac{1}{\hbar}\left[\boldsymbol{d}_2^{\mathrm{T}} \overleftrightarrow{\chi}_{\mathrm{re}}(\boldsymbol{r}_{12})\, \boldsymbol{d}_1\right]. \tag{3.10}$$

Note that we assumed real dipole moments $\boldsymbol{d}_1$ and $\boldsymbol{d}_2$.

In the following, we will investigate the fluorescence intensity emitted by the pair of atoms and measured by a detector at point $\boldsymbol{R} = R\hat{\boldsymbol{R}}$. It is proportional to the normally ordered correlation function

$$I = \left\langle \hat{\boldsymbol{E}}^{(-)}(\boldsymbol{R},t)\, \hat{\boldsymbol{E}}^{(+)}(\boldsymbol{R},t)\right\rangle, \tag{3.11}$$

where $\hat{\boldsymbol{E}}(\boldsymbol{r},t) = \hat{\boldsymbol{E}}^{(+)}(\boldsymbol{r},t) + \hat{\boldsymbol{E}}^{(-)}(\boldsymbol{r},t)$ and $\hat{\boldsymbol{E}}^{(\pm)}(\boldsymbol{r},t)$ are the positive and negative frequency parts of the vacuum field with $[\hat{\boldsymbol{E}}^{(+)}(\boldsymbol{r},t)]^\dagger = \hat{\boldsymbol{E}}^{(-)}(\boldsymbol{r},t)$. We write the positive frequency part of the electric field operator as

$$\hat{\boldsymbol{E}}^{(+)}(\boldsymbol{r},t) = i\hbar \sum_{\boldsymbol{k}s} \boldsymbol{u}_{\boldsymbol{k}s}(\boldsymbol{r})\, a_{\boldsymbol{k}s}\,, \tag{3.12}$$

where the mode function $\boldsymbol{u}_{\boldsymbol{k}s}(\boldsymbol{r})$ is defined in Eq. (1.8). The Heisenberg equation of motion for the annihilation operator $a_{\boldsymbol{k}s}$ is given by

$$\begin{aligned}\frac{d}{dt}a_{\boldsymbol{k}s} &= \frac{1}{i\hbar}[a_{\boldsymbol{k}s}, H_{\mathrm{A}} + H_{\mathrm{F}} + H_{\mathrm{L}} + V] \\ &= -i\omega_k a_{\boldsymbol{k}s} + \sum_{\mu=1}^{2}\left[\boldsymbol{d}_1\left(S_{1+}^{(\mu)} + S_{1-}^{(\mu)}\right) + \boldsymbol{d}_2\left(S_{2+}^{(\mu)} + S_{2-}^{(\mu)}\right)\right]\boldsymbol{u}_{\boldsymbol{k}s}^*(\boldsymbol{r}_\mu)\,,\end{aligned} \tag{3.13}$$

where H_A and H_L are given in Eqs. (3.1) and (3.2), respectively. H_F is the free Hamiltonian of the radiation field which is defined in Eq. (1.4), and

$$V = -\sum_{\mu=1}^{2}\left[\left(\boldsymbol{d}_1 S_{1+}^{(\mu)} + \boldsymbol{d}_2 S_{2+}^{(\mu)}\right)\cdot\hat{\boldsymbol{E}}(\boldsymbol{r}_\mu) + \mathrm{H.c.}\right] \tag{3.14}$$

describes the interaction of the atoms with the quantized modes of the radiation field. By formally integrating the expression for $a_{\boldsymbol{k}s}$, the electric field operator in the far field limit $R \gg r_{12}$ can be derived. It can be split up in a source part and a free part, where the latter can be neglected if the detector is placed outside of the laser field. The source part $\hat{\boldsymbol{E}}_S^{(+)}(\boldsymbol{R},t)$ of the electric field operator evaluates to

$$\hat{\boldsymbol{E}}_S^{(+)}(\boldsymbol{R},t) = -\frac{1}{4\pi\varepsilon_0 R}\sum_{\mu=1}^{2}\sum_{j=1}^{2}\frac{\omega_{3j}^2}{c^2}\hat{\boldsymbol{R}}\times(\hat{\boldsymbol{R}}\times\boldsymbol{d}_j)S_{j-}^{(\mu)}(t)\,e^{-ik_j\hat{\boldsymbol{R}}\cdot\boldsymbol{r}_\mu}\,. \tag{3.15}$$

Here, we have ignored retardation effects [98]. Then the intensity can be written as

$$\begin{aligned} I = &\sum_{j=1}^{2}\left(w_j^2\sum_{\mu,\nu=1}^{2}\left\langle S_{j+}^{(\mu)}S_{j-}^{(\nu)}\right\rangle e^{ik_j\hat{\boldsymbol{R}}\cdot(\boldsymbol{r}_\mu-\boldsymbol{r}_\nu)}\right) \\ &-\bar{w}_1\,\bar{w}_2\sum_{\mu,\nu=1}^{2}\left(\left\langle S_{1+}^{(\mu)}S_{2-}^{(\nu)}\right\rangle e^{i\hat{\boldsymbol{R}}\cdot(k_1\boldsymbol{r}_\mu-k_2\boldsymbol{r}_\nu)} + \left\langle S_{2+}^{(\mu)}S_{1-}^{(\nu)}\right\rangle e^{i\hat{\boldsymbol{R}}\cdot(k_2\boldsymbol{r}_\mu-k_1\boldsymbol{r}_\nu)}\right), \end{aligned} \tag{3.16}$$

with prefactors $w_j = \alpha_j\sin\varphi_j$ and $\bar{w}_j = \alpha_j\cos\varphi_j$, where $\alpha_j = (\omega_{3j}^2 d_j)/(4\pi\varepsilon_0 c^2 R)$. The angle between the observation direction $\hat{\boldsymbol{R}}$ and the dipole moment $\boldsymbol{d}_j$ is φ_j. Note that the expectation values in Eq. (3.16) should be evaluated with respect to the Schrödinger picture density matrix of the system. The first line of Eq. (3.16) contains the individual emission of each of the two transitions $1 \leftrightarrow 3$ and $2 \leftrightarrow 3$ from both of the atoms. The other two lines are cross terms which contain contributions of both transitions. In the following, we assume our detector to be placed on the y axis, i.e. $\hat{\boldsymbol{R}} = (0,1,0)^\mathrm{T}$. Then $\sin\varphi_2 = 0 = \cos\varphi_1$, and the intensity reduces to

$$I_y = w_1^2\sum_{\mu,\nu=1}^{2}\left\langle S_{1+}^{(\mu)}S_{1-}^{(\nu)}\right\rangle e^{ik_1\hat{\boldsymbol{R}}\cdot(\boldsymbol{r}_\mu-\boldsymbol{r}_\nu)}\,. \tag{3.17}$$

3.3 Numerical results

In this section, we numerically integrate the density matrix Eq. (3.6) for the configuration outlined in the previous section. Thus the first atom is at the coordinate origin, the second atom is at position $\boldsymbol{r}_{12}$, the laser fields propagate in the z direction, and the detector is placed in the y direction. We fix all parameters except for the angles θ and ϕ which determine the 3D orientation of the two-atom system. As

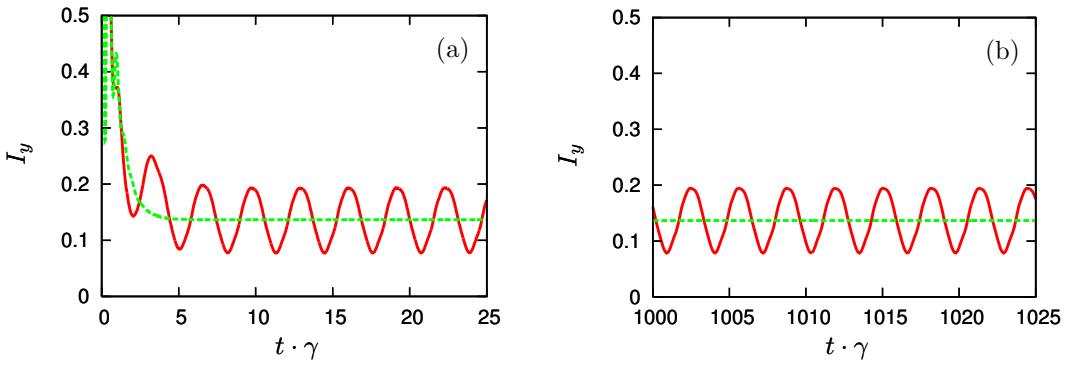

Figure 3.3: The time-dependent fluorescence intensity I_y. The parameters chosen are $\Omega_1 = 3\gamma$, $\Omega_2 = 5\gamma$, $\delta = 0$, $\Delta_1 = 0$, $\Delta_2 = 2\gamma$, $r_{12} = 0.1\lambda$, and $\phi = \pi/4$. The solid line corresponds to $\theta = \pi/2$, the dashed line is for $\theta = 0$. (a) Short-time evolution, (b) long-time limit. The oscillatory behavior of the intensity for $\theta = \pi/2$ remains undamped in the long-time limit.

initial conditions, we choose both atoms to be in the excited state $|3\rangle$. Our main observable is the total fluorescence intensity I_y given in Eq. (3.17).

Fig. 3.3 shows the intensity I_y for $\Omega_1 = 3\gamma$, $\Omega_2 = 5\gamma$, $\delta = 0$, $\Delta_1 = 0$, $\Delta_2 = 2\gamma$, $r_{12} = 0.1\lambda$, $\phi = \pi/4$, and for two different values of θ: $\theta = 0, \pi/2$. It can be seen that after an initial phase of rapid changes in the intensity, the sample comes to a time-independent steady state for $\theta = 0$, whereas it undergoes periodic changes for $\theta = \pi/2$. These changes persist undamped in the dynamics, as can be seen in Fig. 3.3(b), which shows the intensity for same parameters as in Fig. 3.3(a), but for times $t > 1000\gamma^{-1}$.

The interpretation of this effect is straightforward: For $\theta = 0$, the dipole-dipole cross-couplings Γ_{vc}^{dd} and Ω_{vc}^{dd} are zero. Thus the coefficients on the right hand side

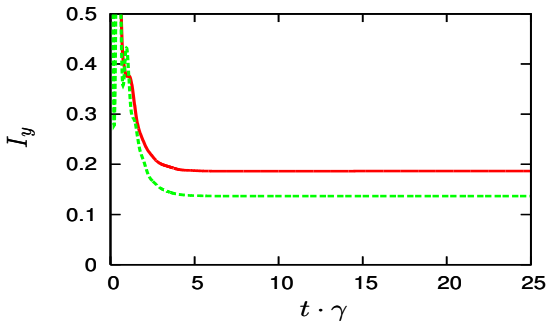

Figure 3.4: Same as in Fig. 3.3, but with $\delta = -2\gamma$ and thus $\Delta = 0$. In this case, both for $\theta = 0$ and $\theta = \pi/2$, the long-time limit intensity is time-independent.

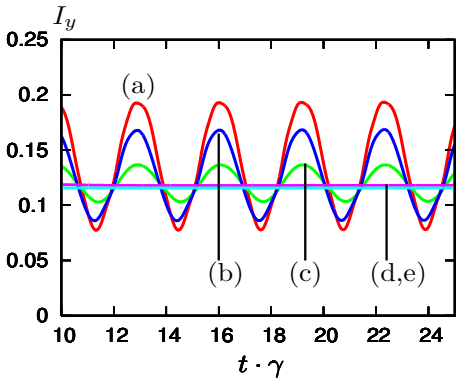

Figure 3.5: Dependence of the modulation of the fluorescence in the long-time limit on the angle ϕ. (a) $\phi = 0.25\pi$, (b) $\phi = 0.1\pi$, (c) $\phi = 0.4\pi$, (d) $\phi = 0$, (e) $\phi = 0.5\pi$. The other parameters are as in Fig. 3.3 with $\theta = \pi/2$.

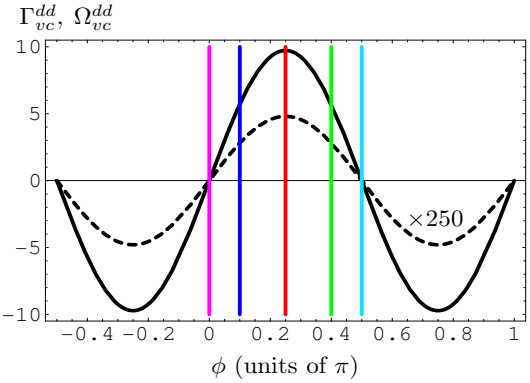

Figure 3.6: Dependence of the coupling constants Γ_{vc}^{dd} and Ω_{vc}^{dd} on the angle ϕ. The parameters are as in Fig. 3.5. The solid curve shows Ω_{vc}^{dd}, the dashed curve is for $250 \times \Gamma_{vc}^{dd}$. The vertical lines indicate the phase values shown in Fig. 3.5.

of the master equation Eq. (3.6) are time-independent, and the system approaches a time-independent steady state. For $\theta = \pi/2$, the dipole-dipole cross-couplings Γ_{vc}^{dd} and Ω_{vc}^{dd} are non-zero, and induce an explicit time-dependence in the master equation coefficients, which accounts for the non-stationary long time behavior. This effect is somewhat similar to a two-level system driven by a bichromatic field. Also in this case, the long-time limit is non-stationary. In our system under conditions where the dipole-dipole cross-couplings are non-zero, each transition is driven both by a laser field and by the cross coupling contribution. In general, these two contributions have different detunings, and thus induce the non-stationary behavior. This interpretation can easily be verified. The interaction picture in Eq. (3.6) is chosen such that the only time dependence that may occur is $\exp(\pm i\Delta t)$, where $\Delta = \delta + \Delta_2 - \Delta_1$ is a combination of the laser field detunings and the frequency difference of the two lower states. If the non-stationary behavior is due to this time dependence, then the system should approach a constant steady state for any geometry if $\Delta = 0$. This is indeed the case, as can be seen in Fig. 3.4. Here, the same parameters as in Fig. 3.3 are shown except for $\delta = -2\gamma$, such that $\Delta = 0$. Both for $\theta = 0$ and $\theta = \pi/2$, the system approaches a true steady state. Note that the one may also rewrite the frequency of the time dependence as $\Delta = \nu_2 - \nu_1$, i.e., the difference of the two driving field frequencies. This further substantiates the interpretation along the lines of a bichromatic driving of each of the atomic transitions.

Next we study the dependence of the long-time limit on the angle ϕ. For this, we take parameters as in Fig. 3.3 with $\theta = \pi/2$ and $\phi = 0; 0.1\pi; 0.25\pi; 0.4\pi; 0.5\pi$. The result is shown in Fig. 3.5. It can be seen that the angle ϕ modifies the depth of the intensity modulations. For $\phi = 0$ and $\phi = 0.5\pi$, there a no modulations, as then the dipole-dipole cross coupling vanishes. The maximum modulation occurs

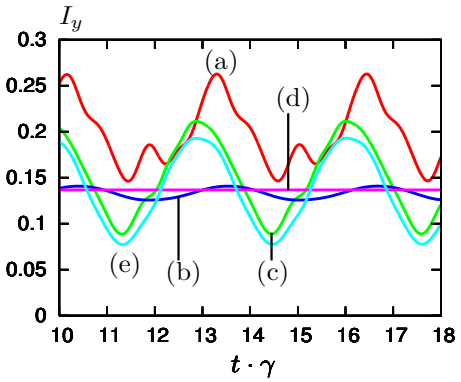

Figure 3.7: Dependence of the modulation of the fluorescence in the long-time limit on the angle θ. (a) $\theta = 0.25\pi$, (b) $\theta = 0.1\pi$, (c) $\theta = 0.4\pi$, (d) $\theta = 0$, (e) $\theta = 0.5\pi$. The other parameters are as in Fig. 3.3 with $\phi = \pi/4$.

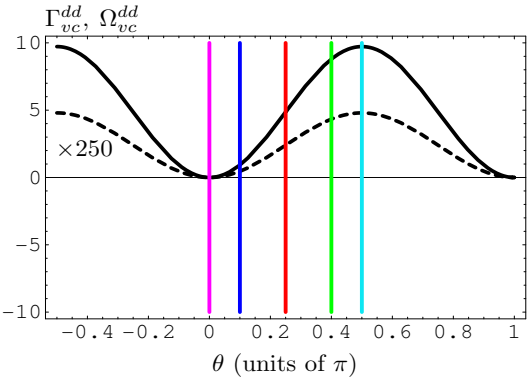

Figure 3.8: Dependence of the coupling constants Γ_{vc}^{dd} and Ω_{vc}^{dd} on the angle θ. The parameters are as in Fig. 3.7. The solid curve shows Ω_{vc}^{dd}, the dashed curve is for $250 \times \Gamma_{vc}^{dd}$. The vertical lines indicate the phase values shown in Fig. 3.7.

for $\phi = 0.25\pi$, intermediate modulations are obtained for $\phi = 0.1\phi$ and $\phi = 0.4\pi$.

The dependence on ϕ can be understood by looking at the ϕ-dependence of the vacuum-induced coupling constants Γ_{vc}^{dd} and Ω_{vc}^{dd}, see Fig. 3.6. The total fluorescence intensity has a time independent long-time behavior for phase values where the coupling constants vanish. For maximum coupling constants, the intensity modulation is maximum. The modulation amplitude cannot, however, be understood in terms of the coupling constants only. For $\phi = 0.1\pi$ and $\phi = 0.4\pi$, the coupling constants have identical values, while the fluorescence intensity has different modulation amplitudes. The reason for this is that the angle ϕ also enters the fluorescence intensity via the exponential of the cross terms in Eq. (3.17), where the two ϕ values yield different results.

The dependence on θ is shown in Fig. 3.7, with the dependence of the corresponding vacuum-induced couplings in Fig. 3.8. As for the angle ϕ, the modulation vanishes for vanishing couplings Γ_{vc}^{dd} and Ω_{vc}^{dd}. The interpretation in terms of the magnitude of the coupling constants, however, is difficult as a change of θ also has impact on other variables. This arises mainly from the fact that θ determines the relative position of the two atoms with respect to the laser propagation direction, such that the Rabi frequencies Ω_j depend on θ.

The study of the influence of the various detunings is somewhat complicated by the fact that for equal detunings of the driving fields, the system moves into a dark state due to coherent population trapping, such that the intensity is zero. Thus in Fig. 3.9, we show the dependence of the intensity long-time limit modulation on the lower-level splitting δ for $\Delta_2 = -\Delta_1 = \gamma$. Thus one has $\Delta = \delta + 2\gamma$, and it is not surprising that the frequency of the modulation decreases with decreasing δ until there is no modulation for $\delta = -2\gamma$.

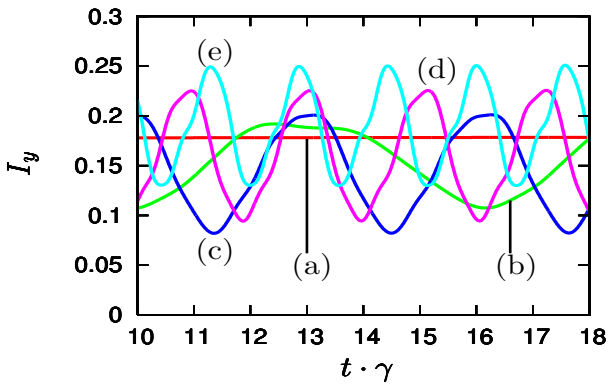

Figure 3.9: Dependence of the modulation of the fluorescence in the long-time limit on the lower-state splitting δ. Parameters are as in Fig. 3.3 with $\theta = \pi/2$, but with $\Delta_1 = -\gamma$ and $\Delta_2 = \gamma$. (a) $\delta = -2\gamma$, (b) $\delta = -\gamma$, (c) $\delta = 0$, (d) $\delta = \gamma$, (e) $\delta = 2\gamma$.

3.4 Physical interpretation of the new coherences

In this section we investigate the physical origin of the cross-coupling terms Γ_{vc}^{dd} and Ω_{vc}^{dd} that arise from the interaction between a dipole of one of the atoms and the *perpendicular* dipole of the other atom.

In general, vacuum-mediated interactions arise from an emission of a photon on one transition and the absorption of the photon on the same or another transition. In a single atom, such interactions where the absorbing and the emitting transition are the same lead to the complex Lamb shift. Any dipole-dipole interaction between different dipole moments, however, for a single atom in plain vacuum strictly requires the dipoles to be non-orthogonal (see chapters 1 and 2). This is clearly the case since the dipole moments must couple to a common set of modes.

In contrast, in the present case of two atoms separated by a distance r_{12}, the cross-coupling terms Γ_{vc}^{dd} and Ω_{vc}^{dd} can be different from zero although the two involved dipole moments are orthogonal. As in a single atom, a coupling between dipole moments of different atoms is only possible if the involved transitions couple to a common set of modes, i.e. photons emitted by one transition can be absorbed on a transition of the other atom. Here we illustrate why this condition can be fulfilled even between orthogonal dipole moments belonging to different atoms. For this, we return to the equation of motion Eq. (3.12) for the field modes $a_{\boldsymbol{k}s}$ and keep only the source contribution from the transition $1 \leftrightarrow 3$ of atom 1. The corresponding

electric field operator reads then

$$\hat{\boldsymbol{E}}^{(1)}_{\boldsymbol{d}_1}(\boldsymbol{r},t) = \sum_{\boldsymbol{k}s} \boldsymbol{u}_{\boldsymbol{k}s}(\boldsymbol{r}) \int_0^t d\tau e^{-i\omega_k \tau} \times \left[\boldsymbol{d}_1 \cdot \boldsymbol{u}^*_{\boldsymbol{k}s}(\boldsymbol{r}_1)\right] \left[S^{(1)}_{1-}(t-\tau) + S^{(1)}_{1+}(t-\tau)\right] + \text{H.c.}\,. \tag{3.18}$$

The aim is to evaluate Eq. (3.18) at the position $\boldsymbol{r}_2$ of atom 2. In contrast to the derivation of Eq. (3.15), the calculation has to be performed without taking the far field limit since the atoms are close to each other. We follow the steps outlined in chapter 8 of [10] and obtain

$$\hat{\boldsymbol{E}}^{(1)}_{\boldsymbol{d}_1}(\boldsymbol{r}_2,t) = S^{(1)}_{1-}(t) \overleftrightarrow{\chi}(\boldsymbol{r}_{12}) \cdot \boldsymbol{d}_1 + \text{H.c.} \tag{3.19}$$

$$= S^{(1)}_{1-}(t) \left[f_1(k_0, r_{12})\, \boldsymbol{d}_1 - f_2(k_0, r_{12})\, \frac{(\boldsymbol{d}_1 \cdot \boldsymbol{r}_{12})\, \boldsymbol{r}_{12}}{r_{12}^2} \right] + \text{H.c.}\,, \tag{3.20}$$

where

$$f_1(k_0, r_{12}) = \frac{k_0^3}{4\pi\varepsilon_0} \left(\frac{1}{\eta} + \frac{i}{\eta^2} - \frac{1}{\eta^3} \right) e^{i\eta}\,,$$

$$f_2(k_0, r_{12}) = \frac{k_0^3}{4\pi\varepsilon_0} \left(\frac{1}{\eta} + \frac{3i}{\eta^2} - \frac{3}{\eta^3} \right) e^{i\eta}\,, \tag{3.21}$$

and $\eta = k_0 r_{12}$. $\hat{\boldsymbol{E}}^{(1)}_{\boldsymbol{d}_1}(\boldsymbol{r}_2,t)$ can be regarded as the field radiated by the dipole $\boldsymbol{d}_1$ of atom 1 at the position of atom 2. Note that a similar expression is obtained in the case of a classical radiating dipole at $\boldsymbol{r}_1$ (see, e.g., chapter 2.2.3 in [99]). Obviously, the polarization of $\hat{\boldsymbol{E}}^{(1)}_{\boldsymbol{d}_1}(\boldsymbol{r}_2,t)$ depends on the relative orientation of the atoms. In particular, from Eq. (3.20) it follows that $\hat{\boldsymbol{E}}^{(1)}_{\boldsymbol{d}_1}(\boldsymbol{r}_2,t)$ contains not only a contribution along $\boldsymbol{d}_1$, but also a term proportional to $\boldsymbol{r}_{12}$. Therefore, a photon emitted by atom 1 on the $1 \leftrightarrow 3$ transition can be absorbed by atom 2 on the $2 \leftrightarrow 3$ transition, provided that the projection of $\boldsymbol{r}_{12}$ onto $\boldsymbol{d}_2$ is different from zero, i.e. $\boldsymbol{r}_{12} \cdot \boldsymbol{d}_2 \neq 0$. The dipole moment $\boldsymbol{d}_1$ of atom 1 can thus be coupled to the orthogonal dipole moment $\boldsymbol{d}_2$ of atom 2 since the field radiated by the former dipole moment may exhibit a component along the latter dipole moment.

In order to verify the consistency of this explanation, we consider the projection of $\hat{\boldsymbol{E}}^{(1)}_{\boldsymbol{d}_1}(\boldsymbol{r}_2,t)$ onto $\boldsymbol{d}_2$. This expression should exhibit the same dependence on the relative position $\boldsymbol{r}_{12}$ of the two atoms as the cross-coupling terms Γ^{dd}_{vc} and Ω^{dd}_{vc}. In fact, with the help of Eqs. (3.9), (3.10) and (3.19) we arrive at

$$\boldsymbol{d}_2 \cdot \hat{\boldsymbol{E}}^{(1)}_{\boldsymbol{d}_1}(\boldsymbol{r}_2,t) = \hbar\Omega^{dd}_{vc} \left(S^{(1)}_{1-}(t) + S^{(1)}_{1+}(t) \right) + i\hbar\Gamma^{dd}_{vc} \left(S^{(1)}_{1-}(t) - S^{(1)}_{1+}(t) \right)\,. \tag{3.22}$$

It follows that the real and imaginary parts of $\boldsymbol{d}_2 \cdot \hat{\boldsymbol{E}}^{(1)}_{\boldsymbol{d}_1}(\boldsymbol{r}_2,t)$ show indeed the same dependence on r_{12}, θ and ϕ as the coupling coefficients Ω^{dd}_{vc} and Γ^{dd}_{vc}, respectively.

From another point of view, the preceding discussion shows that for certain relative positions of the atoms each dipole of atom 2 interacts with both dipoles of atom 1 and vice versa. We finally perform a thought experiment and replace atom 2 by a photodetector with a polarization filter in front of it. The question is now if this detector is able to discriminate between photons that stem from dipole moments $\boldsymbol{d}_1$ and $\boldsymbol{d}_2$ of atom 1. Surprisingly, the answer is no since the fields radiated by $\boldsymbol{d}_1$ and $\boldsymbol{d}_2$ are never orthogonal to each other at any position where Γ_{vc}^{dd} and Ω_{vc}^{dd} are different from zero. In this sense, the orthogonal dipole moments of different atoms are forced to interact, since the absorbing atom cannot distinguish between photons originating from the two transitions of the emitting atom.

3.5 Summary and discussion

In the previous Sec. 3.4, we have shown that the peculiar vacuum-induced coupling of orthogonal transition dipole moments can be understood in terms of the dipole radiation pattern. For certain geometries, the field emitted by one transition of the first atom has components parallel to each of the transition dipole moments of the second atom, even if the emitting and absorbing dipoles are orthogonal. Thus the second atom cannot decide on which transition the photon was emitted by the first atom.

Speaking generally, this result is of relevance for experimental realizations of collective few-level systems. In real atoms, the realization of simple level schemes like a Λ system or even a two-level system typically involves the omission of Zeeman sublevels. The usual justification for this few-level approximation is that the relevant transitions can be selected via the polarization of the driving fields. Since the vacuum-induced coupling of orthogonal dipole moments may populate unwanted extra energy levels, even if they are not driven by the laser field, the few-level approximation may lead to incorrect results (see chapter 4).

The collective effects in samples of atoms arise from vacuum-induced dipole-dipole couplings between transitions in different atoms. These couplings are analogous to virtual interactions of a single transition and the vacuum, which gives rise to the complex Lamb shift, and to virtual interactions between different transitions in a single atom, responsible for spontaneously generated coherences between a pair of atomic states. The coupling of orthogonal dipole moments by the exchange of photons discussed here, however, is not possible in single atoms interacting with the plain isotropic vacuum. Therefore the vacuum-coupling of orthogonal dipole moments observed here is a collective effect.

In summary, we have discussed the dynamics of a pair of nearby three-level systems in Λ-configuration. We have shown that in contrast to the single-atom case, transitions in the two atoms can be dipole-dipole coupled via the vacuum field even if the transition dipole moments are orthogonal. This additional coupling can strongly affect the system dynamics. For otherwise fixed parameters, the relative position of the two atoms alone can decide whether the system has a stationary steady state

or not. As a consequence, the total fluorescence intensity emitted by the composite system is either stationary or "blinks" at a characteristic frequency in the long-time limit, depending on the alignment of the two atoms. The coupling of orthogonal dipole moments occurs if the absorbing atom is unable to distinguish between photons emitted by the two transitions of the other atom.

Chapter 4

Breakdown of the few-level approximation in collective systems

4.1 Introduction

The theoretical analysis of any non-trivial physical problem typically requires the use of approximations. A key approximation facilitated in most areas of physics reduces the complete configuration space of the system of interest to a smaller set of relevant system states. In the theoretical description of atom-field interactions, the essential state approximation entails neglecting most of the bound and continuum atomic states [1, 10, 11]. The seminal Jaynes-Cummings-Model [100] takes this reduction to the extreme in that only two atomic states are retained. Obviously, it is essential to in detail explore the validity range of this reduction of the configuration space. The few-level approximation usually leads to theoretical predictions that are well verified experimentally [1, 11], and is generally considered as understood for single-atom systems. It fails, however, to reproduce results of quantum electrodynamics, where in general all possible intermediate atomic states need to be considered in order to obtain quantitatively correct results [101]. The situation becomes even less clear in collective systems, where the individual constituents interact via the dipole-dipole interaction, despite the relevance of collectivity to many areas of physics. Examples for such systems can be found in ultracold quantum gases [102–104], trapped atoms [94, 96, 105], or solid state systems [97, 106], with possible applications, e.g., in quantum information theory [91, 107–109].

Therefore, we discuss the validity of the few-level approximation in dipole-dipole interacting collective systems. For this, we study the archetype case of two dipole-dipole interacting atoms, see Fig. 4.1(a). Experiments of this type have become possible recently [94, 96, 106]. In order to remain general, each atom is modelled by complete sets of angular momentum multiplets, as shown in Fig. 4.1(b). We

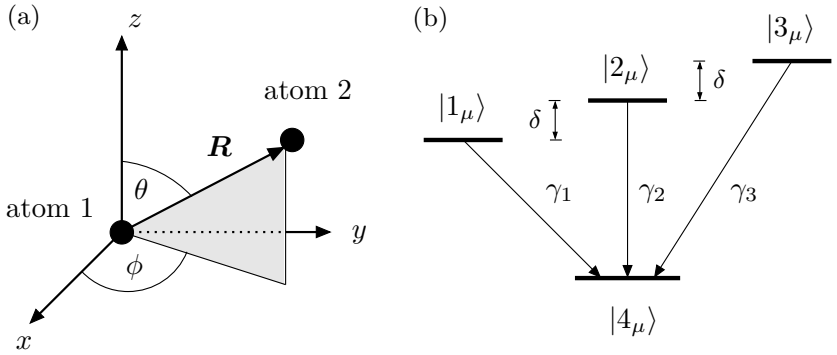

Figure 4.1: (a) The system under consideration is comprised of two atoms that are located at $\boldsymbol{r}_1$ and $\boldsymbol{r}_2$, respectively. The relative position $\boldsymbol{R} = \boldsymbol{r}_2 - \boldsymbol{r}_1$ of atom 2 with respect to atom 1 is expressed in terms of spherical coordinates. (b) Internal level structure of atom $\mu \in \{1, 2\}$. The ground state of each of the atoms is a S_0 state, and the three excited levels are Zeeman sublevels of a P_1 triplet. The states $|1_\mu\rangle$, $|2_\mu\rangle$ and $|3_\mu\rangle$ correspond to the magnetic quantum numbers $m_j = -1$, 0 and 1, respectively. The frequency splitting of the upper levels is denoted by $\delta = \omega_3 - \omega_2 = \omega_2 - \omega_1$, where $\hbar\omega_i$ is the energy of state $|i_\mu\rangle$.

find that the few-level approximation in general leads to incorrect predictions if it is applied to the magnetic sublevels of this system. For this, we first establish a general statement about the system behavior under rotations of the atomic separation vector $\boldsymbol{R}$. As a first conclusion from this result, we derive the intuitive outcome that the dipole-dipole induced energy shifts between collective two-atom states are invariant under rotations of the separation vector $\boldsymbol{R}$ if complete and degenerate multiplets are considered. This result can only be established if also dipole-dipole interactions between orthogonal transition dipole moments are included in the analysis. From this, we conclude that the artificial omission of any of the Zeeman sublevels of a multiplet leads to a spurious dependence of the energy shifts on the orientation, and thus to incorrect predictions.

For example, if in the well-known two-level approximation only one excited state $|e\rangle$ and the ground state $|g\rangle$ are retained, then we recover the position-dependent energy splitting between the entangled two-particle states $(|e, g\rangle \pm |g, e\rangle)/\sqrt{2}$ that has previously been reported for a pair of two-level systems [10, 11]. This geometry-dependence is at odds with the rotational invariance of the collective energy splitting expected for the degenerate system with all Zeeman sublevels. Therefore, in general the few-level approximation cannot be applied to this system.

This chapter is organized as follows. In Sec. 4.2, we describe the master equation for the system depicted in Fig. 4.1. A motivation for our work is provided in Sec. 4.3, where we show on the basis of an example that the few-level approximation may fail. The rigorous analysis of this result is carried out in Sec. 4.4, and a discussion and summary of our findings is given in Sec. 4.5.

4.2 Equation of motion

We describe each atom by a $S_0 \leftrightarrow P_1$ transition shown in Fig. 4.1(b) that can be found, e.g., in ^{40}Ca atoms. We choose the z axis as the quantization axis, which is distinguished by an external magnetic field that induces a Zeeman splitting δ of the excited states. The orientation of $\boldsymbol{R}$ is defined relative to this quantization axis. We begin with the introduction of the master equation which governs the atomic evolution of the system shown in Fig. 4.1. The internal state $|i_\mu\rangle$ of atom μ is an eigenstate of $J_z^{(\mu)}$, where $\boldsymbol{J}^{(\mu)}$ is the angular momentum operator of atom μ ($\mu \in \{1,2\}$). In particular, the P_1 multiplet with $J = 1$ corresponds to the excited states $|1_\mu\rangle$, $|2_\mu\rangle$ and $|3_\mu\rangle$ with magnetic quantum numbers $m = -1$, 0 and 1, respectively, and the S_0 state is the ground state $|4_\mu\rangle$ with $J = m = 0$.

The free time evolution of the of the two identical atoms is governed by the Hamiltonian

$$H_\mathrm{A} = \hbar \sum_{i=1}^{3} \sum_{\mu=1}^{2} \omega_i \, S_{i+}^{(\mu)} S_{i-}^{(\mu)} \,, \tag{4.1}$$

where $\hbar\omega_i$ is the energy of state $|i_\mu\rangle$ and we choose $\hbar\omega_4 = 0$. The raising and lowering operators on the $|4_\mu\rangle \leftrightarrow |i_\mu\rangle$ transition of atom μ are ($i \in \{1,2,3\}$)

$$S_{i+}^{(\mu)} = |i_\mu\rangle\langle 4_\mu| \quad \text{and} \quad S_{i-}^{(\mu)} = |4_\mu\rangle\langle i_\mu| \,. \tag{4.2}$$

We determine the electric-dipole moment operator of atom μ via the Wigner-Eckart theorem [54] and arrive at

$$\hat{\boldsymbol{d}}^{(\mu)} = \sum_{i=1}^{3} \left[\boldsymbol{d}_i S_{i+}^{(\mu)} + \mathrm{H.c.} \right] , \tag{4.3}$$

where the dipole moments $\boldsymbol{d}_i = \langle i|\hat{\boldsymbol{d}}|4\rangle$ are given by

$$\begin{aligned} \boldsymbol{d}_1 &= \mathcal{D}\,\boldsymbol{\epsilon}^{(+)} \,, \qquad \boldsymbol{d}_2 = \mathcal{D}\,\boldsymbol{e}_z \,, \\ \boldsymbol{d}_3 &= -\mathcal{D}\,\boldsymbol{\epsilon}^{(-)} \,; \quad \boldsymbol{\epsilon}^{(\pm)} = \tfrac{1}{\sqrt{2}}(\boldsymbol{e}_x \pm i\boldsymbol{e}_y) \,, \end{aligned} \tag{4.4}$$

and $\mathcal{D}$ is the reduced dipole matrix element.

According to Eq. (1.44) in chapter 1, the master equation for the reduced atomic density operator ϱ of the system shown in Fig. 4.1 can be written as

$$\partial_t \varrho = -\frac{i}{\hbar}[H_\mathrm{A}, \varrho] - \frac{i}{\hbar}[H_\Omega, \varrho] + \mathcal{L}_\gamma \varrho \,. \tag{4.5}$$

The coherent evolution of the atomic states is determined by $H_\mathrm{A} + H_\Omega$, where H_A is defined in Eq. (4.1). The Hamiltonian H_Ω arises from the vacuum-mediated dipole-

dipole interaction between the two atoms and is given by

$$\begin{aligned} H_\Omega &= -\hbar\sum_{i=1}^{3}\left\{\Omega_{ii}S_{i+}^{(2)}S_{i-}^{(1)} + \text{H.c.}\right\} \\ &\quad -\hbar\left\{\Omega_{21}\left(S_{2+}^{(2)}S_{1-}^{(1)} + S_{2+}^{(1)}S_{1-}^{(2)}\right) + \text{H.c.}\right\} \\ &\quad -\hbar\left\{\Omega_{31}\left(S_{3+}^{(2)}S_{1-}^{(1)} + S_{3+}^{(1)}S_{1-}^{(2)}\right) + \text{H.c.}\right\} \\ &\quad -\hbar\left\{\Omega_{32}\left(S_{3+}^{(2)}S_{2-}^{(1)} + S_{3+}^{(1)}S_{2-}^{(2)}\right) + \text{H.c.}\right\}. \end{aligned} \tag{4.6}$$

The coefficients Ω_{ij} cause an energy shift of the collective atomic levels (see Sec. 5.3) and are defined as

$$\Omega_{ij} = \frac{1}{\hbar}\left[\boldsymbol{d}_i^{\mathrm{T}} \overleftrightarrow{\chi}_{\mathrm{re}}(\boldsymbol{R})\, \boldsymbol{d}_j^*\right]. \tag{4.7}$$

The vector $\boldsymbol{R}$ denotes the relative coordinates of atom 2 with respect to atom 1 (see Fig. 4.1), and $\eta = k_0 R$. In the derivation of Eq. (4.6), the three transition frequencies ω_1, ω_2 and ω_3 have been approximated by their mean value $\omega_0 = ck_0$ (see chapter 1). This is justified since the Zeeman splitting δ is small as compared to the resonance frequencies ω_i. For $i = j$, the coupling constants in Eq. (4.6) account for the coherent interaction between a dipole of one of the atoms and the corresponding dipole of the other atom. Since the three dipoles of the system depicted in Fig. 4.1(b) are mutually orthogonal [see Eq. (4.4)], the terms Ω_{ij} for $i \neq j$ reflect the interaction between orthogonal dipoles of different atoms. The physical origin of these cross-coupling terms has been explained in chapter 3.

The last term in Eq. (4.5) accounts for spontaneous emission and reads

$$\begin{aligned} \mathcal{L}_\gamma\varrho = &-\sum_{\mu=1}^{2}\sum_{i=1}^{3}\gamma_i\left(S_{i+}^{(\mu)}S_{i-}^{(\mu)}\varrho + \varrho S_{i+}^{(\mu)}S_{i-}^{(\mu)} - 2S_{i-}^{(\mu)}\varrho S_{i+}^{(\mu)}\right) \\ &-\sum_{i=1}^{3}\left\{\Gamma_{ii}\left(S_{i+}^{(2)}S_{i-}^{(1)}\varrho + \varrho S_{i+}^{(2)}S_{i-}^{(1)} - 2S_{i-}^{(1)}\varrho S_{i+}^{(2)}\right) + \text{H.c.}\right\} \\ &-\sum_{\substack{\mu,\nu=1\\ \mu\neq\nu}}^{2}\Big\{\Gamma_{21}\left(S_{2+}^{(\mu)}S_{1-}^{(\nu)}\varrho + \varrho S_{2+}^{(\mu)}S_{1-}^{(\nu)} - 2S_{1-}^{(\nu)}\varrho S_{2+}^{(\mu)}\right) \\ &\qquad + \Gamma_{31}\left(S_{3+}^{(\mu)}S_{1-}^{(\nu)}\varrho + \varrho S_{3+}^{(\mu)}S_{1-}^{(\nu)} - 2S_{1-}^{(\nu)}\varrho S_{3+}^{(\mu)}\right) \\ &\qquad + \Gamma_{32}\left(S_{3+}^{(\mu)}S_{2-}^{(\nu)}\varrho + \varrho S_{3+}^{(\mu)}S_{2-}^{(\nu)} - 2S_{2-}^{(\nu)}\varrho S_{3+}^{(\mu)}\right) + \text{H.c.}\Big\}. \end{aligned} \tag{4.8}$$

The total decay rate of the exited state $|i\rangle$ of each of the atoms is given by $2\gamma_i$, where

$$\gamma_i = \frac{1}{4\pi\epsilon_0}\frac{2|\boldsymbol{d}_i|^2\omega_0^3}{3\hbar c^3} = \gamma\,, \tag{4.9}$$

and we again employed the approximation $\omega_i \approx \omega_0$. The collective decay rates Γ_{ij} result from the vacuum-mediated dipole-dipole coupling between the two atoms and are determined by

$$\Gamma_{ij} = \frac{1}{\hbar}\left[\boldsymbol{d}_i^{\mathrm{T}} \overleftrightarrow{\chi}_{\mathrm{im}}(\boldsymbol{R})\, \boldsymbol{d}_j^*\right] . \tag{4.10}$$

The parameters Γ_{ii} arise from the interaction between a dipole of one of the atoms and the corresponding dipole of the other atom, and the cross-decay rates Γ_{ij} for $i \neq j$ originate from the interaction between orthogonal dipoles of different atoms (see chapter 3). Note that if the master equation (4.5) is transformed into the interaction picture with respect to H_{A}, terms proportional to the parameters Ω_{ij} and Γ_{ij} with $i \neq j$ rotate at frequencies $\pm\delta$ or $\pm 2\delta$. Similar to the usual rotating-wave approximation, the cross terms are negligible as compared to terms proportional to Ω_{ii} and Γ_{ii} if the level splitting δ is large, i.e. $|\delta| \gg |\Omega_{ij}|, |\Gamma_{ij}|$ $(i \neq j)$.

In order to evaluate the expressions for the various coupling terms Ω_{ij} and the decay rates Γ_{ij} in Eqs. (4.7) and (4.10), we express the relative position of the two atoms in spherical coordinates (see Fig. 4.1),

$$\boldsymbol{R} = R\,(\sin\theta\cos\phi,\, \sin\theta\sin\phi,\, \cos\theta)^{\mathrm{T}} . \tag{4.11}$$

Together with the definition of the tensor $\overleftrightarrow{\chi}$ in Eq. (1.48) and Eq. (4.4), we obtain

$$\begin{aligned}
\Omega_{31} &= \gamma\frac{3}{4\eta^3}\left[\left(\eta^2-3\right)\cos\eta - 3\eta\sin\eta\right]\sin^2\theta e^{-2i\phi} ,\\
\Omega_{11} &= 3\frac{\gamma}{8\eta^3}\left[\left(3\eta^2 - 1 + \left(\eta^2-3\right)\cos 2\theta\right)\cos\eta - \eta\left(1+3\cos 2\theta\right)\sin\eta\right] ,\\
\Omega_{21} &= -\sqrt{2}\cot\theta\;\Omega_{31}e^{i\phi} ,\\
\Omega_{22} &= \Omega_{11} - (2\cot^2\theta - 1)\Omega_{31}e^{2i\phi} ,\\
\Omega_{32} &= -\Omega_{21} , \quad \Omega_{33} = \Omega_{11} ,
\end{aligned} \tag{4.12}$$

and the collective decay rates are found to be

$$\begin{aligned}
\Gamma_{31} &= \gamma\frac{3}{4\eta^3}\left[\left(\eta^2-3\right)\sin\eta + 3\eta\cos\eta\right]\sin^2\theta e^{-2i\phi} ,\\
\Gamma_{11} &= 3\frac{\gamma}{8\eta^3}\left[\left(3\eta^2 - 1 + \left(\eta^2-3\right)\cos 2\theta\right)\sin\eta + \eta\left(1+3\cos 2\theta\right)\cos\eta\right] ,\\
\Gamma_{21} &= -\sqrt{2}\cot\theta\;\Gamma_{31}e^{i\phi} ,\\
\Gamma_{22} &= \Gamma_{11} - (2\cot^2\theta - 1)\Gamma_{31}e^{2i\phi} ,\\
\Gamma_{32} &= -\Gamma_{21} , \quad \Gamma_{33} = \Gamma_{11} .
\end{aligned} \tag{4.13}$$

The coupling terms Ω_{11}, Ω_{31} and the collective decay rates Γ_{11}, Γ_{31} are shown in Fig. 4.2 as a function of the interatomic distance R.

Finally, we consider the case where the two atoms are driven by an external laser field,

$$\boldsymbol{E}_L = \left[\mathcal{E}_x\boldsymbol{e}_x + \mathcal{E}_y\boldsymbol{e}_y\right] e^{i\boldsymbol{k}_L\cdot\boldsymbol{r}}\, e^{-i\omega_L t} + \text{c.c.} , \tag{4.14}$$

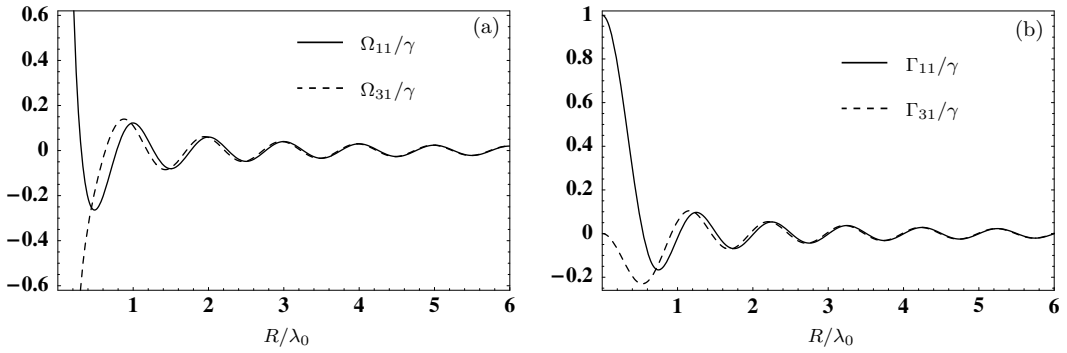

Figure 4.2: (a) Plot of the vacuum-induced coupling terms Ω_{11} and Ω_{31} according to Eq. (4.12). λ_0 is the mean transition wavelength. If the interatomic distance R approaches zero, the parameters Ω_{11} and Ω_{31} diverge. (b) Plot of the collective decay rates Γ_{11} and Γ_{31} according to Eq. (4.13). Γ_{11} and Γ_{31} remain finite in the limit $R \to 0$. The parameters in (a) and (b) are given by $\theta = \pi/2$ and $\phi = 0$.

where $\mathcal{E}_x$, $\mathcal{E}_y$ and $\boldsymbol{e}_x$, $\boldsymbol{e}_y$ denote the field amplitudes and polarization vectors, respectively, ω_L is the laser frequency and c.c. stands for the complex conjugate. The wave vector $\boldsymbol{k}_L = k_L \boldsymbol{e}_z$ of the laser field points in the positive z direction. In the presence of the laser field and in a frame rotating with the laser frequency, the master equation (4.5) becomes

$$\partial_t \tilde{\varrho} = -\frac{i}{\hbar}[\tilde{H}_{\rm L} + \tilde{H}_{\rm A}, \tilde{\varrho}] - \frac{i}{\hbar}[H_\Omega, \tilde{\varrho}] + \mathcal{L}_\gamma \tilde{\varrho}\,. \tag{4.15}$$

In this equation, $\tilde{H}_A$ is the transformed Hamiltonian of the free atomic evolution,

$$\tilde{H}_{\rm A} = -\hbar \sum_{i=1}^{3} \sum_{\mu=1}^{2} \Delta_i \, S_{i+}^{(\mu)} S_{i-}^{(\mu)}\,. \tag{4.16}$$

The detunings with the state $|i\rangle$ are labeled by $\Delta_i = \omega_L - \omega_i$ ($i \in \{1,2,3\}$), and we have $\Delta_1 = \Delta_2 + \delta$, $\Delta_3 = \Delta_2 - \delta$. The Hamiltonian $\tilde{H}_{\rm L}$ describes the atom-laser interaction in the electric-dipole and rotating-wave approximation,

$$\tilde{H}_{\rm L} = -\hbar \sum_{\mu=1}^{2} \Big\{ [\Omega_x(\boldsymbol{r}_\mu) + i\,\Omega_y(\boldsymbol{r}_\mu)]\; S_{1+}^{(\mu)} + [-\Omega_x(\boldsymbol{r}_\mu) + i\,\Omega_y(\boldsymbol{r}_\mu)]\; S_{3+}^{(\mu)} + \text{H.c.} \Big\}\,, \tag{4.17}$$

and the position-dependent Rabi frequencies are defined as

$$\begin{aligned} \Omega_x(\boldsymbol{r}) &= \mathcal{D}\mathcal{E}_x/(\sqrt{2}\hbar)\, \exp\left[i\boldsymbol{k}_L \cdot \boldsymbol{r}\right]\,, \\ \Omega_y(\boldsymbol{r}) &= \mathcal{D}\mathcal{E}_y/(\sqrt{2}\hbar)\, \exp\left[i\boldsymbol{k}_L \cdot \boldsymbol{r}\right]\,. \end{aligned} \tag{4.18}$$

4.3 Physical motivation

In the following section 4.4, we will provide a rigorous treatment of the behavior of our model system under rotations of the atomic separation vector in order to study the geometrical properties of the different coupling terms in the master equation (4.5). In order to motivate this analysis, we first discuss a simple example for our results. This example employs an external laser field driving the atoms. On the other hand, our main results starting from Sec. 4.4 will not rely on external driving fields.

We consider the geometrical setup shown in Fig. 4.3, where the atoms with internal structure as in Fig. 4.1(b) are aligned along the y axis. Each atom interacts with a σ^+ polarized laser beam with frequency ω_L that propagates in z direction. Since the laser polarization is σ^+, it couples only to the transition $|3\rangle \leftrightarrow |4\rangle$ in each atom. To describe this setup, one might be tempted to employ the usual few-level approximation, and thus neglect the excited states $|1\rangle$ and $|2\rangle$ in each atom, since they are not populated by the laser field. If this were correct, the seemingly relevant subsystem would be

$$\mathcal{C} = \mathrm{Span}(|4,4\rangle,\ |3,3\rangle,\ |3,4\rangle,\ |4,3\rangle)\,. \tag{4.19}$$

However, it is easy to prove that the state space of the two atoms can *not* be reduced to the subspace $\mathcal{C}$, i.e., that the few-level approximation cannot be applied in its usual form. In order to show this, we solve the master equation (4.15) numerically with the initial condition $\tilde{\varrho}(t=0) = |4,4\rangle\langle 4,4|$, i.e. it is assumed that both atoms are initially in their ground states.

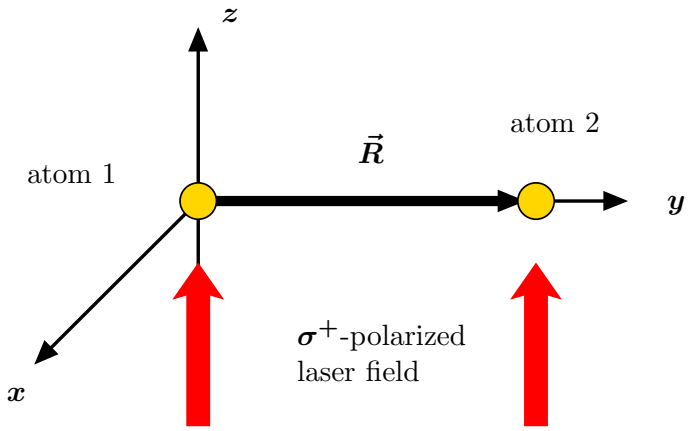

Figure 4.3: Setup considered in Sec. 4.3, where the breakdown of the few-level approximation is illustrated by means of an example. The atoms are aligned along the y axis, and the σ^+ polarized laser field propagates in z direction. Note that our main results starting from Section 4.4 do not rely on external driving fields.

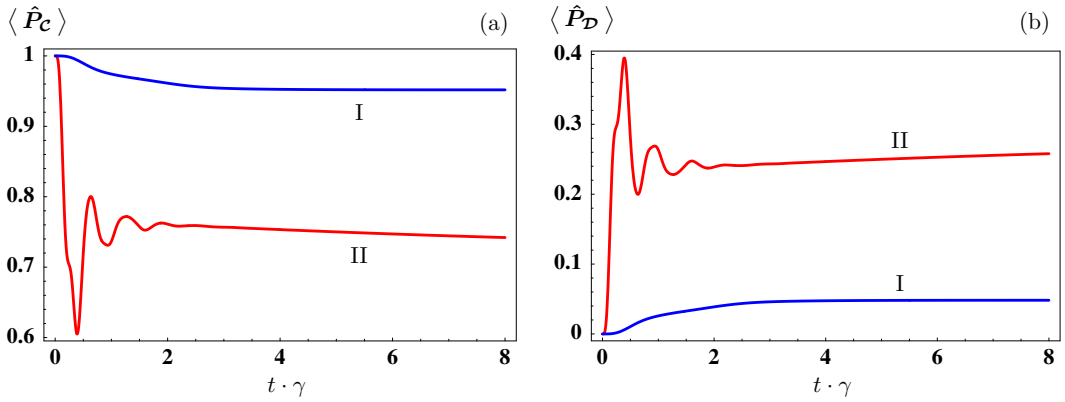

Figure 4.4: (a) Population in the seemingly relevant subspace $\mathcal{C}$ [see Eq. (4.19)] for the setup shown in Fig. 4.3. The common parameters are $\theta = \pi/2$, $\phi = \pi/2$, and $\delta = 0$. In I, we have $\Omega_x(\boldsymbol{r}_1) = \Omega_x(\boldsymbol{r}_2) = \gamma$, $\Omega_y(\boldsymbol{r}_1) = \Omega_y(\boldsymbol{r}_2) = i\gamma$, $R = 0.3\lambda_0$, and $\Delta = 0.58\gamma$. Curve II shows the case $\Omega_x(\boldsymbol{r}_1) = \Omega_x(\boldsymbol{r}_2) = 2.7\gamma$, $\Omega_y(\boldsymbol{r}_1) = \Omega_y(\boldsymbol{r}_2) = 2.7i\gamma$, $R = 0.1\lambda_0$, and $\Delta = 5.2\gamma$. (b) Population in the subspace $\mathcal{D}$ [see Eq. (4.21)] for the same parameters than in (a). Note that the population in $\mathcal{C} + \mathcal{D}$ remains unity for all times.

Figure 4.4(a) shows the total population confined to the subspace $\mathcal{C}$,

$$\left\langle \hat{P}_{\mathcal{C}} \right\rangle = \mathrm{Tr}\left[\varrho(t)\,\hat{P}_{\mathcal{C}}\right] , \tag{4.20}$$

where $P_{\mathcal{C}}$ is the projector onto the subspace $\mathcal{C}$. It can easily be seen that for both sets of parameters, population is lost from the subspace $\mathcal{C}$. Since all states but the excited states $|1\rangle$ and $|2\rangle$ are contained in $\mathcal{C}$, it is clear that it is not sufficient to take only the excited state $|3\rangle$ into account in the usual few-level approximation.

The explanation of this outcome is straightforward. According to Eq. (4.6), the dipole transition $|3\rangle \leftrightarrow |4\rangle$ of one atom is coupled by the cross-coupling term Ω_{31} to the $|1\rangle \leftrightarrow |4\rangle$ transition of the other atom. This coupling results in a population of state $|1\rangle$, even though the transition dipoles of the two considered transitions are orthogonal. Consequently, the dipole-dipole interaction between transitions with orthogonal dipole moments will result in the (partial) population of the states $|1,1\rangle$, $|1,3\rangle$, $|3,1\rangle$, $|1,4\rangle$, $|4,1\rangle$, although none of these states is directly coupled to the laser field.

The numerical verification of these statements is shown in Figure 4.4(b), which depicts the population of the subspace

$$\mathcal{D} = \mathrm{Span}(|1,1\rangle,\ |1,3\rangle,\ |3,1\rangle,\ |1,4\rangle,\ |4,1\rangle)\,. \tag{4.21}$$

$\hat{P}_{\mathcal{D}}$ is the projector onto the subspace $\mathcal{D}$, and the parameters are the same as above. Note that we have verified that all population is contained in the subspace $\mathcal{C} + \mathcal{D}$, i.e. $\left\langle \hat{P}_{\mathcal{C}} \right\rangle + \left\langle \hat{P}_{\mathcal{D}} \right\rangle = 1$ at all times.

It is important to note that the sufficient subspace $\mathcal{S} + \mathcal{D}$ still does not contain all possible states of the two atoms, because the excited state $|2\rangle$ of each atom is neglected. The justification for this is that in the chosen geometry, the cross-coupling terms Ω_{21}, Γ_{21} and Ω_{32}, Γ_{32} vanish such that the transition $|2\rangle \leftrightarrow |4\rangle$ of one atom is not coupled to the transitions $|1\rangle \leftrightarrow |4\rangle$ and $|3\rangle \leftrightarrow |4\rangle$ of the other atom, see Eqs. (4.12) and (4.13). This is important since it demonstrates that it is also not correct to simply state that all atomic states have to be taken into account for all parameter configurations.

The above example clearly demonstrates that the few-level approximation is rendered impossible by the coupling terms between transitions with *orthogonal dipole moments*. Therefore, it is the nature of the dipole-dipole coupling itself which enforces that generally all Zeeman sublevels have to be taken into account, and not the orientation external laser fields, as one may be tempted to assume in the usual few-level approximation.

A physical interpretation for the origin of the vacuum-induced coupling of transitions with orthogonal dipole moments has been given in chapter 3. In essence, these couplings occur if the polarization of a (virtual) photon emitted on one of the transitions in the first atom has non-zero projection on different dipole moments of the second atom.

4.4 Breakdown of the few-level approximation

For the remaining parts of this chapter, we omit the laser fields considered in Sec. 4.3 and return to our original setup in Fig. 4.1. We first derive a general statement about the behavior of the master equation (4.5) under rotations of the separation vector $\boldsymbol{R}$. This will provide the theoretical foundation for our central results and physical interpretations that follow after the formal proof of the statement.

4.4.1 Central theorem

In addition to a given relative position $\boldsymbol{R}$ of the two atoms, we consider a different geometrical setup where the separation vector $\boldsymbol{P}$ is obtained from $\boldsymbol{R}$ by a rotation, $\boldsymbol{P} = \mathcal{R}_{\boldsymbol{u}}(\alpha)\boldsymbol{R}$. Here, $\mathcal{R}_u(\alpha)$ is an orthogonal 3×3 matrix that describes a rotation in the three-dimensional real vector space $\mathbb{R}^3$ around the axis $\boldsymbol{u}$ by an angle α. We show that there exists a unitary operator W such that

$$H_\Omega(\boldsymbol{P}) = W H_\Omega(\boldsymbol{R}) W^\dagger \,, \tag{4.22a}$$

$$\mathcal{L}_\gamma(\boldsymbol{P})\varrho = W \left[\mathcal{L}_\gamma(\boldsymbol{R}) W^\dagger \varrho W\right] W^\dagger \,, \tag{4.22b}$$

where $W = W_{\boldsymbol{u}}(\alpha)$ is given by

$$W_{\boldsymbol{u}}(\alpha) = \exp[-i\alpha\, \boldsymbol{J}^{(1)} \cdot \boldsymbol{u}/\hbar] \exp[-i\alpha\, \boldsymbol{J}^{(2)} \cdot \boldsymbol{u}/\hbar] \,. \tag{4.23}$$

Here the operator $\exp[-i\alpha\, \boldsymbol{J}^{(\mu)} \cdot \boldsymbol{u}/\hbar]$ describes a rotation around the axis $\boldsymbol{u}$ by an angle α in the state space of atom μ. The notation $H_\Omega(\boldsymbol{R})$ and $\mathcal{L}_\gamma(\boldsymbol{R})$ means that the coupling constants and collective decay rates in Eqs. (4.7) and (4.8) have to be evaluated at $\boldsymbol{R}$.

Before we turn to the proof of Eq. (4.22), we recall the general master equation in Born approximation (see chapter 1),

$$\partial_t \varrho = -\frac{i}{\hbar}[H_\mathrm{A}, \varrho] - \frac{1}{\hbar^2}\int_0^t d\tau \mathrm{Tr}_\mathrm{F}\Big(\big[V, U(\tau)\big[V, \varrho_\mathrm{F}\otimes\varrho(t-\tau)\big]U^\dagger(\tau)\big]\Big)\,, \tag{4.24}$$

where $U(\tau) = \exp[-i(H_\mathrm{A}+H_\mathrm{F})\tau/\hbar]$ and H_F denotes the free Hamiltonian of the radiation field [see Eq. (1.4)]. For the system shown in Fig. 4.1, the free Hamiltonian of the atoms H_A is given in Eq. (4.1). The interaction of the atoms with the vacuum modes is described by

$$V = -\hat{\boldsymbol{d}}^{(1)}\cdot\hat{\boldsymbol{E}}(\boldsymbol{r}_1) - \hat{\boldsymbol{d}}^{(2)}\cdot\hat{\boldsymbol{E}}(\boldsymbol{r}_2)\,, \tag{4.25}$$

the dipole operator $\hat{\boldsymbol{d}}^{(\mu)}$ of atom μ is given in Eq. (4.3) and $\hat{\boldsymbol{E}}(\boldsymbol{r})$ is the electric field operator [see Eq. (1.7)]. If we apply the Markov- and the rotating-wave approximations, and ignore all terms associated with the Lamb shift of the atomic levels, the master equation (4.5) is obtained. These steps were carried out explicitly in Sec. 1.3.

We proceed with the proof of Eq. (4.22). In a first step, we introduce the auxiliary operator $A_{\boldsymbol{R}} = WV_{\boldsymbol{R}}W^\dagger$, where $V_{\boldsymbol{R}}$ is the interaction Hamiltonian for a relative position of the atoms given by $\boldsymbol{R}$, and $W = W_{\boldsymbol{u}}(\alpha)$ is defined in Eq. (4.23). The evaluation of $A_{\boldsymbol{R}}$ involves only the transformation of the dipole operator of each atom. Since the matrix elements of vector operators transform like classical vectors under rotations (see, e.g., Sec. 3.10. in [54]), we find

$$W\,\hat{\boldsymbol{d}}^{(\mu)}\,W^\dagger = \sum_{i=1}^{3}\big[\tilde{\boldsymbol{d}}_i\, S_{i+}^{(\mu)} + \mathrm{H.c.}\big]\,, \tag{4.26}$$

where $\tilde{\boldsymbol{d}}_i = \mathcal{R}_{\boldsymbol{u}}^{-1}(\alpha)\boldsymbol{d}_i$. This shows that the only difference between the auxiliary operator $A_{\boldsymbol{R}}$ and $V_{\boldsymbol{R}}$ is that the dipole moments of the former are determined by $\tilde{\boldsymbol{d}}_i$ instead of $\boldsymbol{d}_i$. In a second step, we employ the tensor properties of $\overleftrightarrow{\chi}$ to find the following expression for the parameters $\Omega_{ij}(\boldsymbol{P})$ and $\Gamma_{ij}(\boldsymbol{P})$ [see Eqs. (4.7) and (4.10)],

$$\hbar\Omega_{ij}(\boldsymbol{P}) = \big[\mathcal{R}_{\boldsymbol{u}}^{-1}(\alpha)\boldsymbol{d}_i\big]^\mathrm{T}\overleftrightarrow{\chi}_\mathrm{re}(\boldsymbol{R})\big[\mathcal{R}_{\boldsymbol{u}}^{-1}(\alpha)\boldsymbol{d}_j^*\big]\,, \tag{4.27}$$

$$\hbar\Gamma_{ij}(\boldsymbol{P}) = \big[\mathcal{R}_{\boldsymbol{u}}^{-1}(\alpha)\boldsymbol{d}_i\big]^\mathrm{T}\overleftrightarrow{\chi}_\mathrm{im}(\boldsymbol{R})\big[\mathcal{R}_{\boldsymbol{u}}^{-1}(\alpha)\boldsymbol{d}_j^*\big]\,. \tag{4.28}$$

This important result shows that a rotation of the dipole moments $\boldsymbol{d}_i$ by $\mathcal{R}_{\boldsymbol{u}}^{-1}(\alpha)$ is formally equivalent to a rotation of $\boldsymbol{R}$ by $\mathcal{R}_{\boldsymbol{u}}(\alpha)$ in the master equation (4.5). From the combination of the results obtained in step one and two, we conclude that the

exchange of $V_{\boldsymbol{R}}$ by $A_{\boldsymbol{R}}$ in the integral of Eq. (4.24) is equivalent to a rotation of the separation vector from $\boldsymbol{R}$ to $\boldsymbol{P} = \mathcal{R}_{\boldsymbol{u}}(\alpha)\boldsymbol{R}$,

$$I = -\frac{1}{\hbar^2}\int_0^t d\tau \mathrm{Tr}_\mathrm{F}\Big(\big[A_{\boldsymbol{R}}, \big[U(\tau)A_{\boldsymbol{R}}U^\dagger(\tau), \sigma(\hat{\tau})\big]\big]\Big) \tag{4.29}$$

$$= -\frac{i}{\hbar}[H_\Omega(\boldsymbol{P}), \varrho] + \mathcal{L}_\gamma(\boldsymbol{P})\varrho\,, \tag{4.30}$$

where $\hat{\tau} = t - \tau$ and

$$\sigma(\hat{\tau}) = U(\tau)\left[\varrho_\mathrm{F} \otimes \varrho(\hat{\tau})\right] U^\dagger(\tau)\,. \tag{4.31}$$

Note that the equality of Eqs. (4.29) and (4.30) holds under the same assumptions that led from Eqs. (4.24) to (4.5).

In the second part of the proof we evaluate the integral in Eq. (4.29) in a different way. In the discussion following Eq. (4.7), we justified that $\mathcal{L}_\gamma$ and H_Ω depend only on the mean transition frequency ω_0. Here we employ exactly the same approximation and replace the frequencies ω_i appearing in $U(\tau)A_{\boldsymbol{R}}U^\dagger(\tau)$ by ω_0. The equivalence of these approximations becomes apparent by a detailed study of the derivation of the master equation in Sec. (1.3). Since H_A commutes with $\boldsymbol{J}^{(\mu)}$ if all frequencies ω_i are replaced by the mean transition frequency ω_0, we have $[W, U] = 0$ and hence

$$U(\tau)A_{\boldsymbol{R}}U^\dagger(\tau) = U(\tau)WV_{\boldsymbol{R}}W^\dagger U^\dagger(\tau) = WU(\tau)V_{\boldsymbol{R}}U^\dagger(\tau)W^\dagger\,. \tag{4.32}$$

It follows that the argument of the trace in Eq. (4.29) can be written as

$$W\big[V_{\boldsymbol{R}}, \big[U(\tau)V_{\boldsymbol{R}}U^\dagger(\tau), W^\dagger\sigma(\hat{\tau})W\big]\big]W^\dagger\,. \tag{4.33}$$

In contrast to Eq. (4.29), the double commutator contains now the original interaction Hamiltonian $V_{\boldsymbol{R}}$ that corresponds to a setting with separation vector $\boldsymbol{R}$. We thus obtain

$$I = -\frac{i}{\hbar}[WH_\Omega(\boldsymbol{R})W^\dagger, \varrho] + W\Big[\mathcal{L}_\gamma(\boldsymbol{R})W^\dagger\varrho W\Big]W^\dagger\,. \tag{4.34}$$

Finally, the comparison of Eqs. (4.34) and (4.30) establishes Eq. (4.22) which concludes the proof.

4.4.2 Implications of the theorem

Diagonalization of H_Ω

We now turn to the discussion of Eq. (4.22), which will lead to our central results. The Hamiltonian H_Ω describes the coherent part of the dipole-dipole interaction between the atoms. From Eq. (4.22a), it is immediately clear that the eigenvalues of H_Ω depend only on the interatomic distance, but not on the orientation of the separation vector $\boldsymbol{R}$. The reason is that the spectrum of two operators, which are related by a unitary transformation, is identical. In our case, the Hamiltonian

$H_\Omega(\boldsymbol{R})$ and $H_\Omega(\boldsymbol{P})$ for different orientations $\boldsymbol{R}$ and $\boldsymbol{P}$ are related by the unitary transformation W, and since $\boldsymbol{P}$ is obtained from $\boldsymbol{R}$ by an arbitrary rotation, the eigenvalues of H_Ω are identical for any orientation.

Next we re-obtain this result in a more explicit way and derive symbolic expressions for the eigenvalues and eigenstates of H_Ω. This Hamiltonian can be written as

$$H_\Omega = \sum_{i,j=1}^{3} \langle a_i|H_\Omega|a_j\rangle |a_i\rangle\langle a_j| + \sum_{i,j=1}^{3} \langle s_i|H_\Omega|s_j\rangle |s_i\rangle\langle s_j|\,, \tag{4.35}$$

where the symmetric and antisymmetric states are defined as

$$|s_i\rangle = (\,|i,4\rangle + |4,i\rangle\,)/\sqrt{2}\,, \tag{4.36a}$$

$$|a_i\rangle = (\,|i,4\rangle - |4,i\rangle\,)/\sqrt{2}\,, \tag{4.36b}$$

and $|i,j\rangle = |i_1\rangle \otimes |j_2\rangle$. Since all matrix elements $\langle s_i|H_\Omega|a_j\rangle$ of H_Ω between a symmetric and an antisymmetric state vanish, the set of eigenstates decomposes into a symmetric subspace $\mathcal{S}$ and an antisymmetric subspace $\mathcal{A}$. The matrix elements of H_Ω in the subspace $\mathcal{S}$ spanned by the symmetric states $\{|s_1\rangle, |s_2\rangle, |s_3\rangle\}$ are

$$[H_\Omega]_\mathcal{S} = -\hbar \begin{pmatrix} \Omega_{11} & \Omega_{21}^* & \Omega_{31}^* \\ \Omega_{21} & \Omega_{22} & \Omega_{32}^* \\ \Omega_{31} & \Omega_{32} & \Omega_{33} \end{pmatrix}, \tag{4.37}$$

and the representation of H_Ω in the subspace $\mathcal{A}$ spanned by the antisymmetric states $\{|a_1\rangle, |a_2\rangle, |a_3\rangle\}$ is given by $[H_\Omega]_\mathcal{A} = -[H_\Omega]_\mathcal{S}$. Note that the collective ground state $|4,4\rangle$ and the states $|i,j\rangle$ $(i,j \in \{1,2,3\})$ where each atom is in an excited state are not influenced by the dipole-dipole interaction and thus not part of the expansion (4.37).

In Section 4.4.1, we have derived a general relation between any two orientations of the atomic separation vector. In order to apply this result, we define the vector $\boldsymbol{R}_z$ to be parallel to the z axis, i.e. $\boldsymbol{R}_z = R\,\boldsymbol{e}_z$. This corresponds to the choice $\theta = 0$ in Eq. (4.11). Any separation vector $\boldsymbol{P}$ can then be obtained from $\boldsymbol{R}_z$ as $\boldsymbol{P} = \mathcal{R}_{\boldsymbol{u}}(\alpha)\boldsymbol{R}_z$ by a suitable choice of the rotation axis $\boldsymbol{u}$ and the angle α.

We then proceed with the diagonalization of the Hamiltonian $H_\Omega(\boldsymbol{R}_z)$ with atomic separation vector $\boldsymbol{R}_z$. The explicit calculation of the coupling constants Ω_{ij} shows that the off-diagonal elements in Eq. (4.37) vanish if the atoms are aligned along the z axis, see Eqs. (4.12) and (4.13) with $\theta = 0$. It follows that the Hamiltonian $H_\Omega(\boldsymbol{R}_z)$ is already diagonalized by the symmetric and antisymmetric states Eq. (4.36), and the eigenvalues of $[H_\Omega]_\mathcal{S}$ and $[H_\Omega]_\mathcal{A}$ are given by $\lambda_i^\mathcal{S} = -\hbar\Omega_{ii}(\boldsymbol{R}_z)$ and $\lambda_i^\mathcal{A} = \hbar\Omega_{ii}(\boldsymbol{R}_z)$, respectively.

According to Eq. (4.22a), the Hamiltonian $H_\Omega(\boldsymbol{P})$ is the unitary transform of $H_\Omega(\boldsymbol{R}_z)$ by W. The normalized eigenstates of $H_\Omega(\boldsymbol{P})$ are thus determined by $W|s_i\rangle$ and $W|a_i\rangle$, and their eigenvalues are again $\lambda_i^\mathcal{S}$ and $\lambda_i^\mathcal{A}$, respectively. Since the orientation of $\boldsymbol{P}$ is arbitrary, the eigenvalues of $H_\Omega(\boldsymbol{P})$ depend only on the interatomic distance $|\boldsymbol{P}| = |\boldsymbol{R}_z| = R$, but not on the orientation of the separation vector.

Thus, it follows from our theorem in Sec. 4.4.1 that the eigenvalues of $H_\Omega(\boldsymbol{P})$ are invariant under rotation of the atomic separation vector.

Diagonalization of $H_\mathbf{A} + H_\Omega$

An additional conclusion can be drawn from Eq. (4.22) if the operator H_A commutes with the transformation $W = W_{\boldsymbol{u}}(\alpha)$, i.e.,

$$[H_\mathrm{A}, W] = 0\,. \tag{4.38}$$

Then, Eq. (4.22a) implies that $H_\mathrm{A} + H_\Omega(\boldsymbol{P})$ is the unitary transform of $H_\mathrm{A} + H_\Omega(\boldsymbol{R})$ by W. A straightforward realization of this is the case of vanishing Zeeman splitting δ, in which the relation holds for an arbitrary orientation of $\boldsymbol{P}$. Then, the energy levels of the full system Hamiltonian $H_\mathrm{A} + H_\Omega$ do not depend on the orientation of the separation vector.

This result can be understood as follows. In the absence of a magnetic field ($\delta = 0$), there is no distinguished direction in space. Since the vacuum is isotropic in free space, one expects that the energy levels of the system are invariant under rotations of the separation vector $\boldsymbol{R}$.

By contrast, the application of a magnetic field in z direction breaks the full rotational symmetry. For $\delta \neq 0$, the atomic Hamiltonian H_A only commutes with transformations $W_{\boldsymbol{u}}(\alpha)$ that correspond to a rotation of the separation vector around the z axis, $\boldsymbol{u} = \boldsymbol{e}_z$. If we express the atomic separation vector in terms of spherical coordinates as in Eq. (4.11), this means that the eigenvalues of the full system Hamiltonian $H_\mathrm{A} + H_\Omega$ do only depend on the interatomic distance R and the angle θ, but not on the angle ϕ. This result reflects the symmetry of our system with respect to rotations around the z axis.

Unitary equivalence of time evolution in different orientations

If the operator H_A commutes with the transformation $W = W_{\boldsymbol{u}}(\alpha)$, another conclusion can be drawn. Then, the result in Eq. (4.22) implies that the density operator $W\varrho(\boldsymbol{R})W^\dagger$ obeys the same master equation than $\varrho(\boldsymbol{P})$ for $\boldsymbol{P} = \mathcal{R}_{\boldsymbol{u}}(\alpha)\boldsymbol{R}$. It follows that $\boldsymbol{P}$ is the unitary transform of $\varrho(\boldsymbol{R})$ by W, i.e.

$$\varrho(\boldsymbol{P}) = W\varrho(\boldsymbol{R})W^\dagger\,. \tag{4.39}$$

As discussed above, the free atomic Hamiltonian H_A commutes with $W_{\boldsymbol{u}}(\alpha)$ for an arbitrary choice of the rotation axis $\boldsymbol{u}$ and angle α if the Zeeman splitting δ vanishes.

We thus conclude that it suffices to determine the solution of the master equation (4.5) for only one particular geometry if $\delta = 0$. Any other solution can then be generated simply by applying the transformation $W = W_{\boldsymbol{u}}(\alpha)$ with suitable values of $\boldsymbol{u}$ and α to the solution for the particular geometry.

Establishment of the breakdown

The breakdown of the few-level approximation for collective systems is established by noting that the result in Eq. (4.22) and all its just discussed implications cannot be recovered if any of the Zeeman sublevels of the P_1 triplet are neglected. In this case, the unitary operator W does not exist since it is impossible to define an angular momentum or vector operator in a state space where magnetic sublevels have been removed artificially. For example, an artificially reduced sublevel scheme will exhibit eigenenergies with a spurious dependence on the orientation of the atomic separation vector. This is in contrast to our finding that the energy levels of the collective states are invariant under rotations of the atomic separation vector if complete and degenerate multiplets are considered. We thus conclude that all Zeeman sublevels generally have to be taken into account.

The intuitive explanation of this has already been hinted at in Sec. 4.3. For a more formal discussion, we return to the matrix representation of $[H_\Omega]_\mathcal{S}$ in Eq. (4.37). The diagonal elements proportional to Ω_{ii} account for the coherent interaction between a dipole of one of the atoms and the corresponding dipole of the other atom. By contrast, the off-diagonal terms proportional to Ω_{ij} with $i \neq j$ arise from the vacuum-mediated interaction between orthogonal dipoles of different atoms (see chapter 3). It is the presence of these terms that renders the simplification of the atomic level scheme impossible since they couple an excited state $|i\rangle$ of one atom to a different excited state $|j\rangle$ $(i \neq j)$ of the other atom. A similar argument applies to the collective decay rates Γ_{ij} appearing in $\mathcal{L}_\gamma \varrho$. Thus, if any Zeeman sublevel of the excited state multiplet is artificially removed, then some of these vacuum-induced couplings Ω_{ij} and Γ_{ij} with $i \neq j$ are neglected, which leads to incorrect results. Now, it is also apparent why the breakdown of the few-level approximation appears exclusively in collective systems. For single atoms in free space, a coupling of orthogonal transition dipole moments via the vacuum is impossible.

Recovery of the few-level approximation in special geometries

The identification of the vacuum-induced couplings Ω_{ij} and Γ_{ij} between orthogonal transition dipole moments as the cause of the breakdown enables one to conjecture that few-level approximations are justified if some or all of the cross-coupling terms can be neglected. As we pointed out in the discussion below Eq. (4.10), the influence of the cross-coupling terms in the master equation (4.5) is negligible if the Zeeman splitting is large such that the inequality $|\delta| \gg |\Omega_{ij}|, |\Gamma_{ij}|$ $(i \neq j)$ holds. Independent of the actual value of δ, some or all of the cross-coupling terms are exactly equal to zero for particular geometrical setups.

For example, we mentioned earlier that all cross-coupling terms vanish if the atoms are aligned along the z axis. This corresponds to the case $\theta = 0$ in Eqs. (4.11)-(4.13). Then, the $S_0 \leftrightarrow P_1$ transition may be reduced to a two-level system, formed by an arbitrary sublevel of the P_1 triplet and the ground state S_0.

As a second example, we assume the atoms to be aligned in the x-y plane, i.e., $\theta = \pi/2$ in Eq. (4.11). Then the terms Ω_{21}, Γ_{21} and Ω_{32}, Γ_{32} vanish, see Eqs. (4.12) and (4.13). In effect, the excited state $|2\rangle$ may be disregarded such that the atomic level scheme simplifies to a V-system formed by the states $|1\rangle$ and $|3\rangle$ of the P_1 multiplet and the ground state S_0.

4.5 Discussion and summary

In this chapter, we have studied the properties of various parts of the system Hamiltonian as well as the full density operator under rotations of the atomic separation vector. This discussion was based on a general theorem in Sec. 4.4.1 which relates the master equations for different orientations of the atomic separation vector.

First, we have discussed the Hamiltonian H_Ω, which describes the coherent coupling between different transitions in the two atoms induced by the vacuum field. Armed with our main theorem, it is possible to first diagonalize H_Ω in a special geometry, where the eigenvectors and eigenenergies assume a particularly simple form. The eigenvectors and eigenenergies for an arbitrary system geometry are then derived via the theorem. Our main result of this first part of Sec. 4.4.2 is that the eigenvalues of H_Ω are invariant under rotations of the atomic separation vector.

In a second step, we have studied the eigenenergies of the full system Hamiltonian $H_A + H_\Omega$, which in general are *not* invariant under rotations of the atomic separation vector. The invariance, however, is recovered if H_A commutes with the transformation $W = W_{\boldsymbol{u}}(\alpha)$, which is given in explicit form as a result of our theorem. Most importantly, this additional condition is fulfilled for a degenerate excited state multiplet, i.e., if the Zeeman splitting δ vanishes. Then, there is no preferred direction in space, such that the invariance of the eigenenergies, which are observables, can be expected.

We then conclude the breakdown of the few-level approximation, since our results of the previous sections are violated if any of the excited state multiplet sublevels are artificially removed. Possible consequences are, for example, a spurious dependence of the eigenenergies on the orientation of the atomic separation vector, and thus of all observables that depend on the transition frequencies among the various eigenstates of the system. In experiments, in addition, a loss of population from the subspace considered in the few-level approximation would be observed. We have identified the vacuum-induced dipole-dipole coupling between transitions with orthogonal dipole moments as the origin of the breakdown. On the one hand, this explains why the breakdown exclusively occurs in collective systems, since such orthogonal couplings are impossible in single atoms in free space. On the other hand, the interpretation enables one to identify special geometries where some of the Zeeman sublevels can be omitted. This also allows to connect our results to previous studies involving dipole-dipole interacting few-level systems. In these studies involving the few-level approximation, typically a very special geometry was chosen, e.g., with atomic separation vector and transition dipole moments orthogonal or parallel to each other.

These results remain valid if a geometry can be found such that the full Zeeman sublevel scheme reduces to the chosen level scheme as discussed in Sec. 4.4.2. It should be noted, however, that there are physical realizations of interest which in general do not allow for a particular system geometry that leads to the validity of a few-level approximation, such as quantum gases.

On a more technical side, our results can also be applied to considerably simplify the computational effort required for the treatment of such dipole-dipole interacting multilevel systems with arbitrary alignment of the two atoms. First, our theorem both allows for a convenient evaluation of eigenvalues and eigenenergies for arbitrary orientations of the atomic separation vector based on the results found in a single, special alignment. Second, we have found in Sec. 4.4.2 that for the degenerate system, the density matrices for different orientations are related to each other by the unitary transformation W defined in our theorem. Thus the solution for any orientation can be obtained from a single time integration simply by applying this transformation.

Finally, we point out that the theorem derived in Sec. 4.4 does not only apply to a pair of atoms with internal level structure as shown in Fig. 4.1(b). On the contrary, the theorem and its implications can easily be generalized to systems where the level scheme of each atom is comprised of other angular momentum multiplets than the $S_0 \leftrightarrow P_1$ transition considered here.

Chapter 5

Coherent control in a decoherence-free subspace of a collective multi-level system

5.1 Introduction

The fields of quantum computation and quantum information processing have attracted a lot of attention due to their promising applications such as the speedup of classical computations [5, 110, 111]. Although the physical implementation of basic quantum information processors has been achieved recently [7], the realization of powerful and useable devices is still a challenging and as yet unresolved problem. A major difficulty arises from the interaction of a quantum system with its environment, which leads to decoherence [8, 9]. One possible solution to this problem is provided by the concept of decoherence-free subspaces (DFS) [112–117]. Under certain conditions, a subspace of a physical system is decoupled from its environment such that the dynamics within this subspace is purely unitary. Experimental realizations of DFS have been achieved with photons [118–121] and in nuclear spin systems [122–124]. A decoherence-free quantum memory for one qubit has been realized experimentally with two trapped ions [125, 126].

The physical implementation of most quantum computation and quantum information schemes involves the generation of entanglement and the realization of quantum gates. It has been shown that dipole-dipole interacting systems are both a resource for entanglement and suitable candidates for the implementation of gate operations between two qubits [14, 91, 93, 107–109, 127]. The creation of entanglement in collective two-atom systems is discussed in [14, 93]. Several schemes employ the dipole-dipole induced energy shifts of collective states to realize quantum gates, for example, in systems of two atoms [91, 107, 108, 127] or quantum dots [109]. In order to ensure that the induced dynamics is fast as compared to decoherence processes, the dipole-dipole interaction must be strong, and thus the distance between the par-

ticles must be small. On the other hand, it is well known that a system of particles which are closer together than the relevant transition wavelength displays collective states which are immune against spontaneous emission [4, 10, 11, 14, 73]. The space spanned by these subradiant states is an example for a DFS, and hence the question arises whether qubits and gate operations enabled by the coherent part of the dipole-dipole interaction can be embedded into this DFS. In the simple model of a pair of interacting two-level systems, there exists only a single subradiant state. Larger DFS which are suitable for the storage and processing of quantum information can be found, e.g., in systems of many two-level systems [128, 129].

Here, we pursue a different approach and consider a pair of dipole-dipole interacting multi-level atoms (see Fig. 4.1). The level scheme of each of the atoms is modeled by a $S_0 \leftrightarrow P_1$ transition that can be found, e.g., in ^{40}Ca atoms. The excited state multiplet P_1 consists of three Zeeman sublevels, and the ground state is a S_0 singlet state. We consider arbitrary geometrical alignments of the atoms, i.e. the length and orientation of the vector $\boldsymbol{R}$ connecting the atoms can be freely adjusted. In this case, the analysis in chapter 4 shows that all Zeeman sublevels of the atomic multiplets have to be taken into account. Experimental studies of such systems have become feasible recently [94, 96, 106].

As our main results, we demonstrate that the state space of the two atoms contains a four-dimensional DFS if the interatomic distance R approaches zero. A careful analysis of both the coherent and the incoherent dynamics reveals that the antisymmetric states of the DFS can be populated with a laser field, and that coherent dynamics can be induced within the DFS via an external static magnetic or a radio-frequency field. Finally, it is shown that the system can be prepared in long-lived entangled states.

More specifically, all features of the collective two-atom system will be derived from the master equation for the two atoms which we discussed in Sec. 4.2. To set the stage, we prove the existence of the four-dimensional DFS in the case of small interatomic distance R in Sec. 5.2.

Subsequent sections of this chapter address the question whether this DFS can be employed to store and process quantum information. In a first step, we provide a detailed analysis of the coherent and incoherent system dynamics (Sec. 5.3). The eigenstates and energies in the case where the Zeeman splitting δ of the excited states vanishes are presented in Sec. 5.3.1. In Sec. 5.3.2, we calculate the decay rates of the collective two-atom states which are formed by the coherent part of the dipole-dipole interaction. It is shown that spontaneous emission in the DFS is strongly suppressed if the distance between the atoms is small as compared to the wavelength of the $S_0 \leftrightarrow P_1$ transition. The full energy spectrum in the presence of a magnetic field is investigated in Sec. 5.3.3.

The DFS is comprised of the collective ground state and three antisymmetric collective states. In Sec. 5.4, we show that the antisymmetric states can be populated selectively by means of an external laser field. The probability to find the system in a (pure) antisymmetric state is 1/4 in steady state. In particular, the described

method does not require a field gradient between the position of the two atoms.

We then address coherent control within the DFS, and demonstrate that the coherent time evolution of two states in the DFS can be controlled via the Zeeman splitting δ of the excited states and therefore by means of an external magnetic field (Sec. 5.5). Both static magnetic fields and radio-frequency (RF) fields are considered. The time evolution of the two states is visualized in the Bloch sphere picture. While a static magnetic field can only induce a limited dynamics, any single-qubit operation can be performed by an RF field.

In Sec. 5.6, we determine the degree of entanglement of the symmetric and antisymmetric collective states which are formed by the coherent part of the dipole-dipole interaction. We employ the concurrence as a measure of entanglement and show that the symmetric and antisymmetric states are entangled. The degree of entanglement of the collective states is the same as in the case of two two-level atoms. But in contrast to a pair of two-level atoms, the symmetric and antisymmetric states of our system are not maximally entangled. A brief summary and discussion of our results is provided in Sec. 5.7.

5.2 Decoherence-free subspace

In this section we show that the system described in Sec. 4.2 exhibits a decoherence-free subspace. By definition, a subspace $\mathcal{V}$ of a Hilbert space $\mathcal{H}$ is said to be decoherence-free if the time evolution inside $\mathcal{V}$ is purely unitary [113, 114, 117]. For the moment, we assume that the system initially is prepared in a pure or mixed state in the subspace $\mathcal{V}$. The system state is then represented by a positive semi-definite Hermitian density operator $\varrho_{\mathcal{V}} \in \mathrm{End}(\mathcal{V})$ with $\mathrm{Tr}(\varrho_{\mathcal{V}}) = 1$. It follows that $\mathcal{V}$ is a decoherence-free subspace if two conditions are met. First, the time evolution of $\varrho_{\mathcal{V}}$ can only be unitary if the decohering dynamics is zero, and therefore we must have [see Eq. (4.5)]

$$\mathcal{L}_\gamma \varrho_{\mathcal{V}} = 0 \tag{5.1}$$

for all density operators $\varrho_{\mathcal{V}}$ that represent a physical system over $\mathcal{V}$. Second, the unitary time evolution governed by $H_\mathrm{A} + H_\Omega$ must not couple states in $\mathcal{V}$ to any states outside of $\mathcal{V}$. Consequently, $\mathcal{V}$ has to be invariant under the action of $H_\mathrm{A} + H_\Omega$,

$$|\psi\rangle \in \mathcal{V} \quad \Longrightarrow \quad (H_\mathrm{A} + H_\Omega)|\psi\rangle \in \mathcal{V}\,. \tag{5.2}$$

Note that since $(H_\mathrm{A} + H_\Omega)$ is Hermitian, this condition also implies that it cannot couple states outside of $\mathcal{V}$ to states in $\mathcal{V}$.

In a first step we seek a solution of Eq. (5.1). To this end we denote the state space of the two atoms by $\mathcal{H}_\mathrm{sys}$ and choose the 16 vectors $|i,j\rangle = |i_1\rangle \otimes |j_2\rangle$ ($i,\, j \in \{1,2,3,4\}$) as a basis of $\mathcal{H}_\mathrm{sys}$. The density operator ϱ can then be expanded in terms of the 256 operators

$$|i,j\rangle\langle k,l|\,, \qquad i,\, j,\, k,\, l \in \{1,2,3,4\}\,, \tag{5.3}$$

that constitute a basis in the space of all operators acting on $\mathcal{H}_{\rm sys}$,

$$\varrho = \sum_{i,j=1}^{4} \sum_{k,l=1}^{4} \varrho_{ij,kl} |i,j\rangle\langle k,l| \,. \tag{5.4}$$

It follows that ϱ can be regarded as a vector with 256 components $\varrho_{ij,kl}$ and the linear superoperator $\mathcal{L}_\gamma$ is represented by a 256×256 matrix. Equation (5.1) can thus be transformed into a homogeneous system of linear equations which can be solved by standard methods.

For a finite distance of the two atoms, the only exact solution of Eq. (5.1) is given by $|4,4\rangle\langle 4,4|$, i.e. only the state $|4,4\rangle$ where each of the atoms occupies its ground state is immune against spontaneous emission. A different situation arises if the interatomic distance R approaches zero. In this case, the collective decay rates obey the relations

$$\begin{aligned} \lim_{R\to 0} \Gamma_{31} = \lim_{R\to 0} \Gamma_{32} = \lim_{R\to 0} \Gamma_{21} = 0 \\ \lim_{R\to 0} \Gamma_{11} = \lim_{R\to 0} \Gamma_{22} = \lim_{R\to 0} \Gamma_{33} = \gamma \,. \end{aligned} \tag{5.5}$$

In order to characterize the general solution of Eq. (5.1) in the limit $R \to 0$, we introduce the three antisymmetric states

$$|a_i\rangle = \frac{1}{\sqrt{2}} \big[\, |i,4\rangle - |4,i\rangle \,\big] \,, \quad i \in \{1,2,3\} \,, \tag{5.6}$$

as well as the 4 dimensional subspace

$$\mathcal{V} = \mathrm{Span}(|4,4\rangle,\, |a_1\rangle,\, |a_2\rangle,\, |a_3\rangle) \,. \tag{5.7}$$

The set of operators acting on $\mathcal{V}$ forms the 16 dimensional operator subspace $\mathrm{End}(\mathcal{V})$. We find that the solution of Eq. (5.1) in the limit $R \to 0$ is determined by

$$\mathcal{L}_\gamma \hat{O} = 0 \quad \Longleftrightarrow \quad \hat{O} \in \mathrm{End}(\mathcal{V}) \,. \tag{5.8}$$

In particular, any positive semi-definite Hermitian operator $\varrho_{\mathcal{V}} \in \mathrm{End}(\mathcal{V})$ that represents a state over $\mathcal{V}$ does not decay by spontaneous emission provided that $R \to 0$.

We now turn to the case of imperfect initialization, i.e., the initial state is not entirely contained in the subspace $\mathcal{V}$. Then, states outside of $\mathcal{V}$ spontaneously decay into the DFS [117]. This strictly speaking disturbs the unitary time evolution inside the DFS, but does not mean that population leaks out of the DFS. Also, this perturbing decay into the DFS only occurs on a short timescale on the order of γ^{-1} at the beginning of the time evolution.

These results can be understood as follows. In the Dicke model [14, 73] of two nearby 2-level atoms, the antisymmetric collective state is radiatively stable if the interatomic distance approaches zero. In the system shown in Fig. 4.1, each of the three allowed dipole transitions in one of the atoms and the corresponding transition

in the other atom form a system that can be thought of as two 2-level atoms. This picture is supported by the fact that the cross-decay rates originating from the interaction between orthogonal dipoles of different atoms vanish as R approaches zero [see Eq. (5.5)]. Consequently, the suppressed decay of one of the antisymmetric states $|a_i\rangle$ is independent of the other states.

In contrast to the cross-decay rates, the coherent dipole-dipole interaction between orthogonal dipoles of different atoms is not negligible as R goes to zero. It is thus important to verify condition (5.2) that requires $\mathcal{V}$ to be invariant under the action of $H_\mathrm{A} + H_\Omega$. To show that Eq. (5.2) holds, we calculate the matrix representation of H_Ω in the subspace $\mathcal{A}$ spanned by the antisymmetric states $\{|a_1\rangle, |a_2\rangle, |a_3\rangle\}$,

$$[H_\Omega]_\mathcal{A} = \hbar \begin{pmatrix} \Omega_{11} & \Omega_{21}^* & \Omega_{31}^* \\ \Omega_{21} & \Omega_{22} & \Omega_{32}^* \\ \Omega_{31} & \Omega_{32} & \Omega_{33} \end{pmatrix} . \tag{5.9}$$

Similarly, we introduce the symmetric states

$$|s_i\rangle = \frac{1}{\sqrt{2}} \big[\, |i,4\rangle + |4,i\rangle \,\big] , \quad i \in \{1,2,3\} , \tag{5.10}$$

and the representation of H_Ω on the subspace $\mathcal{S}$ spanned by the states $\{|s_1\rangle, |s_2\rangle, |s_3\rangle\}$ is described by

$$[H_\Omega]_\mathcal{S} = -\hbar \begin{pmatrix} \Omega_{11} & \Omega_{21}^* & \Omega_{31}^* \\ \Omega_{21} & \Omega_{22} & \Omega_{32}^* \\ \Omega_{31} & \Omega_{32} & \Omega_{33} \end{pmatrix} . \tag{5.11}$$

It is found that H_Ω can be written as

$$H_\Omega = \sum_{i,j=1}^{3} \langle a_i|H_\Omega|a_j\rangle |a_i\rangle\langle a_j| + \sum_{i,j=1}^{3} \langle s_i|H_\Omega|s_j\rangle |s_i\rangle\langle s_j| , \tag{5.12}$$

i.e., all matrix elements $\langle a_i|H_\Omega|s_j\rangle$ between a symmetric and an antisymmetric state vanish. This result implies that H_Ω couples the antisymmetric states among themselves, but none of them is coupled to a state outside of $\mathcal{A}$. Moreover, the ground state $|4,4\rangle$ is not coupled to any other state by H_Ω. It follows that the subspace $\mathcal{V}$ is invariant under the action of H_Ω.

It remains to demonstrate that $\mathcal{V}$ is invariant under the action of the free Hamiltonian H_A in Eq. (4.1). With the help of the definitions of $|a_i\rangle$ and $|s_i\rangle$ in Eqs. (5.6) and (5.10), it is easy to verify that H_A is diagonal within the subspaces $\mathcal{A}$ and $\mathcal{S}$. In particular, H_A does not introduce a coupling between the states $|a_i\rangle$ and $|s_i\rangle$,

$$\begin{aligned} \langle s_i|H_\mathrm{A}|a_i\rangle &= \frac{1}{2} \left[\langle i,4|H_\mathrm{A}|i,4\rangle - \langle 4,i|H_\mathrm{A}|4,i\rangle \right] \\ &= \frac{\hbar}{2} \left(\omega_i \, \langle i_1|S_{i+}^{(1)} S_{i-}^{(1)}|i_1\rangle - \omega_i \, \langle i_2|S_{i+}^{(2)} S_{i-}^{(2)}|i_2\rangle \right) \\ &= 0 . \end{aligned} \tag{5.13}$$

Note that these matrix elements vanish since we assumed that the two atoms are identical, i.e. we suppose that the energy $\hbar\omega_i$ of the internal state $|i_\mu\rangle$ does not depend on the index μ which labels the atoms.

In conclusion, we have shown that the system of two nearby four-level atoms exhibits a four-dimensional decoherence-free subspace $\mathcal{V} \subset \mathcal{H}_{\rm sys}$ if the interatomic distance R approaches zero. However, in any real situation the distance between the two atoms remains finite. In this case, condition Eq. (5.1) holds approximately and spontaneous emission in $\mathcal{V}$ is suppressed as long as R is sufficiently small. In Sec. 5.3.2, we demonstrate that the decay rates of states in $\mathcal{V}$ are smaller than in the single-atom case provided that $R \lesssim 0.43 \times \lambda_0$.

5.3 System dynamics – eigenvalues and decay rates

The aim of this section is to determine the energies and decay rates of the eigenstates of the system Hamiltonian $H_{\rm A} + H_\Omega$. We demonstrated in chapter 4 that this diagonalization procedure is facilitated by the implications of the theorem derived in Sec. 4.4. However, here we find the eigenvalues and eigenvectors with conventional methods and compare our results with the predictions of the theorem. In a first step (Sec. 5.3.1), we determine the eigenstates and eigenvalues of H_Ω. It will turn out that the eigenstates of H_Ω are also eigenstates of $H_{\rm A}$, provided that the Zeeman splitting of the excited states vanishes ($\delta = 0$). Section 5.3.2 discusses the spontaneous decay rates of the eigenstates of H_Ω, and Sec. 5.3.3 is concerned with the full diagonalization of $H_{\rm A} + H_\Omega$ for $\delta \neq 0$.

5.3.1 Diagonalization of H_Ω

We find the eigenstates and eigenenergies of H_Ω by the diagonalization of the two 3×3 matrices $[H_\Omega]_{\mathcal{A}}$ and $[H_\Omega]_{\mathcal{S}}$ which are defined in Eq. (5.9) and Eq. (5.11), respectively. The eigenstates of H_Ω in the subspace $\mathcal{A}$ spanned by the antisymmetric states are given by

$$\begin{aligned} |\psi_a^1\rangle &= \sin\theta|a_2\rangle - \cos\theta|\psi_a^-\rangle\,, \\ |\psi_a^2\rangle &= |\psi_a^+\rangle\,, \\ |\psi_a^3\rangle &= \cos\theta|a_2\rangle + \sin\theta|\psi_a^-\rangle\,, \end{aligned} \tag{5.14}$$

where

$$|\psi_a^\pm\rangle = \frac{1}{\sqrt{2}}\big[\, e^{i\phi}|a_1\rangle \pm e^{-i\phi}|a_3\rangle\,\big]\,. \tag{5.15}$$

We denote the eigenvalue of the state $|\psi_a^i\rangle$ by λ_a^i and find

$$\lambda_a^1 = \lambda_a^2 = \hbar\Omega_F\,, \qquad \lambda_a^3 = \hbar\Omega_N\,, \tag{5.16}$$

where

$$\begin{aligned}\Omega_F &= -\gamma\frac{3}{2\eta^3}\left[\left(1-\eta^2\right)\cos(\eta)+\eta\sin(\eta)\right]\,,\\ \Omega_N &= \gamma\frac{3}{\eta^3}\left[\cos(\eta)+\eta\sin(\eta)\right]\,,\end{aligned} \tag{5.17}$$

and $\eta = k_0 R$. The parameters Ω_F and Ω_N are shown in Fig. 5.1 as a function of the interatomic distance R.

The eigenstates of H_Ω in the subspace $\mathcal{S}$ spanned by the symmetric states are found to be

$$\begin{aligned}|\psi_s^1\rangle &= \sin\theta|s_2\rangle - \cos\theta|\psi_s^-\rangle\,,\\ |\psi_s^2\rangle &= |\psi_s^+\rangle\,,\\ |\psi_s^3\rangle &= \cos\theta|s_2\rangle + \sin\theta|\psi_s^-\rangle\,,\end{aligned} \tag{5.18}$$

where

$$|\psi_s^\pm\rangle = \frac{1}{\sqrt{2}}\left[\,e^{i\phi}|s_1\rangle \pm e^{-i\phi}|s_3\rangle\,\right], \tag{5.19}$$

and the corresponding eigenvalues read

$$\lambda_s^1 = \lambda_s^2 = -\hbar\Omega_F\,, \quad \lambda_s^3 = -\hbar\Omega_N\,. \tag{5.20}$$

Next we discuss several features of the eigenstates and eigenenergies of H_Ω. First, note that two of the symmetric (antisymmetric) states are degenerate. Second, we point out that the matrices $[H_\Omega]_\mathcal{A}$ and $[H_\Omega]_\mathcal{S}$ consist of the coupling terms Ω_{ij} which depend on the interatomic distance R and the angles θ and ϕ [see Fig. 4.1

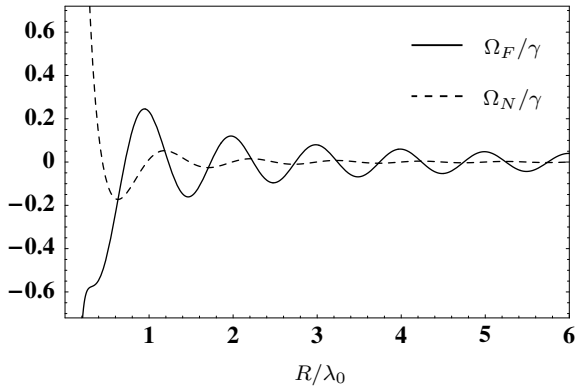

Figure 5.1: Plot of the vacuum induced energy shifts Ω_F and Ω_N as a function of the interatomic distance R according to Eq. (5.17). These shifts enter the expressions for the eigenvalues of H_Ω in Eqs. (5.16) and (5.20). Note that Ω_F decreases with $1/R$ for large values of R, while Ω_N vanishes with $1/R^2$.

and Eq. (4.12)]. On the contrary, the eigenstates $|\psi_a^i\rangle$ and $|\psi_s^i\rangle$ depend only on the angles θ and ϕ, but not on the interatomic distance R. Conversely, the eigenvalues of H_Ω are only functions of the atomic separation R and do not depend on the angles θ and ϕ. This remarkable result is consistent with the theorem that has been derived in Sec. 4.4. The theorem states that the dipole-dipole induced energy shifts between collective two-atom states depend on the length of the vector connecting the atoms, but not on its orientation, provided that the level scheme of each atom is modelled by complete sets of angular momentum multiplets. Since we take all magnetic sublevels of the $S_0 \leftrightarrow P_1$ transition into account, the theorem applies to the system shown in Fig. 4.1.

In Sec. 5.3.3, we show that the eigenstates $|\psi_a^i\rangle$ and $|\psi_s^i\rangle$ of H_Ω are also eigenstates of H_A, provided that the Zeeman splitting δ of the excited states vanishes. This implies that the energy levels of the degenerate system ($\delta = 0$) do not depend on the angles θ and ϕ, but only on the interatomic distance R. From a physical point of view, this result can be understood as follows. In the absence of a magnetic field ($\delta = 0$), there is no distinguished direction in space. Since the vacuum is isotropic in free space, one expects that the energy levels of the system are invariant under rotations of the separation vector $\boldsymbol{R}$.

5.3.2 Decay rates

In order to find the decay rates that correspond to the Eigenstates $|\psi_a^i\rangle$ and $|\psi_s^i\rangle$ of the Hamiltonian H_Ω, we project Eq. (4.8) onto these states and arrive at

$$\begin{aligned} \partial_t \langle\psi_a^i|\varrho|\psi_a^i\rangle &= -2\,\Gamma_a^i \langle\psi_a^i|\varrho|\psi_a^i\rangle + C_a^i(t)\,, \\ \partial_t \langle\psi_s^i|\varrho|\psi_s^i\rangle &= -2\,\Gamma_s^i \langle\psi_s^i|\varrho|\psi_s^i\rangle + C_s^i(t)\,. \end{aligned} \tag{5.21}$$

In these equations, $2\,\Gamma_a^i$ and $2\,\Gamma_s^i$ denote the decay rates of the states $|\psi_a^i\rangle$ and $|\psi_s^i\rangle$, respectively. The time-dependent functions $C_a^i(t)$ and $C_s^i(t)$ describe the increase of the populations $\langle\psi_a^i|\varrho|\psi_a^i\rangle$ and $\langle\psi_s^i|\varrho|\psi_s^i\rangle$ due to spontaneous emission from states $|i,j\rangle$ ($i,j \in \{1,2,3\}$) where both atoms occupy an excited state. The explicit expressions for the coefficients Γ_a^i and Γ_s^i as a function of the parameter $\eta = k_0 R$ are given by

$$\begin{aligned} \Gamma_a^1 &= \Gamma_a^2 = \gamma\frac{1}{2\eta^3}\left[2\eta^3 - 3\eta\cos(\eta) + 3\left(1-\eta^2\right)\sin(\eta)\right]\,, \\ \Gamma_a^3 &= \gamma\frac{1}{\eta^3}\left[\eta^3 + 3\eta\cos(\eta) - 3\sin(\eta)\right]\,, \\ \Gamma_s^1 &= \Gamma_s^2 = \gamma\frac{1}{2\eta^3}\left[2\eta^3 + 3\eta\cos(\eta) - 3\left(1-\eta^2\right)\sin(\eta)\right]\,, \\ \Gamma_s^3 &= \gamma\frac{1}{\eta^3}\left[\eta^3 - 3\eta\cos(\eta) + 3\sin(\eta)\right]\,. \end{aligned} \tag{5.22}$$

These functions do not depend on the angles θ and ϕ, but only on the interatomic distance R. As for the dipole-dipole induced energy shifts of the states $|\psi_a^i\rangle$ and $|\psi_s^i\rangle$ (see Sec. 5.3.1), this result is in agreement with the theorem derived in Sec 4.4.1.

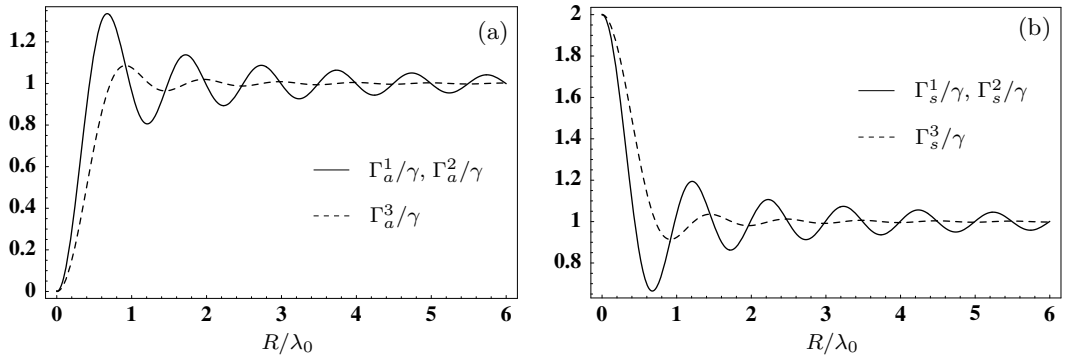

Figure 5.2: Dependence of the parameters Γ_a^i and Γ_s^i on the interatomic distance R according to Eq. (5.22). (a) In the limit $R \to 0$, the Γ_a^i tend to zero, and the antisymmetric states $|\psi_a^i\rangle$ are subradiant. (b) The symmetric states $|\psi_s^i\rangle$ decay twice as fast as compared to two independent atoms if R approaches zero.

While Λ_a^1 and Λ_a^2 tend to $-\infty$ in the limit $R \to 0$, Λ_a^3 tends to $+\infty$. The frequency splitting of the excited states is $\delta = \gamma$. In (d), the Λ_a^i are shown as a function of the interatomic distance R, the parameters are $\theta = \pi/2$ and $\delta = \gamma$.

Figure 5.2(a) shows the parameters Γ_a^i as a function of R. The oscillations of Γ_a^1 and Γ_a^2 around γ are damped with $1/R$ as R increases, and those of Γ_a^3 decrease with $1/R^2$. Note that the oscillations of the frequency shifts λ_a^i display similar features for $R \gg \lambda_0$ (see Sec. 5.3.1). It has been shown in Sec. 5.2 that any state within the subspace $\mathcal{A}$ of antisymmetric states is completely stable for $R \to 0$. Consequently, the decay rates $2\Gamma_a^i$ of the states $|\psi_a^i\rangle$ tend to zero as R approaches zero. It can be verified by numerical methods that Γ_a^1 and Γ_a^2 are smaller than the parameter γ provided that $R \lesssim 0.44 \times \lambda_0$, and Γ_a^3 does not exceed γ if $R \lesssim 0.72 \times \lambda_0$. For $R = 0.1 \times \lambda_0$, the coefficients Γ_a^i are smaller than $0.1 \times \gamma$. Although R is larger than zero in an experiment, the states $|\psi_a^i\rangle$ decay much slower as compared to two non-interacting atoms if R is sufficiently small. This shows that spontaneous emission can be strongly suppressed within the subspace $\mathcal{A}$ of the antisymmetric states, even for a realistic value of the interatomic distance R.

The parameters Γ_s^i are depicted in Fig. 5.2(b). In the limit $R \to 0$, the coefficients Γ_s^i tend to 2γ. The symmetric states within the subspace $\mathcal{S}$ display thus superradiant features since they decay faster as compared to two independent atoms.

5.3.3 Non-degenerate system

Here we discuss the diagonalization of $H_\mathrm{A} + H_\Omega$ in the most general case where the Zeeman splitting δ of the excited states is different from zero. The matrix representation of this Hamiltonian with respect to the states $\{|\psi_a^1\rangle, |\psi_a^2\rangle, |\psi_a^3\rangle\}$ defined in

Eq. (5.14) reads

$$[H_{\rm A}+H_\Omega]_{\mathcal{A}} = \hbar \begin{pmatrix} \omega_0+\Omega_F & \delta\cos\theta & 0 \\ \delta\cos\theta & \omega_0+\Omega_F & -\delta\sin\theta \\ 0 & -\delta\sin\theta & \omega_0+\Omega_N \end{pmatrix} . \tag{5.23}$$

In general, the eigenvalues of this matrix can be written in the form

$$\begin{aligned} E_a^1 &= \hbar\left(\omega_0+\Lambda_a^1\right) , \\ E_a^2 &= \hbar\left(\omega_0+\Lambda_a^2\right) , \\ E_a^3 &= \hbar\left(\omega_0+\Lambda_a^3\right) , \end{aligned} \tag{5.24}$$

where the frequency shifts Λ_a^i depend only on the interatomic distance R and the azimuthal angle θ, but not on the angle ϕ. To illustrate this result, we consider a plane spanned by $\boldsymbol{e}_z$ and $\boldsymbol{e}_\phi = (\cos\phi, \sin\phi, 0)$, see Fig. 5.3. Within this plane, the vector $\boldsymbol{R} = z\,\boldsymbol{e}_z + l\,\boldsymbol{e}_\phi$ is described by the parameters z and l, and Fig. 5.4(a)-(c) shows $\Lambda_a^i(l,z)$ as a function of these variables. Since the Λ_a^i do not depend on ϕ, the energy surfaces shown in Fig. 5.4(a)-(c) remain the same if $\boldsymbol{e}_\phi$ is rotated around the z axis. This result follows from the fact that the Hamiltonian $H_{\rm A}$ in Eq. (4.1) is invariant under rotations around the z axis (see Sec. 4.4.2).

In Sec. 5.5, we will focus on the geometrical setup where the atoms are aligned in the x-y plane ($\theta = \pi/2$). In this case, the frequency shifts Λ_a^i of the antisymmetric states are found to be

$$\begin{aligned} \Lambda_a^1 &= \Omega_F\,, \\ \Lambda_a^2 &= (\Omega_F+\Omega_N)/2 - \omega_B/2\,, \\ \Lambda_a^3 &= (\Omega_F+\Omega_N)/2 + \omega_B/2\,, \end{aligned} \tag{5.25}$$

where the Bohr frequency is given by

$$\omega_B = \sqrt{4\delta^2 + (\Omega_F-\Omega_N)^2}\,. \tag{5.26}$$

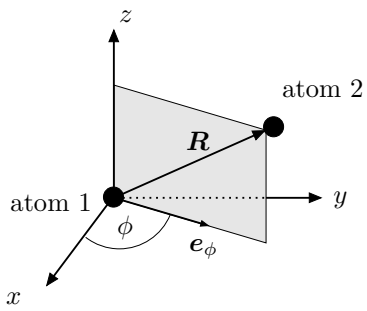

Figure 5.3: The atoms are aligned in a plane spanned by the unit vectors $\boldsymbol{e}_z$ and $\boldsymbol{e}_\phi = (\cos\phi, \sin\phi, 0)$. Within this plane, the relative position of the two atoms $\boldsymbol{R} = z\,\boldsymbol{e}_z + l\,\boldsymbol{e}_\phi$ is described by the parameters z and l. The energies of the eigenstates of $H_{\rm A}+H_\Omega$ depend only on z and l, but not on ϕ.

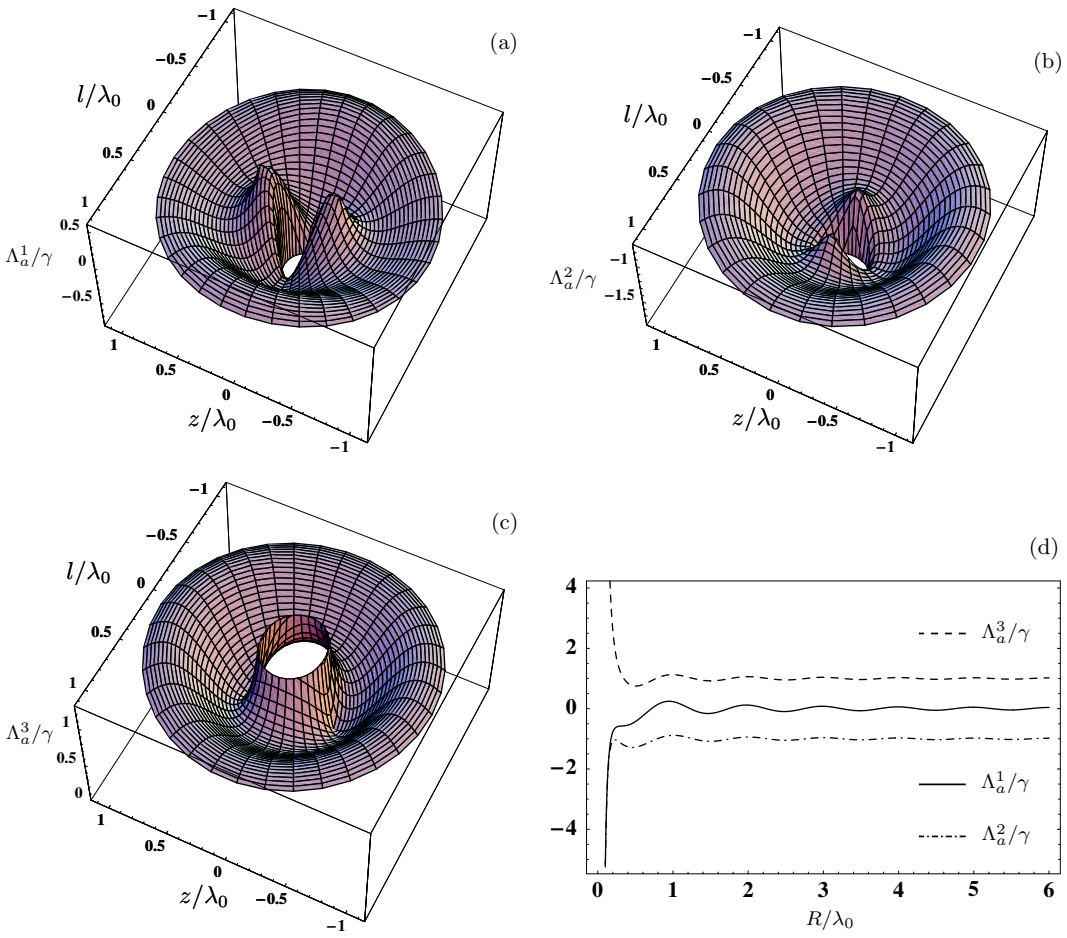

Figure 5.4: Plot of the energy shifts that determine the energy levels of the antisymmetric states according to Eq. (5.24). In (a)-(c), the parameters Λ_a^i are shown in a plane spanned by $\boldsymbol{e}_z$ and $\boldsymbol{e}_\phi = (\cos\phi, \sin\phi, 0)$. The relative position $\boldsymbol{R} = z\,\boldsymbol{e}_z + l\,\boldsymbol{e}_\phi$ of the atoms in this plane is parameterized by z and l (see also Fig. 5.3). Since the Λ_a^i do not depend on ϕ, the energy surfaces shown in (a)-(c) do not change if $\boldsymbol{e}_\phi$ is rotated around the z axis.

A plot of the frequency shifts Λ_a^i as a function of the interatomic distance R and for $\theta = \pi/2$ is shown in Fig. 5.4(d). Note that the degeneracy and the level crossing of the eigenvalues λ_a^i is removed for $\delta \neq 0$ (see Sec. 5.3.1). The eigenstates that correspond to the frequency shifts in Eq. (5.25) read

$$\begin{aligned} |\varphi_a^1\rangle &= |a_2\rangle\,, \\ |\varphi_a^2\rangle &= e^{i\xi}\sin\vartheta_a|\psi_a^+\rangle + \cos\vartheta_a|\psi_a^-\rangle\,, \\ |\varphi_a^3\rangle &= -e^{i\xi}\cos\vartheta_a|\psi_a^+\rangle + \sin\vartheta_a|\psi_a^-\rangle\,, \end{aligned} \tag{5.27}$$

where $\delta = |\delta|e^{i\xi}$ ($\xi \in \{0, \pi\}$), the states $|\psi_a^\pm\rangle$ are defined in Eq. (5.15), and the angle

ϑ_a is determined by

$$\tan 2\vartheta_a = \frac{|\delta|}{\Omega_F - \Omega_N}\,, \quad 0 < \vartheta_a < \frac{\pi}{2}\,. \tag{5.28}$$

If the distance between the atoms is small such that $R \lesssim 0.63\times\lambda_0$, we have $\Omega_F < \Omega_N$. In this case, we find $\lim_{\delta\to 0}|\varphi_a^i\rangle = |\psi_a^i\rangle$ and $\lim_{\delta\to 0}\Lambda_a^i = \lambda_a^i$, where the eigenstates $|\psi_a^i\rangle$ and the frequency shifts λ_a^i of the degenerate system are defined in Eqs. (5.14) and (5.16), respectively.

The matrix representation of $H_{\rm A} + H_\Omega$ with respect to the symmetric states $\{|\psi_s^1\rangle, |\psi_s^2\rangle, |\psi_s^3\rangle\}$ defined in Eq. (5.18) is found to be

$$[H_{\rm A} + H_\Omega]_{\mathcal{S}} = \hbar \begin{pmatrix} \omega_0 - \Omega_F & \delta\cos\theta & 0 \\ \delta\cos\theta & \omega_0 - \Omega_F & -\delta\sin\theta \\ 0 & -\delta\sin\theta & \omega_0 - \Omega_N \end{pmatrix}. \tag{5.29}$$

Just as in the case of the antisymmetric states, the eigenvalues of $[H_{\rm A} + H_\Omega]_{\mathcal{S}}$ are written as

$$\begin{aligned} E_s^1 &= \hbar\left(\omega_0 + \Lambda_s^1\right), \\ E_s^2 &= \hbar\left(\omega_0 + \Lambda_s^2\right), \\ E_s^3 &= \hbar\left(\omega_0 + \Lambda_s^3\right), \end{aligned} \tag{5.30}$$

and the frequency shifts Λ_s^i depend only on the interatomic distance R and the azimuthal angle θ.

If the atoms are aligned in the x-y plane ($\theta = \pi/2$), the frequency shifts Λ_s^i of the symmetric states are given by

$$\begin{aligned} \Lambda_s^1 &= -\Omega_F\,, \\ \Lambda_s^2 &= -(\Omega_F + \Omega_N)/2 + \omega_B/2\,, \\ \Lambda_s^3 &= -(\Omega_F + \Omega_N)/2 - \omega_B/2\,, \end{aligned} \tag{5.31}$$

and the corresponding eigenstates are

$$\begin{aligned} |\varphi_s^1\rangle &= |s_2\rangle\,, \\ |\varphi_s^2\rangle &= -e^{i\xi}\cos\vartheta_s|\psi_s^+\rangle + \sin\vartheta_s|\psi_s^-\rangle\,, \\ |\varphi_s^3\rangle &= e^{i\xi}\sin\vartheta_s|\psi_s^+\rangle + \cos\vartheta_s|\psi_s^-\rangle\,. \end{aligned} \tag{5.32}$$

The states $|\psi_s^\pm\rangle$ are defined in Eq. (5.19), $\delta = |\delta|e^{i\xi}$ ($\xi \in \{0, \pi\}$), and the angle ϑ_s is determined by

$$\tan 2\vartheta_s = \frac{|\delta|}{\Omega_N - \Omega_F}\,, \quad 0 < \vartheta_s < \frac{\pi}{2}\,. \tag{5.33}$$

For small values of the interatomic distance R such that $\Omega_F < \Omega_N$, we find $\lim_{\delta\to 0}|\varphi_s^i\rangle = |\psi_s^i\rangle$ and $\lim_{\delta\to 0}\Lambda_s^i = \lambda_s^i$, where the eigenstates $|\psi_s^i\rangle$ and the frequency shifts λ_s^i of the degenerate system are defined in Eqs. (5.18) and (5.20), respectively.

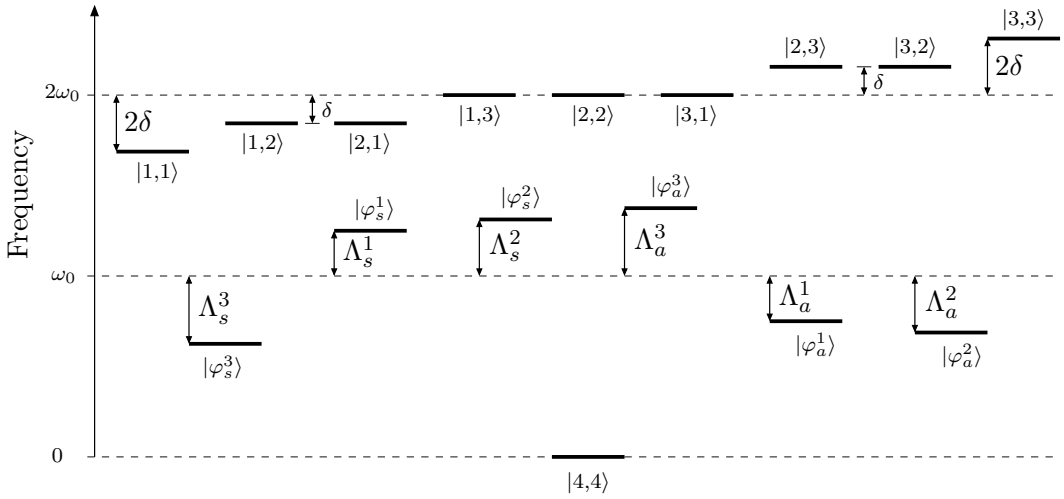

Figure 5.5: Complete level scheme of the non-degenerate system ($\delta \neq 0$). For the special geometrical setup where the atoms are aligned in the x-y plane ($\theta = \pi/2$), the analytical expressions for the states $|\varphi_a^i\rangle$, $|\varphi_s^i\rangle$ and the frequency shifts Λ_a^i, Λ_s^i are given in Eqs. (5.27), (5.32), (5.25) and (5.31), respectively. The frequency shifts Λ_a^i (Λ_s^i) of the antisymmetric (symmetric) states and the splitting of the excited states are not to scale. Note that the frequency shifts Λ_a^i and Λ_s^i depend on the relative position of the atoms.

Finally, we note that the ground state $|4,4\rangle$ and the excited states $|i,j\rangle$ ($i,j \in \{1,2,3\}$) are eigenstates of $H_\mathrm{A} + H_\Omega$. These states together with the symmetric and antisymmetric eigenstates of $H_\mathrm{A} + H_\Omega$ form the new basis of the total state space $\mathcal{H}_\mathrm{sys}$. The complete level scheme of the non-degenerate system is shown in Fig. 5.5.

5.4 Population of the decoherence free subspace

In this section we describe a method that allows to populate the subspace $\mathcal{A}$ spanned by the antisymmetric states. For simplicity, we restrict the analysis to the degenerate system ($\delta = 0$) and show how the states $|\psi_a^i\rangle$ can be populated selectively by means of an external laser field. However, a laser field cannot induce direct transitions between the ground state $|4,4\rangle$ and $|\psi_a^i\rangle$ as long as the electric field at the position of atom 1 is identical to the field at the location of atom 2. By contrast, a direct driving of the antisymmetric states is possible provided that one can realize a field gradient between the positions of the two atoms. Since we consider an interatomic spacing R that is smaller than $\lambda_0/2$ such that the states in $\mathcal{A}$ are subradiant, the realization of this field gradient is an experimentally challenging task. Several authors proposed a setup where the atoms are placed symmetrically around the node of a standing light field [14, 107], and this method also allows to address the states of our system individually. Other methods [11, 14, 130] rest on the assumption that the atoms

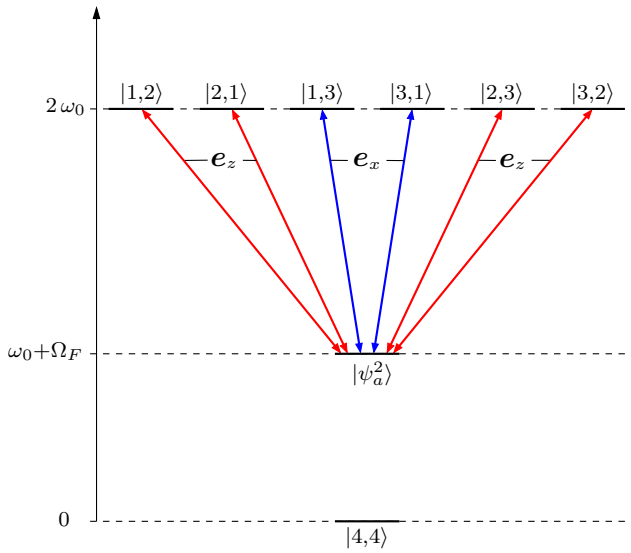

Figure 5.6: Laser-induced coupling of $|\psi_a^2\rangle$ to the excited states $|i,j\rangle$ $(i,j \in \{1,2,3\})$ in the case of the degenerate system. States that are not directly coupled to $|\psi_a^2\rangle$ have been omitted (except for the ground state). The laser polarization that couples the antisymmetric state $|\psi_a^2\rangle$ to a state $|i,j\rangle$ $(i,j \in \{1,2,3\})$ is indicated next to the respective transition. $|\psi_a^2\rangle$ is completely decoupled from a y-polarized laser field.

are *non-identical* and cannot be applied to our system comprised of two identical atoms.

Here we describe a method that allows to populate the states $|\psi_a^i\rangle$ individually and that does not require a field gradient between the positions of the two atoms. It rests on a finite distance between the atoms and exploits the fact that the antisymmetric states may be populated by spontaneous emission from the excited states $|i,j\rangle$ $(i,j \in \{1,2,3\})$. For a given geometrical setup, we choose a coordinate system where the unit vector $\boldsymbol{e}_x$ coincides with the separation vector $\boldsymbol{R}$. In this case, we have $\theta = \pi/2$ and $\phi = 0$. The z direction is determined by the external magnetic field and can be chosen in any direction perpendicular to $\boldsymbol{R}$. The polarization vector of the laser field propagating in z direction lies in the x-y plane and can be adjusted as needed, see Eq. (4.14). In the presence of the laser, the atomic evolution is governed by the master equation (4.15). We find that the coupling of the states $|\psi_a^i\rangle$ to the excited states $|i,j\rangle$ $(i,j \in \{1,2,3\})$ depends on the polarization of the laser field (see Table 5.1 and Fig. 5.6). In particular, it is found that $|\psi_a^1\rangle$ does not couple to z-polarized light, $|\psi_a^2\rangle$ does not couple to y-polarized light and $|\psi_a^3\rangle$ does not couple to x-polarized light. At the same time, the states $|\psi_a^i\rangle$ are populated by spontaneous emission from the excited states. This fact together with the polarization dependent coupling of the antisymmetric states allows to populate the states $|\psi_a^i\rangle$ selectively. In order to populate state $|\psi_a^2\rangle$, for example, one has to shine in a y-polarized field. Since the spontaneous decay of $|\psi_a^2\rangle$ is slow and since $|\psi_a^2\rangle$ is decoupled from the

	$\|\psi_a^1\rangle$	$\|\psi_a^2\rangle$	$\|\psi_a^3\rangle$
$\|1,2\rangle$	$\boldsymbol{e}_x$, $\boldsymbol{e}_y$	$\boldsymbol{e}_z$	$\boldsymbol{e}_z$
$\|2,1\rangle$	$\boldsymbol{e}_x$, $\boldsymbol{e}_y$	$\boldsymbol{e}_z$	$\boldsymbol{e}_z$
$\|1,3\rangle$	-	$\boldsymbol{e}_x$	$\boldsymbol{e}_y$
$\|3,1\rangle$	-	$\boldsymbol{e}_x$	$\boldsymbol{e}_y$
$\|2,3\rangle$	$\boldsymbol{e}_x$, $\boldsymbol{e}_y$	$\boldsymbol{e}_z$	$\boldsymbol{e}_z$
$\|3,2\rangle$	$\boldsymbol{e}_x$, $\boldsymbol{e}_y$	$\boldsymbol{e}_z$	$\boldsymbol{e}_z$

Table 5.1: Polarization of the external laser field that couples an antisymmetric state $|\psi_a^i\rangle$ to an excited state $|i,j\rangle$ ($i,j \in \{1,2,3\}$) for $\delta = 0$. Note that $|\psi_a^1\rangle$ does not couple to z-polarized light, $|\psi_a^2\rangle$ does not couple to y-polarized light and $|\psi_a^1\rangle$ does not couple to x-polarized light. See also Fig. 5.6.

laser, population can accumulate in this state. On the other hand, the states $|\psi_a^1\rangle$ and $|\psi_a^3\rangle$ are depopulated by the laser coupling to the excited states. This situation is shown in Fig. 5.7(a) for two different values of the interatomic distance R. The initial state at $t = 0$ is $|4,4\rangle$, and for $t\cdot\gamma = 20$ the population of $|\psi_a^2\rangle$ is approximately 1/4. Since all coherences between $|\psi_a^2\rangle$ and any other state are zero, the probability to find the system at $t = 20/\gamma$ in the pure state $|\psi_a^2\rangle$ is given by 1/4.

The exact steady state solution of Eq. (4.15) is difficult to obtain analytically. However, one can determine the steady state value of $\langle\psi_a^2|\varrho|\psi_a^2\rangle$ with the help of Eq. (5.21),

$$\langle\psi_a^2|\varrho_{\rm st}|\psi_a^2\rangle = \left[\lim_{t\to\infty} C_a^2(t)\right]/(2\Gamma_a^2)\,. \tag{5.34}$$

The population of $|\psi_a^2\rangle$ in steady state is thus limited by the population of the relevant excited states that are populated by the y-polarized laser field and that decay spontaneously to $|\psi_a^2\rangle$. Furthermore, it is possible to gain some insight into the time evolution of $\langle\psi_a^2|\varrho|\psi_a^2\rangle$. For a strong laser field and for a small value of R, C_a^2 reaches the steady state on a timescale that is fast as compared to $1/(2\Gamma_a^2)$. We may thus replace C_a^2 by its steady state value in Eq. (5.21). The solution of this differential equation is

$$\langle\psi_a^i|\varrho(t)|\psi_a^i\rangle \approx \frac{\left[\lim_{t\to\infty} C_a^i(t)\right]}{2\Gamma_a^i}\left[1 - e^{-2\Gamma_a^2 t}\right] \tag{5.35}$$

and reproduces the exact time evolution of $\langle\psi_a^2|\varrho|\psi_a^2\rangle$ according to Fig. 5.7(a) quite well. Moreover, it becomes now clear why it takes longer until the population of $|\psi_a^2\rangle$ reaches its steady state if the interatomic distance R is reduced since the decay rate $2\Gamma_a^2$ approaches zero as $R \to 0$.

So far, we considered only the population of $|\psi_a^2\rangle$, but the treatment of $|\psi_a^1\rangle$ and $|\psi_a^3\rangle$ is completely analogous. The population of $|\psi_a^3\rangle$ by a x-polarized field is shown

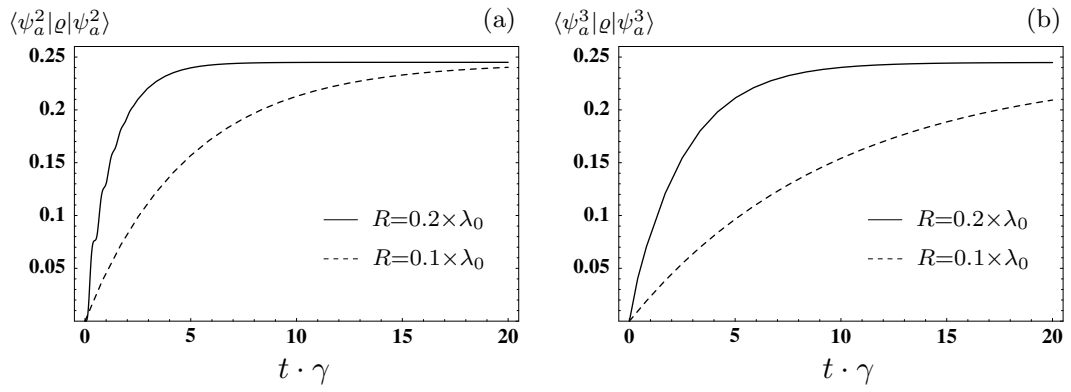

Figure 5.7: Time-dependent population of the states $|\psi_a^i\rangle$ for different polarizations of the driving field. The initial state at $t = 0$ is $|4, 4\rangle$. The parameters are $\theta = \pi/2$, $\phi = 0$, $\delta = 0$ and $\Delta_2 = 0$. (a) Population of $|\psi_a^2\rangle$ for $\Omega_y(\boldsymbol{r}_1) = \Omega_y(\boldsymbol{r}_2) = 5\gamma$. The states $|\psi_a^1\rangle$ and $|\psi_a^3\rangle$ are not populated. (b) Population of $|\psi_a^3\rangle$ for $\Omega_x(\boldsymbol{r}_1) = \Omega_x(\boldsymbol{r}_2) = 5\gamma$. The states $|\psi_a^1\rangle$ and $|\psi_a^2\rangle$ are not populated.

in Fig. 5.7(b). The differences between plot (a) and (b) arise since the decay rates of $|\psi_a^2\rangle$ and $|\psi_a^3\rangle$ are different for the same value of R (see Sec. 5.3.2). In general, the presented method may also be employed to populate the antisymmetric states of the non-degenerate system selectively. In this case, the polarization of the field needed to populate a state $|\varphi_a^i\rangle$ is a function of the detuning δ.

In conclusion, the discussed method allows to populate the antisymmetric states selectively, provided that the interatomic distance is larger than zero. If the interatomic distance is reduced, a longer interaction time with the laser field is required to reach the maximal value of $\langle\psi_a^i|\varrho|\psi_a^i\rangle \approx 1/4$. Note that a finite distance between the atoms is also required in the case of other schemes where the atoms are placed symmetrically around the node of a standing light field [14, 107]. While the latter method allows, at least in principle, for a complete population transfer to the antisymmetric states, its experimental realization is difficult for two nearby atoms. By contrast, our scheme does not require a field gradient between the atoms and is thus easier to implement. It has been pointed out that the population transfer to the antisymmetric states is limited by the population of the excited states that spontaneously decay to an antisymmetric state $|\psi_a^i\rangle$. Although this limit is difficult to overcome, an improvement can be achieved if the fluorescence intensity is observed while the atom is irradiated by the laser. As soon as the system decays into one of the states $|\psi_a^i\rangle$, the fluorescence signal is interrupted for a time period that is on the order of $1/(2\Gamma_a^i)$ (see Sec. 5.3.2). The dark periods in the fluorescence signal reveal thus the spontaneous emission events that lead to the population of one of the antisymmetric states.

5.5 Inducing dynamics within the subspace $\mathcal{A}$

In this Section we assume that the system has been prepared in the antisymmetric state $|\psi_a^2\rangle$, for example by one of the methods described in Sec. 5.4. The aim is to induce a controlled dynamics in the subspace $\mathcal{A}$ of the antisymmetric states. We suppose that the atoms are aligned along the x axis, i.e. $\theta = \pi/2$ and $\phi = 0$. According to Eq. (5.23), the state $|\psi_a^2\rangle$ is then only coupled to $|\psi_a^3\rangle$. Apart from a constant, the Hamiltonian $H_\mathcal{Q}$ that governs the unitary time evolution in the space $\mathcal{Q}$ spanned by $\{|\psi_a^2\rangle, |\psi_a^3\rangle\}$ can be written as

$$H_\mathcal{Q} = \hbar \begin{pmatrix} -(\Omega_N - \Omega_F)/2 & -\delta \\ -\delta & (\Omega_N - \Omega_F)/2 \end{pmatrix}$$

$$= \hbar\omega_B \hat{\boldsymbol{n}} \cdot \boldsymbol{\sigma}/2\,, \tag{5.36}$$

where the vector $\boldsymbol{\sigma} = \{\sigma_x, \sigma_y, \sigma_z\}$ consists of the Pauli matrices σ_i, and the unit vector $\hat{\boldsymbol{n}}$ is defined as

$$\hat{\boldsymbol{n}} = -\left(2\delta, 0, \Omega_N - \Omega_F\right)/\omega_B\,. \tag{5.37}$$

The Bohr frequency ω_B is the difference between the eigenvalues of $H_\mathcal{Q}$ and is given in Eq. (5.26) of Sec. 5.3.3. Equation (5.36) implies that the parameter δ which can be adjusted by means of the external magnetic field introduces a coupling between the states $|\psi_a^2\rangle$ and $|\psi_a^3\rangle$. If the initial state is $|\psi_a^2\rangle$, the final state $|\psi_F\rangle$ reads

$$|\psi_F(t)\rangle = U(t,0)|\psi_a^2\rangle, \tag{5.38}$$

where $U = \exp(-iH_\mathcal{Q}t/\hbar)$ is the time evolution operator. The time evolution induced by $H_\mathcal{Q}$ can be described in a simple way in the Bloch sphere picture [5]. The Bloch vector of the state $|\psi_F(t)\rangle$ is defined as

$$\boldsymbol{B}(t) = \langle\psi_F(t)|\boldsymbol{\sigma}|\psi_F(t)\rangle\,. \tag{5.39}$$

Initially, this vector points into the positive z direction. The time evolution operator U rotates this vector on the Bloch sphere around the axis $\hat{\boldsymbol{n}}$ by an angle $\omega_B t$. According to Eq. (5.37), the axis of rotation lies in the x-z plane and its orientation depends on the parameter δ which can be controlled by means of the magnetic field. In order to demonstrate these analytical considerations, we numerically integrate the master equation (4.5) with the initial condition $\varrho(t=0) = |\psi_a^2\rangle\langle\psi_a^2|$. We define a projector onto the space spanned by $\{|\psi_a^2\rangle, |\psi_a^3\rangle\}$,

$$\hat{P} = |\psi_a^2\rangle\langle\psi_a^2| + |\psi_a^3\rangle\langle\psi_a^3|\,. \tag{5.40}$$

The generalized Bloch vector is then defined as

$$\boldsymbol{B}_N(t) = \mathrm{Tr}\left[\boldsymbol{\sigma}\hat{P}\varrho(t)\hat{P}\right]\,. \tag{5.41}$$

In contrast to $\boldsymbol{B}$, $\boldsymbol{B}_N$ is not necessarily a unit vector, but its length can be smaller than unity due to spontaneous emission from $|\psi_a^2\rangle$ and $|\psi_a^3\rangle$ to the ground state.

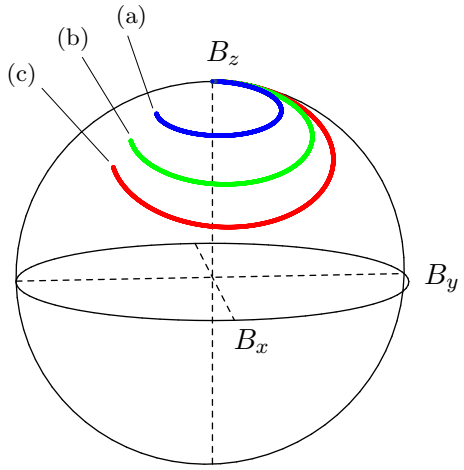

Figure 5.8: Bloch sphere representation of the system dynamics in the subspace $\mathcal{Q}$ spanned by the states $\{|\psi_a^2\rangle, |\psi_a^3\rangle\}$. At $t = 0$, the system is in the pure state $|\psi_a^2\rangle$ and a static magnetic field is switched on. The Bloch vector is rotated around an axis in the x-z plane, and the tilt of this axis in x direction increases with the magnetic field strength. The value of the parameter δ is (a) $\delta = 3.15 \times \gamma$, (b) $\delta = 4.83 \times \gamma$ and (c) $\delta = 6.22 \times \gamma$, and we chose $R = 0.1 \times \lambda_0$.

Figure 5.8 shows the evolution of $\boldsymbol{B}_N$ for different values of the parameter δ which depends on the magnetic field strength. Let $\boldsymbol{S} = \{S_x, S_y, S_z\}$ be a point on the Bloch sphere that lies not in the y-z plane ($S_x \neq 0$). If one chooses the parameter δ according to

$$\delta = \frac{1 - S_z}{2|S_x|} |\Omega_F - \Omega_N| \, \mathrm{Sign}(S_x) \,, \tag{5.42}$$

then $\boldsymbol{S}$ lies on the orbit of the rotating Bloch vector $\boldsymbol{B}$ if spontaneous emission is negligible. According to Eq. (5.42), any point close to the y-z plane requires large values of δ since $|\delta|$ diverges for $S_x \to 0$. The dynamics that can be induced by a static magnetic field is thus restricted, particularly because we are only considering the regime of the linear Zeeman effect.

These limitations can be overcome if a radio-frequency (RF) field is applied instead of a static magnetic field. If the RF field oscillates along the z axis, the Hamiltonian H_A in Eq. (4.1) has to be replaced by

$$H_\mathrm{A}^\mathrm{rf}(t) = \hbar\omega_0 \sum_{i=1}^{3} \sum_{\mu=1}^{2} S_{i+}^{(\mu)} S_{i-}^{(\mu)} + V_\mathrm{rf}(t) \,, \tag{5.43}$$

where

$$V_\mathrm{rf}(t) = 2\hbar\delta(t) \sum_{\mu=1}^{2} \left(S_{3+}^{(\mu)} S_{3-}^{(\mu)} - S_{1+}^{(\mu)} S_{1-}^{(\mu)} \right) \tag{5.44}$$

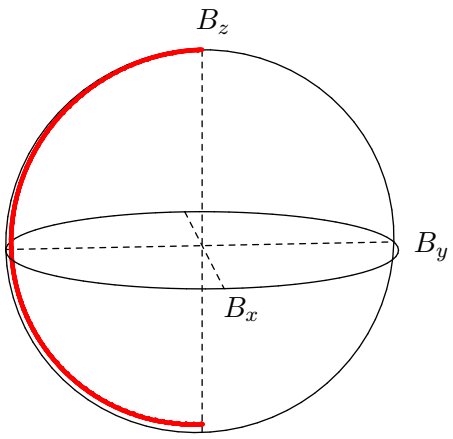

Figure 5.9: Complete population transfer from $|\psi_a^2\rangle$ to $|\psi_a^3\rangle$ by means of a resonant RF field. At $t = 0$, the Bloch vector $\boldsymbol{B}_N$ points into the positive z direction. At $t = \pi/\Omega_{\rm rf}$, the state of the system is $|\psi_a^3\rangle$ and $\boldsymbol{B}_N$ points into the negative z direction. Note that the length of $\boldsymbol{B}_N$ is slightly smaller than unity for $t > 0$ due to the small probability of spontaneous emission to the ground state. The parameters are $R = 0.05 \times \lambda_0$, $\delta_0 = \gamma$, $\phi_{\rm rf} = \pi$ and $\Delta_{\rm rf} = 0$.

describes the interaction with the RF field and

$$\delta(t) = \delta_0 \cos(\omega_{\rm rf}\, t + \phi_{\rm rf})\,. \tag{5.45}$$

In this equation, the magnitude of $\delta_0 (> 0)$ depends on the amplitude of the RF field, and $\omega_{\rm rf}$ and $\phi_{\rm rf}$ are the frequency and phase of the RF field, respectively. We assume that the interatomic distance of the atoms is smaller than $R = 0.63 \times \lambda_0$. In this case, the dipole-dipole interaction raises the energy of $|\psi_a^3\rangle$ with respect to $|\psi_a^2\rangle$, and the frequency difference between these two states is $\Omega_N - \Omega_F > 0$. Furthermore, we suppose that the detuning $\Delta_{\rm rf} = \omega_{\rm rf} - (\Omega_N - \Omega_F)$ of the RF field with the $|\psi_a^2\rangle \leftrightarrow |\psi_a^3\rangle$ transition and the parameter δ_0 are small as compared to $(\Omega_N - \Omega_F)$ such that the rotating-wave approximation can be employed. In a frame rotating with $\omega_{\rm rf}$, the system dynamics in the subspace $\mathcal{Q}$ spanned by $\{|\psi_a^2\rangle, |\psi_a^3\rangle\}$ is then governed by the Hamiltonian

$$\begin{aligned} H_{\mathcal{Q}}^{\rm rf} &= \hbar \begin{pmatrix} \Delta_{\rm rf}/2 & -\delta_0 \exp(i\phi_{\rm rf}) \\ -\delta_0 \exp(-i\phi_{\rm rf}) & -\Delta_{\rm rf}/2 \end{pmatrix} \\ &= \hbar\Omega_{\rm rf}\, \hat{\boldsymbol{n}}_{\rm rf} \cdot \boldsymbol{\sigma}/2\,, \end{aligned} \tag{5.46}$$

where

$$\hat{\boldsymbol{n}}_{\rm rf} = \left(-2\delta_0 \cos\phi_{\rm rf}, -2\delta_0 \sin\phi_{\rm rf}, \Delta_{\rm rf}\right)/\Omega_{\rm rf} \tag{5.47}$$

and $\Omega_{\rm rf} = \sqrt{\Delta_{\rm rf}^2 + 4|\delta_0|^2}$. For a resonant RF field ($\Delta_{\rm rf} = 0$), the axis $\hat{\boldsymbol{n}}_{\rm rf}$ lies in the x-y plane of the Bloch sphere, and its orientation can be adjusted at will by

the phase $\phi_{\rm rf}$ of the RF field. Any single-qubit operation can thus be realized by a sequence of suitable RF pulses [5]. In particular, a complete transfer of population from $|\psi_a^2\rangle$ to $|\psi_a^3\rangle$ can be achieved by a resonant RF pulse with a duration of $\pi/\Omega_{\rm rf}$ and an arbitrary phase $\phi_{\rm rf}$.

Next we demonstrate that the Hamiltonian $H_{\mathcal{Q}}^{\rm rf}$ in Eq. (5.46) describes the system dynamics quite well if the atoms are close to each other such that spontaneous emission is strongly suppressed. For this, we transform the master equation (4.5) with $H_{\rm A}^{\rm rf}$ instead of $H_{\rm A}$ in a frame rotating with $\omega_{\rm rf}$. The resulting equation is integrated numerically without making the rotating-wave approximation. We suppose that the system is initially in the state $|\psi_a^2\rangle$, and the phase of the resonant RF field has been set to $\phi_{\rm rf} = \pi$. Figure 5.9 shows the time evolution of the Bloch vector $\boldsymbol{B}_N$. As predicted by Eq. (5.46), the Bloch vector is rotated around the x axis and at $t = \pi/\Omega_{\rm rf}$, $\boldsymbol{B}_N$ points in the negative z direction. Due to the small probability of spontaneous emission to the ground state, the length of $\boldsymbol{B}_N$ is slightly smaller than unity ($|\boldsymbol{B}_N| = 0.95$) at $t = \pi/\Omega_{\rm rf}$.

Finally, we briefly discuss how the final state $|\psi_F(t)\rangle$ could be measured. In principle, one can exploit the polarization-dependent coupling of the states $|\psi_a^2\rangle$ and $|\psi_a^3\rangle$ to the excited states (see Sec. 5.4). For example, one could ionize the system in a two-step process, where $|\psi_a^2\rangle$ ($|\psi_a^3\rangle$) is first resonantly coupled to the excited states $|i,j\rangle$ ($i,j \in \{1,2,3\}$). A second laser then ionizes the system, and the ionization rate is a measure for the population of state $|\psi_a^2\rangle$ ($|\psi_a^3\rangle$). Another possibility is to shine in a single laser whose frequency is just high enough to ionize the system starting from $|\psi_a^3\rangle$. Since the energy of $|\psi_a^3\rangle$ is higher than those of $|\psi_a^2\rangle$, the ionization rate is a measure for the population of state $|\psi_a^3\rangle$.

5.6 Entanglement of the collective two-atom states

In Sec. 5.3.1, we determined the collective two-atom states $|\psi_a^i\rangle$ and $|\psi_s^i\rangle$ that are formed by the coherent part of the dipole-dipole interaction. Here we show that these states are entangled, i.e. they cannot be written as a single tensor product $|\psi_1\rangle \otimes |\psi_2\rangle$ of two single-atom states. In order to quantify the degree of entanglement, we calculate the concurrence [131, 132] of the pure states $|\psi_a^i\rangle$ and $|\psi_s^i\rangle$. The concurrence for a pure state $|\psi_{12}\rangle$ of the two-atom state space $\mathcal{H}_{\rm sys} = \mathcal{H}_1 \otimes \mathcal{H}_2$ is defined as [132]

$$C(|\psi_{12}\rangle) = \sqrt{2[1 - {\rm Tr}(\varrho_1^2)]}\,. \tag{5.48}$$

Here $\varrho_1 = {\rm Tr}_2(\varrho)$ denotes the reduced density operator of atom 1. The concurrence C of a maximally entangled state in $\mathcal{H}_{\rm sys}$ is $C_{\rm max} = \sqrt{3/2}$, and C is zero for product states [132]. We find that the antisymmetric and symmetric states $|\psi_a^i\rangle$ and $|\psi_s^i\rangle$ are entangled, but the degree of entanglement is not maximal,

$$C(|\psi_a^i\rangle) = C(|\psi_s^i\rangle) = 1 < C_{\rm max}\,. \tag{5.49}$$

Next we compare this result to the corresponding results for a pair of interacting two-level systems with ground state $|g\rangle$ and excited state $|e\rangle$. In this case, the

exchange interaction gives rise to the entangled states [11, 14, 73]

$$|\pm\rangle = \frac{1}{\sqrt{2}}(|e,g\rangle \pm |g,e\rangle) \tag{5.50}$$

with $C(|\pm\rangle) = 1$. It follows that the degree of entanglement of the states $|\pm\rangle$ is the same than the degree of entanglement of the symmetric and antisymmetric states of two four-level systems. On the other hand, the states $|\pm\rangle$ are maximally entangled in the state space of two two-level systems. This is in contrast to the states $|\psi_a^i\rangle$ and $|\psi_s^i\rangle$ which are not maximally entangled in the state space of two four-level atoms. Note that the system of two four-level atoms shown in Fig. 4.1 may be reduced to a pair of two-level systems if the atoms are aligned along the z axis. For this particular setup, all cross-coupling terms Ω_{ij} and Γ_{ij} with $i \neq j$ vanish [see Eqs. (4.12) and (4.13)] such that an arbitrary sublevel of the P_1 triplet and the ground state S_0 form an effective two-level system.

In Sec. 5.5, we showed that a static magnetic or RF field can induce a controlled dynamics between the states $|\psi_a^2\rangle$ and $|\psi_a^3\rangle$. We find that the degree of entanglement of an arbitrary superposition state

$$|\psi_{\text{sup}}\rangle = a|\psi_a^2\rangle + b|\psi_a^3\rangle \tag{5.51}$$

with $|a|^2 + |b|^2 = 1$ is given by $C(|\psi_{\text{sup}}\rangle) = 1$. It follows that the degree of entanglement is not influenced by the induced dynamics between the states $|\psi_a^2\rangle$ and $|\psi_a^3\rangle$.

Finally, we point out that the antisymmetric states $|\psi_a^i\rangle$ can be populated selectively, for example by the method introduced in Sec. 5.4. Since the spontaneous decay of the antisymmetric states is suppressed if the interatomic distance is small as compared to mean transition wavelength λ_0, we have shown that the system can be prepared in long-lived entangled states.

5.7 Summary and discussion

We have shown that the state space of two dipole-dipole interacting four-level atoms contains a four-dimensional decoherence-free subspace (DFS) if the interatomic distance approaches zero. If the separation of the atoms is larger than zero but small as compared to the wavelength of the $S_0 \leftrightarrow P_1$ transition, the spontaneous decay of states within the DFS is suppressed. In addition, we have shown that the system dynamics within the DFS is closed, i.e., the coherent part of the dipole-dipole interaction does not introduce a coupling between states of the DFS and states outside of the DFS.

In the case of degenerate excited states ($\delta = 0$), we find that the energy levels depend only on the interatomic distance R, but not on the angles θ and ϕ. This result reflects the fact that each atom is modelled by complete sets of angular momentum multiplets (see Sec. 4.4.1). We identified two antisymmetric collective states ($|\psi_a^2\rangle$

and $|\psi_a^3\rangle$) within the DFS that can be employed to represent a qubit. The storing times of the qubit state depend on the interatomic distance R and can be significantly longer than the inverse decay rate of the $S_0 \leftrightarrow P_1$ transition. Moreover, any single-qubit operation can be realized via a sequence of suitable RF pulses. The energy splitting between the states $|\psi_a^2\rangle$ and $|\psi_a^3\rangle$ arises from the coherent dipole-dipole interaction between the atoms and is on the order of $10\gamma \equiv (10 - 1000)$ MHz in the relevant interatomic distance range. The coupling strength between the RF field and the atoms is characterized by the parameter δ_0 which is on the order of $\mu_B B_0$, where μ_B is the Bohr magneton and B_0 is the amplitude of the RF field. Since μ_B is about 3 orders of magnitude larger than the nuclear magneton, typical operation times of our system may be significantly shorter than for a nuclear spin system.

Part IV

Non-classical states of the radiation field

Chapter 6

Two-mode single-atom laser as a source of entangled light

6.1 Introduction

Quantum entanglement is known to be the key resource in many applications of quantum information and quantum computing [5]. These phenomena range from quantum teleportation [133, 134] and quantum cryptography [135] to quantum implementation of Shor's algorithm [136] and quantum search [137]. It is therefore not surprising that there has been a great deal of interest in the generation and measurement of entanglement in recent years.

Entangled states have been considered traditionally between individual qubits. However, it has been shown that continuous variable entanglement can offer an advantage in some situations in quantum information science [138]. One reason for this is that continuous variable entanglement often can be prepared unconditionally, whereas the preparation of discrete entanglement usually relies on an event selection via coincidence measurements. The classic scheme for the generation of continuous variable entanglement is the parametric down-conversion. Starting with the first demonstration by Ou et al. [139], the generation of entanglement in such systems has been achieved in several experiments [138]. It still remains, however, a challenge to generate entanglement in macroscopic light rather than on the few photon level. Promising candidates for the generation of macroscopic light entanglement are optical amplifiers [140–144]. For example, it was shown recently that a two-mode correlated spontaneous emission laser (CEL) [145, 146] can lead to two-mode entanglement even when the average photon number in the field modes are very large [143, 144]. In this setup, the gain medium can be thought of as a stream of suitably prepared atoms.

From a conceptual point of view, a much simpler system relates to a single atom laser, where the gain medium is replaced by a single trapped atom. Such a laser has recently been experimentally demonstrated by Kimble's group [147], where a sin-

gle atom interacts with a single cavity mode. Thus the interesting question arises, whether a two-mode generalization of the single-atom laser also enables one to generate entanglement in macroscopic light.

Therefore, here we consider a single atom that interacts with two quantized modes of a doubly resonant cavity via two lasing transitions. In our model, the atomic level scheme is based on the single-atom laser experiment performed by Kimble's group [147], where dipole transitions between four hyperfine levels of atomic caesium were considered. In contrast to their experiment, we do not work in the strong coupling regime since we are interested in the generation of large photon numbers. We show that, under certain realizable conditions, a two-mode single-atom laser can serve as a source of macroscopic entangled light. Macroscopic entanglement can be achieved over a wide range of control parameters and initial states of the cavity field.

An important technical question in the generation of continuous variable entanglement in quantum optical systems is the way such entanglement can be measured experimentally. This is a hotly discussed subject in recent years. Several inequalities involving the correlation of the field operators have been derived that are based on the separability condition of the field modes [148–155]. A violation of these inequalities provides an evidence of entanglement. These inequalities can, in general, provide only a sufficient condition for entanglement and only, in some very specific instances, lead to sufficient and necessary conditions for entanglement. In this chapter we employ the inequality based on quadrature measurement of the field variables for the test of entanglement.

6.2 Master equation for the density operator of the cavity modes

We consider a single four-level atom trapped in a doubly resonant cavity (see Fig. 6.1). The atom interacts with two (nondegenerate) cavity modes and two classical laser fields. The intensities and frequencies of the two laser fields can be adjusted independently. The aim of this section is to derive an equation of motion for the reduced density operator ϱ_{F} of the two cavity modes.

We begin with a detailed description of the system shown in Fig. 6.1. The first cavity mode with frequency ν_1 couples to the atomic transition $|a\rangle \leftrightarrow |c\rangle$, and the second mode with frequency ν_2 interacts with the atom on the $|b\rangle \leftrightarrow |d\rangle$ transition. In rotating-wave approximation (RWA), the interaction of the atom with the cavity modes is described by the Hamiltonian

$$H_{\mathrm{C}} = \hbar g_1 a_1 |a\rangle\langle c| + \hbar g_2 a_2 |b\rangle\langle d| + \mathrm{H.c.}\,. \tag{6.1}$$

Here a_j ($a_j^\dagger$) is the annihilation (creation) operator of the cavity mode with frequency ν_j and coupling constant g_j ($j \in \{1, 2\}$). The detuning of the first cavity mode with the $|a\rangle \leftrightarrow |c\rangle$ transition is denoted by Δ_1, and Δ_2 is the detuning of the second

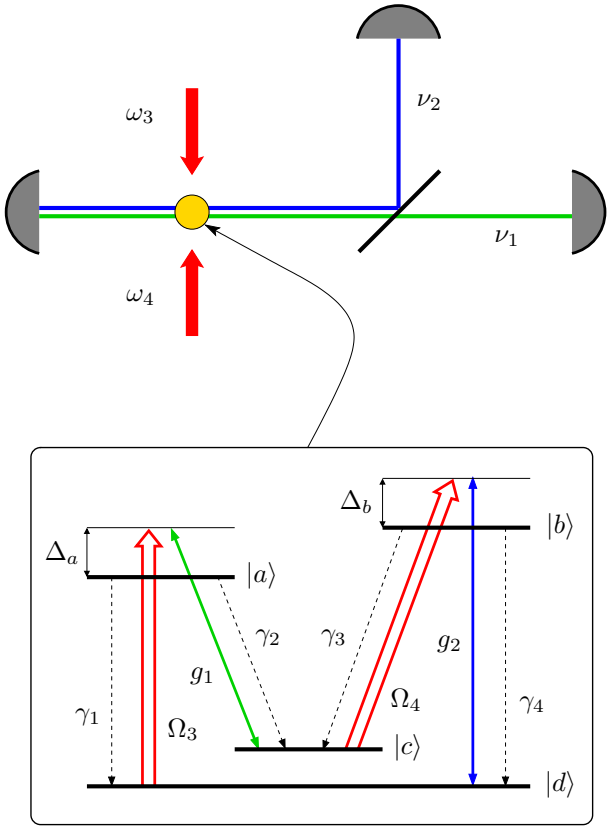

Figure 6.1: A single four-level atom is trapped in a doubly resonant cavity and interacts with two cavity modes and two classical laser fields. The inset shows the atomic level scheme. The laser field with frequency ω_3 and Rabi frequency Ω_3 couples to the $|a\rangle \leftrightarrow |d\rangle$ transition, and the cavity mode with frequency ν_1 and coupling constant g_1 interacts with the $|a\rangle \leftrightarrow |c\rangle$ transition. Δ_a is the detuning of the fields Ω_3 and g_1 with state $|a\rangle$. The laser field with frequency ω_4 and Rabi frequency Ω_4 drives the $|b\rangle \leftrightarrow |c\rangle$ transition, and the second cavity mode with frequency ν_2 and coupling constant g_2 interacts with the $|b\rangle \leftrightarrow |d\rangle$ transition. Δ_b is the detuning of the fields Ω_4 and g_2 with state $|b\rangle$. Spontaneous emission is denoted by dashed arrows, and the parameters γ_i are the decay rates of the various transitions.

mode with the $|b\rangle \leftrightarrow |d\rangle$ transition,

$$\Delta_1 = \nu_1 - \omega_{ac}\,, \qquad \Delta_2 = \nu_2 - \omega_{bd}\,. \tag{6.2}$$

The resonance frequencies on the $|a\rangle \leftrightarrow |c\rangle$ and $|b\rangle \leftrightarrow |d\rangle$ transitions have been labeled by ω_{ac} and ω_{bd}, respectively. In addition, the atom interacts with two classical laser fields. The first laser field with frequency ω_3 and Rabi frequency Ω_3 couples to the $|a\rangle \leftrightarrow |d\rangle$ transition, and the second field with frequency ω_4 and Rabi frequency Ω_4 coherently drives the $|b\rangle \leftrightarrow |c\rangle$ transition. In rotating-wave approximation, the

atom-laser interaction reads

$$H_{\rm L} = -\hbar\Omega_3|a\rangle\langle d|e^{-i\omega_3 t} - \hbar\Omega_4|b\rangle\langle c|e^{-i\omega_4 t} + \text{H.c.}\,. \tag{6.3}$$

Note that the Rabi frequencies $\Omega_3 = |\Omega_3|\exp(i\phi_3)$ and $\Omega_4 = |\Omega_4|\exp(i\phi_4)$ are complex numbers, and ϕ_3 and ϕ_4 are determined by the phase of the laser fields. The detuning of the laser fields with the corresponding atomic transitions are

$$\Delta_3 = \omega_3 - \omega_{ad}\,, \quad \Delta_4 = \omega_4 - \omega_{bc}\,, \tag{6.4}$$

where ω_{ad} and ω_{bc} are the resonance frequencies on the $|a\rangle \leftrightarrow |d\rangle$ and $|b\rangle \leftrightarrow |c\rangle$ transitions, respectively.

The free time evolution of the cavity modes is governed by

$$H_{\rm R} = \hbar\nu_1 a_1^\dagger a_1 + \hbar\nu_2 a_2^\dagger a_2\,, \tag{6.5}$$

and $H_{\rm A}$ is the free Hamiltonian of the atomic degrees of freedom,

$$H_{\rm A} = \hbar\omega_a|a\rangle\langle a| + \hbar\omega_b|b\rangle\langle b| + \hbar\omega_c|c\rangle\langle c| + \hbar\omega_d|d\rangle\langle d|\,. \tag{6.6}$$

With these definitions, we arrive at the master equation for the combined system of the atomic degrees of freedom and the two cavity modes,

$$\dot\varrho = -\frac{i}{\hbar}[H_{\rm R} + H_{\rm A} + H_{\rm L} + H_{\rm C}, \varrho] + \mathcal{L}_\gamma\varrho\,. \tag{6.7}$$

The last term in Eq. (6.7) accounts for spontaneous emission and is given by (see chapter 1)

$$\mathcal{L}_\gamma\varrho = -\frac{1}{2}\sum_{i=1}^{4}\gamma_i\left(S_i^+S_i^-\varrho + \varrho S_i^+S_i^- - 2S_i^-\varrho S_i^+\right)\,, \tag{6.8}$$

where the atomic transition operators are defined as

$$\begin{aligned} S_1^+ &= |a\rangle\langle d|, \quad S_2^+ = |a\rangle\langle c|\,, \\ S_3^+ &= |b\rangle\langle c|, \quad S_4^+ = |b\rangle\langle d|\,, \quad S_i^- = (S_i^+)^\dagger\,. \end{aligned} \tag{6.9}$$

The parameters γ_i are the decay rates of the various atomic transitions (see Fig. 6.1). Note that the presence of the cavity may change the analytical expression in Eq. (1.46) for the decay rates [11]. In addition, we have neglected all cross-decay terms.

In a next step, we derive from Eq. (2.7) the master equation for the density operator $\varrho_{\rm F}$ of the cavity modes,

$$\varrho_{\rm F} = \text{Tr}_{\rm A}\,\varrho = \varrho_{aa} + \varrho_{bb} + \varrho_{cc} + \varrho_{dd}\,, \tag{6.10}$$

and $\varrho_{\nu\nu}$ denotes $\langle\nu|\varrho|\nu\rangle$. To this end, we apply a unitary transformation $W = W_{\rm R}\otimes W_{\rm A}$ to Eq. (2.7), where $W_{\rm R} = \exp[iH_{\rm R}t/\hbar]$ acts only on the cavity modes, and

$$W_{\rm A} = \exp[i(H_{\rm A} + \hbar\Delta_3|a\rangle\langle a| + \hbar\Delta_4|b\rangle\langle b|)t/\hbar] \tag{6.11}$$

acts only on the atomic degrees of freedom. As indicated in Fig. 6.1, we assume that the condition of two-photon resonance is fulfilled, i.e.

$$\Delta_a = \Delta_1 = \Delta_3\,, \quad \Delta_b = \Delta_2 = \Delta_4\,. \tag{6.12}$$

The density operator in the new frame is denoted by $\tilde{\varrho} = W\varrho W^\dagger$ and obeys the equation of motion

$$\dot{\tilde{\varrho}} = -\frac{i}{\hbar}[H_0 + H_\mathrm{C}, \tilde{\varrho}] + \mathcal{L}_\gamma\tilde{\varrho}\,, \tag{6.13}$$

where

$$H_0 = -\hbar\Delta_a|a\rangle\langle a| - \hbar\Delta_b|b\rangle\langle b| - \hbar\left(\Omega_3|a\rangle\langle d| + \Omega_4|b\rangle\langle c| + \mathrm{H.c.}\right)\,. \tag{6.14}$$

The two-photon condition Eq. (6.12) ensures that the Hamiltonian $H_0 + H_\mathrm{C}$ in Eq. (6.13) is time-independent. The master equation for the transformed density operator $\tilde{\varrho}_\mathrm{F}$ of the cavity modes is obtained if we trace over the atomic degrees of freedom in Eq. (6.13),

$$\dot{\tilde{\varrho}}_\mathrm{F} = -ig_1[a_1^\dagger, \tilde{\varrho}_{ac}] - ig_2[a_2^\dagger, \tilde{\varrho}_{bd}] + \mathrm{H.c.}\,. \tag{6.15}$$

In order to eliminate the coherences $\tilde{\varrho}_{ac}$ and $\tilde{\varrho}_{bd}$ from Eq. (6.15), we apply the standard methods of laser theory (see, e.g., Chapter 14 in [1]). We restrict the analysis to the linear theory and solve Eq. (6.13) to first order in the coupling constants g_1 and g_2. To this end, we expand the density operator $\tilde{\varrho}_\mathrm{F}$ in Eq. (6.13) as $\tilde{\varrho} = \varrho_0 + \varrho_\mathrm{C}$ and retain only terms up to first order with respect to H_C. This procedure yields two uncoupled equations for ϱ_0 and ϱ_C,

$$\dot{\varrho_0} = \mathcal{L}_0\varrho_0\,, \tag{6.16}$$

$$\dot{\varrho_\mathrm{C}} = \mathcal{L}_0\varrho_\mathrm{C} - \frac{i}{\hbar}[H_\mathrm{C}, \varrho_0]\,, \tag{6.17}$$

and the superoperator $\mathcal{L}_0$ is defined as

$$\mathcal{L}_0(\cdot) = -\frac{i}{\hbar}[H_0, \cdot\,] + \mathcal{L}_\gamma(\cdot)\,. \tag{6.18}$$

Here the centered dot denotes the position of the argument of $\mathcal{L}_0$. The zeroth-order equation (6.16) describes the interaction of the atom with the classical laser fields to all orders, and Eq. (6.17) is the first-order equation. The steady state solution for $\tilde{\varrho}_{ac}$ and $\tilde{\varrho}_{bd}$ can be obtained if the steady-state solution for ϱ_0 is plugged in Eq. (6.17). We find

$$\begin{aligned} ig_1\tilde{\varrho}_{ac} &= \alpha_{11}a_1\tilde{\varrho}_\mathrm{F} + \alpha_{12}a_2^\dagger\tilde{\varrho}_\mathrm{F} + \beta_{11}\tilde{\varrho}_\mathrm{F}a_1 + \beta_{12}\tilde{\varrho}_\mathrm{F}a_2^\dagger\,, \\ ig_2\tilde{\varrho}_{bd} &= \alpha_{22}a_2\tilde{\varrho}_\mathrm{F} + \alpha_{21}a_1^\dagger\tilde{\varrho}_\mathrm{F} + \beta_{22}\tilde{\varrho}_\mathrm{F}a_2 + \beta_{21}\tilde{\varrho}_\mathrm{F}a_1^\dagger\,, \end{aligned} \tag{6.19}$$

and the coefficients α_{ij} and β_{ij} are defined in Appendix 6.A. Next we substitute Eq. (6.19) in Eq. (6.15) to obtain the equation of motion for $\tilde{\varrho}_\mathrm{F}$. Finally, we transform

$\tilde{\varrho}_{\rm F}$ back with respect to W_R and obtain the equation of motion for the density operator $\varrho_{\rm F}$ of the cavity modes,

$$\begin{aligned}\dot{\varrho_{\rm F}} =& -i\,\nu_1[a_1^\dagger a_1,\varrho_{\rm F}] - i\,\nu_2[a_2^\dagger a_2,\varrho_{\rm F}] \\ &- \Big[\alpha_{11}a_1^\dagger a_1\varrho_{\rm F} + \alpha_{11}^*\varrho_{\rm F}a_1^\dagger a_1 - (\alpha_{11}+\alpha_{11}^*)a_1\varrho_{\rm F}a_1^\dagger \\ &\qquad -\beta_{11}^* a_1 a_1^\dagger\varrho_{\rm F} - \beta_{11}\varrho_{\rm F}a_1a_1^\dagger + (\beta_{11}+\beta_{11}^*)a_1^\dagger\varrho_{\rm F}a_1\Big] \\ &- \Big[\alpha_{22}a_2^\dagger a_2\varrho_{\rm F} + \alpha_{22}^*\varrho_{\rm F}a_2^\dagger a_2 - (\alpha_{22}+\alpha_{22}^*)a_2\varrho_{\rm F}a_2^\dagger \\ &\qquad -\beta_{22}^* a_2 a_2^\dagger\varrho_{\rm F} - \beta_{22}\varrho_{\rm F}a_2a_2^\dagger + (\beta_{22}+\beta_{22}^*)a_2^\dagger\varrho_{\rm F}a_2\Big] \\ &- \Big[(\alpha_{12}+\alpha_{21})a_1^\dagger a_2^\dagger\varrho_{\rm F} - (\beta_{12}+\beta_{21})\varrho_{\rm F}a_1^\dagger a_2^\dagger \\ &\qquad -(\alpha_{21}-\beta_{12})a_1^\dagger\varrho_{\rm F}a_2^\dagger - (\alpha_{12}-\beta_{21})a_2^\dagger\varrho_{\rm F}a_1^\dagger\Big]\,\exp[-i(\nu_1+\nu_2)t] \\ &- \Big[(\alpha_{12}^*+\alpha_{21}^*)\varrho_{\rm F}a_1a_2 - (\beta_{12}^*+\beta_{21}^*)a_1a_2\varrho_{\rm F} \\ &\qquad -(\alpha_{21}^*-\beta_{12}^*)a_2\varrho_{\rm F}a_1 - (\alpha_{12}^*-\beta_{21}^*)a_1\varrho_{\rm F}a_2\Big]\,\exp[i(\nu_1+\nu_2)t] \\ &- \kappa_1\left(a_1^\dagger a_1\varrho_{\rm F} + \varrho_{\rm F}a_1^\dagger a_1 - 2a_1\varrho_{\rm F}a_1^\dagger\right) - \kappa_2\left(a_2^\dagger a_2\varrho_{\rm F} + \varrho_{\rm F}a_2^\dagger a_2 - 2a_2\varrho_{\rm F}a_2^\dagger\right)\,. \end{aligned} \tag{6.20}$$

In the last line of Eq. (6.20), we included the damping of the cavity field. The damping constants of the cavity modes are denoted by κ_1 and κ_2, respectively.

In the master equation (6.20), the two classical laser fields are taken into account to all orders in the Rabi frequencies Ω_3 and Ω_4. On the contrary, the two quantum fields inside the cavity are only treated to second order in the coupling constants g_1 and g_2. This approximation means that we ignore saturation effects and operate in the regime of linear amplification. It is justified if the Rabi frequencies associated with the quantum fields are small as compared to other system parameters which dominate the time evolution.

6.3 Entanglement of the cavity field

In this Section we show that the system depicted in Fig. 6.1 can serve as a source of macroscopic entangled light. We employ the sufficient inseparability criterion derived in [149] to provide evidence for the entanglement of the two field modes.

By definition, the quantum state $\varrho_{\rm F}$ of the cavity field is said to be entangled if and only if it is nonseparable, and $\varrho_{\rm F}$ is separable if and only if it can be written as

$$\varrho_{\rm F} = \sum_j p_j \varrho_j^{(1)} \otimes \varrho_j^{(2)}\,. \tag{6.21}$$

Here $\varrho_j^{(1)}$ and $\varrho_j^{(2)}$ are normalized states of the modes 1 and 2, respectively, and the parameters $p_j \geq 0$ comply with $\sum_j p_j = 1$. The criterion derived in [149] states that the system is in an entangled quantum state if the total variance of two Einstein-Podolsky-Rosen (EPR) type operators $\hat{u}$ and $\hat{v}$ of the two modes satisfy the inequality

$$\left\langle \, (\Delta\hat{u})^2 + (\Delta\hat{v})^2 \, \right\rangle < 2\,, \tag{6.22}$$

where

$$\hat{u} = \hat{x}_1 + \hat{x}_2\,, \qquad \hat{v} = \hat{p}_1 - \hat{p}_2\,. \tag{6.23}$$

Here $\hat{x}_k$ and $\hat{p}_k$ are local operators which correspond to mode k with frequency ν_k. They must obey the commutation relation

$$[\hat{x}_k, \hat{p}_l] = i\delta_{kl}\,, \tag{6.24}$$

but are otherwise arbitrary. For the physical system considered here, it turns out that the following quadrature operators

$$\hat{x}_k = (b_k + b_k^\dagger)/\sqrt{2} \quad \text{and} \quad \hat{p}_k = (b_k - b_k^\dagger)/(\sqrt{2}i) \tag{6.25}$$

are the best choice, where

$$b_k(t) = a_k \exp[i\nu_k t] \quad \text{and} \quad b_k^\dagger(t) = a_k^\dagger \exp[-i\nu_k t]\,. \tag{6.26}$$

With the help of Eqs. (6.23) and (6.25), we express the total variance of the operators $\hat{u}$ and $\hat{v}$ in terms of the operators b_k and $b_k^\dagger$,

$$\begin{aligned}\left\langle \, (\Delta\hat{u})^2 + (\Delta\hat{v})^2 \, \right\rangle = 2\Big[1 &+ \langle\, b_1^\dagger b_1 \,\rangle + \langle\, b_2^\dagger b_2 \,\rangle + \langle\, b_1 b_2 \,\rangle + \langle\, b_1^\dagger b_2^\dagger \,\rangle \\ &- \langle\, b_1 \,\rangle\langle\, b_1^\dagger \,\rangle - \langle\, b_2 \,\rangle\langle\, b_2^\dagger \,\rangle - \langle\, b_1 \,\rangle\langle\, b_2 \,\rangle - \langle\, b_1^\dagger \,\rangle\langle\, b_2^\dagger \,\rangle\Big]\,.\end{aligned} \tag{6.27}$$

In Appendix 6.A, we outline the calculation of the mean values that enter Eq. (6.27).

Next we classify several parameter regimes for which the inequality (6.22) is fulfilled. In a first step, we consider the case where the Rabi frequency $|\Omega_3|$ and the detuning Δ_b are much larger than the parameters $|\Delta_a|$, $|\Omega_4|$, γ_i ($i \in \{1,2,3,4\}$), i.e.

$$|\Omega_3|,\, |\Delta_b| \gg |\Delta_a|,\, |\Omega_4|,\, \gamma_i\,. \tag{6.28}$$

If these conditions are fulfilled, the parameters α_{ij} and β_{ij} in Eqs. (6.36)-(6.43) of Appendix 6.A reduce to

$$\begin{aligned}&\alpha_{11} \approx 0,\, \alpha_{22} \approx 0,\, \beta_{11} \approx 0,\, \beta_{22} \approx 0\,,\\ &\alpha_{21} \approx 0,\, \beta_{12} \approx 0,\, \alpha_{12} \approx \beta_{21} \approx -i\alpha \exp[i(\phi_3 + \phi_4)t]\,,\\ &\alpha = g_1 g_2 \frac{|\Omega_4|}{|\Omega_3|\Delta_b}\,.\end{aligned} \tag{6.29}$$

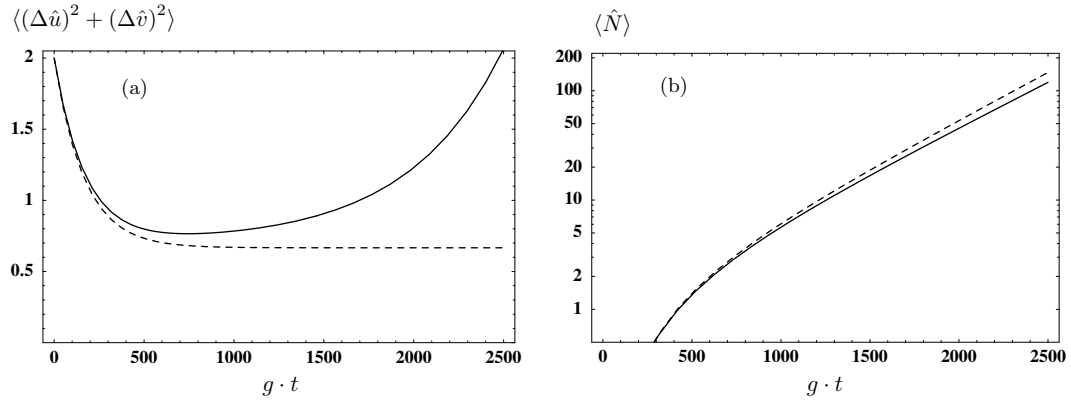

Figure 6.2: (a) Time evolution of $\langle\,(\Delta\hat{u})^2+(\Delta\hat{v})^2\,\rangle$. The mean value of the total number of photons $\langle\,\hat{N}\,\rangle$ is shown in (b) on a logarithmic scale. At $t=0$, the cavity field is assumed to be in the vacuum state. The dashed curves were obtained with the density operator of the parametric oscillator in Eq. (6.30), and the solid curves correspond to the full density operator in Eq. (6.20). The parameters are $g_1=g_2=g$, $|\Omega_3|=25g$, $|\Omega_4|=2g$, $\gamma_1=\gamma_2=\gamma_3=\gamma_4=5g$, $\Delta_a=0$, $\Delta_b=40g$, $\kappa_1=\kappa_2=10^{-3}g$ and $\phi_3+\phi_4=\pi/2$.

In these equations, ϕ_3 and ϕ_4 are the phases of the classical laser fields with Rabi frequencies $\Omega_3=|\Omega_3|\exp(i\phi_3)$ and $|\Omega_4|\exp(i\phi_4)$, respectively (see Sec. 6.2). If the approximate parameters in Eq. (6.29) are plugged in Eq. (6.20), we obtain the equation of motion for the density operator $\varrho_{\rm F}$ of the cavity modes in the limit (6.28),

$$\begin{aligned}\dot{\varrho_{\rm F}} =& -i\,\nu_1[a_1^\dagger a_1,\varrho_{\rm F}]-i\,\nu_2[a_2^\dagger a_2,\varrho_{\rm F}]+i[H_{\rm P},\varrho_{\rm F}]\\ &-\kappa\left(a_1^\dagger a_1\varrho_{\rm F}+\varrho_{\rm F}a_1^\dagger a_1-2a_1\varrho_{\rm F}a_1^\dagger+a_2^\dagger a_2\varrho_{\rm F}+\varrho_{\rm F}a_2^\dagger a_2-2a_2\varrho_{\rm F}a_2^\dagger\right),\end{aligned}\tag{6.30}$$

where

$$\begin{aligned}H_{\rm P}=&\alpha a_1^\dagger a_2^\dagger\exp[i(\phi_3+\phi_4)t]\exp[-i(\nu_1+\nu_2)t]\\ &+\alpha a_1a_2\exp[-i(\phi_3+\phi_4)t]\exp[i(\nu_1+\nu_2)t]\,.\end{aligned}\tag{6.31}$$

Here we assumed for the sake of simplicity that the decay rates of the cavity modes are equal, $\kappa_1=\kappa_2=\kappa$. We identify Eq. (6.30) as the master equation for a nondegenerate parametric oscillator in the parametric approximation [1]. Note that this parametric limit was also obtained in the case of a two-mode correlated spontaneous emission laser discussed in [143]. Next we evaluate the total variance of the operators $\hat{u}$ and $\hat{v}$ in Eq. (6.27) and the mean number of photons $\langle\,\hat{N}\,\rangle=\langle\,a_1^\dagger a_1+a_2^\dagger a_2\,\rangle=\langle\,b_1^\dagger b_1+b_2^\dagger b_2\,\rangle$ with the approximate density operator $\varrho_{\rm F}$ in

Eq. (6.30). If the sum of the laser phases obeys $\phi_3 + \phi_4 = \pi/2$, we obtain [143]

$$\left\langle\, (\Delta\hat{u})^2 + (\Delta\hat{v})^2 \,\right\rangle(t) = \left[\left\langle\, (\Delta\hat{u})^2 + (\Delta\hat{v})^2 \,\right\rangle(0) - \frac{2\kappa}{\alpha+\kappa}\right] e^{-2(\alpha+\kappa)t} + \frac{2\kappa}{\alpha+\kappa}\,, \quad (6.32)$$

$$\left\langle\, \hat{N} \,\right\rangle(t) = \left[\left\langle\, \hat{N} \,\right\rangle(0) - \frac{\alpha^2}{\kappa^2-\alpha^2}\right] \cosh(2\alpha t) e^{-2\kappa t} - \left[\frac{\alpha\kappa}{\kappa^2-\alpha^2} + \left\langle\, a_1 a_2 + a_1^\dagger a_2^\dagger \,\right\rangle(0)\right] \sinh(2\alpha t) e^{-2\kappa t} + \frac{\alpha^2}{\kappa^2-\alpha^2}\,. \quad (6.33)$$

It follows from Eq. (6.32) that the entanglement criterion in Eq. (6.22) is satisfied for any initial state of the cavity field if $(\alpha+\kappa)t \gg 1$ and $\alpha > 0$ [143] . The time evolution of the total variance of the operators $\hat{u}$ and $\hat{v}$ is shown in Fig. 6.2(a). The dashed curve shows $\langle\, (\Delta\hat{u})^2 + (\Delta\hat{v})^2 \,\rangle$ according to Eq. (6.32), and the solid line corresponds to the general case where the mean values in Eq. (6.27) are evaluated with the full density operator $\varrho_{\rm F}$ in Eq. (6.20). The cavity modes are assumed to be in the vacuum state initially, and the parameters comply with condition (6.28). It follows from Fig. 6.2 that the approximate result in Eq. (6.32) is only in good agreement with the exact solution if $gt < 300$. While the light field remains in an entangled state in the parametric case, the exact solution demonstrates that the entanglement of the cavity field exists only for a finite period of time.

Next we discuss the time evolution of the mean number of photons $\langle\, \hat{N} \,\rangle$. According to Eq. (6.33), $\langle\, \hat{N} \,\rangle$ grows exponentially with time for any initial state of the cavity field, provided that $(\alpha-\kappa)t \gg 1$ and $\alpha > \kappa$ [143]. The time evolution of $\langle\, \hat{N} \,\rangle$ is shown in Fig. 6.2(b) on a logarithmic scale. In contrast to $\langle\, (\Delta\hat{u})^2 + (\Delta\hat{v})^2 \,\rangle$, the result for $\langle\, \hat{N} \,\rangle$ in the parametric approximation (dashed line) is in good agreement with the exact solution (solid line) even for $gt \gg 300$. Moreover, Fig. 6.2(b) shows that the mean number of photons grows exponentially if the scaled time gt is sufficiently large.

According to Fig. 6.2, the entangled state of the cavity field contains up to $\langle\, \hat{N} \,\rangle \approx 110$ photons on average. It follows that the single-atom laser depicted in Fig. 6.1 can give rise to an entangled quantum state of the two cavity modes if the parameters are in agreement with condition (6.28). If this condition holds, level $|b\rangle$ is almost not excited due to the large detuning Δ_b, and states $|c\rangle$ and $|d\rangle$ are coupled via a two-photon process. In contrast, the transitions $|d\rangle \leftrightarrow |a\rangle$ and $|c\rangle \leftrightarrow |a\rangle$ are driven resonantly. In this situation, the structure of the Hamiltonian $H_{\rm P}$ in Eq. (6.31) implies that the system can only emit photons into the cavity fields in pairs, where one photon is emitted in mode 1 and the other photon in mode 2. If the cavity field is initially in the vacuum state $|0,0\rangle$, it will evolve under the influence of $H_{\rm P}$ into the entangled state

$$a\,|0,0\rangle + b\,|1,1\rangle + c\,|2,2\rangle + \ldots\,, \quad (6.34)$$

where a, b and c are complex coefficients. If the complicated master equation (6.20) can be reduced under certain conditions to the parametric equation (6.30), it is thus clear that a macroscopic entangled state is generated.

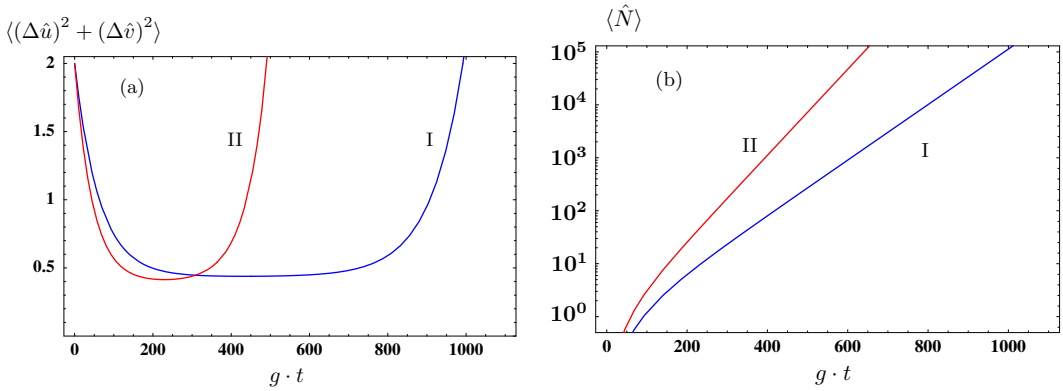

Figure 6.3: (a) Time evolution of $\langle\,(\Delta\hat{u})^2+(\Delta\hat{v})^2\,\rangle$. The mean value of the total number of photons $\langle\,\hat{N}\,\rangle$ is shown in (b) on a logarithmic scale. At $t=0$, the cavity field is assumed to be in the vacuum state, and we set $\gamma_1=\gamma_2=\gamma_3=\gamma_4=5g$, $g_1=g_2=g$, $\kappa_1=\kappa_2=10^{-3}g$ and $\phi_3+\phi_4=\pi/2$. The parameters for the curves labeled with I are $|\Omega_3|=25g$, $|\Omega_4|=9.8g$, $\Delta_a=0$, $\Delta_b=43g$, and for II we have $|\Omega_3|=15g$, $|\Omega_4|=6g$, $\Delta_a=0$, $\Delta_b=32.5g$.

Due to the symmetry in the atomic level scheme, it is possible to reverse the role of the transitions $|d\rangle\leftrightarrow|a\rangle\leftrightarrow|c\rangle$ and $|c\rangle\leftrightarrow|b\rangle\leftrightarrow|d\rangle$. In this case, the detuning Δ_a is large and the transitions $|d\rangle\leftrightarrow|b\rangle$ and $|c\rangle\leftrightarrow|b\rangle$ are driven resonantly. Condition (6.28) then has to be replaced by

$$|\Omega_4|,\,|\Delta_a|\gg|\Delta_b|,\,|\Omega_3|,\,\gamma_i\,, \tag{6.35}$$

and the only nonvanishing coefficients in Eq. (6.20) are now determined by $\alpha_{21}\approx\beta_{12}\approx-i\alpha'\exp[i(\phi_3+\phi_4)t]$, where $\alpha'=g_1g_2|\Omega_3|/(|\Omega_4|\Delta_a)$. It follows that the results in Eqs. (6.30), (6.32) and (6.33) are also valid if condition (6.35) holds, provided that α is replaced by α'.

We now demonstrate that it can be advantageous to consider parameters which do not comply with conditions (6.28) or (6.35). Since the approximate results in Eqs. (6.32) and (6.33) do not apply in this case, we evaluate the mean values $\langle\,(\Delta\hat{u})^2+(\Delta\hat{v})^2\,\rangle$ and $\langle\,\hat{N}\,\rangle$ only with the exact density operator $\varrho_{\rm F}$ in Eq. (6.20). The time evolution of $\langle\,(\Delta\hat{u})^2+(\Delta\hat{v})^2\,\rangle$ is shown in Fig. 6.3(a) for two sets of parameters. As compared to the parameters chosen for Fig. (6.2), the magnitude of the Rabi frequency Ω_4 has been increased such that $|\Omega_3|$ is still larger, but not much larger than $|\Omega_4|$. It follows from Fig. 6.3(a) that the entanglement criterion in Eq. (6.22) is fulfilled for shorter times as compared to the solid line in Fig. 6.2(a). On the other hand, Fig. 6.3(b) shows that the mean number of photons can be much larger as compared to Fig. 6.2(b). For curve I of Fig. 6.3(a), the maximum mean number of photons for which the entanglement criterion (6.22) is still fulfilled is $\langle\,\hat{N}\,\rangle\approx10.2\times10^4$. The same number for the parameters of curve II reads $\langle\,\hat{N}\,\rangle\approx6100$. As compared to Fig. 6.2, the maximum mean number of photons can be enhanced by several orders of magnitude.

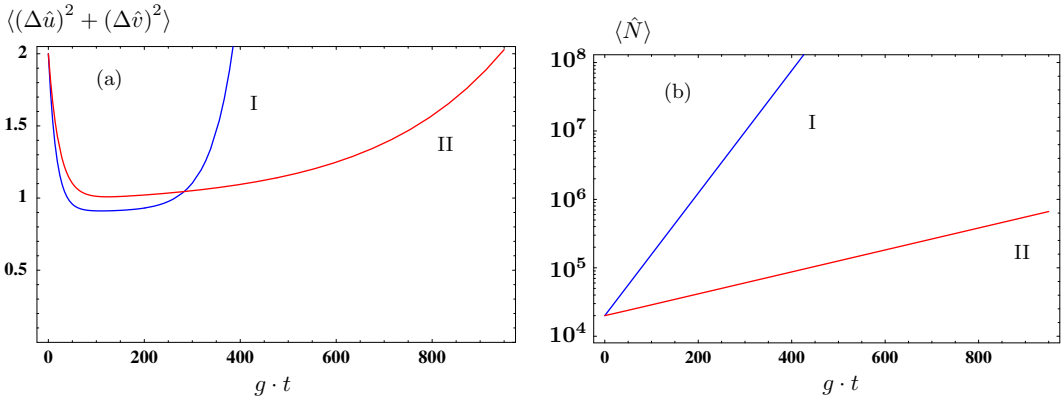

Figure 6.4: (a) Time evolution of $\langle\,(\Delta\hat{u})^2+(\Delta\hat{v})^2\,\rangle$. The mean value of the total number of photons $\langle\,\hat{N}\,\rangle$ is shown in (b) on a logarithmic scale. At $t=0$, the cavity field is assumed to be in the coherent state $|100,-100\rangle$, and we set $\gamma_1=\gamma_2=\gamma_3=\gamma_4=2g$, $g_1=g_2=g$, $\kappa_1=\kappa_2=10^{-2}g$ and $\phi_3+\phi_4=\pi/2$. The parameters for the curves labeled with I are $|\Omega_3|=10g$, $|\Omega_4|=5g$, $\Delta_a=0$, $\Delta_b=15g$, and for II we have $|\Omega_3|=10g$, $|\Omega_4|=2g$, $\Delta_a=0$, $\Delta_b=15g$.

Finally, we consider the case where the quantum state of the cavity field is initially the coherent state $|100,-100\rangle$. The time evolution of $\langle\,(\Delta\hat{u})^2+(\Delta\hat{v})^2\,\rangle$ and $\langle\,\hat{N}\,\rangle$ is shown in Fig. 6.4 for two sets of parameters. All mean values were evaluated with the exact density operator in Eq. (6.20). For curve I, the magnitude of the Rabi frequency Ω_4 is larger as compared to curve II. All other parameters are the same for curve I and II. It can be seen from Fig. 6.4(a) that the entanglement criterion is fulfilled for shorter times if $|\Omega_4|$ is increased. In contrast, the mean number of photons can be greatly enhanced if the value of $|\Omega_4|$ is increased, as can be seen from Fig. 6.4(b). Similar conclusions can be drawn from Fig. 6.3, where the initial state of the cavity field is the vacuum. The comparison of Figs. 6.3 and 6.4 shows that the mean number of photons can be much larger than in Fig. 6.3 if the cavity field is initially prepared in a coherent state. Due to the large mean number of photons in the cavity modes, the system may leave the regime of linear amplification such that saturation effects modify the curve progression in Fig. 6.4. These effects are described by terms that go beyond the second-order expansion of the atom-cavity coupling and are neglected here. According to the linear theory, the maximum mean number of photons for which the entanglement criterion (6.22) is still fulfilled is $\langle\,\hat{N}\,\rangle\approx 6.5\times 10^5$ in the case of curve II of Fig. 6.4, and in the case of curve I the entangled cavity field contains up to $\langle\,\hat{N}\,\rangle\approx 5.4\times 10^7$ photons.

6.4 Summary

We have shown that a two-mode single-atom laser can serve as a source of macroscopic entangled light. We identified two parameter regimes for which the quantum

state of the cavity field is entangled for a long period of time. For these parameters, the master equation for the density operator of the two cavity modes can be approximately reduced to the master equation for a nondegenerate parametric oscillator in the parametric approximation.

The mean number of photons in the cavity field can be strongly increased if parameters beyond the parametric limit are chosen. This enhancement of the mean photon numbers is accompanied by a shortening of the time slice for which the entanglement criterion is fulfilled. As the initial state of the cavity field, we chose either the vacuum or a coherent state. We demonstrated that the mean number of photons of the entangled cavity field can increase by several orders of magnitude if a coherent state instead of the vacuum is chosen as an initial state.

6.A Coefficients α_{ij}, β_{ij} and field correlation functions

Here we give the explicit definitions of the coefficients α_{ij} and β_{ij} which enter the master equation (6.20) for the density operator ϱ_{F} of the two cavity modes

$$\alpha_{11} = \frac{2g_1^2\gamma_2 \left|\Omega_3\right|^2 \left|\Omega_4\right|^2}{P_3 P_4} \left[4\left(P_2^* + 4i\Delta_b\right)\left|\Omega_4\right|^2 + P_1^*\left(4\left|\Omega_3\right|^2 + P_1\left(P_1 + P_2^*\right)\right)\right], \tag{6.36}$$

$$\beta_{11} = -\frac{2g_1^2\gamma_4 \left|\Omega_3\right|^2 \left|\Omega_4\right|^2}{P_3 P_4} \left[4P_1\left|\Omega_4\right|^2 + P_2^*\left(4\left|\Omega_3\right|^2 + P_1\left(P_1 + P_2^*\right)\right)\right], \tag{6.37}$$

$$\alpha_{12} = -\frac{2g_1 g_2\gamma_2\Omega_3\Omega_4 \left|\Omega_3\right|^2}{P_3 P_4} \left[4P_1\left|\Omega_3\right|^2 + P_1^2\left(P_1 + P_2^*\right) - 4\left|\Omega_4\right|^2\left(2P_1 + P_2^*\right)\right], \tag{6.38}$$

$$\beta_{12} = -\frac{2g_1 g_2\gamma_4\Omega_3\Omega_4 \left|\Omega_4\right|^2}{P_3 P_4} \left[\left(P_1 + P_2^*\right)\left|P_2\right|^2 + 4\left|\Omega_4\right|^2 P_2 + 4\left|\Omega_3\right|^2\left(P_1 - 4i\Delta_a\right)\right], \tag{6.39}$$

$$\alpha_{22} = \frac{2g_2^2\gamma_4 \left|\Omega_3\right|^2 \left|\Omega_4\right|^2}{P_3 P_5} \left[4\left(P_1^* + 4i\Delta_a\right)\left|\Omega_3\right|^2 + P_2^*\left(4\left|\Omega_4\right|^2 + P_2\left(P_2 + P_1^*\right)\right)\right], \tag{6.40}$$

$$\beta_{22} = -\frac{2g_2^2\gamma_2 \left|\Omega_3\right|^2 \left|\Omega_4\right|^2}{P_3 P_5} \left[4P_2\left|\Omega_3\right|^2 + P_1^*\left(4\left|\Omega_4\right|^2 + P_2\left(P_2 + P_1^*\right)\right)\right], \tag{6.41}$$

$$\alpha_{21} = -\frac{2g_1 g_2\gamma_4\Omega_3\Omega_4 \left|\Omega_4\right|^2}{P_3 P_5} \left[4P_2\left|\Omega_4\right|^2 + P_2^2\left(P_2 + P_1^*\right) - 4\left|\Omega_3\right|^2\left(2P_2 + P_1^*\right)\right], \tag{6.42}$$

$$\beta_{21} = -\frac{2g_1 g_2\gamma_2\Omega_3\Omega_4 \left|\Omega_3\right|^2}{P_3 P_5} \left[\left(P_2 + P_1^*\right)\left|P_1\right|^2 + 4\left|\Omega_3\right|^2 P_1 + 4\left|\Omega_4\right|^2\left(P_2 - 4i\Delta_b\right)\right]. \tag{6.43}$$

The parameters P_1, P_2, P_3, P_4 and P_5 in Eqs. (6.36)-(6.43) are defined as

$$P_1 = \gamma_3 + \gamma_4 + 2i\Delta_b\,, \tag{6.44}$$

$$P_2 = \gamma_1 + \gamma_2 + 2i\Delta_a\,, \tag{6.45}$$

$$P_3 = \gamma_2\left|P_1\right|^2\left|\Omega_3\right|^2 + \gamma_4\left|P_2\right|^2\left|\Omega_4\right|^2 + 8\left|\Omega_3\right|^2\left|\Omega_4\right|^2\left(\gamma_2 + \gamma_4\right), \tag{6.46}$$

$$P_4 = 4\left(\left|\Omega_3\right|^2 - \left|\Omega_4\right|^2\right)^2 + P_1\left(P_1 + P_2^*\right)\left|\Omega_3\right|^2 + P_2^*\left(P_1 + P_2^*\right)\left|\Omega_4\right|^2, \tag{6.47}$$

$$P_5 = 4\left(\left|\Omega_3\right|^2 - \left|\Omega_4\right|^2\right)^2 + P_1^*\left(P_2 + P_1^*\right)\left|\Omega_3\right|^2 + P_2\left(P_2 + P_1^*\right)\left|\Omega_4\right|^2. \tag{6.48}$$

In the following, we outline the calculation of the mean values that enter the total variance of the operators $\hat{u}$ and $\hat{v}$ in Eq. (6.27). We begin with the mean values of

the quadrature operators defined in Eq. (6.25) with respect to the density operator $\varrho_{\rm F}$ of the two cavity modes. With the help of Eq. (6.20), we derive the following system of differential equations for the mean values $\langle\, b_1 \,\rangle$ and $\langle\, b_2^\dagger \,\rangle$,

$$\partial_t \begin{pmatrix} \langle\, b_1 \,\rangle \\ \langle\, b_2^\dagger \,\rangle \end{pmatrix} = - \begin{pmatrix} C_{11} + \kappa_1 & C_{12} \\ C_{21}^* & C_{22}^* + \kappa_2 \end{pmatrix} \begin{pmatrix} \langle\, b_1 \,\rangle \\ \langle\, b_2^\dagger \,\rangle \end{pmatrix} , \tag{6.49}$$

and $C_{ij} = \alpha_{ij} + \beta_{ij}$. The solution to this set of coupled equations is

$$\begin{aligned} \langle\, b_1 \,\rangle =& e^{w_2 t} \left[\cosh(w_1 t) \langle b_1 \rangle_0 \right. \qquad (6.50) \\ & \left. + \frac{1}{2w_1} \left(\langle b_1 \rangle_0 \left(C_{22}^* - C_{11} - \kappa_1 + \kappa_2 \right) - 2 \langle b_2^\dagger \rangle_0 C_{12} \right) \sinh(w_1 t) \right] \\ \langle\, b_2^\dagger \,\rangle =& e^{w_2 t} \left[\cosh(w_1 t) \langle b_2^\dagger \rangle_0 \right. \qquad (6.51) \\ & \left. + \frac{1}{2w_1} \left(\langle b_2^\dagger \rangle_0 \left(C_{11} - C_{22}^* + \kappa_1 - \kappa_2 \right) - 2 \langle b_1 \rangle_0 C_{21}^* \right) \sinh(w_1 t) \right] , \end{aligned}$$

where

$$\begin{aligned} w_1 =& \frac{1}{2} \sqrt{4 C_{12} C_{21}^* + (C_{11} - C_{22}^* + \kappa_1 - \kappa_2)^2} \,, \\ w_2 =& -\frac{1}{2} (C_{11} + C_{22}^* + \kappa_1 + \kappa_2) \,, \end{aligned} \tag{6.52}$$

and $\langle \cdot \rangle_0 = \langle\, \cdot \,\rangle(t=0)$ denotes the initial mean value at $t = 0$. Note that the mean values $\langle\, b_1^\dagger \,\rangle$ and $\langle\, b_2 \,\rangle$ can be obtained from $\langle\, b_1 \,\rangle$ and $\langle\, b_2^\dagger \,\rangle$ by complex conjugation, i.e. $\langle\, b_1^\dagger \,\rangle = \langle\, b_1 \,\rangle^*$ and $\langle\, b_2 \,\rangle = \langle\, b_2^\dagger \,\rangle^*$.

The remaining mean values in Eq. (6.27) involve products of the operators b_i and $b_i^\dagger$. With the aid of Eq. (6.20), we obtain the following set of differential equations,

$$\partial_t \boldsymbol{R} = M \boldsymbol{R} + \boldsymbol{I} \,, \tag{6.53}$$

where $\boldsymbol{R} = \left(\langle\, b_1^\dagger b_1 \,\rangle, \langle\, b_2^\dagger b_2 \,\rangle, \langle\, b_1 b_2 \,\rangle, \langle\, b_1^\dagger b_2^\dagger \,\rangle \right)$ and

$$M = - \begin{pmatrix} D_{11} & 0 & C_{12}^* & C_{12} \\ 0 & D_{22} & C_{21}^* & C_{21} \\ C_{21} & C_{12} & D_{12} & 0 \\ C_{21}^* & C_{12}^* & 0 & D_{12}^* \end{pmatrix} \quad , \quad \boldsymbol{I} = - \begin{pmatrix} \beta_{11} + \beta_{11}^* \\ \beta_{22} + \beta_{22}^* \\ \alpha_{12} + \alpha_{21} \\ \alpha_{12}^* + \alpha_{21}^* \end{pmatrix} . \tag{6.54}$$

The elements of the matrix M are defined as

$$\begin{aligned} C_{ij} &= \alpha_{ij} + \beta_{ij} \,, \\ D_{ii} &= \alpha_{ii} + \alpha_{ii}^* + \beta_{ii} + \beta_{ii}^* + 2\kappa_i \,, \\ D_{12} &= C_{11} + C_{22} + \kappa_1 + \kappa_2 \,. \end{aligned} \tag{6.55}$$

The differential equation Eq. (6.53) can be solved numerically without difficulties. Analytic results can be obtained, for example, by means of the Laplace transform method which yields the following results for the components R_i of the vector $\boldsymbol{R}$,

$$R_i = \sum_{k=1}^{4} \big[\mathrm{Res}(f_i, \lambda_k) \,+\, \mathrm{Res}(g_i, \lambda_k)\big] e^{\lambda_k t} + \mathrm{Res}(g_i, 0)\,. \tag{6.56}$$

In this equation, expressions of the type $\mathrm{Res}(h, z)$ denote the residue of the function h evaluated at z, and the functions $\boldsymbol{f} = (f_1,\, f_2,\, f_3,\, f_4)$ and $\boldsymbol{g} = (g_1,\, g_2,\, g_3,\, g_4)$ are determined by

$$\boldsymbol{f}(s) = [s\;\mathbb{1}_4 - M]^{-1}\,\boldsymbol{R}_0 \qquad \text{and} \qquad \boldsymbol{g}(s) = [s\;\mathbb{1}_4 - M]^{-1}\,(\boldsymbol{I}/s)\,, \tag{6.57}$$

respectively. Here $\mathbb{1}_4$ denotes the 4×4 identity matrix, and the vector $\boldsymbol{R}_0$ is the initial value of $\boldsymbol{R}$ at $t = 0$, $\boldsymbol{R}_0 = \Big(\langle\, b_1^\dagger b_1 \,\rangle_0,\, \langle\, b_2^\dagger b_2 \,\rangle_0,\, \langle\, b_1 b_2 \,\rangle_0,\, \langle\, b_1^\dagger b_2^\dagger \,\rangle_0\Big)$. Finally, the parameters λ_k are the four (complex) eigenvalues of the matrix M which is defined in Eq. (6.54).

Summary

In this thesis we studied a number of fundamentally different interference and coherence effects in the interaction of atoms with the quantized electromagnetic field. The common foundation for our analysis is a rather general master equation that applies to an arbitrary number of multi-level atoms located at different positions in the isotropic vacuum. This master equation has been derived in chapter 1, and the different contributions arising from the interaction of the atoms with the surrounding electromagnetic vacuum field have been identified and investigated in detail. For single-atom systems, it accounts for spontaneous emission on individual dipole transitions as well as for vacuum-induced quantum interference effects associated with the cross-decay of two dipole transitions (see chapter 2). In addition, the master equation encompasses collective effects that occur in systems with more than one atom. Various parameters like collective decay rates and coherent coupling terms that give rise to energy shifts of collective states have been investigated in detail in part III of this thesis. A point of particular importance is that our master equation accounts for the coupling between orthogonal transition dipole moments of different atoms. While these terms were frequently neglected in the previous literature, our detailed analysis in part III demonstrates the evident significance of these unusual coupling terms.

In chapter 2, we focused on vacuum-induced coherence effects in a single-atom system. For this, we investigated the fluorescence light emitted by a four-level system in $J = 1/2$ to $J = 1/2$ configuration driven by a monochromatic laser field and in an external magnetic field. The distinguished feature of this level scheme is that the dipole moments of the two π transitions are antiparallel. We investigated two standard observables of the system, namely the total intensity and the spectrum of resonance fluorescence emitted by the atom. A polarization dependent detection scheme served to distinguish between the contributions of the π and the σ transitions to these photodetection signals. It was found that the spectrum of resonance fluorescence emitted on the π transitions exhibits a clear signature of quantum interference, whereas the total intensity is not affected by interference. Since the π transitions do neither share a common initial nor a common final state, the presence of the interference effect in the fluorescence spectrum is a surprising and counterintuitive result. We have shown that our findings can be explained in terms of the principle of complementarity, applied to time and energy. For the system considered here, it claims that it is impossible to observe the temporal and the energy aspect

of the radiative cascade of the atom at the same time. If the fluorescence spectrum is observed, the photon emission times are indeterminate. The interference in the fluorescence spectrum can thus be explained in terms of interferences between transition amplitudes that correspond to different time orders of photon emissions. This interpretation was supported by a detailed study of the measured fluorescence spectrum in dependence on the frequency resolution of the detector. An additional consistency check of our interpretation follows from the possibility to control the degree of interference in the fluorescence spectrum emitted on the π transitions by means of an external magnetic field. In particular, we found that the degree of interference in the coherent part of the spectrum can be adjusted from perfect constructive to perfect destructive interference. Under conditions of perfect destructive interference, we found the remarkable result that the weight of the Rayleigh line is completely suppressed, despite of the coherent driving by the laser field. Moreover, we also discussed the spectrum emitted on the σ transitions that contains only an incoherent part, and it was shown that this spectrum displays an indirect signature of the quantum interference effect.
Finally, we point out that the interference terms in the expression for the fluorescence spectrum emitted on the π transitions are proportional to $\sqrt{\gamma_1\gamma_2}$. Here γ_1 and γ_2 represent the spontaneous emission rates of the respective π transition. The factor $\sqrt{\gamma_1\gamma_2}$ can be assessed as the formal signature of vacuum induced interference effects, and terms proportional to it only contribute to the fluorescence spectrum since the dipole moments of the π transitions are antiparallel. While vacuum-induced interference effects have been studied extensively by theoretical means, e.g., in V-type three-level atoms, they could not be confirmed experimentally in atomic systems due to the stringent conditions of near-degenerate levels and non-orthogonal dipole moments that are not fulfilled for V-type systems in real atoms. Since the four-level system with antiparallel dipole moments can be found, e.g., in $^{198}Hg^{+}$ ions, our model system turns out to be an ideal candidate to provide evidence for vacuum-induced interference effects. In particular, we point out that an experiment with individual laser-driven $^{198}Hg^{+}$ ions was already performed [37], and the precise measurement of the fluorescence spectrum of a single atom can be achieved with present technology [156].

In the third part of this thesis, we extended our analysis to collective systems where the vacuum-induced dipole-dipole interaction gives rise to a collective quantum dynamics. The interaction between the individual atoms is reflected by additional contributions to the master equation that are absent in the single-atom case, and the analysis of these collective parameters and their implications are the topic of this part.

In chapter 3, we investigated a novel type of vacuum-induced coupling that is impossible in single-atom systems and that has mostly been neglected in the previous literature. In particular, we considered two nearby three-level systems in Λ-configuration and investigated the dependence of the dipole-dipole coupling on the mutual orientation of the dipole moments associated with the atomic transitions. We have shown that transitions of different atoms can be coupled via the dipole-dipole interaction

even if their dipole moments are perpendicular. This counterintuitive result was explained in terms of the dipole radiation pattern. A coupling between transitions with orthogonal dipole moments occurs if the field radiated by the dipole of one atom has a non-zero projection on the orthogonal dipole of the other atom. This novel type of coupling depends strongly on the geometric alignment of the atoms and may crucially influence the system dynamics. In order to demonstrate this, the resonance fluorescence intensity emitted by the two atoms was discussed. For a fixed setup of driving fields and detectors, the spatial orientation of the two-atom pair decides if the system reaches a true constant steady state or if it exhibits periodic oscillations in the long-time limit. We have shown that these oscillations are directly observable in the total intensity emitted by the two-atom system.

In real atoms, the realization of few-level systems like Λ- or two-level systems usually involves the omission of Zeeman sublevels that belong to the same atomic angular momentum multiplets. Since the analysis in chapter 3 suggests that the interaction between orthogonal dipoles of different atoms may introduce additional couplings to unwanted transitions involving the omitted Zeeman sublevels, we reassessed the validity of the few-level approximation in a pair of dipole-dipole interacting atoms in chapter 4. In order to remain general, each atom is modelled by complete angular momentum multiplets. As a concrete example, we assumed that the ground state of each atom is a S_0 singlet state, and the excited state multiplet is a P_1 triplet which consists of three Zeeman sublevels. In a first step, we employed an example to show that in contrast to single-atom systems, the adjustment of the polarization of an external laser field is not sufficient to select the relevant atomic states in each atom. In particular, we demonstrated that the dipole-dipole interaction can transfer population even to atomic states that are not populated by the laser field. In a second step, we established a general statement about the system behavior under rotations of the atomic separation vector. For the derivation of this statement, we assumed that the atoms are placed in the isotropic vacuum and omitted all external laser fields. Finally, several important conclusions about the system properties were drawn from this statement. As an intuitive result, we found that the energies of the collective states depend on the length of the vector connecting the atoms, but not on its orientation, if complete and degenerate multiplets are considered. We then concluded that the artificial omission of any of the Zeeman sublevels leads to a spurious dependence of the energy levels on the orientation of the atomic separation vector, and thus to incorrect predictions. The careful analysis of our results revealed that this breakdown of the few-level approximation can be traced back to the dipole-dipole coupling of transitions with orthogonal dipole moments that were studied in chapter 3. Our interpretation enabled us to identify special geometries in which one or two of the excited states of each atom can be neglected, such that the few-level approximation is recovered.

On the one hand, the breakdown of the few-level approximation in collective systems entails a definite complication of the theoretical treatment of such systems due to the significantly enlarged number of relevant states. On the other hand, this extended number of degrees of freedom opens the path for new physical phenomena. As an

example for the advantages of dipole-dipole interacting atoms with complete angular momentum multiplets, we investigated the possibility to realize decoherence-free subspaces (DFS) in such systems in chapter 5. Our analysis was based on the system of two dipole-dipole coupled four-level atoms introduced in chapter 4. We have shown that the state space of the two interacting atoms contains a four-dimensional DFS if the interatomic distance approaches zero. This is a strong improvement as compared to a pair of two-level atoms, where only the collective ground state and a single antisymmetric state are immune against spontaneous emission. Since the separation of the two atoms is always larger than zero in an experiment, we demonstrated that the spontaneous decay of states within the DFS is strongly suppressed if the interatomic distance is small as compared to the wavelength of the $S_0 \leftrightarrow P_1$ transition. In addition, we verified that the system dynamics within the DFS is closed, i.e., the coherent part of the dipole-dipole interaction does not introduce a coupling between states of the DFS and states outside of the DFS. Possible applications of this DFS for the storage and processing of quantum information were discussed. For this, we described a method that allows to populate the antisymmetric states of the DFS by means of a laser field without the need of a field gradient between the atoms. Two antisymmetric collective states within the DFS were employed to represent a qubit. The storing times of the qubit state depend on the interatomic distance and can be significantly longer than the inverse decay rate of the $S_0 \leftrightarrow P_1$ transition. Moreover, any single-qubit operation can be realized via a sequence of suitable radio-frequency pulses. Typical operation times of our system may be significantly shorter than for a nuclear spin system due to the stronger coupling between the electronic states and the radio-frequency field. Finally, we demonstrated that the symmetric and antisymmetric collective states are entangled, and this entanglement is created by the coherent part of the dipole-dipole interaction.

While the atom-field interaction in the system considered in chapter 5 gives rise to entanglement between atomic states, several schemes of quantum information and quantum computation theory are based on an entangled state of the radiation field [5]. Therefore, we investigated the possibility to create entanglement between the field modes of the electromagnetic field in chapter 6. For this, we considered a single atom trapped inside a two-mode cavity as the gain medium. Our model system can be regarded as a generalization of the setup employed in a recent experiment [147], where a single-atom laser was realized. In order to prove that the quantum state of the cavity field created by the atom is entangled, we employed an inequality based on the correlation of the field operators. Note that this inequality is only one of several known sufficient criteria for continuous variable entanglement. We demonstrated that a single atom is a source for an entangled state of the radiation field over a wide range of control parameters and initial states of the cavity field. In contrast to other schemes like parametric down-conversion, a quantum state with a macroscopic number of photons can be generated. Two parameter regimes for which the quantum state of the cavity field is entangled for a long period of time were identified. For these parameters, the master equation for the density operator of the two cavity modes can be approximately reduced to the master equation for

a nondegenerate parametric oscillator in the parametric approximation. The mean number of photons in the cavity field can be strongly increased if parameters beyond the parametric limit are chosen. This enhancement of the mean photon numbers is accompanied by a shortening of the time slice for which the entanglement criterion is fulfilled. As the initial state of the cavity field, we chose either the vacuum or a coherent state. We demonstrated that the mean number of photons of the entangled cavity field can be significantly increased if a coherent state instead of the vacuum is chosen as an initial state.

In conclusion, we presented several examples that demonstrate the rich variety of physical phenomena emerging from the interaction of atoms with the electromagnetic radiation field. In particular, these phenomena do not only allow for studies of fundamental concepts like interference and complementarity that aim at an improved understanding of quantum mechanics, but prove to be valuable for applications, e.g., in quantum information and quantum computation theory. Throughout the thesis we focused on some of the elementary physical processes occurring in atom-field interactions on the basis of single-atom and two-atom systems. But our results are well-suited for generalizations in several directions. For example, it can be expected that our interpretation of the interference effect discussed in chapter 2 in terms of time-energy complementarity also applies to other systems. Besides the obvious extension to other emission spectra, variations of the interference mechanism may also play a crucial role in absorption phenomena like electromagnetically induced absorption. It is also interesting to examine how the interference between different time orders of photon emissions affects higher-order correlation functions of the field emitted by the system considered in chapter 2.
Furthermore, the general structure of the master equation derived in chapter 1 suggests the extension to systems comprised of many atoms. Potential systems of interest include regular structures of atoms that could exhibit interesting spatial interference effects in the emitted light. In addition, these systems could turn out to be useful for the storage and the controlled transport of quantum information, e.g., along a line of atoms. On the other hand, it could be promising to extend the analysis to quantum gases. Here the dipole-dipole interaction gives rise to long-range interaction potentials that are frequently derived by an average over the spatial orientation of a pair of atoms [102]. In particular, it could be interesting to investigate whether the coupling terms between orthogonal dipole moments discussed in part III average out, or give rise to new features of the resulting potentials between the atoms. While we have shown in chapter 3 that the coupling between orthogonal dipole moments affects the fluorescence intensity emitted by a two-atom system, a natural extension is to consider other observables like absorption profiles, the propagation of electromagnetic pulses or other quantities related to the dispersive properties of a dipole-dipole interacting system.
An important but presumably difficult generalization of our results is to consider the possibility to create higher-dimensional decoherence-free subspaces (DFS) with many dipole-dipole interacting multi-level atoms. Due to the intricate nature of the dipole-dipole interaction, it is not obvious how the dimension of the DFS scales with

the number of atoms. In addition, the computational effort increases dramatically if more complex systems are considered. While the system of two four-level atoms in chapter 5 is large but still controllable, calculations involving five four-level atoms, for example, would be almost impracticable.
Finally, the generation and characterization of entanglement are two of the strongest ambitions of current research in quantum optics. While the strange features of entanglement are known since the early days of quantum mechanics, an unambiguous and comprehensive measure of entanglement is still not available, and it will be exciting to see if there ever will be.

Bibliography

[1] M. O. Scully and M. S. Zubairy, *Quantum optics* (Cambridge University Press, Cambridge, 1997).

[2] N. Bohr, in *Albert Einstein: Philosopher-Scientist*, edited by P. A. Schilpp (Library of Living Philosophers, Evanston, 1949), pp. 200-241; reprinted in *Quantum Theory and Measurement*, edited by J. A. Wheeler and W. H. Zurek (Princeton University Press, Princeton, 1983), pp. 8-49.

[3] R. Hanbury-Brown and R. Q. Twiss, Nature **177**, 27 (1956).

[4] L. Mandel and E. Wolf, *Optical coherence and quantum optics* (Cambridge University Press, London, 1995).

[5] M. A. Nielsen and I. L. Chuang, *Quantum Computation and Quantum Information* (Cambridge University Press, Cambridge, 2000).

[6] A. Einstein, B. Podolsky, and N. Rosen, Phys. Rev. **47**, 777 (1935).

[7] C. Monroe, Nature **416**, 238 (2002).

[8] D. P. DiVincenzo, Science **270**, 255 (1995).

[9] W. G. Unruh, Phys. Rev. A **51**, 992 (1995).

[10] G. S. Agarwal, in *Quantum Statistical Theories of Spontaneous Emission and Their Relation to Other Approaches*, edited by G. Höhler (Springer, Berlin, 1974).

[11] Z. Ficek and S. Swain, *Quantum Interference and Coherence* (Springer, New York, 2005).

[12] R. H. Lehmberg, Phys. Rev. A **2**, 883 (1970).

[13] R. H. Lehmberg, Phys. Rev. A **2**, 889 (1970).

[14] Z. Ficek and R. Tanaś, Phys. Rep. **372**, 369 (2002).

[15] J. Guo and J. Cooper, Phys. Rev. A **51**, 3128 (1995).

[16] G. Kurizki and A. Ben-Reuven, Phys. Rev. A **36**, 90 (1987).

[17] G. S. Agarwal and A. K. Patnaik, Phys. Rev. A **63**, 043805 (2001).

[18] C. Cohen-Tannoudji, J. Dupont-Roc, and G. Grynberg, *Atom-Photon Interactions* (J. Wiley & Sons, 1998).

[19] C. Cohen-Tannoudji, J. Dupont-Roc, and G. Grynberg, *Photons and Atoms* (J. Wiley & Sons, 1997).

[20] R. Zwanzig, in *Lectures in Theoretical Physics*, Vol. **3**, edited by W. E. Brittin, B. W. Downs and J. Downs (Interscience, New York, 1961), p. 106.

[21] H. Lee, P. Polynkin, M. O. Scully, and S.-Y. Zhu, Phys. Rev. A **55**, 4454 (1997).

[22] S.-Y. Zhu, R. C. F. Chan, and C. P. Lee, Phys. Rev. A **52**, 710 (1995).

[23] S.-Y. Zhu and M. O. Scully, Phys. Rev. Lett. **76**, 388 (1996).

[24] E. Paspalakis and P. L. Knight, Phys. Rev. Lett. **81**, 293 (1998).

[25] E. Paspalakis, C. H. Keitel, and P. L. Knight, Phys. Rev. A **58**, 4868 (1998).

[26] C. H. Keitel, Phys. Rev. Lett. **83**, 1307 (1999).

[27] F. Plastina and F. Piperno, Phys. Rev. A **62**, 053801 (2000).

[28] D. A. Cardimona, M. G. Raymer, and J. C. R. Stroud, J. Phys. B **15**, 55 (1982).

[29] G. C. Hegerfeldt and M. B. Plenio, Phys. Rev. A **46**, 373 (1992).

[30] P. Zhou and S. Swain, Phys. Rev. Lett. **77**, 3995 (1996).

[31] P. Zhou and S. Swain, Phys. Rev. A **56**, 3011 (97).

[32] S. Swain, P. Zhou, and Z. Ficek, Phys. Rev. A **61**, 043410 (2000).

[33] S.-Y. Gao, F.-L. Li, and S.-Y. Zhu, Phys. Rev. A **66**, 43806 (2002).

[34] H.-R. Xia, C.-Y. Ye, and S.-Y. Zhu, Phys. Rev. Lett. **77**, 1032 (1996).

[35] L. Li, X. Wang, J. Yang, G. Lazarov, J. Qi, and A. M. Lyyra, Phys. Rev. Lett. **84**, 4016 (2000).

[36] M. V. G. Dutt, J. Cheng, B. Li, X. Xu, X. Li, P. R. Berman, D. G. Steel, A. S. Bracker, D. Gammon, S. E. Economou, et al., Phys. Rev. Lett. **94**, 227403 (2005).

[37] U. Eichmann, J. C. Bergquist, J. J. Bollinger, J. M. Gilligan, W. M. Itano, D. J. Wineland, and M. G. Raizen, Phys. Rev. Lett. **70**, 2359 (1993).

[38] T. Wong, S. M. Tan, M. J. Collett, and D. F. Walls, Phys. Rev. A **55**, 1288 (1997).

[39] W. M. Itano, J. C. Bergquist, J. J. Bollinger, D. J. Wineland, U. Eichmann, and M. G. Raizen, Phys. Rev. A **57**, 4176 (1998).

[40] G. S. Agarwal, J. von Zanthier, C. Skornia, and H. Walther, Phys. Rev. A **65**, 053826 (2002).

[41] R. P. Feynman, R. B. Leighton, and M. Sands, *The Feynman Lectures on Physics*, Vol. III (Addison-Wesley, 1963).

[42] M. O. Scully, B.-G. Englert, and H. Walther, Nature **351**, 111 (1991).

[43] P. Storey, S. Tan, M. Collett, and D. Walls, Nature **367**, 626 (1994).

[44] B.-G. Englert, M. O. Scully, and H. Walther, Nature **375**, 367 (1995).

[45] E. P. Storey, S. M. Tan, M. J. Collett, and D. F. Walls, Nature **375**, 368 (1995).

[46] H. Wiseman and F. Harrison, Nature **377**, 584 (1995).

[47] H. M. Wiseman, F. E. Harrison, M. J. Collett, S. M. Tan, D. F. Walls, and R. B. Killip, Phys. Rev. A **56**, 55 (1997).

[48] A. Luis and L. L. Sánchez-Soto, J. Opt. B: Quantum Semiclass. Opt. **1**, 668 (1999).

[49] S. P. Walborn, M. O. T. Cunha, S. Pádua, and C. H. Monken, Phys. Rev. A **65**, 033818 (2002).

[50] S. Dürr, T. Nonn, and G. Rempe, Nature **395**, 33 (1998).

[51] D. Polder and M. F. H. Schuurmans, Phys. Rev. A **14**, 1468 (1976).

[52] M. Jakob and J. Bergou, Phys. Rev. A **60**, 4179 (1999).

[53] N. Lütkenhaus, J. I. Cirac, and P. Zoller, Phys. Rev. A **57**, 548 (1998).

[54] J. J. Sakurai, *Modern Quantum Mechanics* (Addison-Wesley, Reading, MA, 1994).

[55] B. R. Mollow, J. Phys. A **8**, L130 (1975).

[56] H. J. Kimble and L. Mandel, Phys. Rev. A **13**, 2123 (1976).

[57] C. Cohen-Tannoudji and S. Reynaud, J. Phys. B **10**, 345 (1977).

[58] Y.-H. Kim, R. Yu, S. P. Kulik, Y. Shih, and M. O. Scully, Phys. Rev. Lett. **84**, 1 (2000).

[59] J. H. Eberly and K. Wódkiewicz, J. Opt. Soc. Am. **67**, 1252 (1977).

[60] B.-G. Englert, Phys. Rev. Lett. **77**, 2154 (1996).

[61] G. C. Hegerfeldt and M. B. Plenio, Phys. Rev. A **52**, 3333 (1995).

[62] M. B. Plenio and P. L. Knight, Rev. Mod. Phys. **70**, 101 (1998).

[63] J. Evers and C. H. Keitel, Phys. Rev. A **65**, 33813 (2002).

[64] M. E. Smithers and H. S. Freedhoff, J. Phys. B **8**, 2911 (1975).

[65] C. Cohen-Tannoudji, *Atoms in strong resonant fields* (North-Holland, 1977), in: Frontiers in Laser Spectroscopy, Les Houches Session XXVII (1975).

[66] A. Aspect, G. Roger, S. Reynaud, J. Dalibard, and C. Cohen-Tannoudji, Phys. Rev. Lett. **45**, 617 (1980).

[67] C. A. Schrama, G. Nienhuis, H. A. Dijkerman, C. Steijsiger, and H. G. M. Heideman, Phys. Rev. Lett. **67**, 2443 (1991).

[68] C. A. Schrama, G. Nienhuis, H. A. Dijkerman, C. Steijsiger, and H. G. M. Heideman, Phys. Rev. A **45**, 8045 (1992).

[69] F. Lindner, M. G. Schätzel, H. Walther, A. Baltuška, E. Goulielmakis, F. Krausz, D. B. Milošević, D. Bauer, W. Becker, and G. G. Paulus, Phys. Rev. Lett. **95**, 040401 (2005).

[70] M. Wollenhaupt, A. Präkelt, C. Sarpe-Tudoran, D. Liese, and T. Baumert, J. Opt. B: Quantum Semiclass. Opt. **7**, 270 (2005).

[71] M. Lax, Phys. Rev. **129**, 2342 (1963).

[72] H. Carmichael, *An Open Systems Approach to Quantum Optics* (Springer, 1993).

[73] R. H. Dicke, Phys. Rev. **93**, 99 (1954).

[74] S. S. Hassan, G. P. Hildred, R. R. Puri, and R. K. Bullough, J. Phys. B **15**, 2635 (1982).

[75] M. Gross and S. Haroche, Phys. Rep. **93**, 301 (1982).

[76] P. D. Drummond and H. J. Carmichael, Opt. Commun. **27**, 160 (1978).

[77] S. Y. Kilin, JETP **55**, 38 (1982).

[78] M. Macovei, J. Evers, and C. H. Keitel, Phys. Rev. Lett. **91**, 233601 (2003).

[79] M. Macovei, J. Evers, and C. H. Keitel, Europhys. Lett. **68**, 391 (2004).

[80] M. A. Macovei and J. Evers, Opt. Commun. **240**, 379 (2004).

[81] J. M. Raimond, P. Goy, M. Gross, C. Fabre, and S. Haroche, Phys. Rev. Lett. **49**, 117 (1982).

[82] N. N. Bogolubov, Jr., T. Quang, and A. S. Shumovsky, Phys. Lett. **112**, 323 (1985).

[83] T. J. Carroll, K. Claringbould, A. Goodsell, M. J. Lim, and M. W. Noel, Phys. Rev. Lett. **93**, 153001 (2004).

[84] T. G. Rudolph, Z. Ficek, and B. J. Dalton, Phys. Rev. A **52**, 636 (1995).

[85] M. Macovei and C. H. Keitel, Phys. Rev. Lett. **91**, 123601 (2003).

[86] Z. Ficek, Phys. Rev. A **44**, 7759 (1991).

[87] D. F. V. James, Phys. Rev. A **47**, 1336 (1993).

[88] G. V. Varada and G. S. Agarwal, Phys. Rev. A **45**, 6721 (1992).

[89] M. Lewenstein and J. Javanainen, Phys. Rev. Lett. **59**, 1289 (1987).

[90] A. Beige and G. C. Hegerfeldt, Phys. Rev. A **59**, 2385 (1999).

[91] M. D. Lukin and P. R. Hemmer, Phys. Rev. Lett. **84**, 2818 (2000).

[92] G. Li, K. Allaart, and D. Lenstra, Phys. Rev. A **69**, 055802 (2004).

[93] I. V. Bargatin, B. A. Grishanin, and V. N. Zadkov, Phys. Rev. A **61**, 052305 (2000).

[94] R. G. DeVoe and R. G. Brewer, Phys. Rev. Lett. **76**, 2049 (1996).

[95] P. Mataloni, E. De Angelis, and F. De Martini, Phys. Rev. Lett. **85**, 1420 (2000).

[96] J. Eschner, C. Raab, F. Schmidt-Kaler, and R. Blatt, Nature **413**, 495 (2001).

[97] M. D. Barnes, P. S. Krstic, P. Kumar, A. Mehta, and J. C. Wells, Phys. Rev. B **71**, 241303(R) (2005).

[98] P. W. Milonni and P. L. Knight, Phys. Rev. A **10**, 1096 (1974).

[99] M. Born and E. Wolf, *Principles of optics*, (Cambridge University Press, Cambridge, 1999).

[100] E. T. Jaynes and F. W. Cummings, Proc. IEEE **51**, 89 (1963).

[101] W. E. Lamb, R. R. Schlicher, and M. O. Scully, Phys. Rev. A **36**, 2763 (1987).

[102] T. Thirunamachandran, Mol. Phys. **40**, 393 (1980).

[103] D. O'Dell, S. Giovanazzi, G. Kurizki, and V. M. Akulin, Phys. Rev. Lett. **84**, 5687 (2000).

[104] A. Gero and E. Akkermans, Phys. Rev. Lett. **96**, 093601 (2006).

[105] J. Kästel and M. Fleischhauer, Phys. Rev. A **71**, 011804(R) (2005).

[106] C. Hettich, C. Schmitt, J. Zitzmann, S. Kühn, I. Gerhardt, and V. Sandoghdar, Nature **298**, 385 (2002).

[107] A. Beige, S. F. Huelga, P. L. Knight, M. B. Plenio, and R. C. Thompson, J. Mod. Opt. **47**, 401 (2000).

[108] G. K. Brennen, C. M. Caves, P. S. Jessen, and I. H. Deutsch, Phys. Rev. Lett. **82**, 1060 (1999).

[109] A. Barenco, D. Deutsch, A. Ekert, and R. Jozsa, Phys. Rev. Lett. **74**, 4083 (1995).

[110] I. L. Chuang, R. Laflamme, P. W. Shor, and W. H. Zurek, Science **270**, 1633 (1995).

[111] A. Ekert and R. Jozsa, Rev. Mod. Phys. **68**, 733 (1996).

[112] P. Zanardi and M. Rasetti, Phys. Rev. Lett. **79**, 3306 (1997).

[113] D. A. Lidar, I. L. Chuang, and K. B. Whaley, Phys. Rev. Lett. **81**, 2594 (1998).

[114] D. A. Lidar and K. B. Whaley, in *Irreversible Quantum Dynamics*, edited by F. Benatti and R. Floreanini, (Springer Lecture Notes in Physics vol. **622**, Berlin, 2003), pp. 83-120.

[115] J. Kempe, D. Bacon, D. A. Lidar, and K. B. Whaley, Phys. Rev. A **63**, 042307 (2001).

[116] E. Knill, R. Laflamme, and L. Viola, Phys. Rev. Lett. **84**, 2525 (2000).

[117] A. Shabani and D. A. Lidar, Phys. Rev. A **72**, 042303 (2005).

[118] P. G. Kwiat, A. J. Berglund, J. B. Altepeter, and A. G. White, Science **290**, 498 (2000).

[119] Q. Zhang, J. Yin, T.-Y. Chen, S. Lu, J. Zhang, X.-Q. Li, T. Yang, X.-B. Wang, and J.-W. Pan, Phys. Rev. A **73**, 020301(R) (2006).

[120] J. B. Altepeter, P. G. Hadley, S. M. Wendelken, A. J. Berglund, and P. G. Kwiat, Phys. Rev. Lett. **92**, 147901 (2004).

[121] M. Mohseni, J. S. Lundeen, K. J. Resch, and A. M. Steinberg, Phys. Rev. Lett. **91**, 187903 (2003).

[122] L. Viola, E. M. Fortunato, M. A. Pravia, E. Knill, R. Laflamme, and D. G. Cory, Science **293**, 2059 (2001).

[123] D. Wei, J. Luo, X. Sun, X. Zeng, M. Zhan, and M. Liu, Phys. Rev. Lett. **95**, 020501 (2005).

[124] J. E. Ollerenshaw, D. A. Lidar, and L. E. Kay, Phys. Rev. Lett. **91**, 217904 (2003).

[125] D. Kielpinski, V. Meyer, M. A. Rowe, C. A. Sackett, W. M. Itano, C. Monroe, and D. J. Wineland, Science **291**, 1013 (2001).

[126] C. Langer, R. Ozeri, J. D. Jost, J. Chiaverini, B. DeMarco, A. Ben-Kish, R. B. Blakestad, J. Britton, D. B. Hume, W. M. Itano, D. Leibfried, R. Reichle, T. Rosenband, T. Schaetz, P. O. Schmidt, and D. J. Wineland, Phys. Rev. Lett. **95**, 060502 (2005).

[127] D. Jaksch, J. I. Cirac, P. Zoller, S. L. Rolston, R. Côté, and M. D. Lukin, Phys. Rev. Lett. **85**, 2208 (2000).

[128] P. Zanardi, Phys. Rev. A **56**, 4445 (1997).

[129] L.-M. Duan and G.-C. Guo, Phys. Rev. A **58**, 3491 (1998).

[130] U. Akram, Z. Ficek, and S. Swain, Phys. Rev. A **62**, 013413 (2000).

[131] W. K. Wootters, Phys. Rev. Lett. **80**, 2245 (1998).

[132] P. Rungta, V. Bužek, C. M. Caves, M. Hillery, and G. J. Milburn, Phys. Rev. A **64**, 042315 (2001).

[133] C. H. Bennett, G. Brassard, C. Crepeau, R. Jozsa, A. Peres, and W. K. Wootters, Phys. Rev. Lett. **70**, 1895 (1993).

[134] D. Bouwmeester, J. W. Pan, K. Mattle, M. Eibl, H. Weinfurter, and A. Zeilinger, Nature **390**, 575 (1997).

[135] C. H. Bennett and G. Brassard, *Proceedings of the IEEE International Conference on Computers, Systems and Signal Processing* (IEEE, Los Alamitos, CA), 1984, p. 175.

[136] P. W. Shor, in *Proceedings of the 35th Annual Symposium on Foundations of Computer Science, Santa Fe, NM 1994*, edited by S. Goldwasser (IEEE Computer Society Press, Los Alamitos, CA 1994), pp 124; SIAM J. Comput. **26** 1484 (1997).

[137] L. K. Grover, Phys. Rev. Lett. **79**, 325 (1997).

[138] S. L. Braunstein and P. van Look, Rev. Mod. Phys. **77**, 513 (2005).

[139] Z. Y. Ou, S. F. Pereira, H. J. Kimble, and K. C. Peng, Phys. Rev. Lett. **68**, 3663 (1992).

[140] G. Morigi, J. Eschner, S. Mancini, and D. Vitali, Phys. Rev. Lett. **96**, 023601 (2006).

[141] G. Morigi, J. Eschner, S. Mancini, and D. Vitali, Phys. Rev. A **73**, 033822 (2006).

[142] L. Zhou, H. Xiong, and M. S. Zubairy, Phys. Rev. A **74**, 022321 (2006).

[143] H. Xiong, M. O. Scully, and M. S. Zubairy, Phys. Rev. Lett. **94**, 023601 (2005).

[144] H.-T. Tan, S.-Y. Zhu, and M. S. Zubairy, Phys. Rev. A **72**, 022305 (2005).

[145] M. O. Scully, Phys. Rev. Lett. **55**, 2802 (1985).

[146] M. O. Scully and M. S. Zubairy, Phys. Rev. A **35**, 752 (1987).

[147] J. McKeever, A. Boca, A. D. Boozer, J. R. Buck, and H. J. Kimble, Nature **425**, 268 (2003).

[148] R. Simon, Phys. Rev. Lett. **84**, 2726 (2000).

[149] L.-M. Duan, G. Giedke, J. I. Cirac, and P. Zoller, Phys. Rev. Lett. **84**, 2722 (2000).

[150] E. Shchukin and W. Vogel, Phys. Rev. Lett. **95**, 230502 (2005).

[151] M. Hillery and M. S. Zubairy, Phys. Rev. Lett. **96**, 050503 (2006).

[152] G. S. Agarwal and A. Biswas, New J. Phys. **7**, 211 (2005).

[153] H. Nha and J. Kim, Phys. Rev. A **74**, 012317 (2006).

[154] O. Gühne and N. Lütkenhaus, Phys. Rev. Lett. **96**, 170502 (2006).

[155] V. Giovannetti, S. Mancini, D. Vitali, and P. Tombesi, Phys. Rev. A **67**, 022320 (2003).

[156] V. Bühner and C. Tamm, Phys. Rev. A **61**, 61801(R) (2000).

Thanks

First of all, I would like to thank Prof. Dr. Christoph H. Keitel for giving me the opportunity to do my PhD in his theory group, for the excellent working conditions and for his continuous support. In particular, I appreciate that I had the freedom to follow my own ideas.

I am especially indebted to Dr. Jörg Evers for numerous discussions about physical problems and questions that accumulate during a PhD. In addition, I would like to thank him for the enjoyable collaboration.

It is my pleasure to thank Prof. Dr. M. Suhail Zubairy for the good collaboration, exciting discussions about physics and his commitment for our project.

To Dr. Zbigniew Ficek I would like to express my sincere gratitude for many inspiring and helpful discussions during his extended visits at the MPI-K.

I would also like to thank Dr. Mihai Macovei for dedicated discussions and the good collaboration.

Probably the most important and sometimes the most troublesome resource for a theorist is the computer. Therefore, I very much appreciate Peter Brunner's excellent support for all my computer problems.

My special thanks go to Martina Weizmann for her friendly and qualified assistance with all kinds of administrative problems.

For the enjoyable atmosphere at the institute and the various free time activities that we shared I would like to thank all my colleagues and friends at the MPI-K. In addition, I am grateful for the friendly and pleasant atmosphere in our office thanks to my roommates Mario Verschl, Martin Haas, Robert Fischer, Henrik Hetzheim and Peter Orth.

Finally, I would like to thank my parents and my brother for their continuous encouragement. In particular, I would like to thank my father for his smart support in transportation issues.